

Copy 35

N70-25828

UB

NASA TM SX-1961

NASA TECHNICAL
MEMORANDUM

UB
NASA TM SX-1961

FOR

U.S. AIR FORCE

CASE FILE
COPY

EFFECTS OF ADDITIONAL REVISIONS
ON THE AERODYNAMIC CHARACTERISTICS
OF A TARGET DRONE VEHICLE
AT MACH NUMBERS FROM 1.70 TO 4.63
COORD NO. AF-AM-827



by A. B. Blair, Jr., and Dorothy H. Tudor

Langley Research Center

Langley Station, Hampton, Va.

The distribution of this document should be restricted to those recipients endorsed by the organization for which it was prepared.

TECHNICAL MEMORANDUM SX-1961
for
U.S. Air Force
EFFECTS OF ADDITIONAL REVISIONS ON THE
AERODYNAMIC CHARACTERISTICS OF A TARGET DRONE VEHICLE
AT MACH NUMBERS FROM 1.70 TO 4.63

COORD NO. AF-AM-827

By A. B. Blair, Jr., and Dorothy H. Tudor

Langley Research Center
Langley Station, Hampton, Va.

NATIONAL AERONAUTICS AND SPACE ADMINISTRATION

TECHNICAL MEMORANDUM SX-1961

for

U.S. Air Force

EFFECTS OF ADDITIONAL REVISIONS ON THE
AERODYNAMIC CHARACTERISTICS OF A TARGET DRONE VEHICLE
AT MACH NUMBERS FROM 1.70 TO 4.63

COORD NO. AF-AM-827

By A. B. Blair, Jr., and Dorothy H. Tudor
Langley Research Center

ABSTRACT

An investigation has been conducted in the Langley Unitary Plan wind tunnel to determine the effects of several modifications on the supersonic aerodynamic characteristics of a 1/4-scale target drone. The model with either wing or with a wing-canard combination was longitudinally stable about the selected moment center. Both the large and the small canards were effective as trim devices; the trim power appeared to be a linear function of canard planform area. The model with large vertical fins was directionally stable and had positive effective dihedral throughout the angle-of-attack and Mach number ranges; however, reducing the size of the vertical fins led to a large decrease in directional stability. The ailerons were effective in producing rolling moment throughout the test ranges, although there was a significant decrease in effectiveness with increases in Mach number. Aileron deflection generally produced an adverse yawing moment which tended to increase with angle of attack.

STAR Category 01

EFFECTS OF ADDITIONAL REVISIONS ON THE
AERODYNAMIC CHARACTERISTICS OF A TARGET DRONE VEHICLE
AT MACH NUMBERS FROM 1.70 TO 4.63

By A. B. Blair, Jr., and Dorothy H. Tudor
Langley Research Center

SUMMARY

As part of a continuing program to develop an expendable supersonic target drone, the Langley Research Center has conducted a wind-tunnel investigation to determine the effects of several modifications on the supersonic aerodynamic characteristics of a 1/4-scale target drone vehicle. The investigation was conducted in the Langley Unitary Plan wind tunnel at Mach numbers from 1.70 to 4.63, at angles of attack from about -4° to 16° , at angles of sideslip from about -4° to 6° , and at a Reynolds number of 9.38×10^6 based on model length.

Results of this investigation indicated that the model with either wing or with a wing-canard combination was longitudinally stable about the selected moment center. Both the large and the small canards were effective trim devices, and the trim power appeared to be a linear function of canard planform area. The model with large vertical fins was directionally stable and had positive effective dihedral throughout the angle-of-attack and Mach number ranges; however, reducing the size of the vertical fins led to a large decrease in directional stability throughout the angle-of-attack and Mach number ranges. The ailerons were effective in producing rolling moment throughout the angle-of-attack and Mach number ranges, although there was a significant decrease in effectiveness with increases in Mach number. Aileron deflection generally produced an adverse yawing moment which tended to increase with angle of attack.

INTRODUCTION

The continuing increase in speed and altitude capability of fighter aircraft has led to the necessity of periodically updating target drones. As part of a program to develop an expendable supersonic target drone, the Langley Research Center has conducted a wind-tunnel investigation to determine the supersonic aerodynamic characteristics of a 1/4-scale target drone vehicle. The vehicle is air launched, and except for programed climb-to-cruise altitude, is designed primarily for straight and level flight at Mach

numbers up to 4.00 and altitudes to 90 000 feet (27 432 m). The vehicle is rocket powered and has canard control surfaces and twin outboard vertical stabilizers. The modified drone is an outgrowth of an existing target drone (refs. 1 and 2) and differs from the configuration of reference 2 primarily by having a longer fuselage, a shorter truncated-cone afterbody, and a canard planform which is a delta rather than a trapezoid. The present investigation also included some measurements of the panel loads on the canards and ailerons.

The investigation was conducted in the Langley Unitary Plan wind tunnel at Mach numbers from 1.70 to 4.63, at angles of attack from about -4° to 16° , at angles of sideslip from about -4° to 6° , and at a Reynolds number of 9.38×10^6 based on model length.

SYMBOLS

The forces and moments have been reduced to nondimensional coefficients based on body cross-sectional area and body length. The longitudinal characteristics are referred to the stability-axis system, and the lateral characteristics are referred to the body-axis system. The moment reference point is located 18.500 inches (46.990 cm) forward of the model base. The physical quantities are given both in U.S. Customary Units and in the International System of Units (SI). (See ref. 3.)

A	cross-sectional area of body, 0.0576 foot ² (0.0054 meter ²)
C_D	drag coefficient, $\frac{\text{Drag}}{qA}$
$C_{D,b}$	base-drag coefficient, $\frac{\text{Base drag}}{qA}$
$C_{D,c}$	balance chamber-drag coefficient, $\frac{\text{Chamber drag}}{qA}$
$C_{D,o}$	drag coefficient for zero lift
$C_{h,a}$	aileron hinge-moment coefficient, $\frac{\text{Aileron hinge moment}}{qAl}$
$C_{h,c}$	canard hinge-moment coefficient, $\frac{\text{Canard hinge moment}}{qAl}$
C_L	lift coefficient, $\frac{\text{Lift}}{qA}$
$C_{L\alpha}$	lift-curve slope at $\alpha = 0^\circ$, per degree
C_l	rolling-moment coefficient, $\frac{\text{Rolling moment}}{qAl}$

C_n	yawing-moment coefficient, $\frac{\text{Yawing moment}}{qAl}$
C_Y	side-force coefficient, $\frac{\text{Side force}}{qA}$
$C_{l\beta}$	effective-dihedral parameter, $\frac{\Delta C_l}{\Delta \beta}$, $\beta = 0^\circ, 3^\circ$
$C_{n\beta}$	directional-stability parameter, $\frac{\Delta C_n}{\Delta \beta}$, $\beta = 0^\circ, 3^\circ$
$C_{Y\beta}$	side-force parameter, $\frac{\Delta C_Y}{\Delta \beta}$, $\beta = 0^\circ, 3^\circ$
C_m	pitching-moment coefficient, $\frac{\text{Pitching moment}}{qAl}$
C_{mC_L}	longitudinal-stability parameter at $C_L \approx 0$
$C_{m\delta_c}$	canard effectiveness in pitch, $\frac{\partial C_m}{\partial \delta_c}$, at $\alpha = 0^\circ$, per degree
$C_{N,c}$	canard normal-force coefficient, $\frac{\text{Canard normal force}}{qA}$
L/D	lift-drag ratio
l	body length, 45.000 inches (114.300 centimeters)
M	free-stream Mach number
q	free-stream dynamic pressure
r	radius (see fig. 1)
α	angle of attack of model center line, degrees
β	angle of sideslip of model center line, degrees
δ_a	deflection of left-hand aileron minus deflection of right-hand aileron, deflection positive when left-aileron trailing edge is down, degrees
δ_c	deflection of both canards, positive when trailing edges are down, degrees

Subscript:

max maximum

Model component designations:

B₁ body

C₁ large canard

C₂ small canard

F₁ large vertical fin

F₂ small vertical fin

W₁ small wing

W₂ large wing

APPARATUS

Tunnel

The tests were conducted in both the low and high Mach number test sections of the Langley Unitary Plan wind tunnel, which is a variable-pressure continuous-flow facility. The test sections are 4 feet (1.219 m) square and approximately 7 feet (2.134 m) long. The nozzles leading to the test sections are of the asymmetric sliding-block type which permits a continuous variation in Mach number from about 1.5 to 2.9 in the low Mach number test section and from about 2.3 to 4.7 in the high Mach number test section.

Model

Details of the 1/4-scale model and an alternate canard, wing, and vertical fin are shown in figure 1. Photographs of the model are presented as figure 2. The fuselage consists of a cylinder with a Von Karman nose and a truncated-cone afterbody. Both wing W₁ and wing W₂ have clipped-delta planforms and modified wedge sections. The planform area of W₂ is 9 percent greater than that of W₁ because of an increase in root chord. Provisions were made so that each wing would accept the same full-span aileron. Vertical fins were attached to the wing tips, normal to the wing-chord plane. The alternate fin F₂ has a planform area equivalent to 77 percent of the area of F₁ because of an

increase in leading-edge sweep angle. Two canards C_1 and C_2 were used with the model. The planform area of C_2 is about 63 percent of the area of C_1 because of a decrease in both chord and span.

PROCEDURE

Test Conditions

The model was tested at the conditions outlined in table I.

TABLE I.- TEST CONDITIONS

Mach number	Stagnation temperature		Stagnation pressure	
	°F	°K	psfa	kN/m ²
1.70	150	338	1472	70.48
2.00	150	338	1659	79.43
2.30	150	338	1915	91.69
2.36	150	338	1975	94.56
2.86	150	338	2570	123.05
2.96	150	338	2711	129.80
3.95	175	352	4829	231.21
4.63	175	352	6594	315.72

The Reynolds number for all test conditions was 9.38×10^6 based on model length.

The dewpoint measured at stagnation pressure was maintained below -30° F (240° K) to insure negligible condensation effects. All tests were performed with boundary-layer transition strips on the fuselage 1.20 inches (3.05 cm) aft of the nose, and on both sides of the wing, vertical tails, and canards 0.40 inch (1.02 cm) aft of the leading edge, measured streamwise. The 0.40-inch streamwise measurement for the canards was taken on the root chord with the transition strip terminating at the vertex of the canard tip. The transition strips, which were approximately 0.0625 inch (0.15875 cm) wide, were composed of No. 60 sand grains for $M = 1.70, 2.00, 2.36$, and 2.86 , and of No. 45 sand grains for $M = 2.30, 2.96, 3.95$, and 4.63 . The angle-of-attack range of the tests was from about -4° to 16° . The angle-of-sideslip range was from about -4° to 6° .

Measurements

Aerodynamic forces and moments were measured by means of a six-component, electrical strain-gage balance mounted within the model. The balance was rigidly fastened to a sting-support system. In addition, a two-component balance was used to

measure canard normal forces and hinge moments. Each aileron was equipped with a strain gage to measure aileron hinge moments. Two pressure measurements were made, one within the balance chamber and the other at the fuselage base annulus.

Corrections

Angles of attack have been corrected for tunnel-flow misalignment. Angles of attack and sideslip have been corrected for deflection of sting and balance due to aerodynamic loads. The axial-force and drag data were adjusted to correspond to free-stream static conditions in the balance chamber and at the fuselage base. Typical values of the balance chamber-drag and base-drag corrections are presented in figure 3.

PRESENTATION OF RESULTS

The results of the investigation are presented as follows:

	Figure
Effect of model components on longitudinal aerodynamic characteristics	4
Effect of change in wing and/or vertical-fin planforms on longitudinal aerodynamic characteristics of complete model	5
Effect of canard size on longitudinal aerodynamic characteristics	6
Longitudinal control characteristics:	
$B_1W_1F_1C_1$	7
$B_1W_1F_1C_2$	8
$B_1W_2F_1C_1$	9
$B_1W_1F_2C_1$	10
$B_1W_2F_2C_1$	11
Canard normal-force and hinge-moment coefficients for configuration $B_1W_1F_1C_1$	12
Canard normal-force and hinge-moment coefficients for configuration $B_1W_1F_1C_2$	13
Summary of longitudinal aerodynamic characteristics	14
Lateral aerodynamic characteristics in sideslip for configuration $B_1W_1F_1C_1$. . .	15
Effect of model components on lateral parameters	16
Effect of change in wing and/or vertical-fin planforms on lateral parameters . . .	17
Effect of canard size on lateral parameters	18
Summary of lateral and directional stability parameters	19
Aileron-control effectiveness:	
$B_1W_1F_1C_1$	20
$B_1W_2F_1C_1$	21

	Figure
$B_1W_1F_2C_1$	22
$B_1W_2F_2C_1$	23
Aileron hinge-moment coefficients for $\delta_a = 0^\circ$ and $\delta_c = 0^\circ$	24
Aileron hinge-moment coefficients for $\delta_a = 20^\circ$ and $\delta_c = 0^\circ$	25

DISCUSSION

Longitudinal Characteristics

The effect of model components on the longitudinal aerodynamic characteristics of the model is presented in figure 4. The body-alone results indicate an increase in lift-curve slope with increase in angle of attack. This increase is evident in all stages of the model buildup. The body alone is unstable about the selected moment center, and the addition of canards, as expected, causes a further decrease in the stability level. Addition of the wing, however, provides a stable condition for the model. Addition of the vertical fins leads to a further increase in stability level caused by the increase in lift due to an endplate effect on the wing panels. The configuration $B_1W_1F_1C_1$ is stable throughout the Mach number range. The variations in pitching moment with lift coefficient are relatively linear through $C_L \approx 0$.

The effect of change in wing and/or vertical-fin planforms (W_1 to W_2 and/or F_1 to F_2) on longitudinal aerodynamic characteristics of the complete model is presented in figure 5. Due to an increase in wing area forward of the model center of gravity, a change in wing planform from W_1 to W_2 results in a slight increase in lift-curve slope and a decrease in stability level. The model with the smaller vertical fins (F_2) generally has the lower stability level. The effect of canard size on the longitudinal aerodynamic characteristics is presented in figure 6. The smaller canard (C_2), as expected, leads to higher stability levels for the model for Mach numbers of 1.70, 2.00, and 2.86.

The longitudinal control data presented in figures 7 to 11 show that both the large and small canards are effective trim devices, although at high canard settings and angles of attack (effective canard angles of attack of about 30°), it is believed that a stall condition for the canard exists at the lowest Mach number. The trim power of the canards appears to be a linear function of the canard area, since the small canard has an area about two-thirds that of the large canard and its trim power is about two-thirds that of the large canard for comparable test Mach numbers.

Canard normal-force and hinge-moment coefficients are presented in figures 12 and 13 for canards C_1 and C_2 , respectively. The larger canard, of course, produces the largest normal-force values; however, the smaller canard C_2 has the greater hinge-moment-coefficient values.

A summary of the longitudinal aerodynamic characteristics of the complete configurations is presented in figure 14.

Lateral Characteristics

The lateral aerodynamic characteristics in sideslip for configuration $B_1W_1F_1C_1$ at several angles of attack are presented in figure 15. These data are shown primarily to indicate the linearity of the coefficients with sideslip angles since all lateral parameters were obtained from incremental results of tests made through the angle-of-attack range at $\beta = 0^\circ$ and 3° . The results were generally linear to $\beta = 3^\circ$ and indicated that the comparative results shown for the lateral parameters are valid.

The effect of model components on the lateral parameters is presented in figure 16. These data show that the complete model has positive effective dihedral and is directionally stable throughout the angle-of-attack and Mach number ranges except at $M = 4.63$ where directional stability occurs only above $\alpha \approx 3^\circ$.

There are only small effects of wing change (W_1 to W_2) on the directional stability of the configuration. (See fig. 17.) Reducing the size of the vertical fins (F_1 to F_2), however, leads to a large decrease in $C_{n\beta}$ throughout the angle-of-attack and Mach number ranges. There is little effect of fin or wing change on the effective dihedral of the model. Changing from C_1 to C_2 indicates that canard size has little effect on the lateral parameters. (See fig. 18.)

A summary of the lateral parameter data is presented as figure 19. The large decrease in directional stability with increase in Mach number is shown in this figure.

The aileron-control effectiveness for four complete configurations is shown in figures 20 to 23 for canard deflections of 0° , 5° , and 15° . The ailerons are effective in producing rolling moment throughout the angle-of-attack and Mach number ranges, although there is a significant decrease in effectiveness with increase in Mach number. The ailerons generally produced an adverse yawing moment, particularly at the higher test angles of attack. There is little effect of wing or fin change on the aileron effectiveness of the configuration. In addition, canard deflection has no significant effect on the aileron effectiveness.

Figures 24 and 25 present left- and right-aileron hinge-moment coefficients for $\delta_a = 0^\circ$ and $\delta_a = 20^\circ$, respectively. For a $\delta_a = 0^\circ$, the maximum hinge-moment coefficients are less than 0.001 in the test angle-of-attack and Mach number ranges. In addition, Mach number has little effect on $C_{h,a}$. With the ailerons deflected ($\delta_a = 20^\circ$), values of $C_{h,a}$ become somewhat greater at the lower Mach numbers and higher angles of attack; however, there is a significant decrease in hinge-moment coefficient with increase in Mach number above $M = 2.00$.

CONCLUSIONS

An investigation has been conducted to determine the supersonic aerodynamic characteristics of a 1/4-scale target drone vehicle at Mach numbers from 1.70 to 4.63, at angles of attack from about -4° to 16° , at angles of sideslip from about -4° to 6° , and at a Reynolds number of 9.38×10^6 based on model length. Results of this investigation indicated the following conclusions:

1. The model with either wing or with a wing-canard combination was longitudinally stable about the selected moment center.
2. Both the large and the small canards were effective trim devices, and the trim power appeared to be a linear function of canard planform area.
3. The model with the large vertical fins was directionally stable and had positive effective dihedral throughout the angle-of-attack and Mach number ranges; however, reducing the size of the vertical fins led to a large decrease in directional stability throughout the angle-of-attack and Mach number ranges.
4. The ailerons were effective in producing rolling moment throughout the angle-of-attack and Mach number ranges, although there was a significant decrease in effectiveness with increases in Mach number. Aileron deflection generally produced an adverse yawing moment which tended to increase with angle of attack.

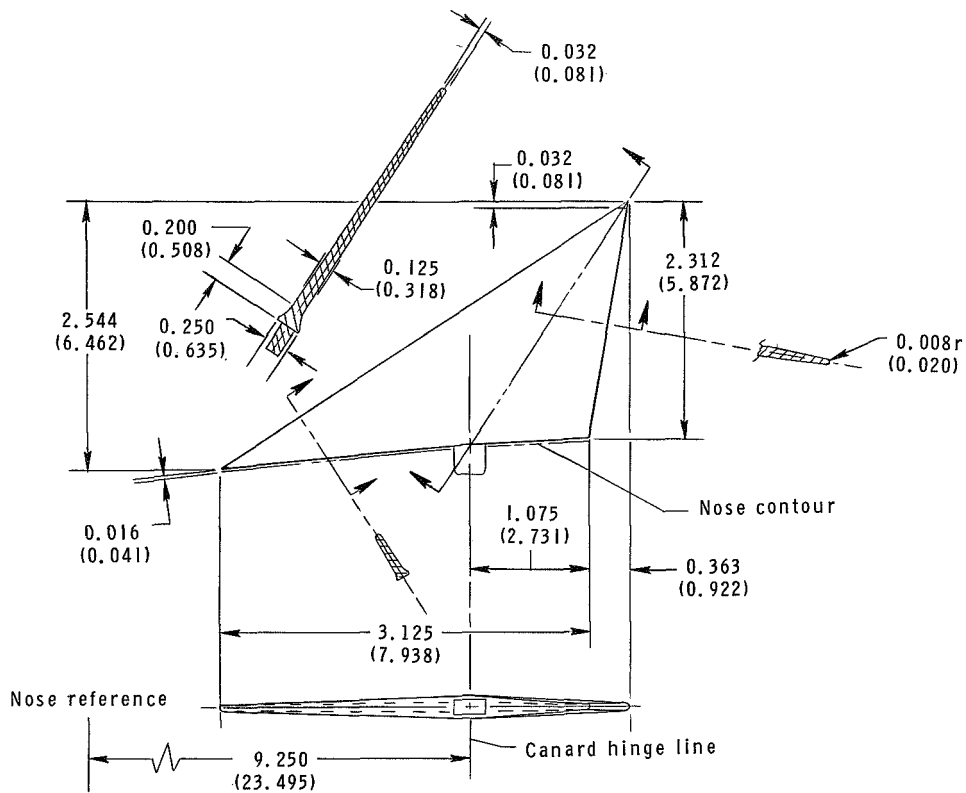
Langley Research Center,
National Aeronautics and Space Administration,
Langley Station, Hampton, Va., January 19, 1970.

REFERENCES

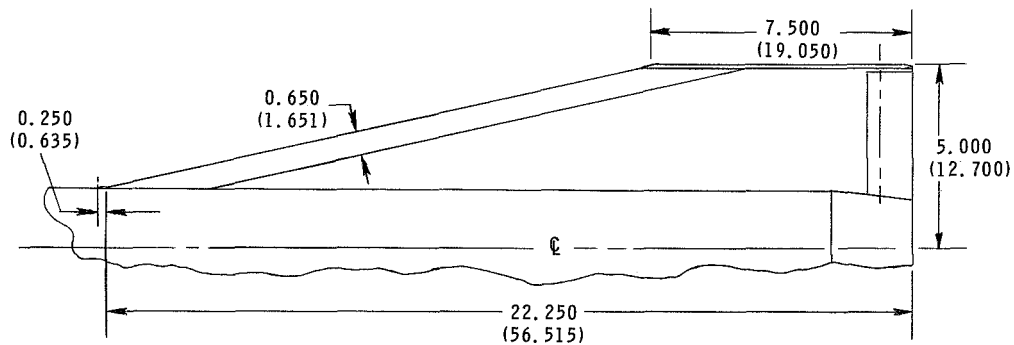
1. Blair, A. B., Jr.; and Fournier, Roger H.: Aerodynamic Characteristics of a Target Drone Vehicle at Mach Numbers From 1.57 to 2.10 - COORD No. AF-AM-627. NASA TM SX-1531, U.S. Air Force, 1968.
2. Blair, A. B., Jr.; and Babb, C. Donald: Aerodynamic Characteristics of a Revised Target Drone Vehicle at Mach Numbers From 1.60 to 2.86 - COORD No. AF-AM-627. NASA TM SX-1532, U.S. Air Force, 1968.
3. Comm. on Metric Pract.: ASTM Metric Practice Guide. NBS Handbook 102, U.S. Dep. Com., Mar. 10, 1967.



Figure 1.- Model details. All dimensions are given in inches and parenthetically in centimeters.



C₂ Canard



W₂ Wing

(b) C₂ canard and W₂ wing.

Figure 1.- Concluded.

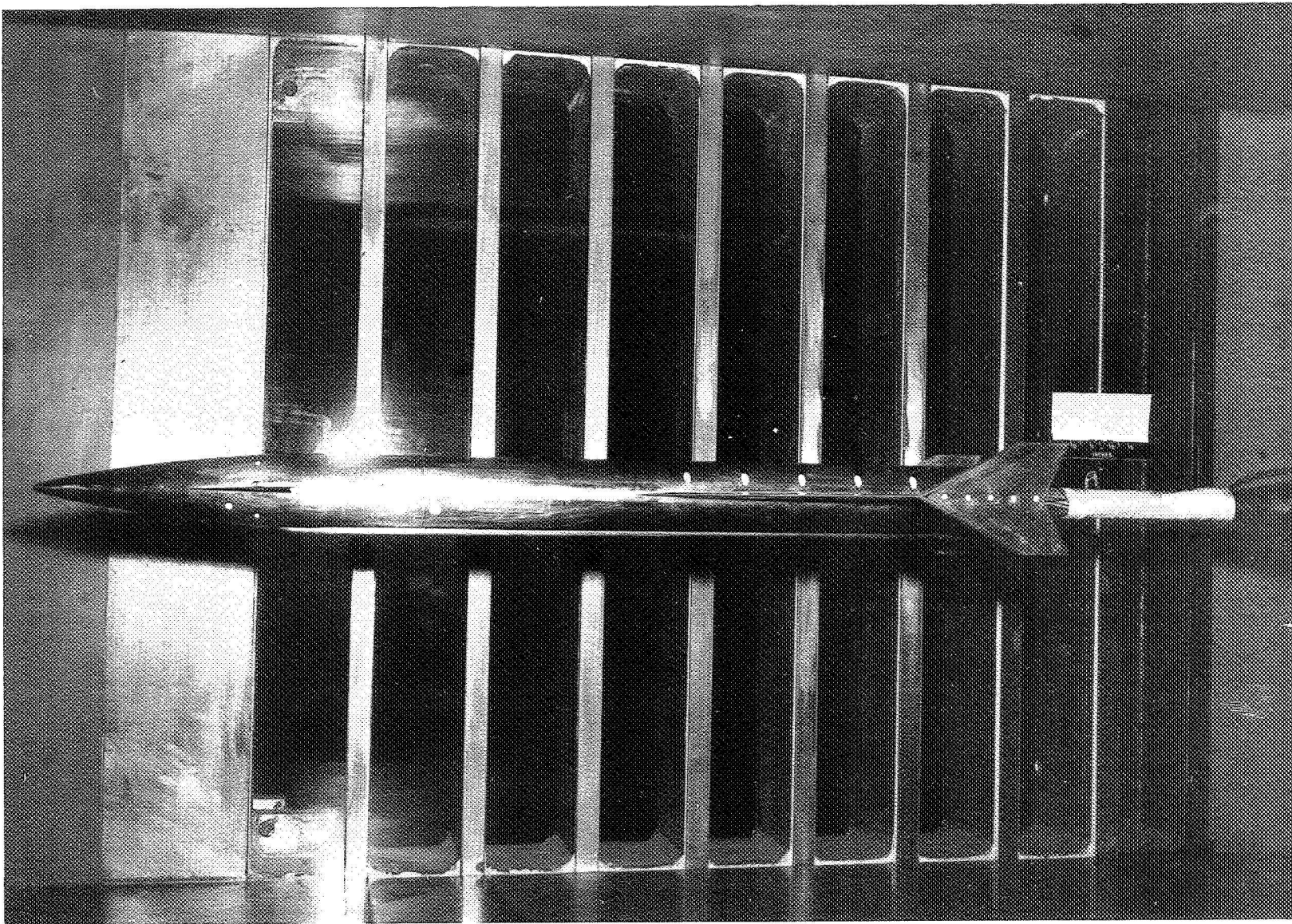


Figure 2.- Photographs of configuration B₁W₁F₁C₁.

L-68-7814

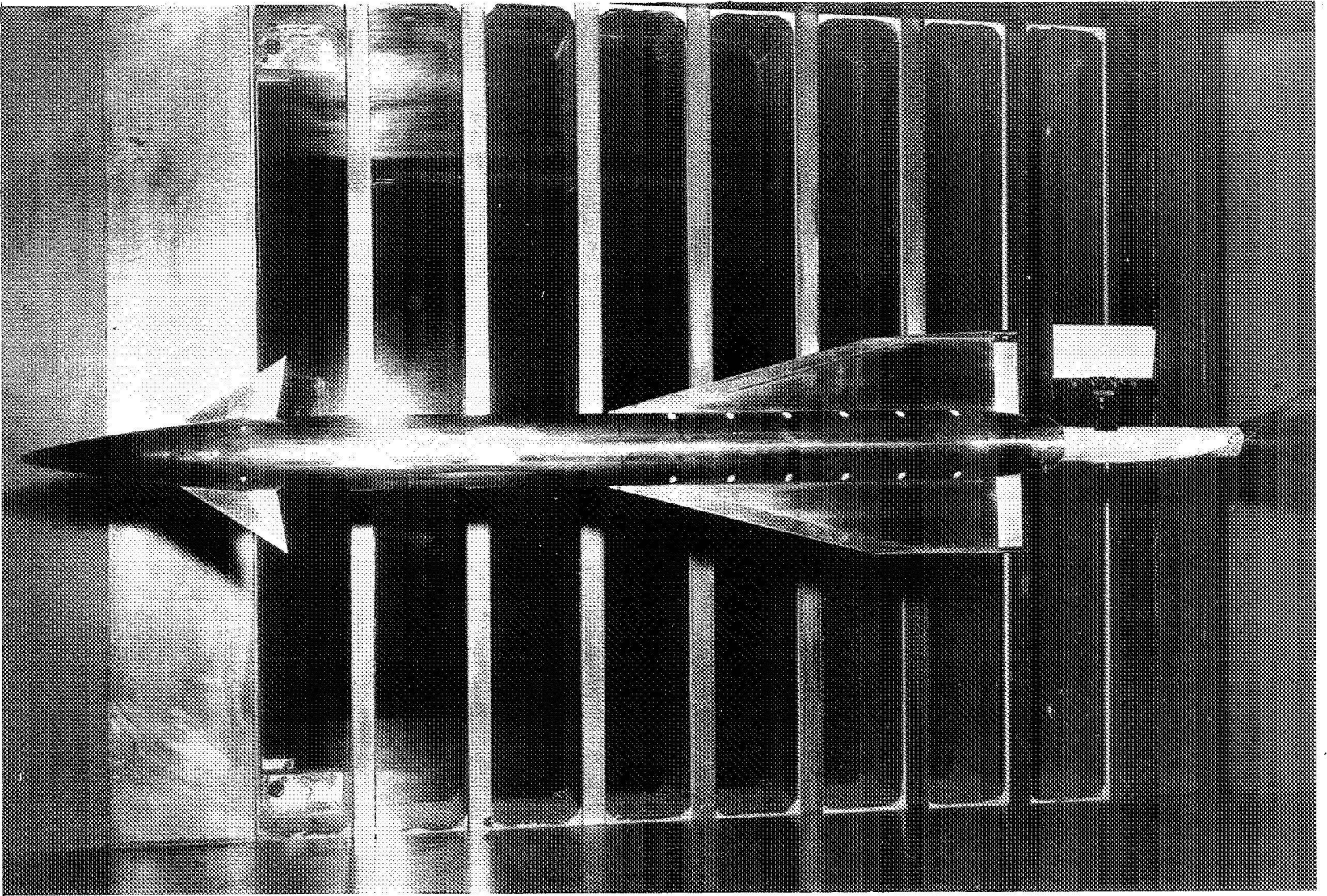


Figure 2.- Concluded.

L-68-7815

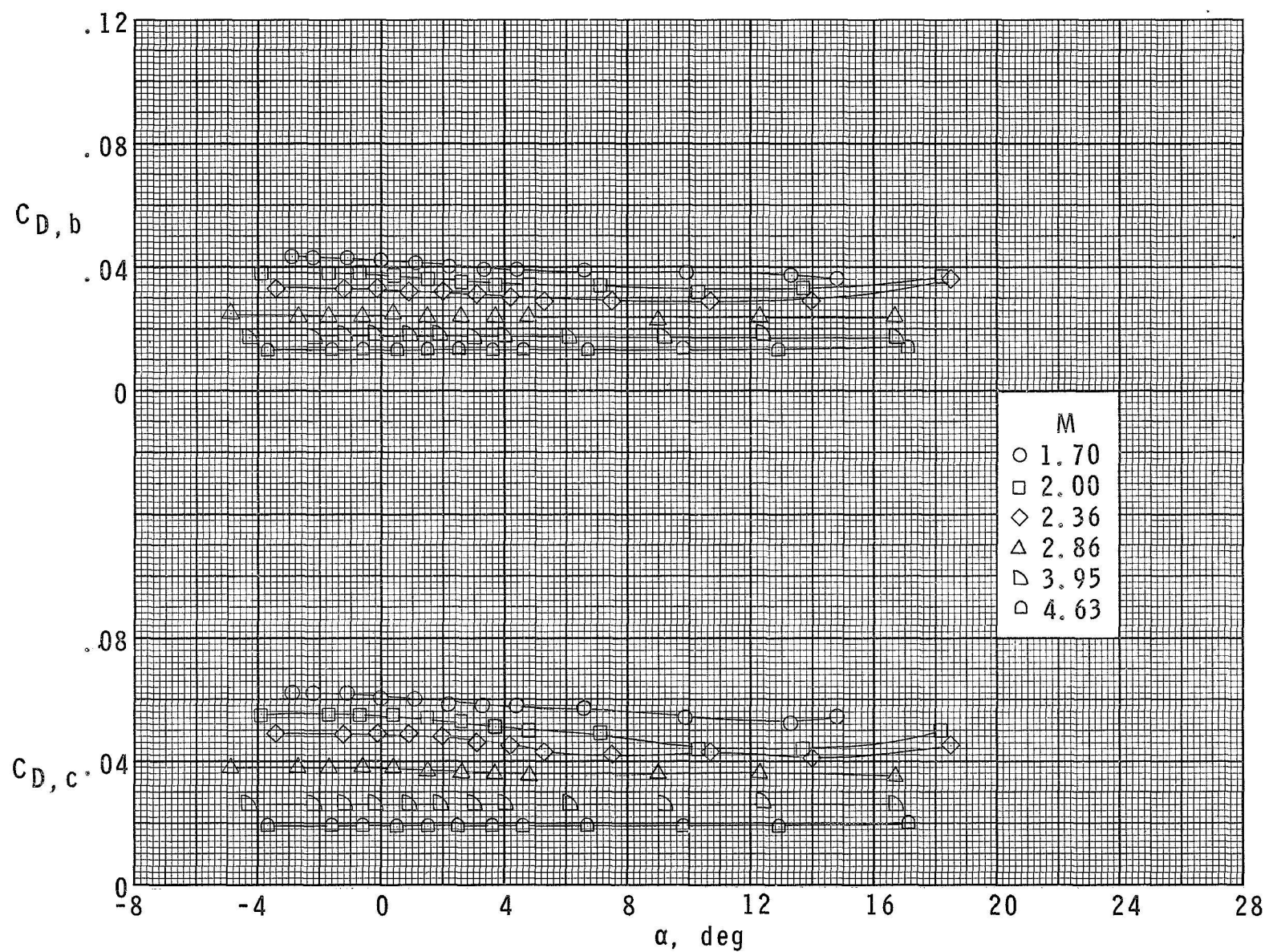
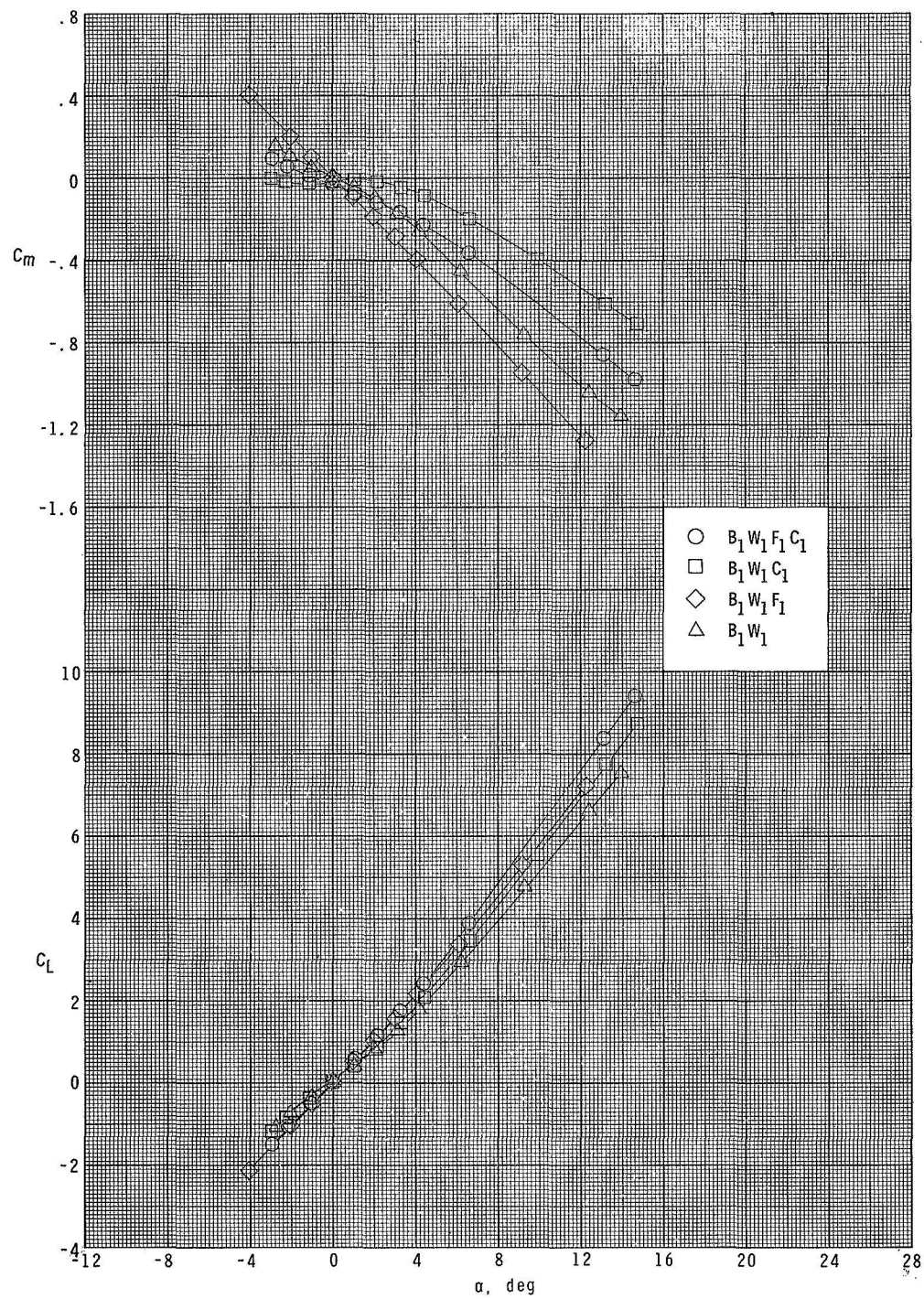
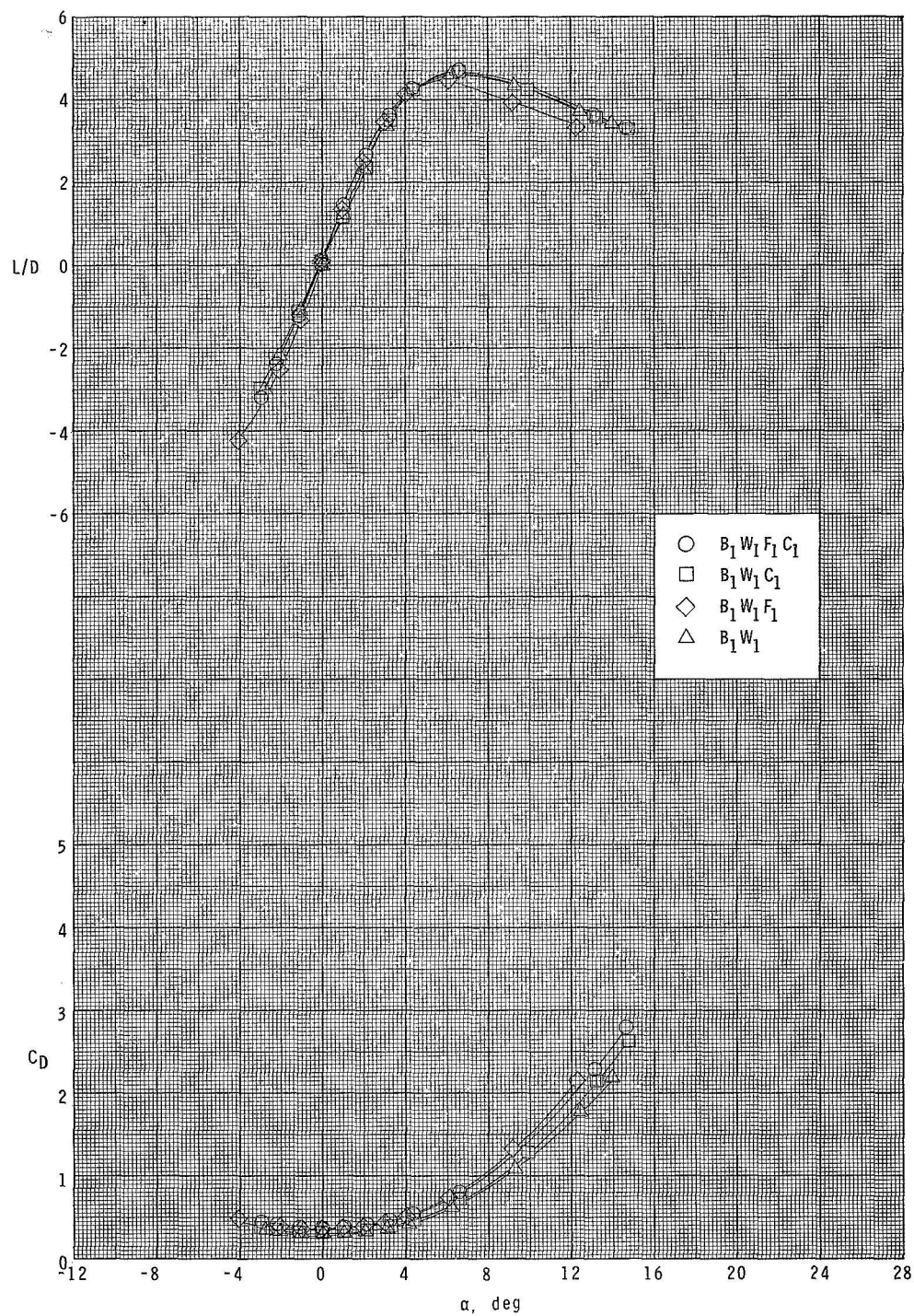


Figure 3.- Typical values of balance chamber-drag and base-drag coefficients of configuration $B_1W_2F_1C_1$.



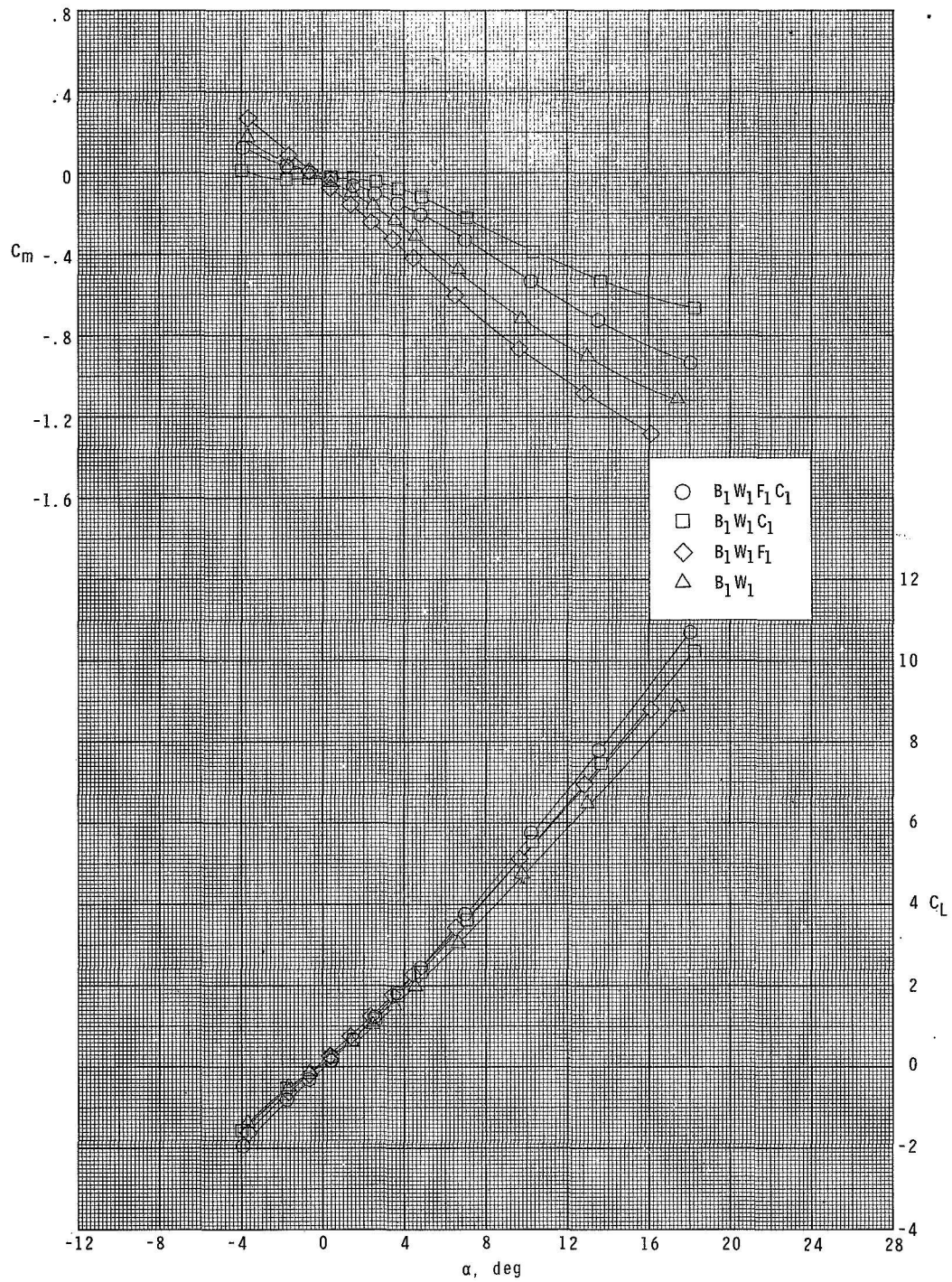
(a) $M = 1.70$.

Figure 4.- Effect of model components on longitudinal aerodynamic characteristics.



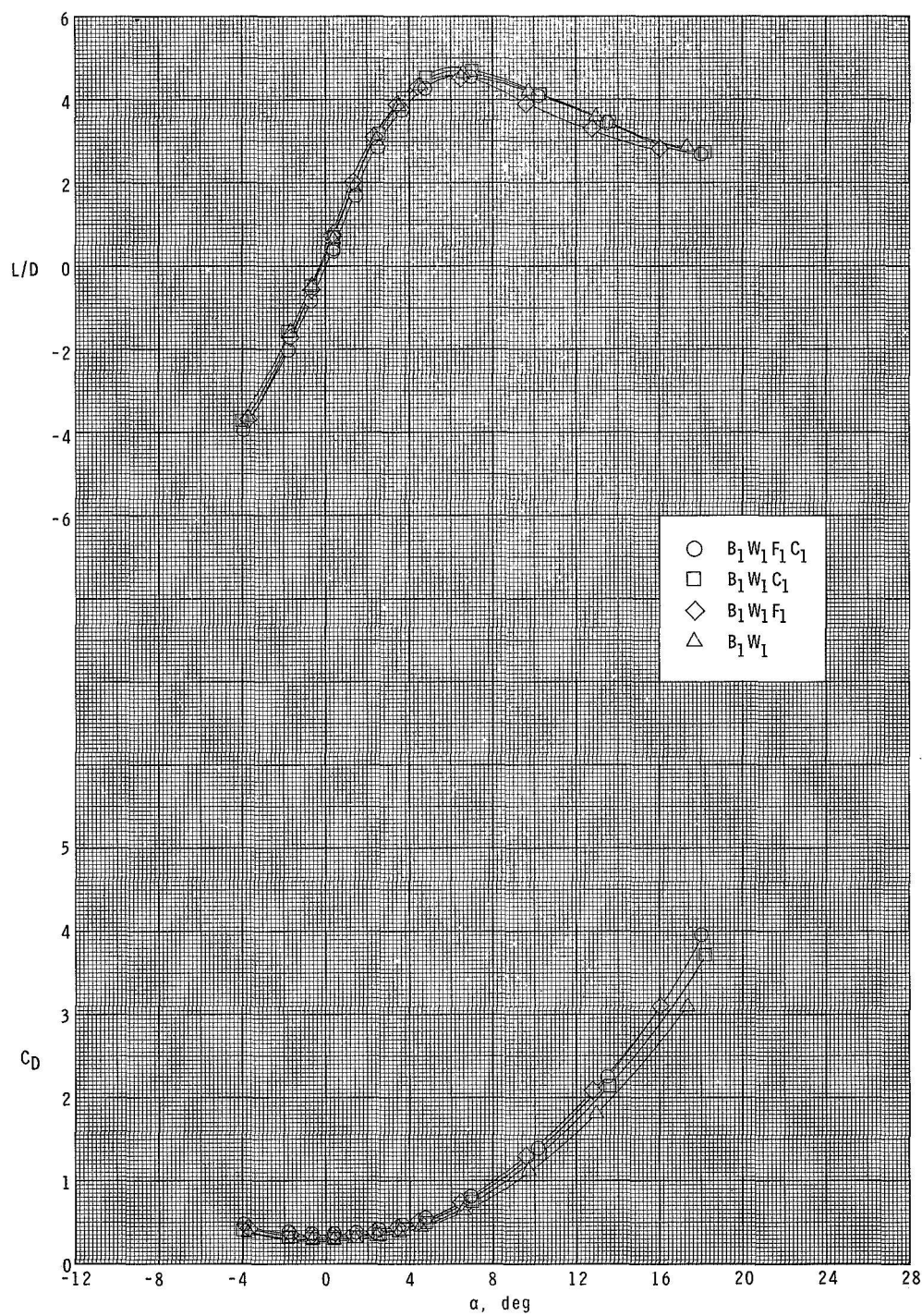
(a) Concluded.

Figure 4.- Continued.



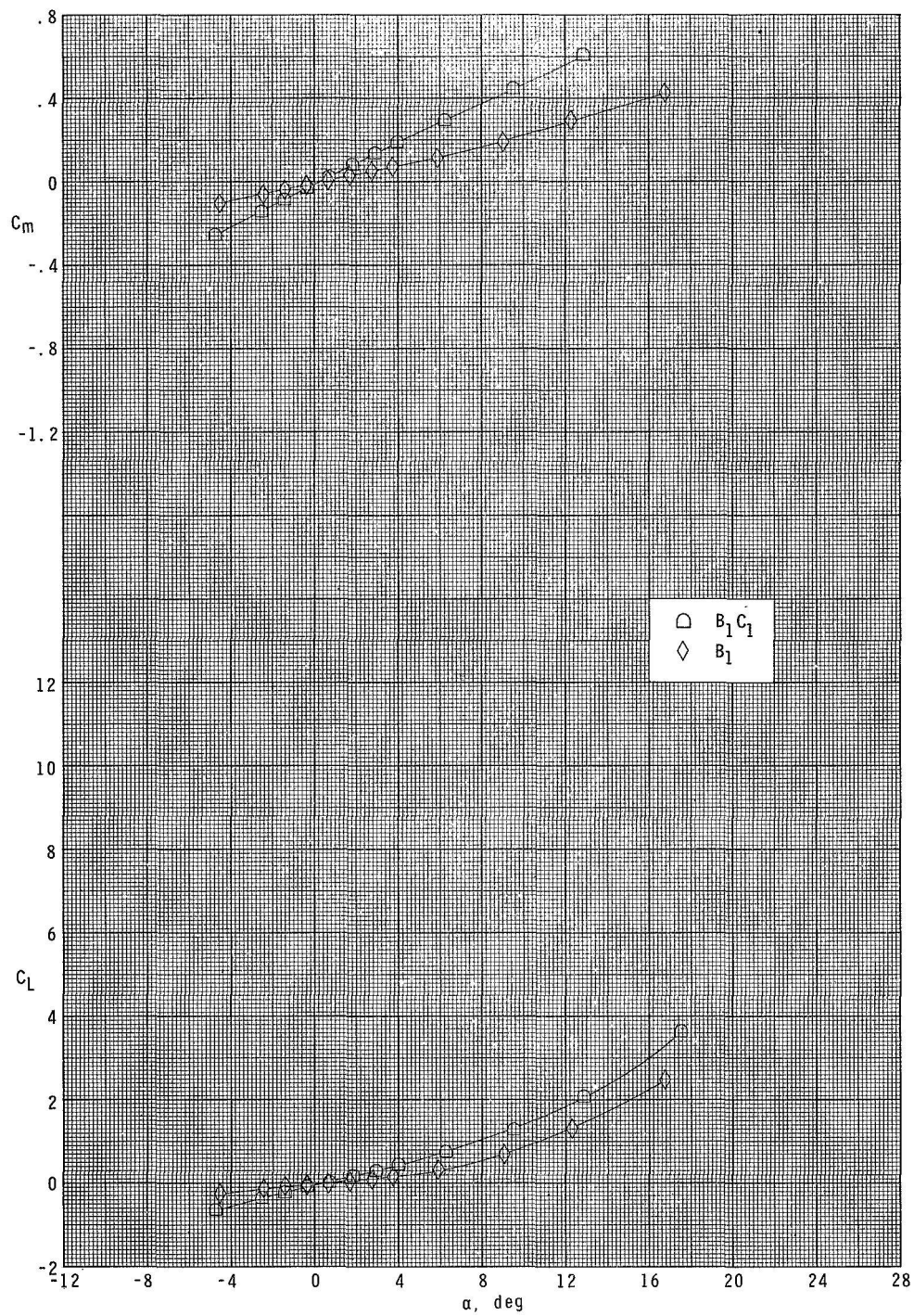
(b) $M = 2.00$.

Figure 4.- Continued.



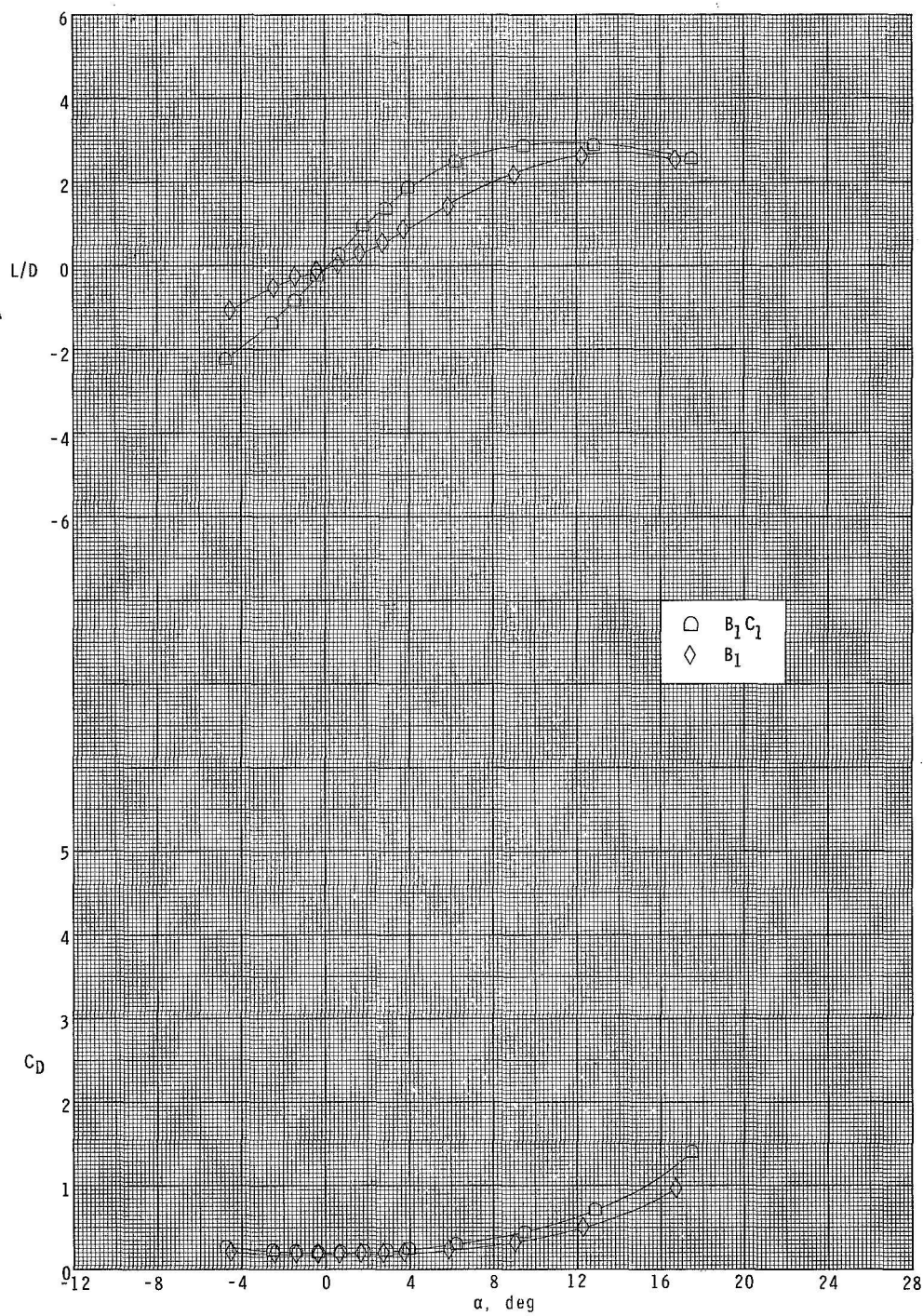
(b) Concluded.

Figure 4.- Continued.



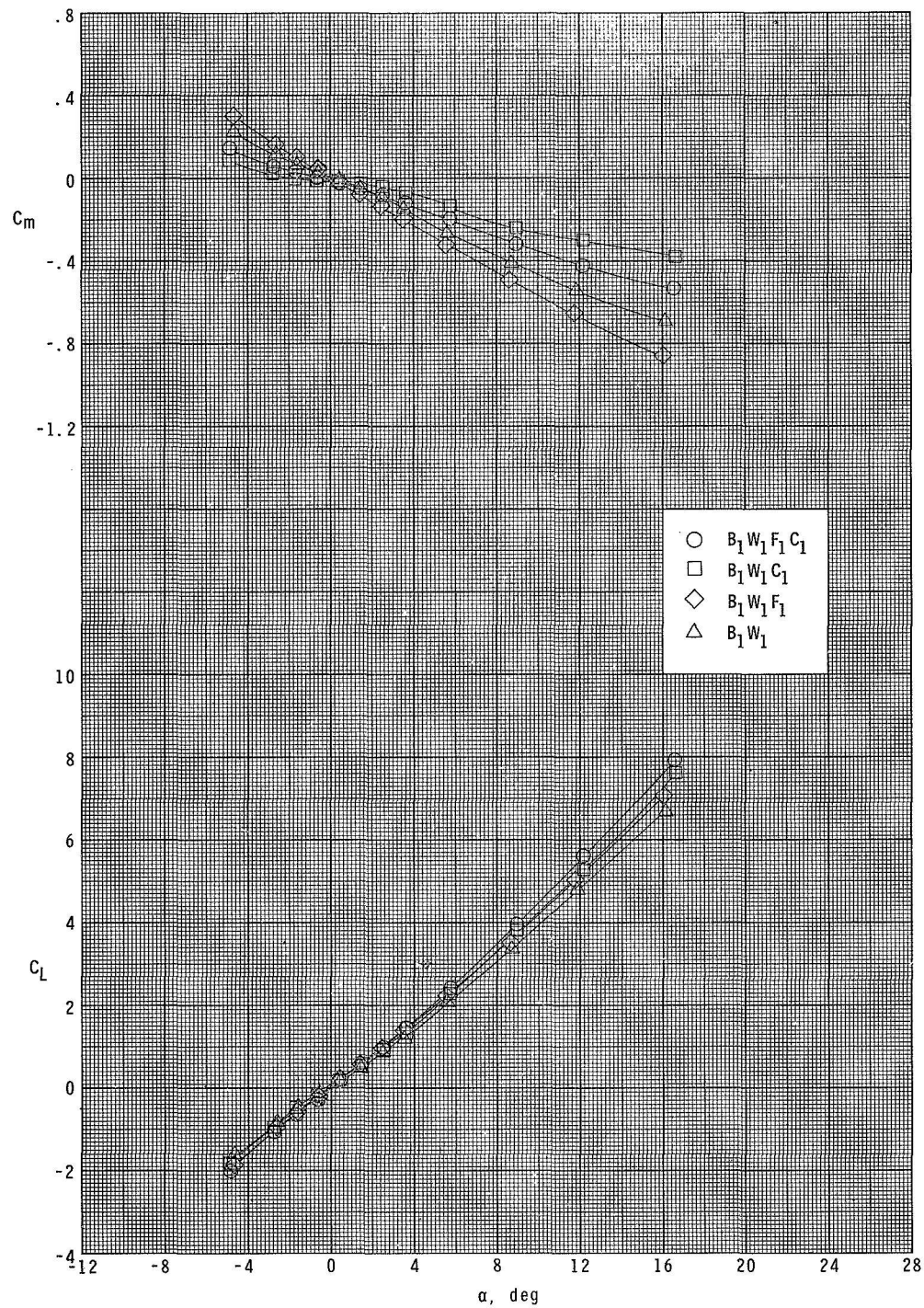
(c) $M = 2.30$.

Figure 4.- Continued.



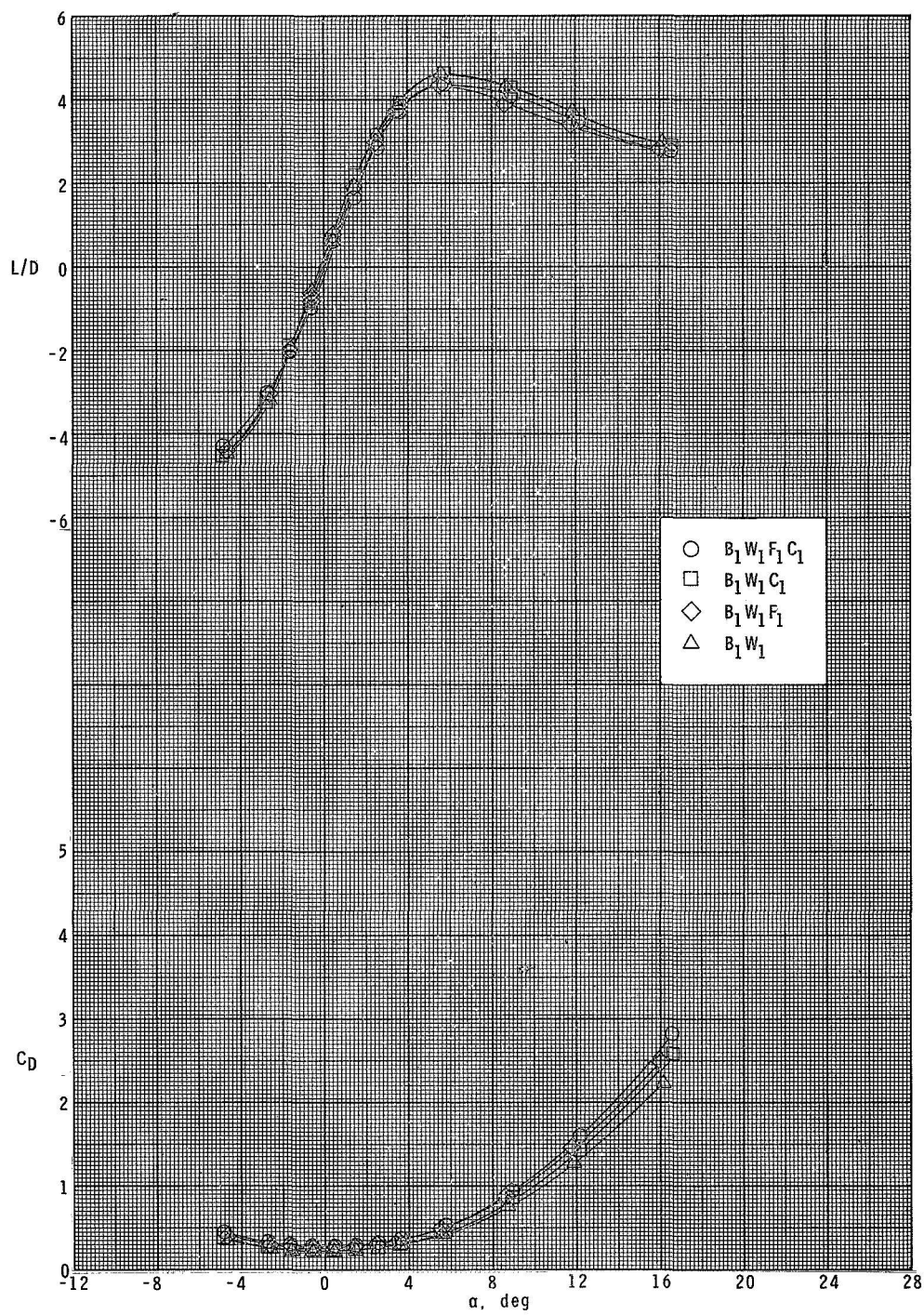
(c) Concluded.

Figure 4.- Continued.



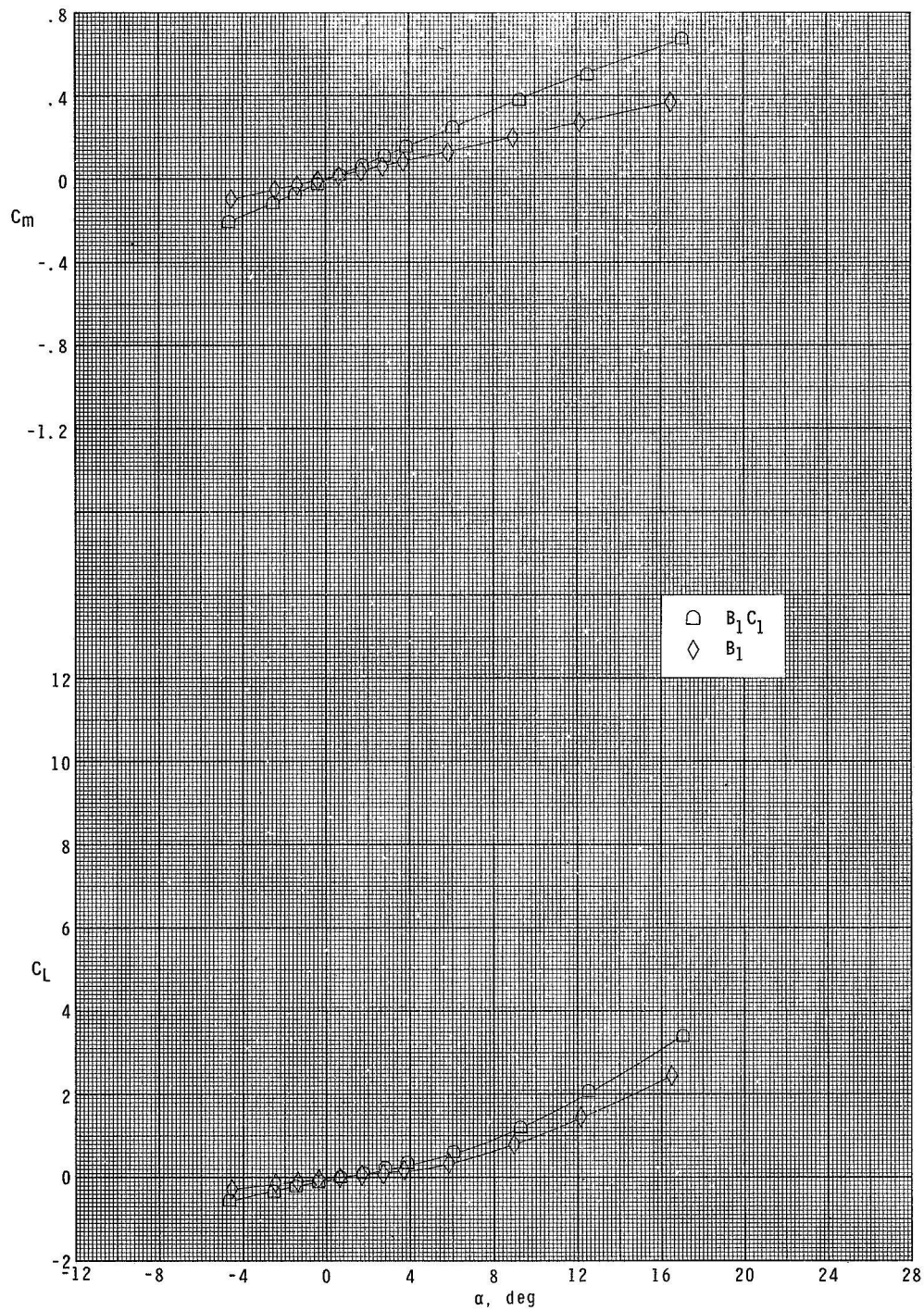
(d) $M = 2.86$.

Figure 4.- Continued.



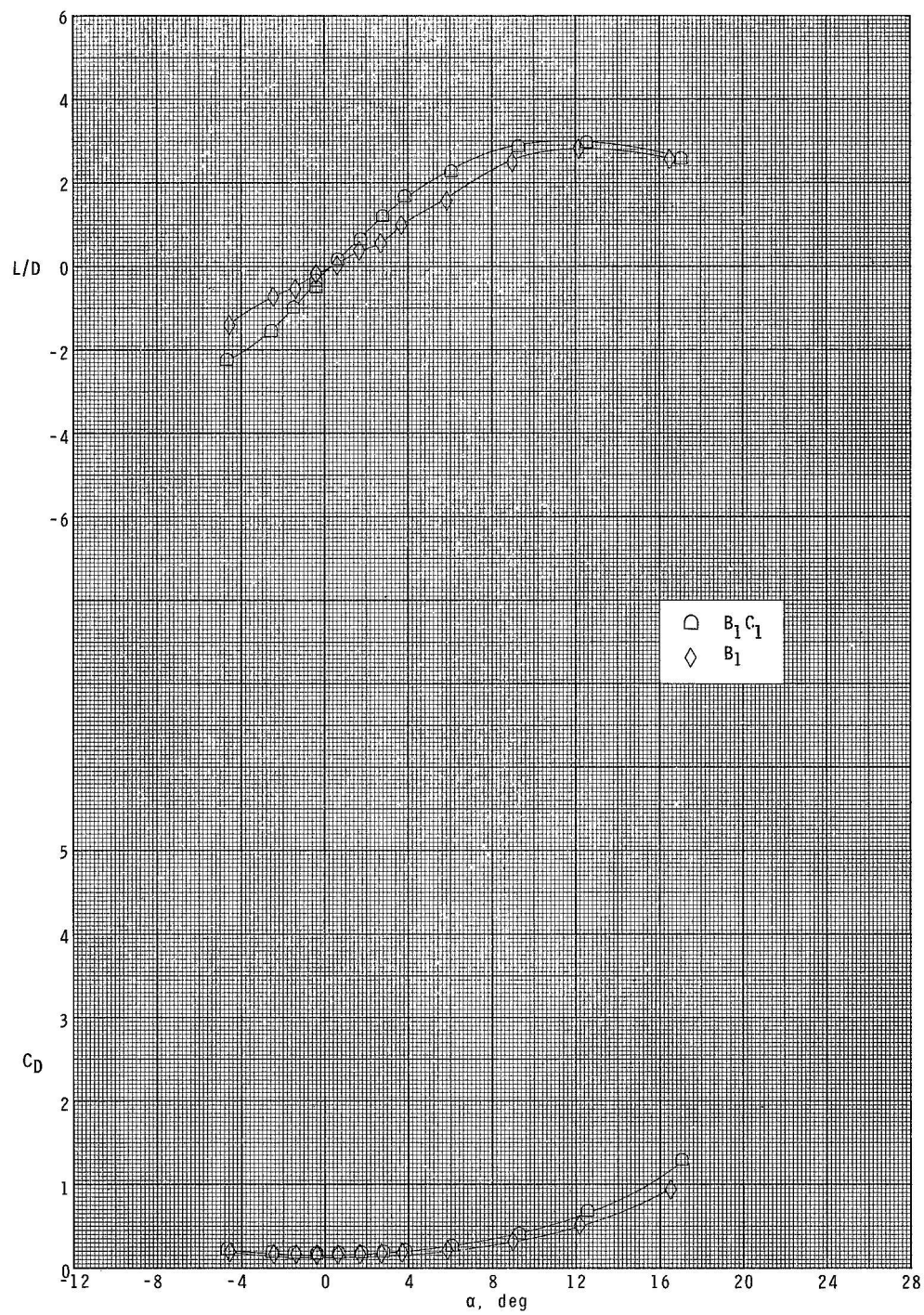
(d) Concluded

Figure 4.- Continued.



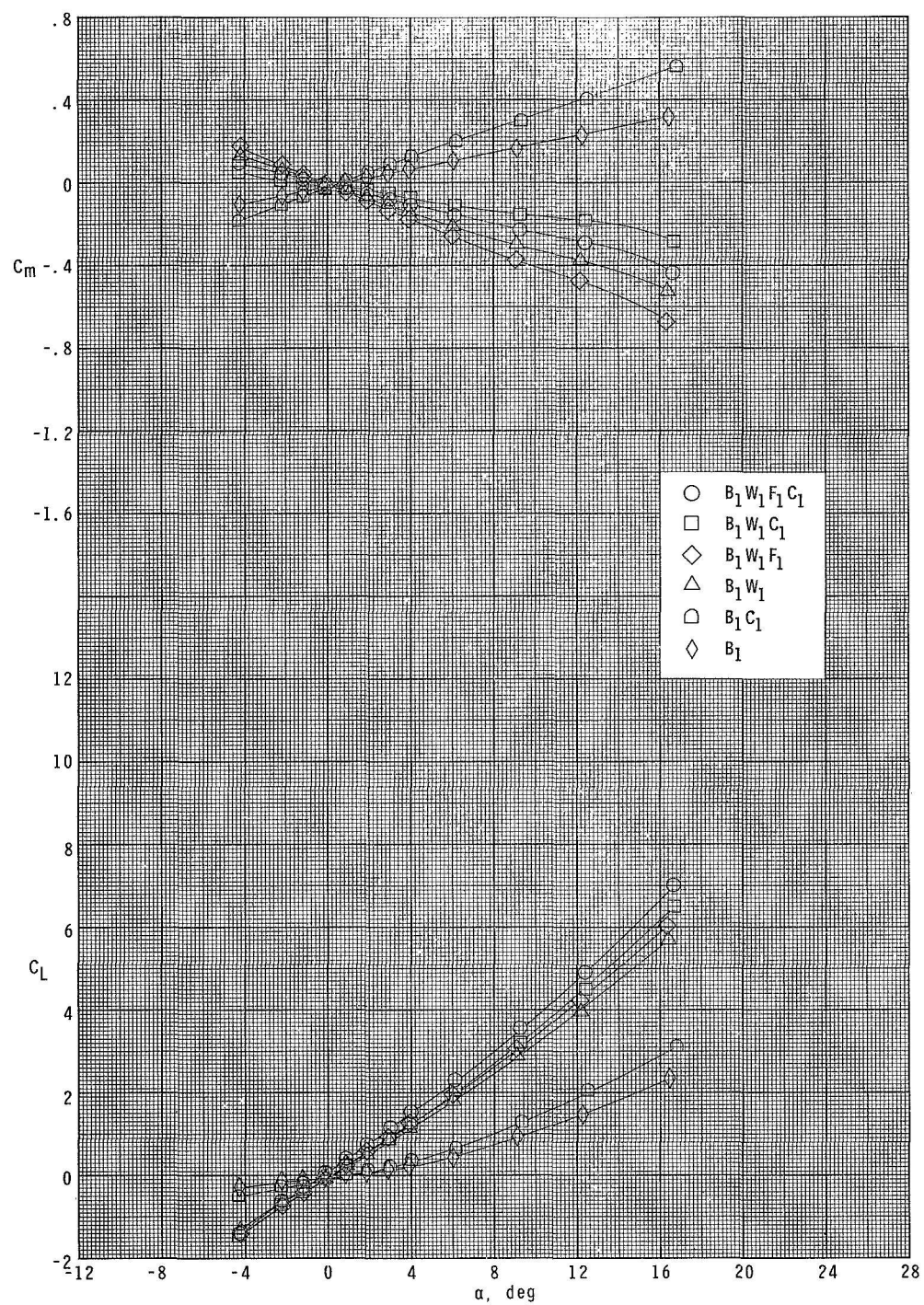
(e) $M = 2.96$.

Figure 4.- Continued.



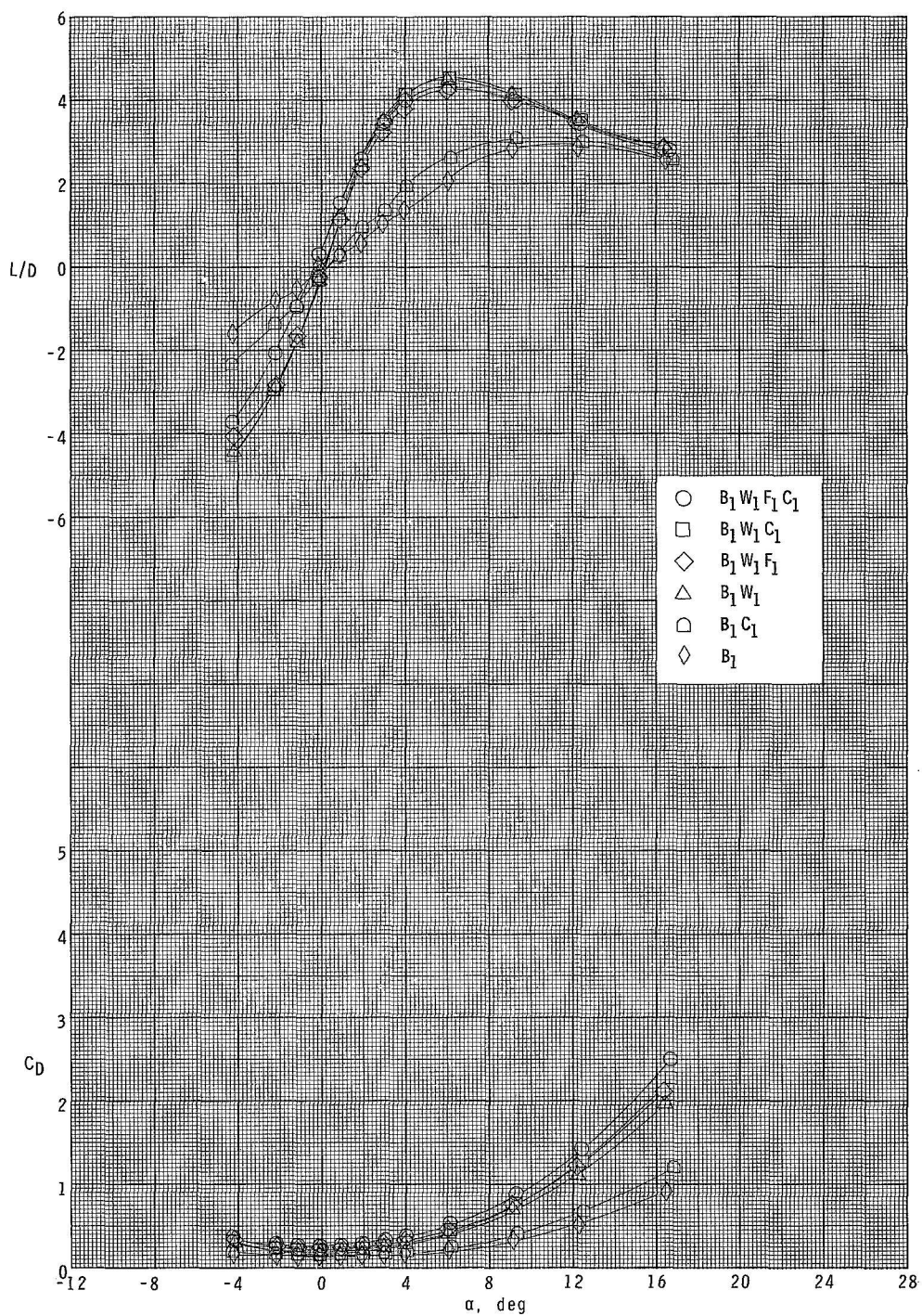
(e) Concluded.

Figure 4.- Continued.



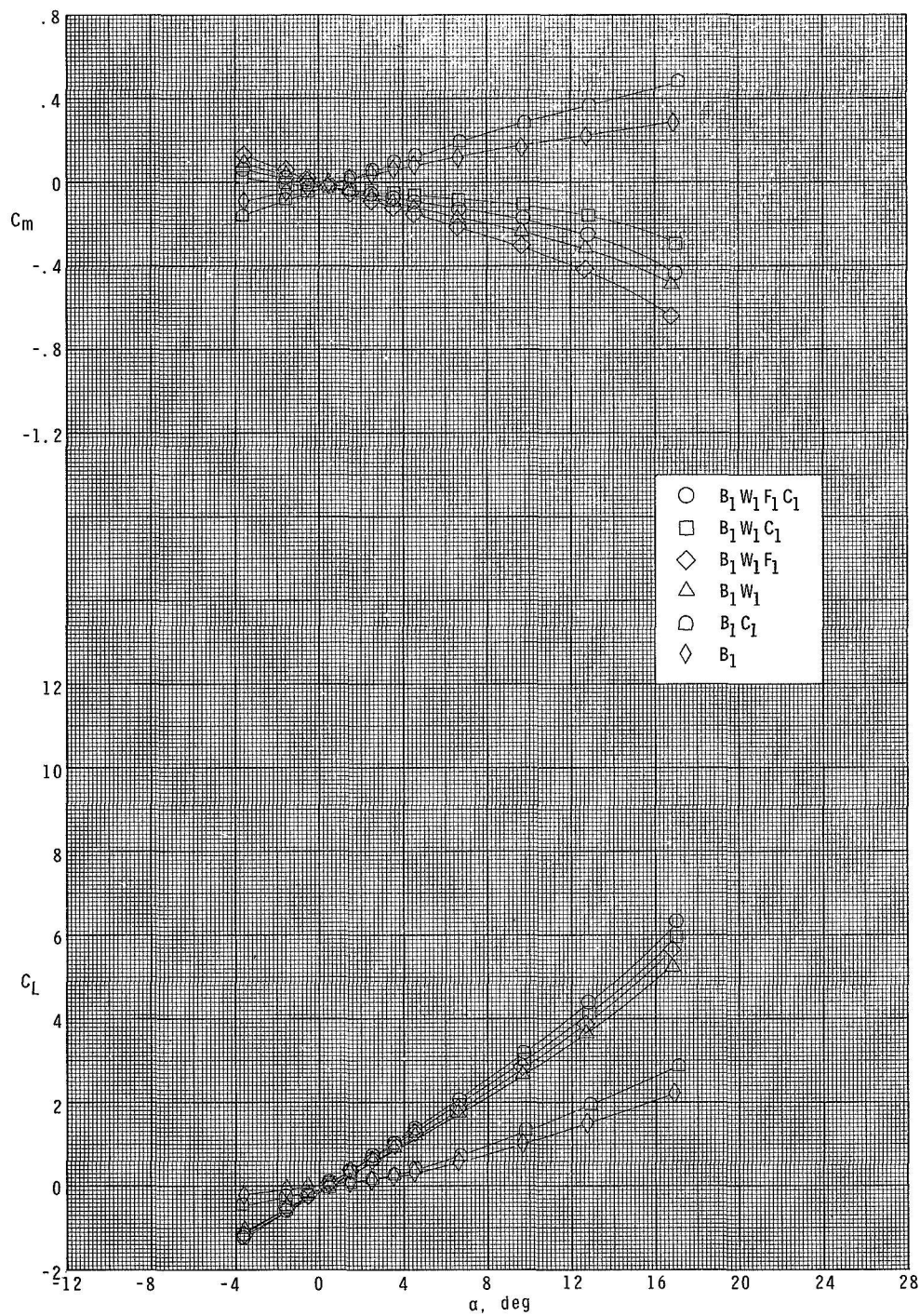
(f) $M = 3.95$.

Figure 4.- Continued.



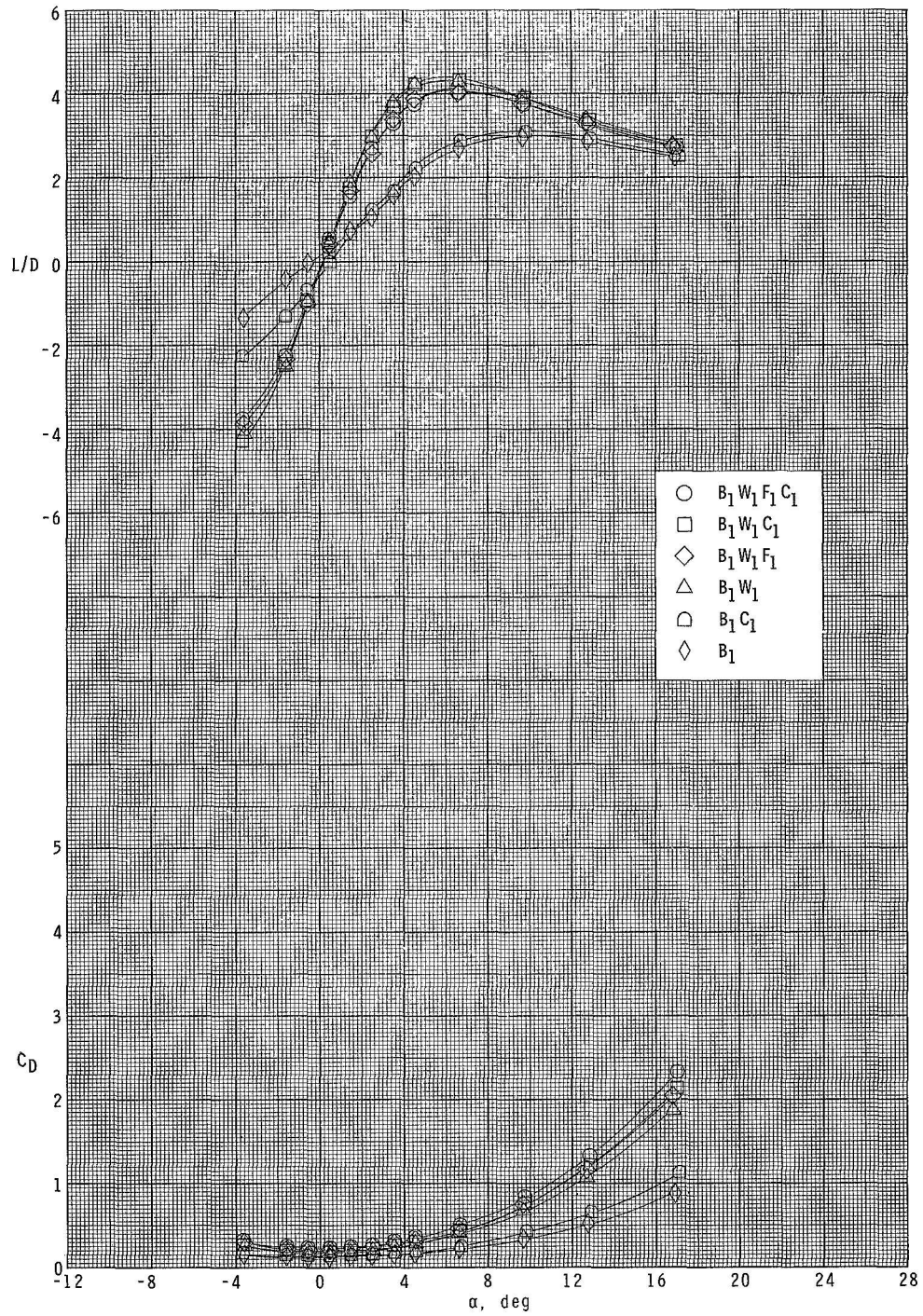
(f) Concluded.

Figure 4.- Continued.



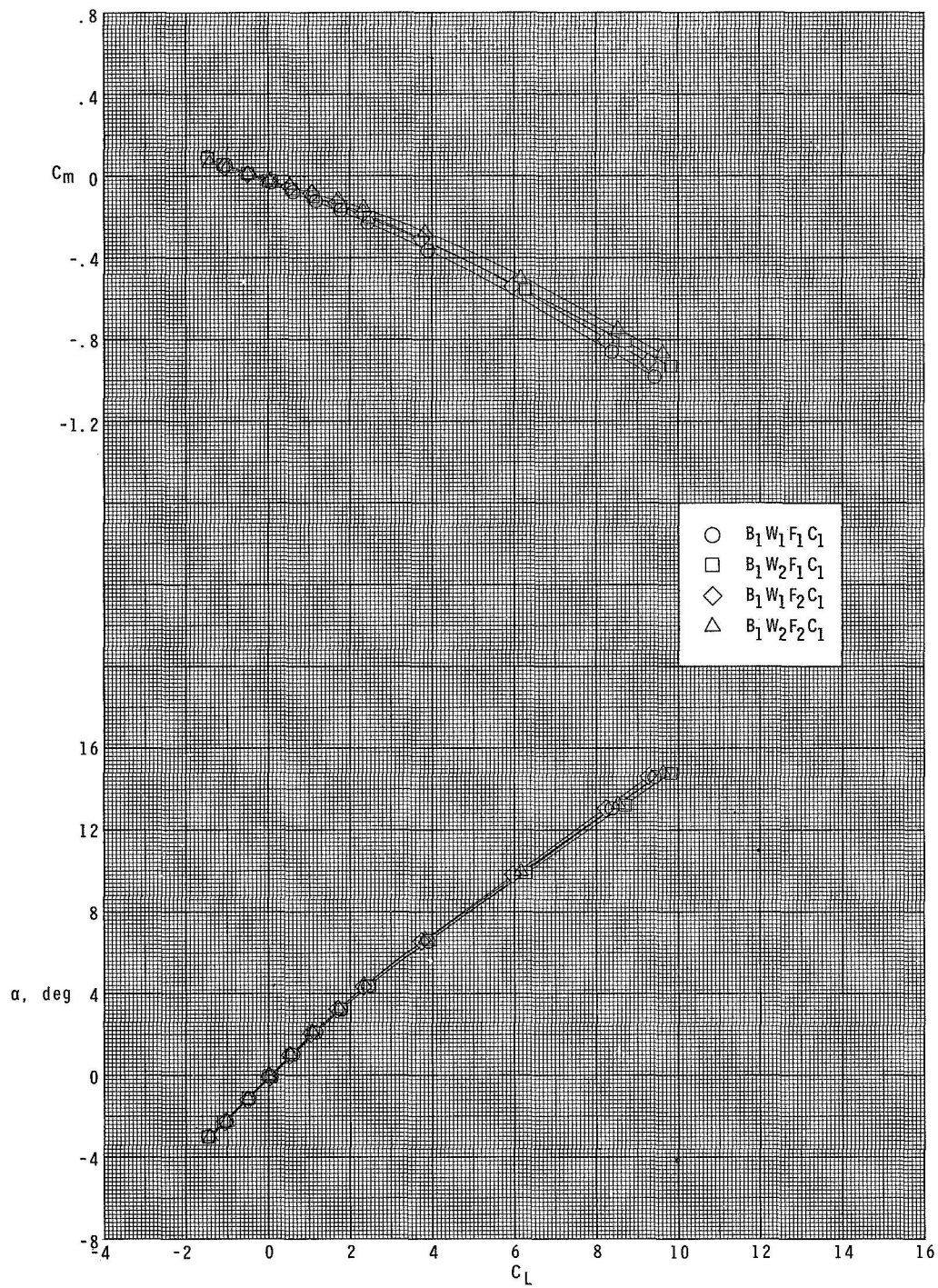
(g) $M = 4.63$.

Figure 4.- Continued.



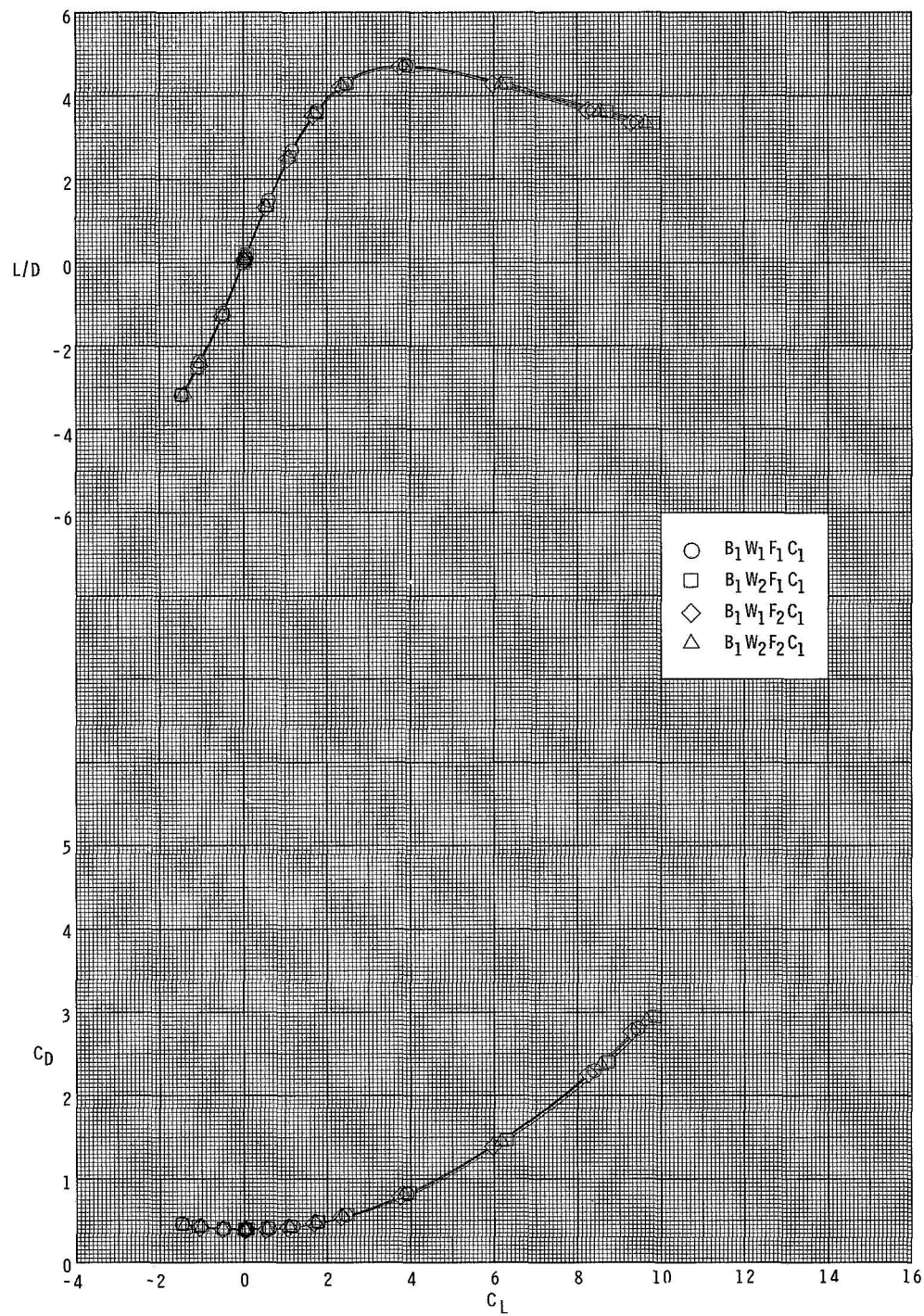
(g) Concluded.

Figure 4.- Concluded.



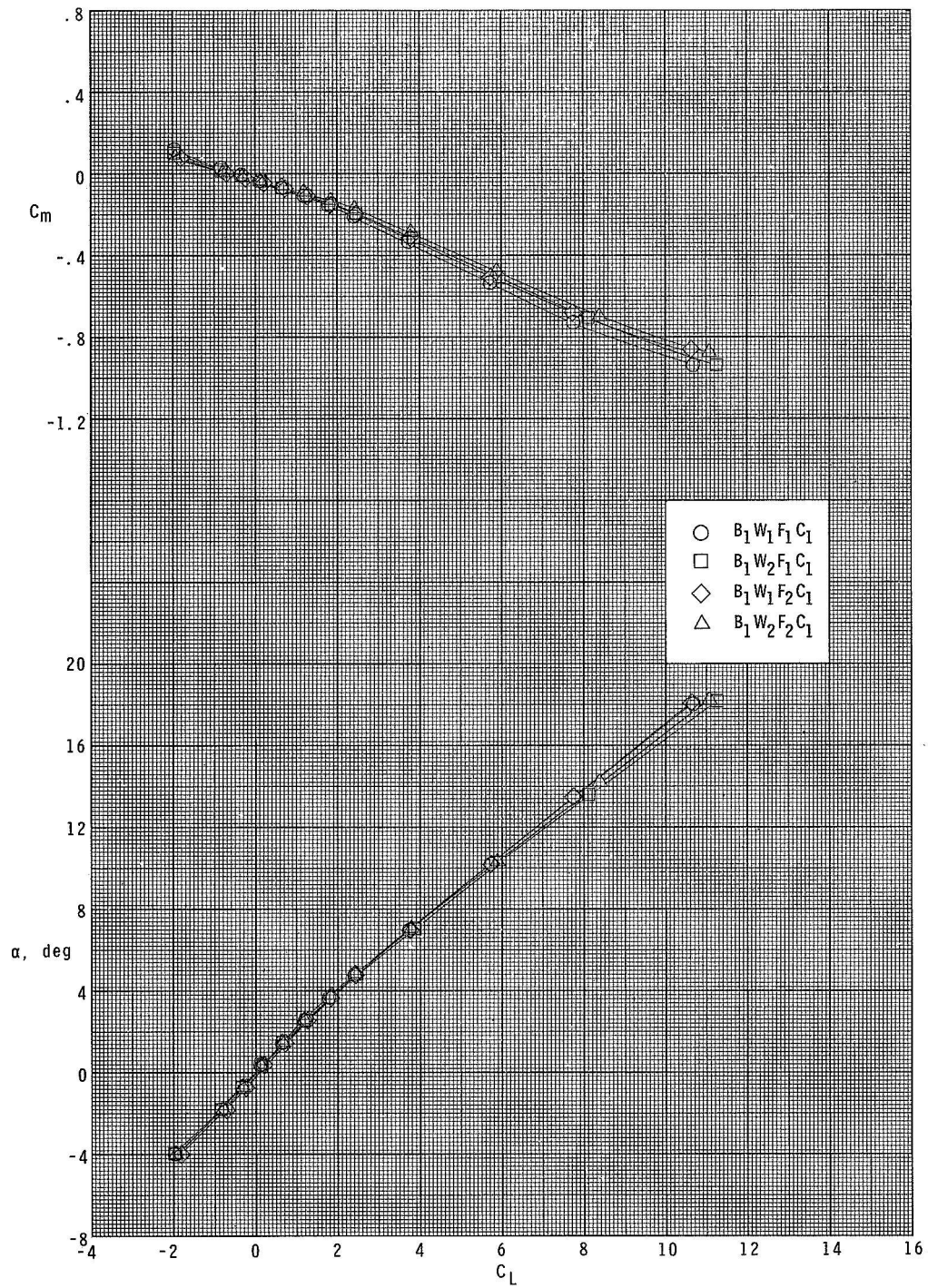
(a) $M = 1.70$.

Figure 5.- Effect of change in wing and/or vertical-fin planforms on longitudinal aerodynamic characteristics of complete model.



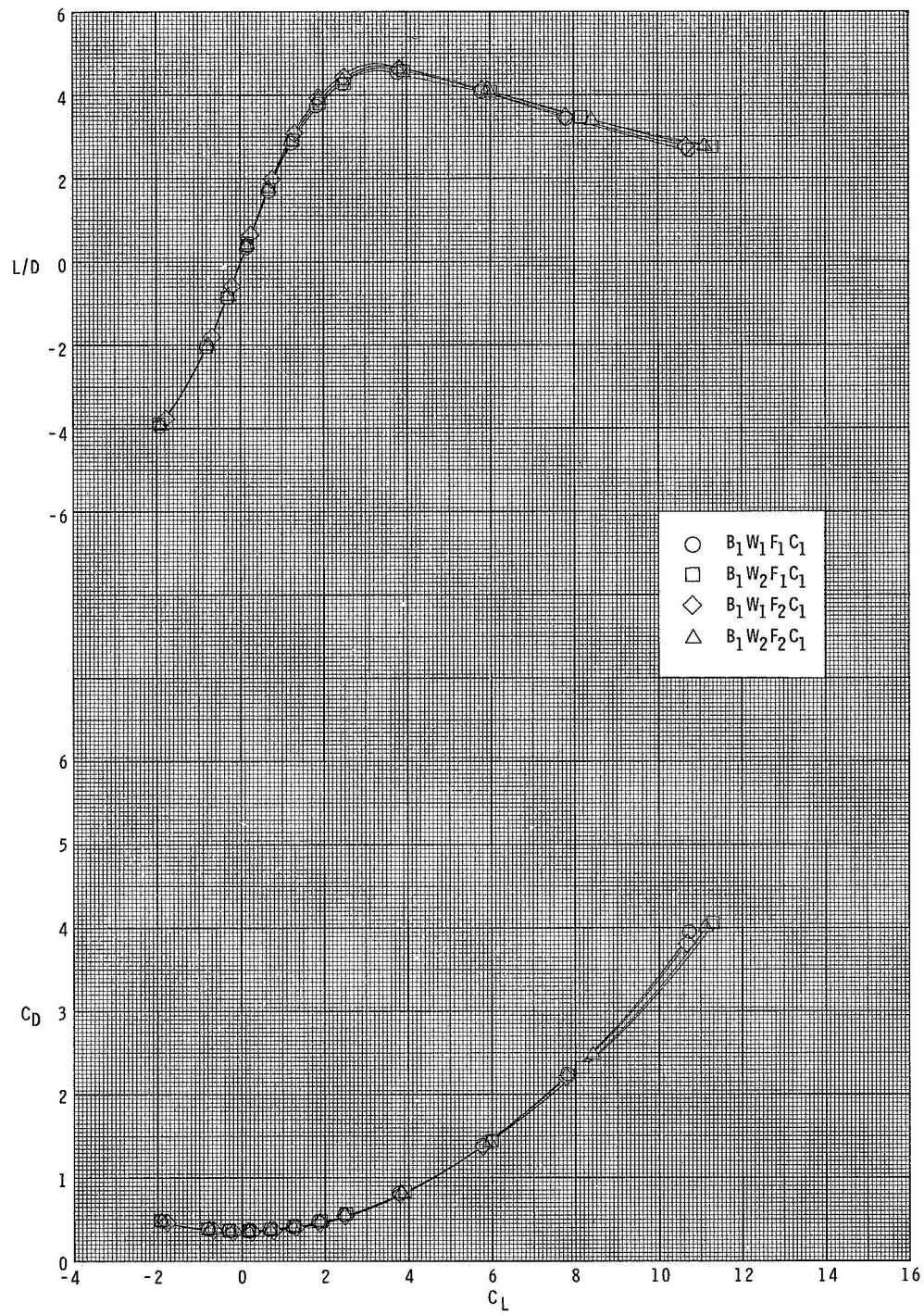
(a) Concluded.

Figure 5.- Continued.



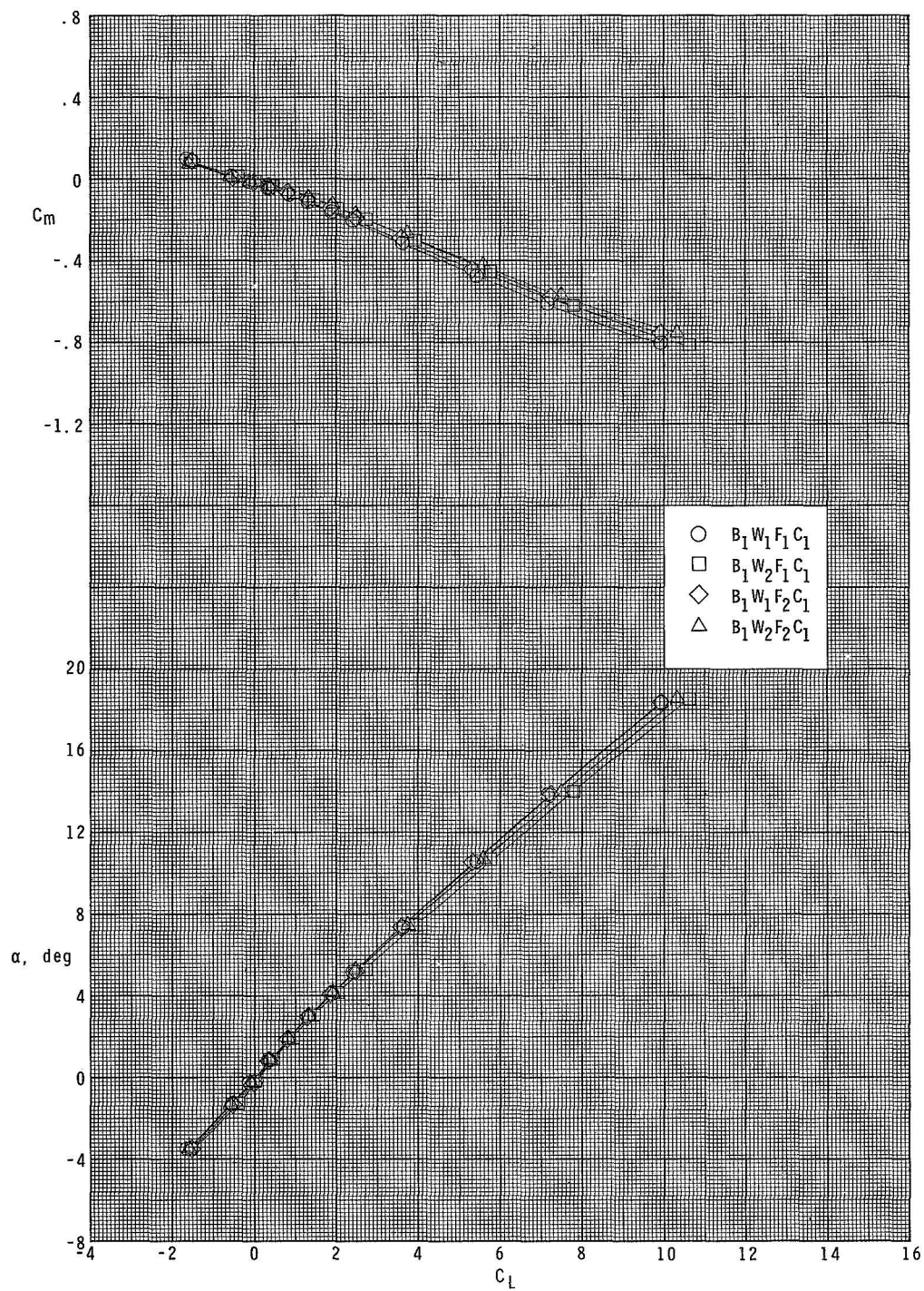
(b) $M = 2.00$.

Figure 5.- Continued.



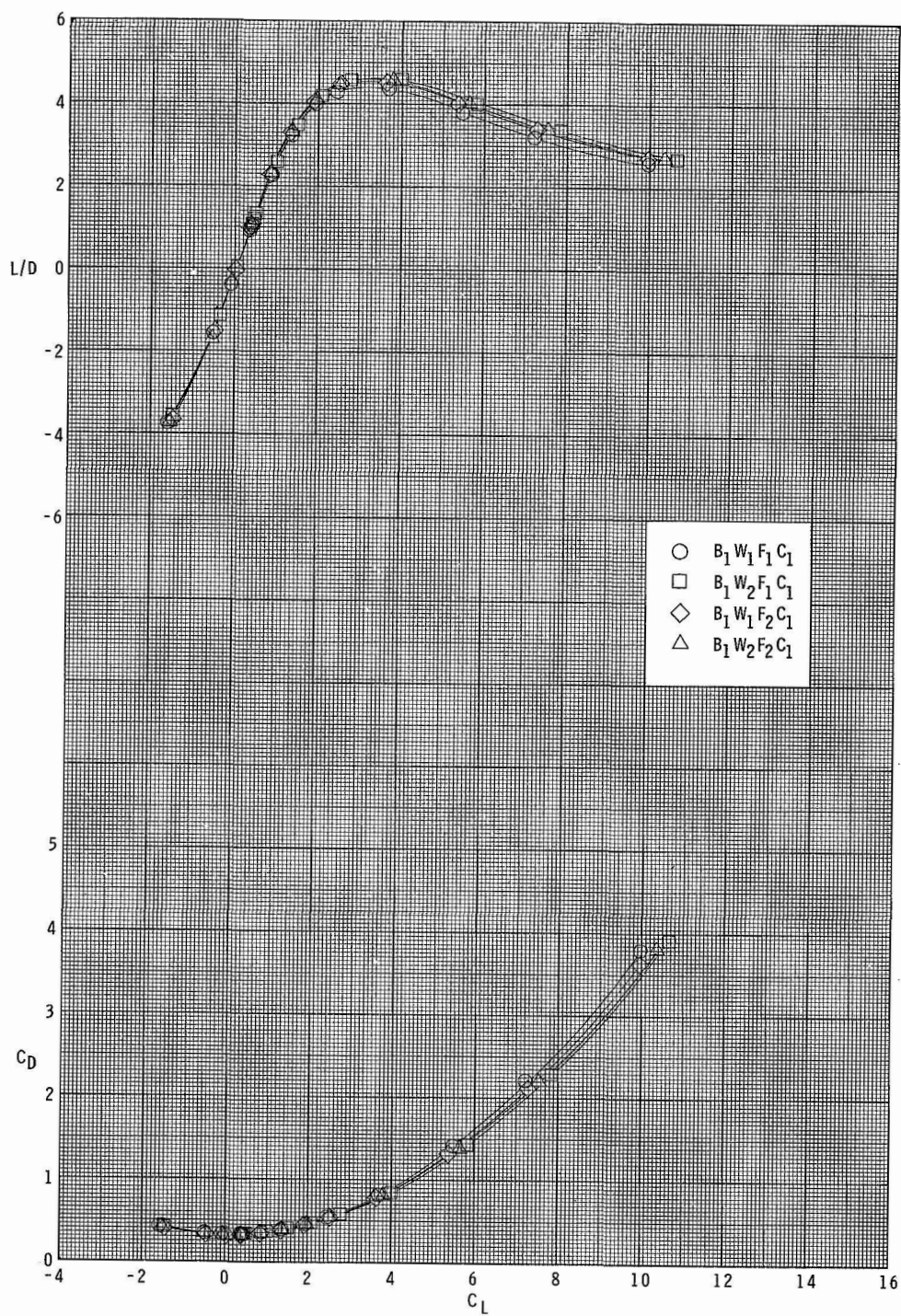
(b) Concluded.

Figure 5.- Continued.



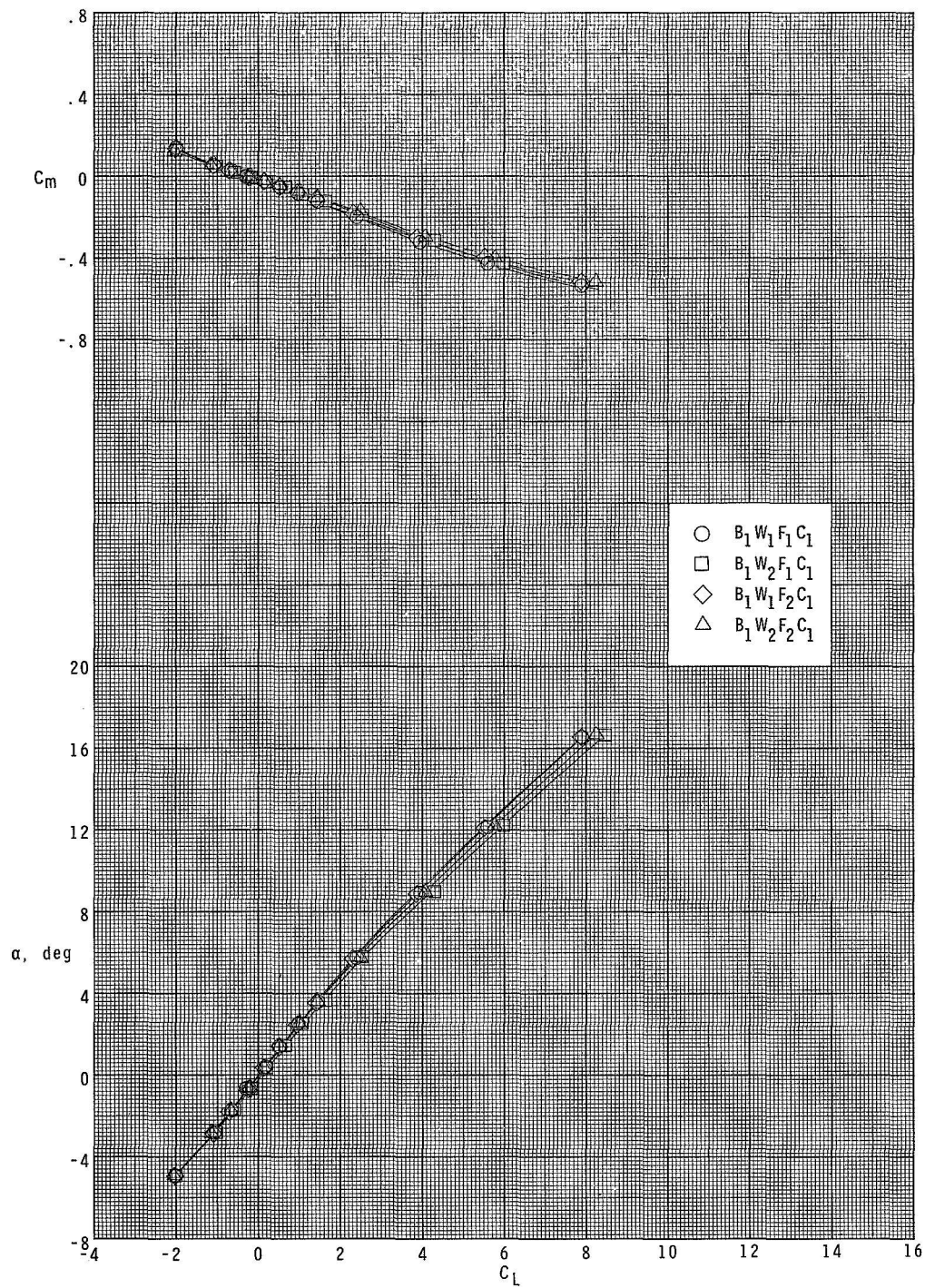
(c) $M = 2.36$.

Figure 5.- Continued.



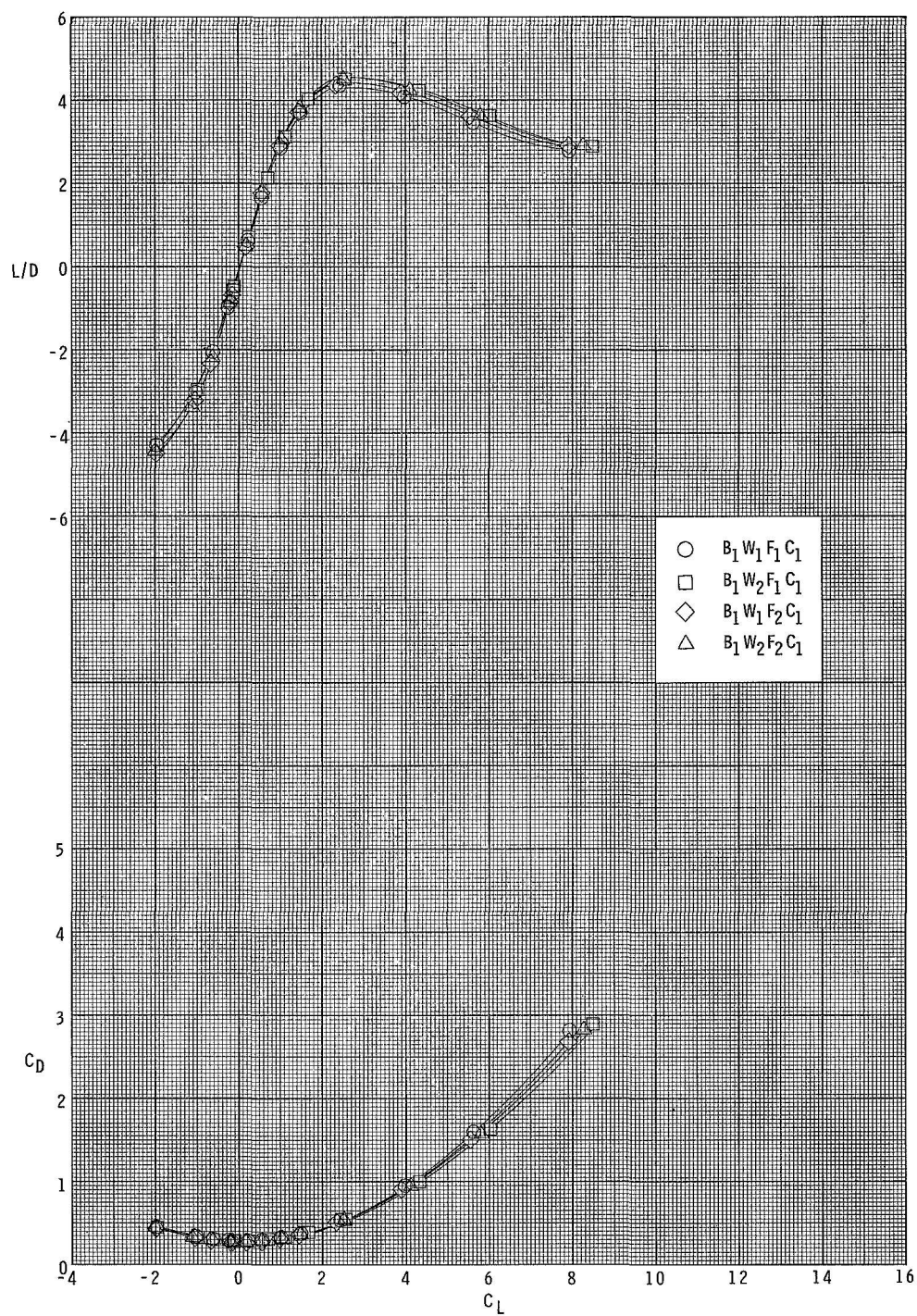
(c) Concluded.

Figure 5.- Continued.



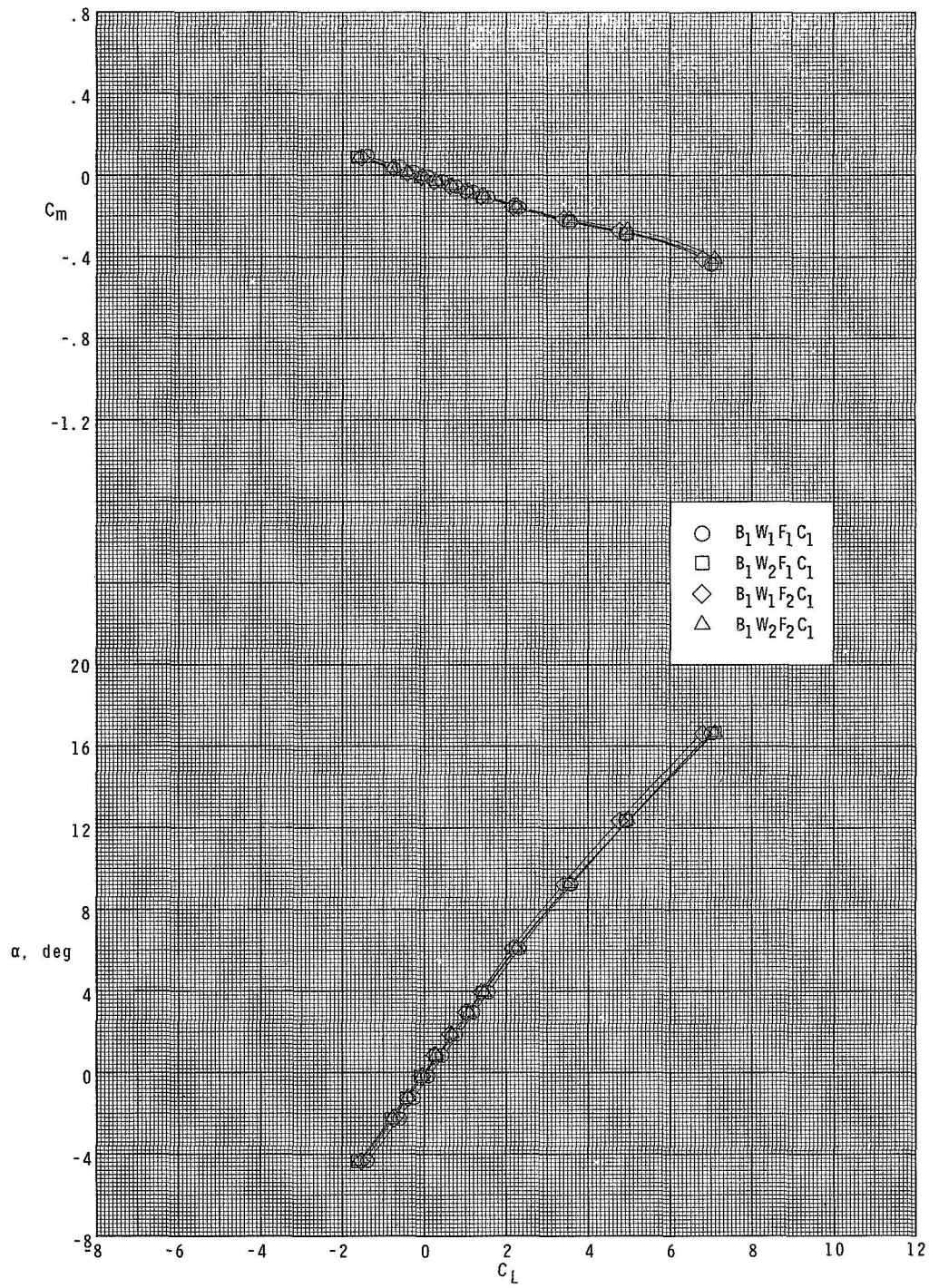
(d) $M = 2.86$.

Figure 5.- Continued.



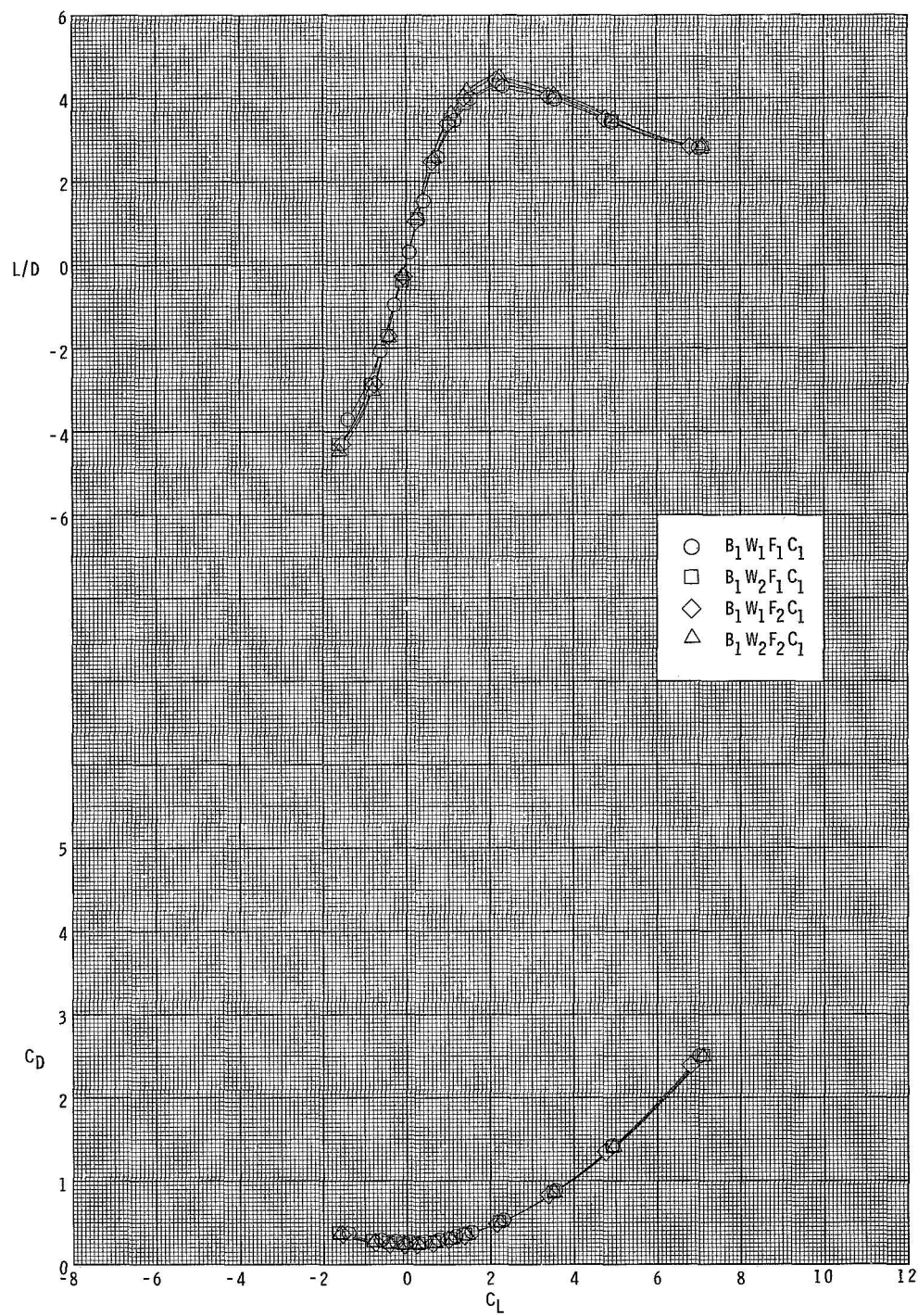
(d) Concluded.

Figure 5.- Continued.



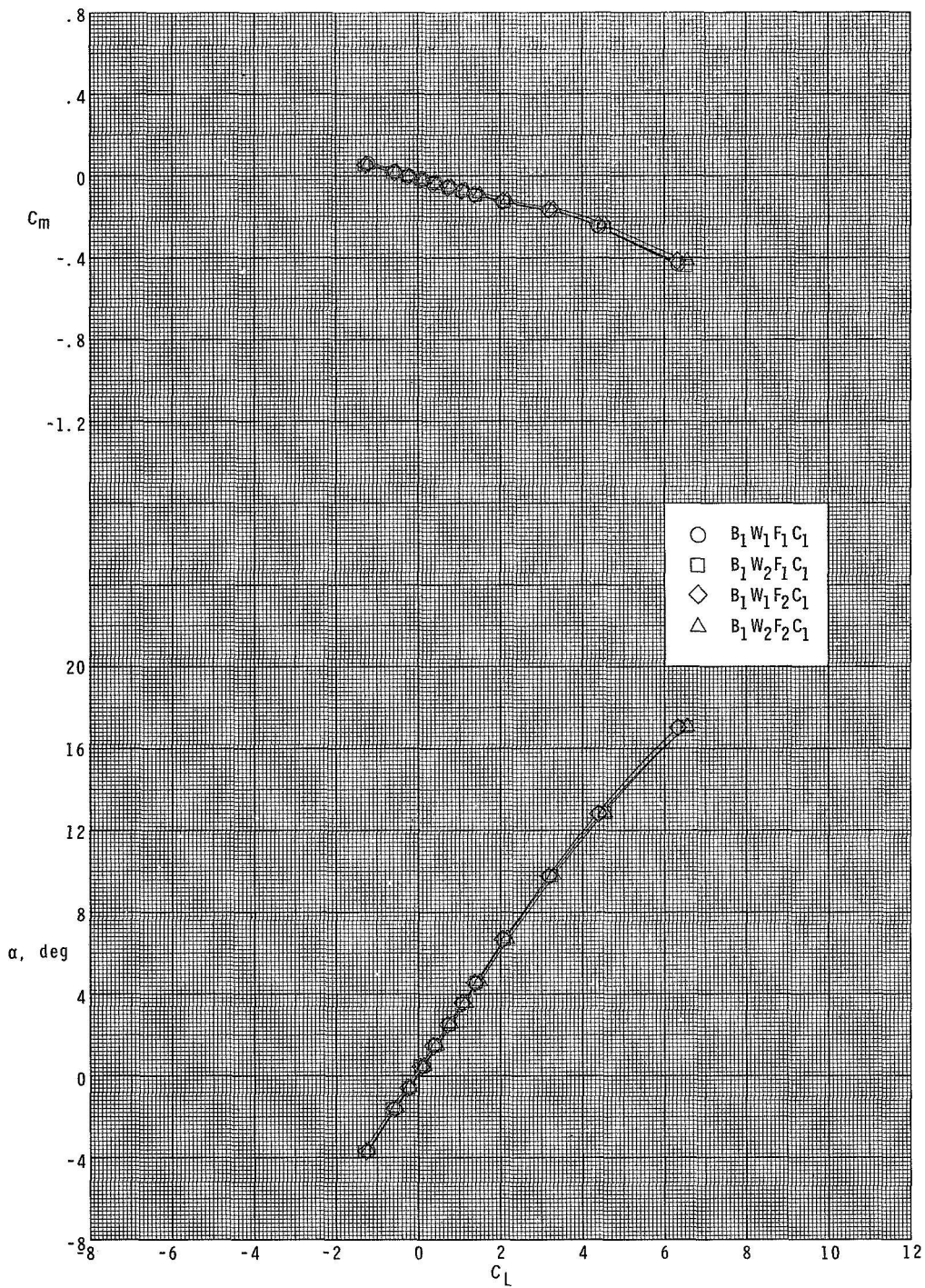
(e) $M = 3.95$.

Figure 5.- Continued.



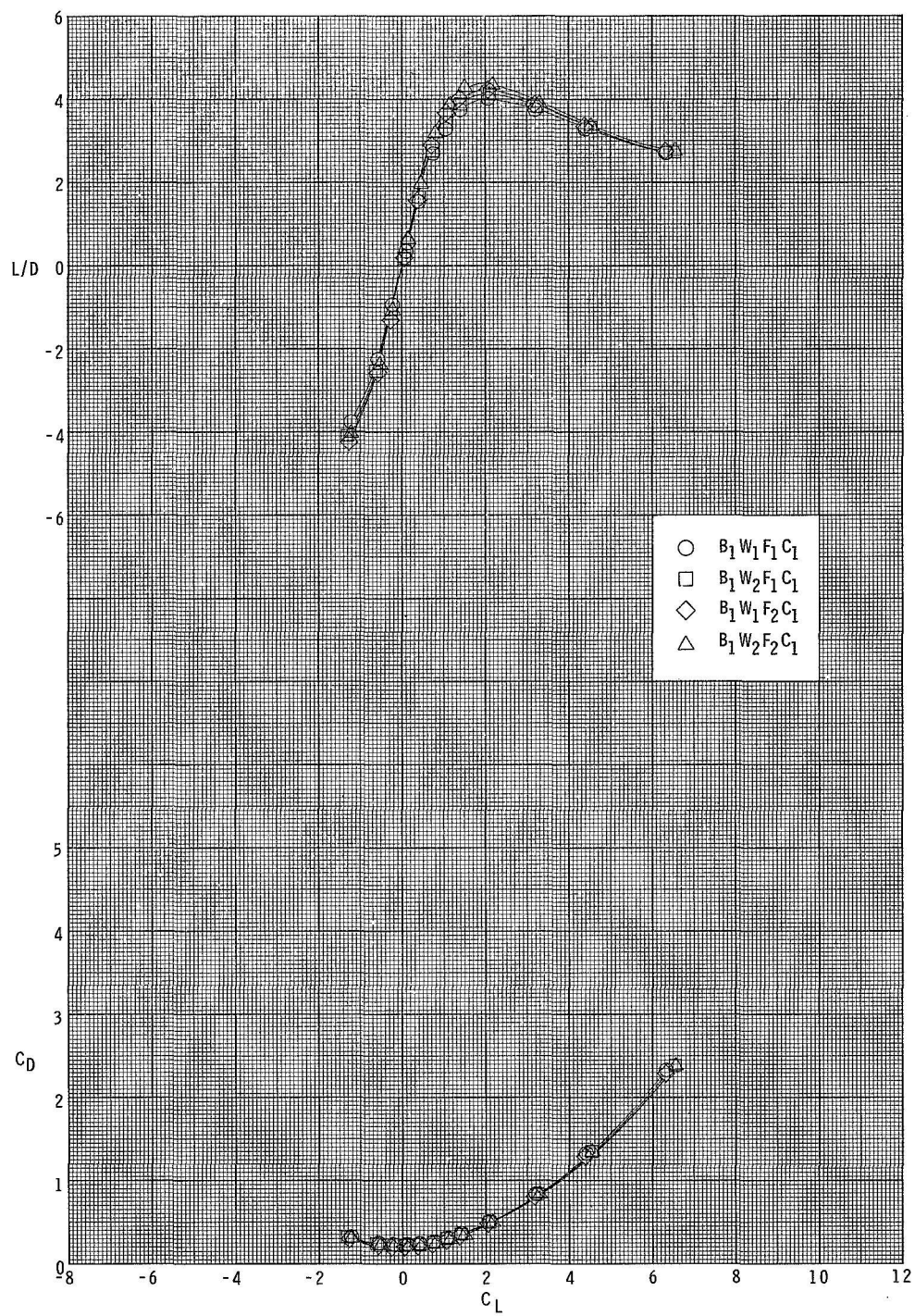
(e) Concluded.

Figure 5.- Continued.



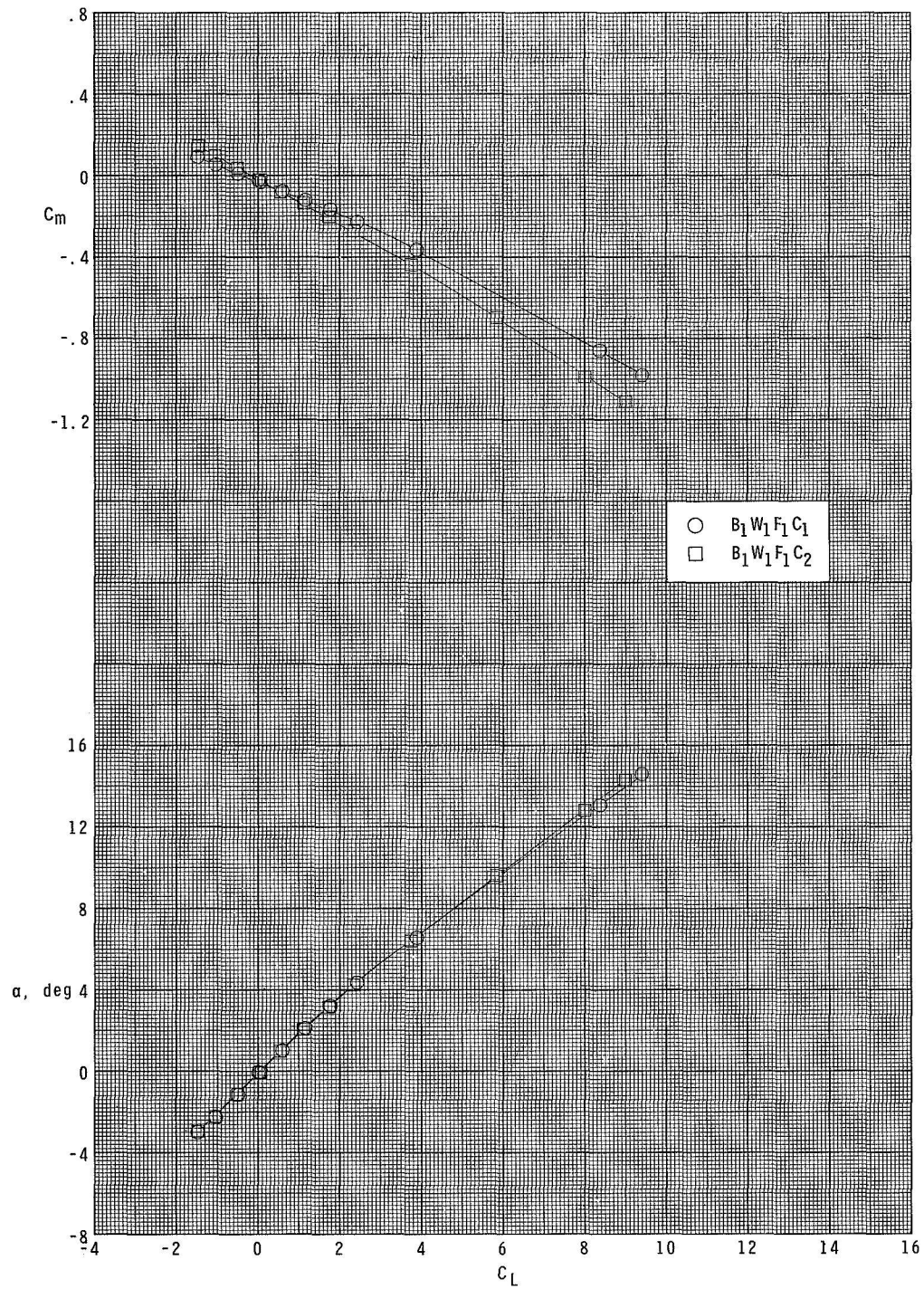
(f) $M = 4.63$.

Figure 5.- Continued.



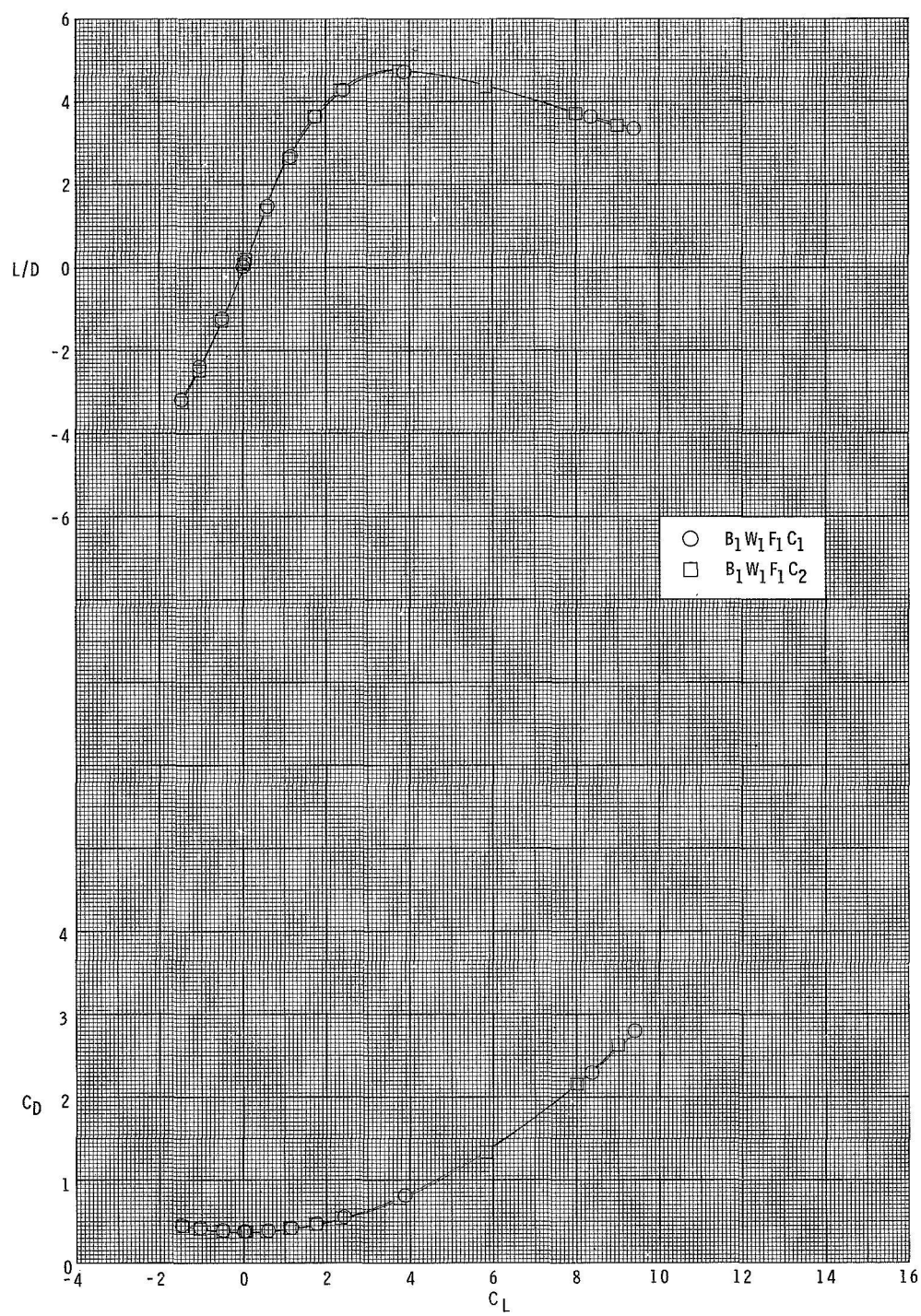
(f) Concluded.

Figure 5.- Concluded.



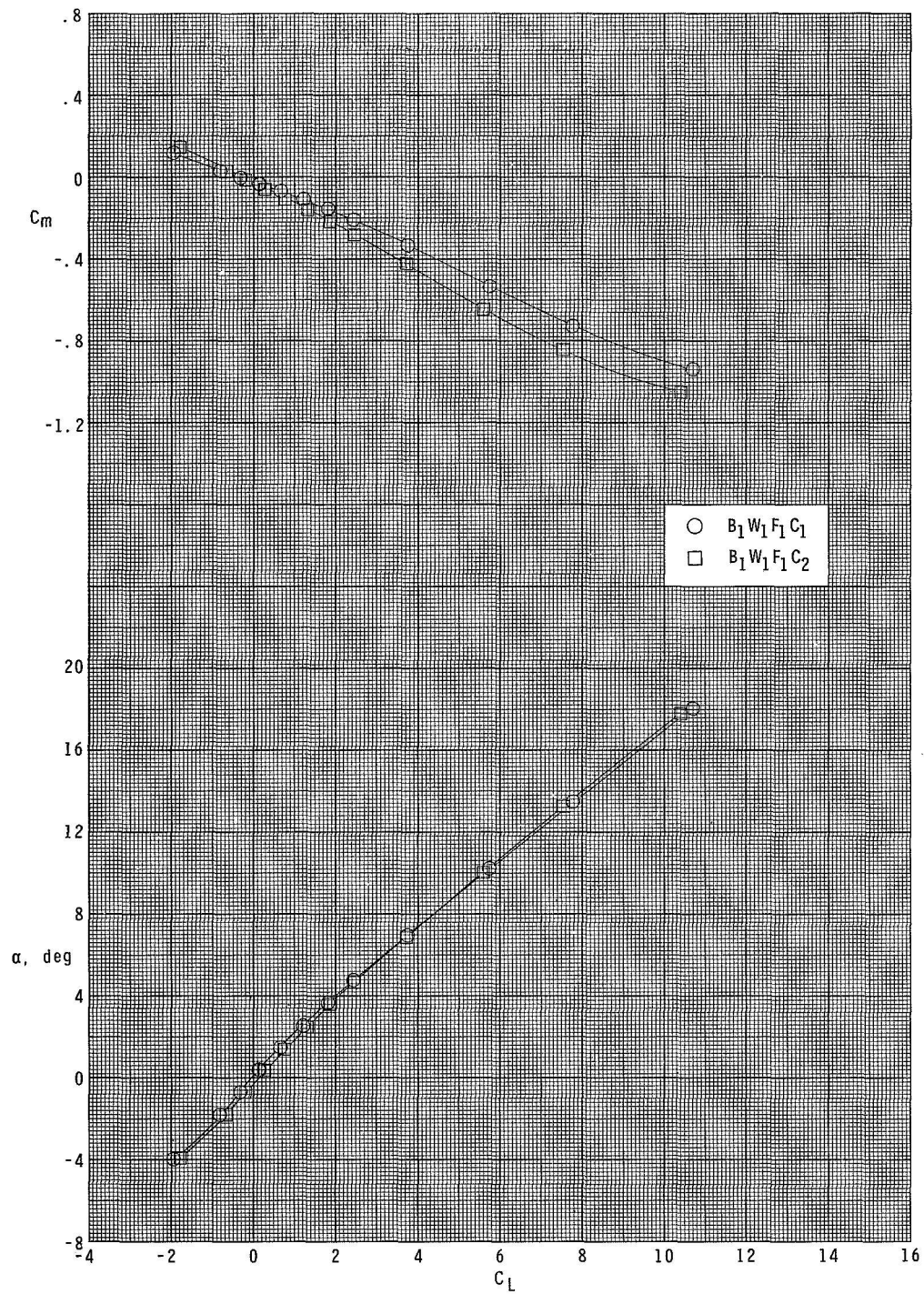
(a) $M = 1.70$.

Figure 6.- Effect of canard size on longitudinal aerodynamic characteristics.



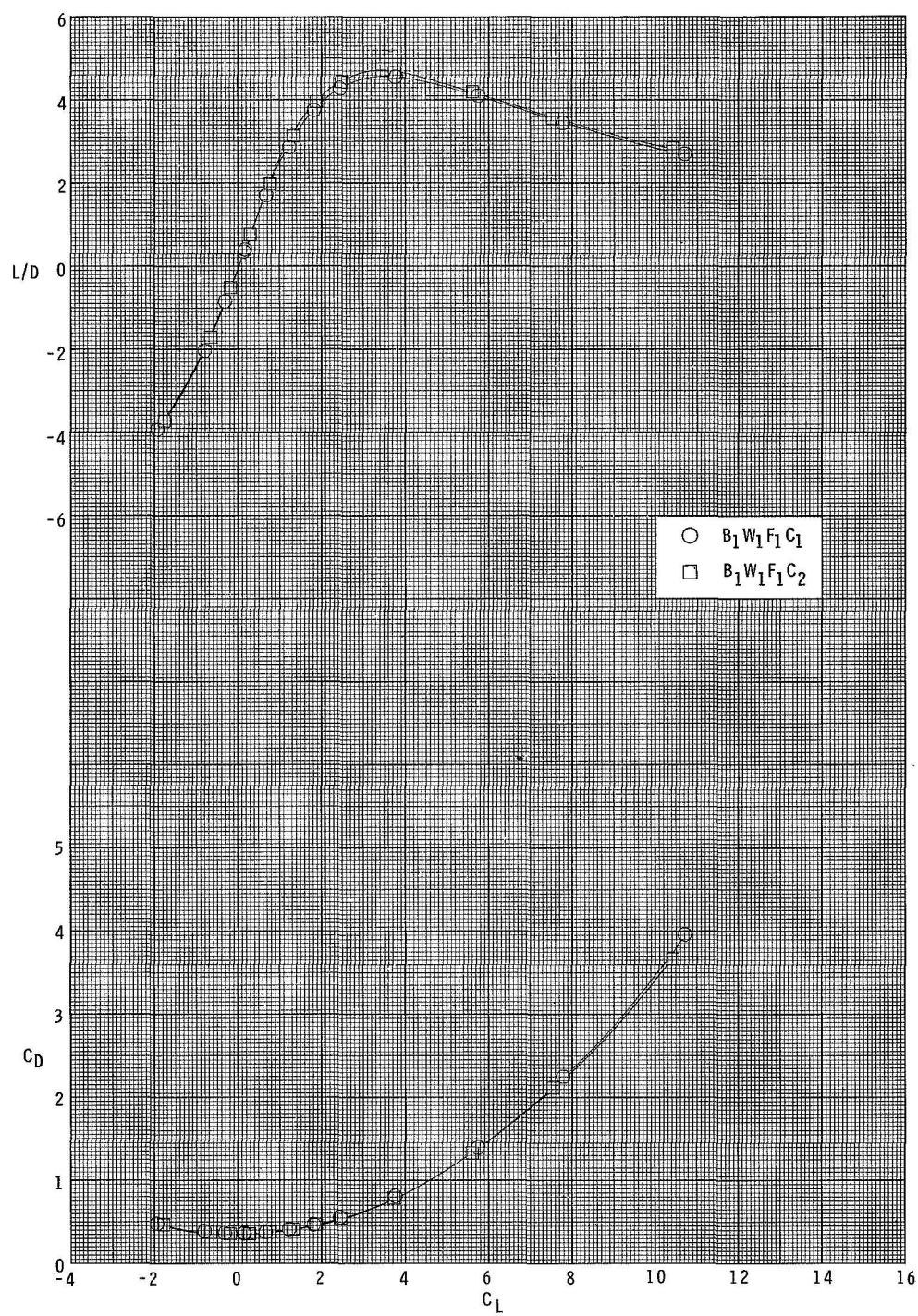
(a) Concluded.

Figure 6.- Continued.



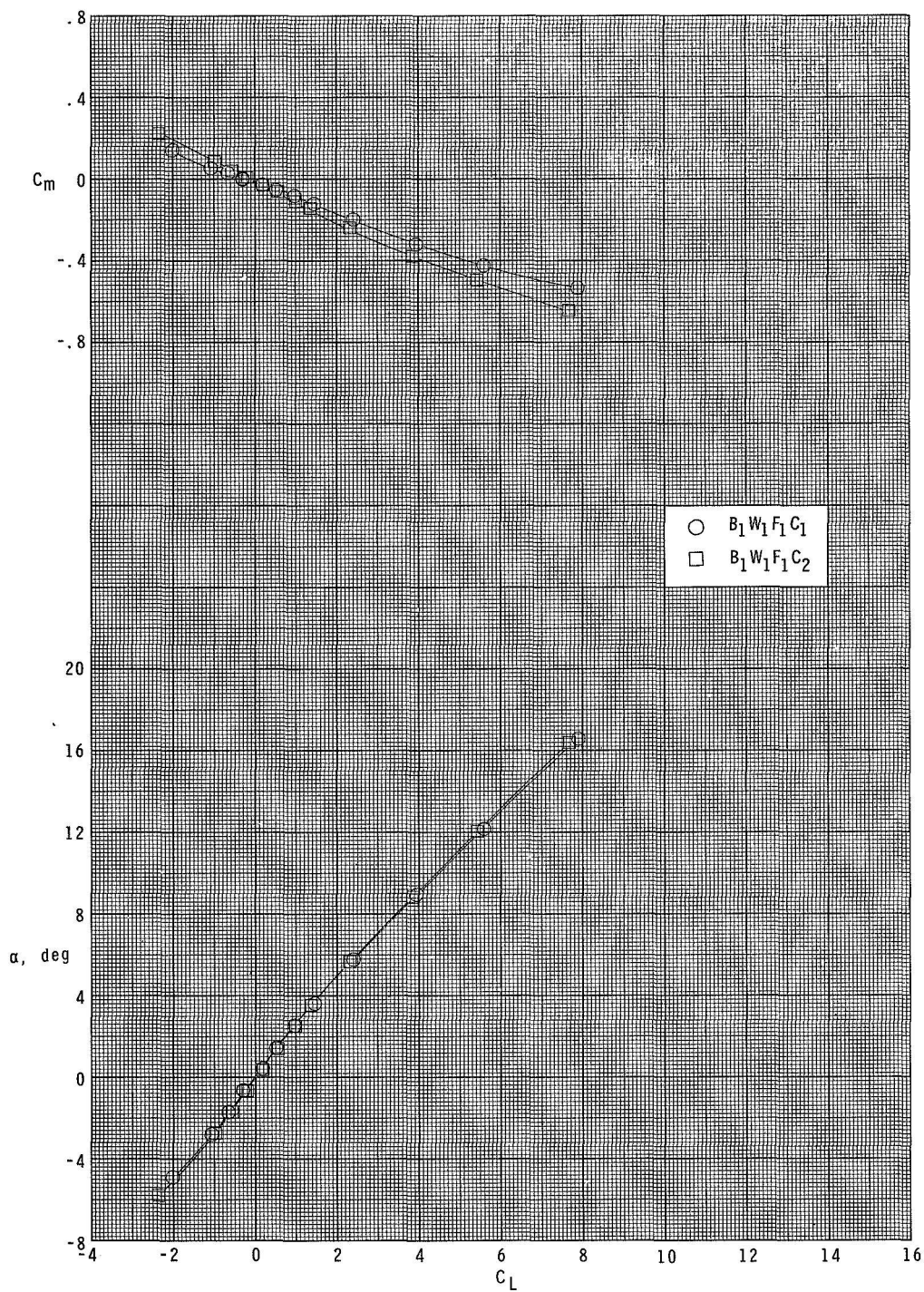
(b) $M = 2.00$.

Figure 6.- Continued.



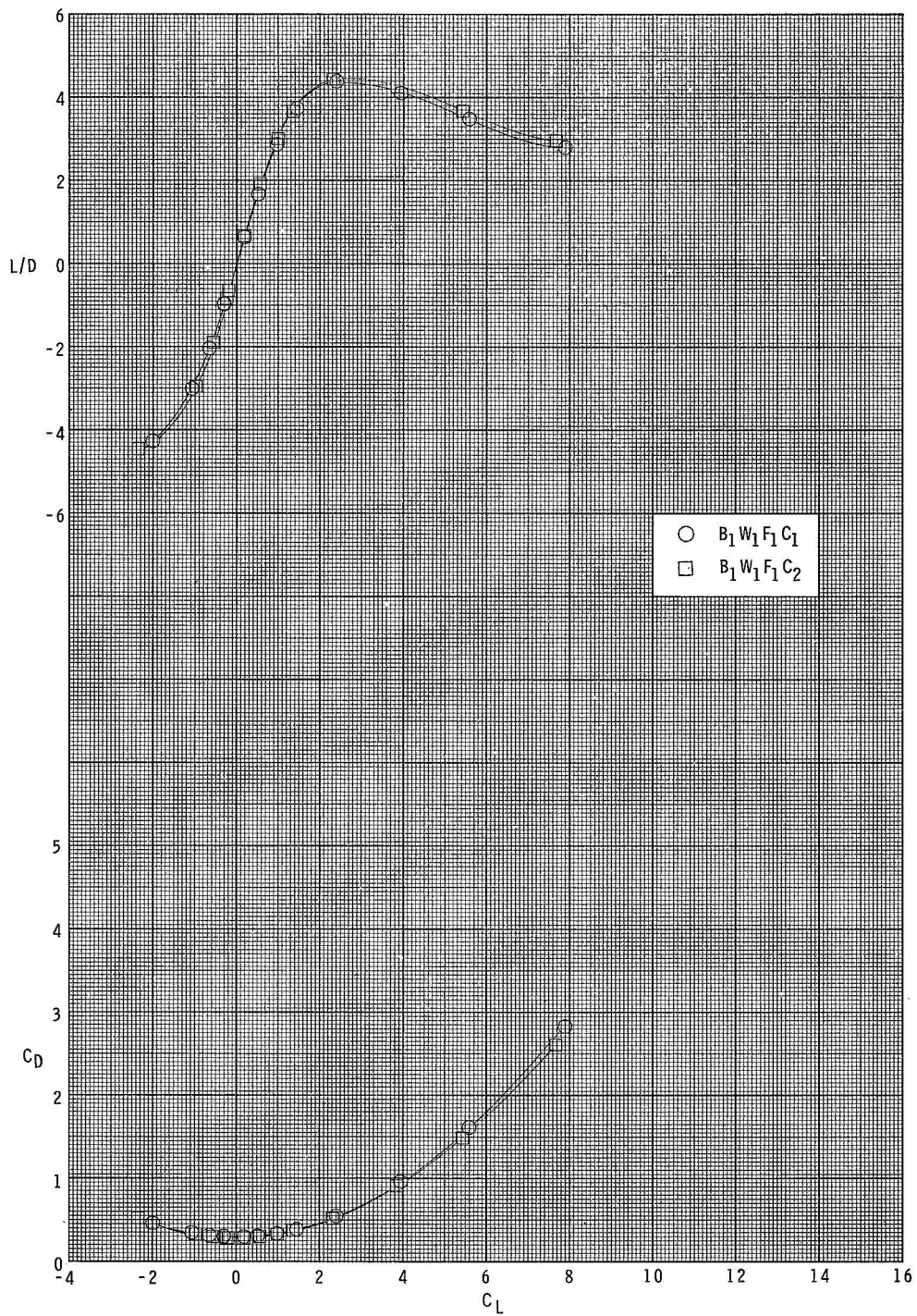
(b) Concluded.

Figure 6.- Continued.



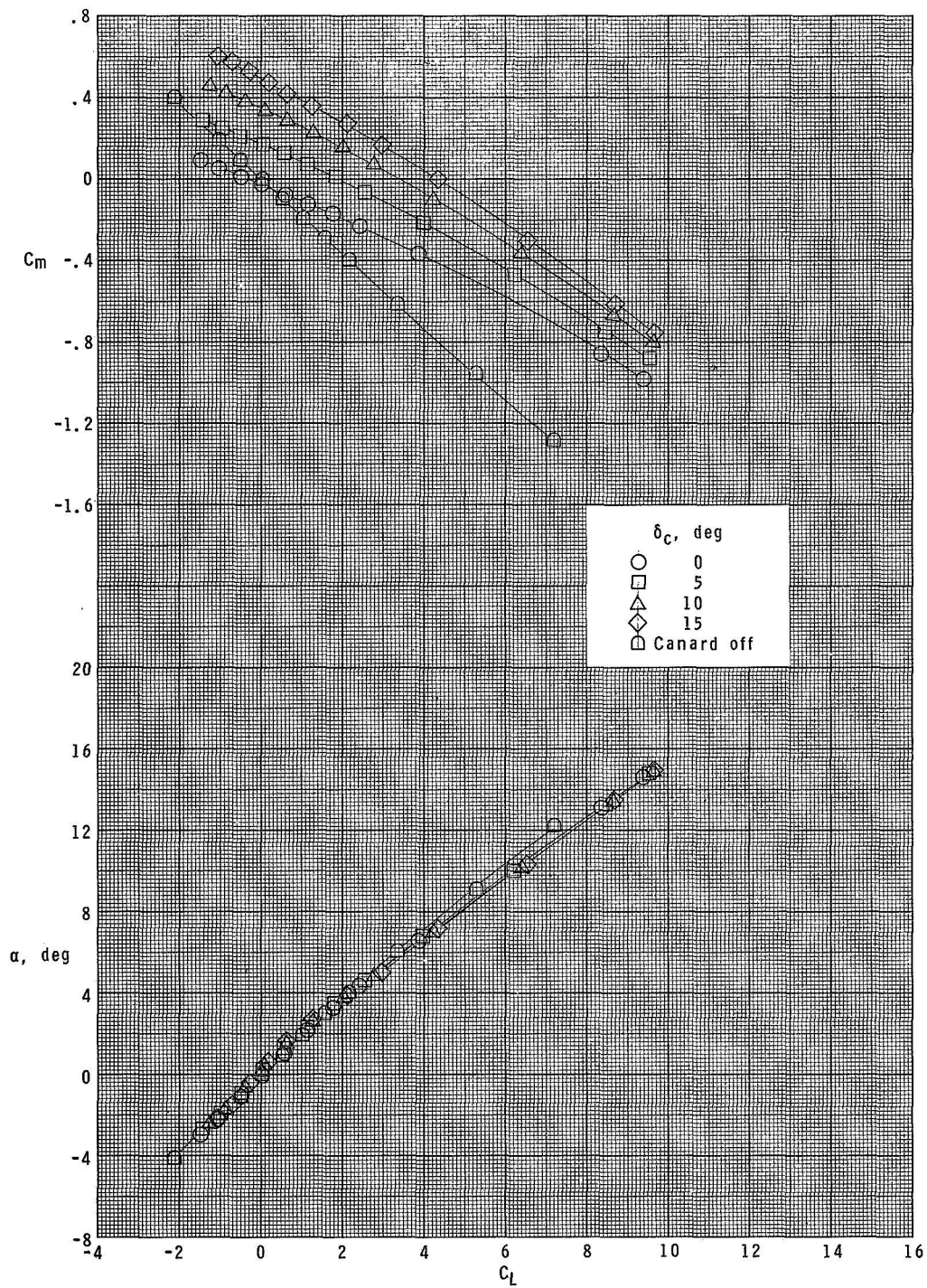
(c) $M = 2.86$.

Figure 6.- Continued.



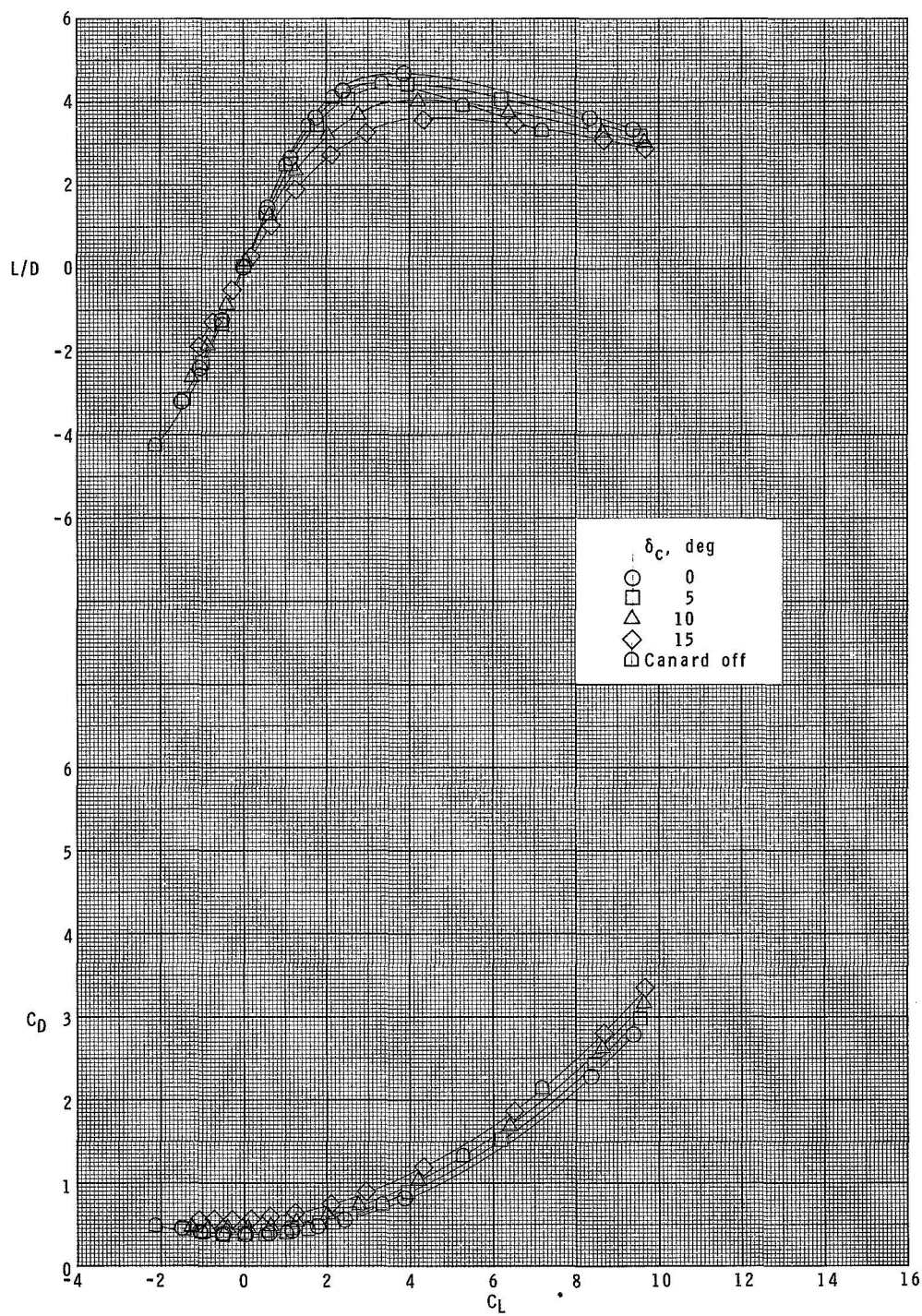
(c) Concluded.

Figure 6.- Concluded.



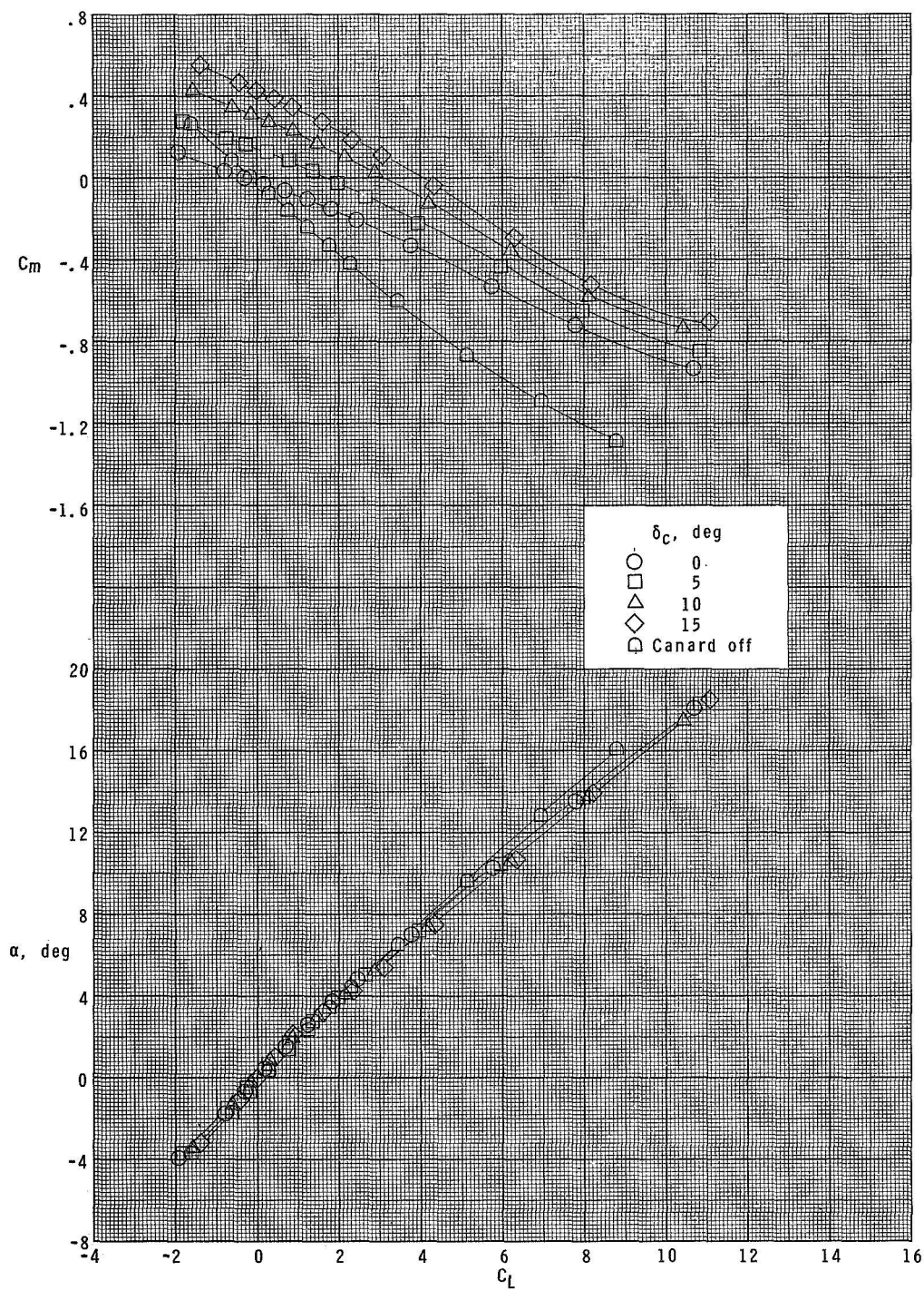
(a) $M = 1.70$.

Figure 7.- Longitudinal control characteristics of configuration B₁W₁F₁C₁.



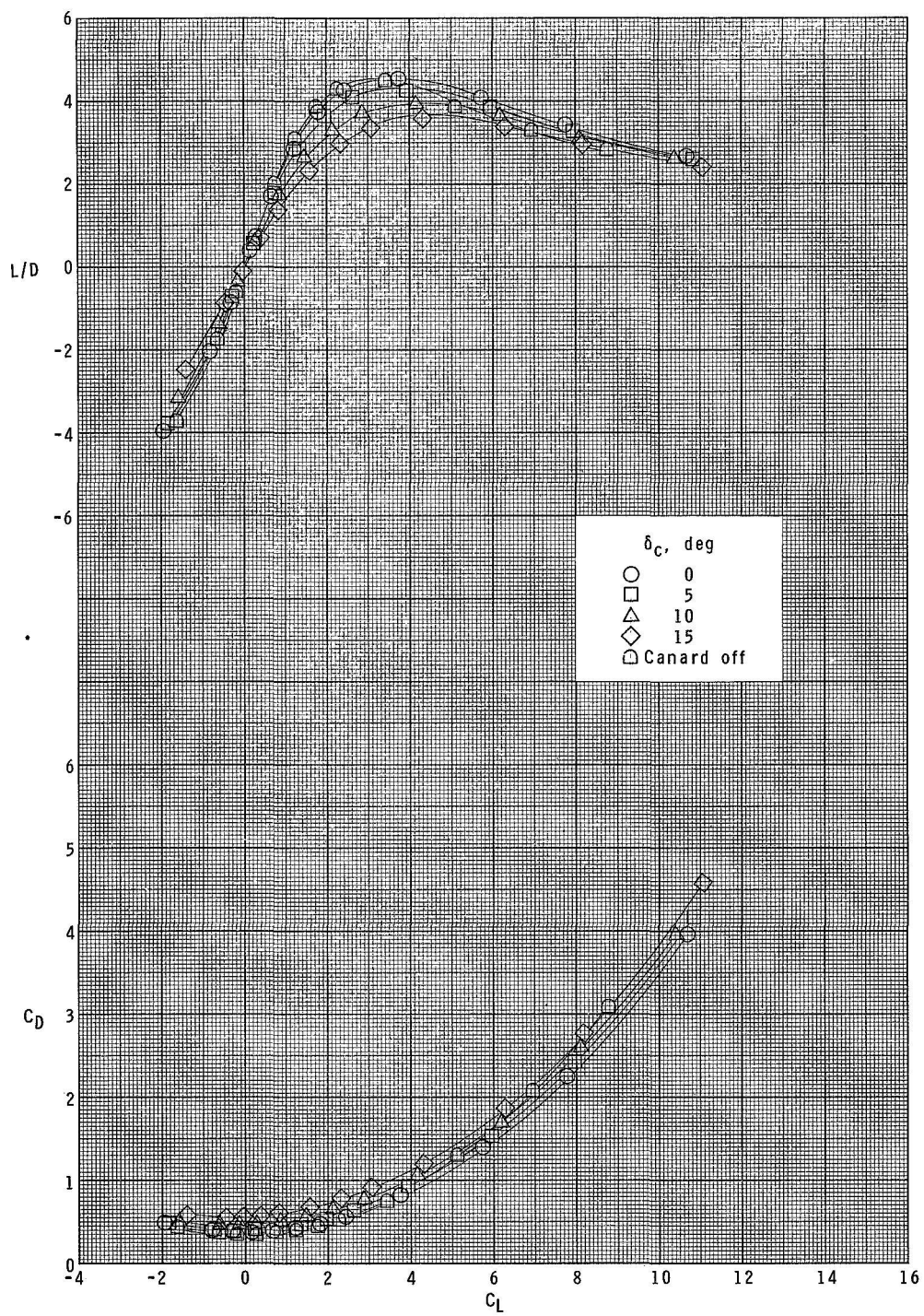
(a) Concluded.

Figure 7.- Continued.



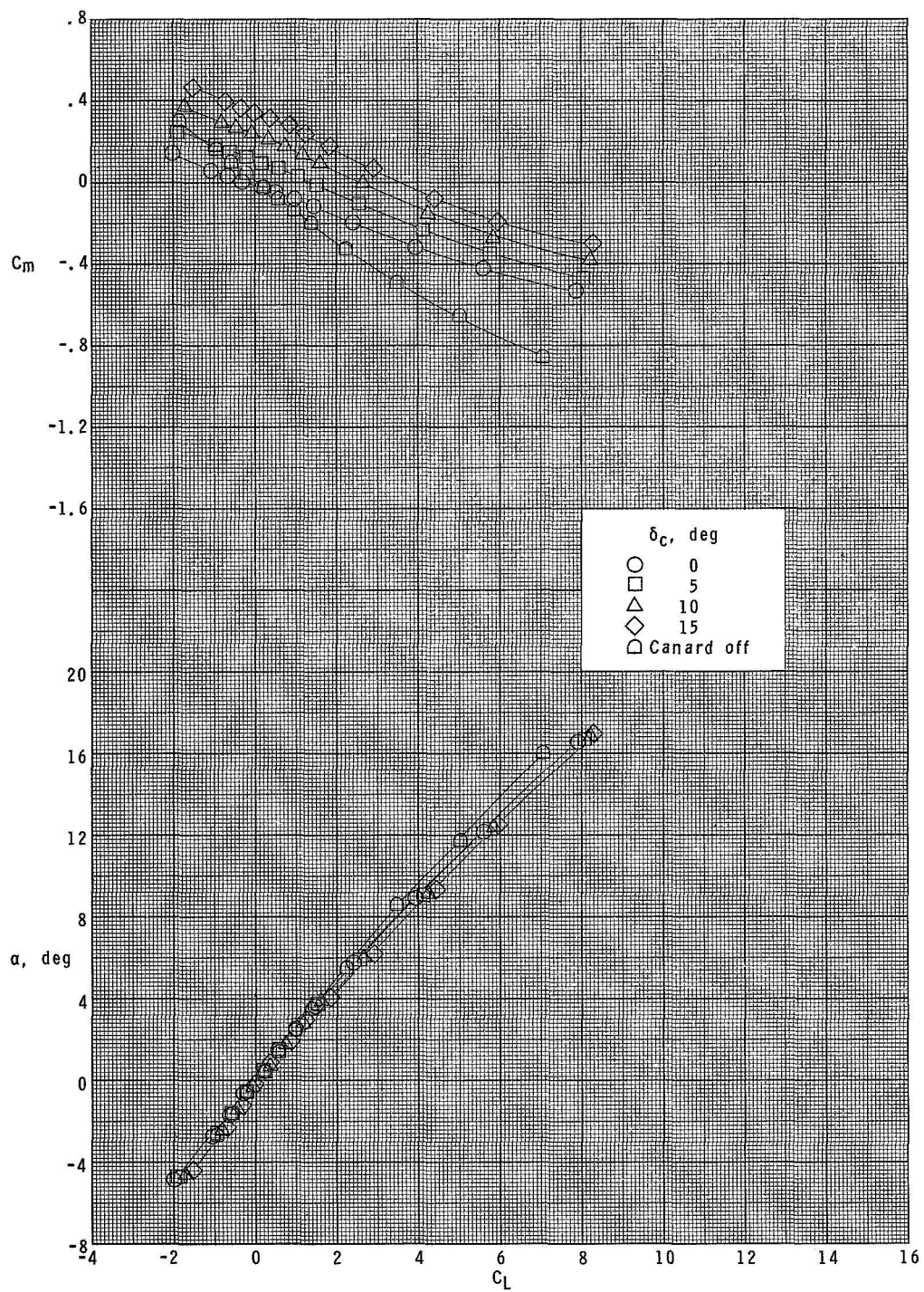
(b) $M = 2.00$.

Figure 7.- Continued.



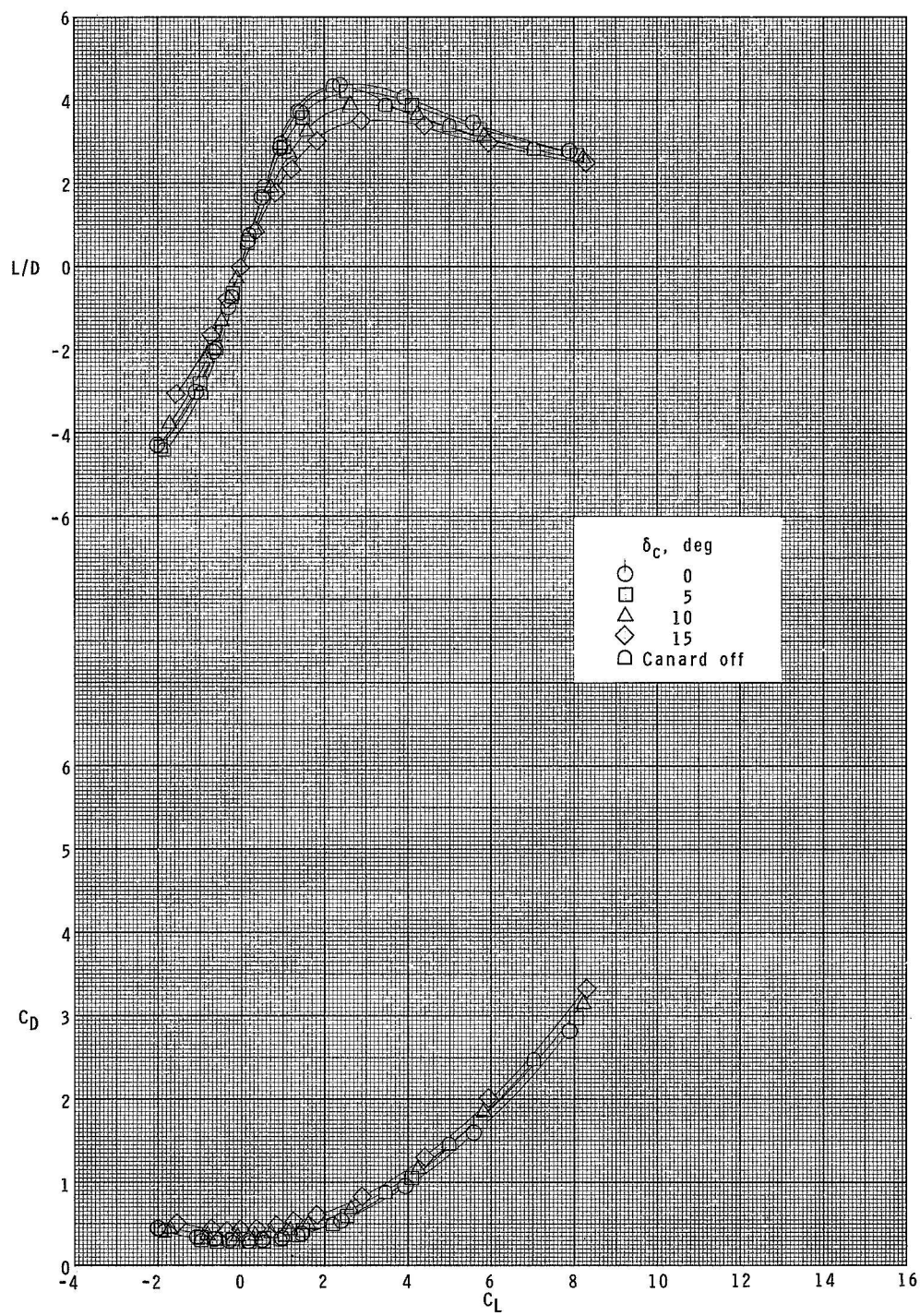
(b) Concluded.

Figure 7.- Continued.



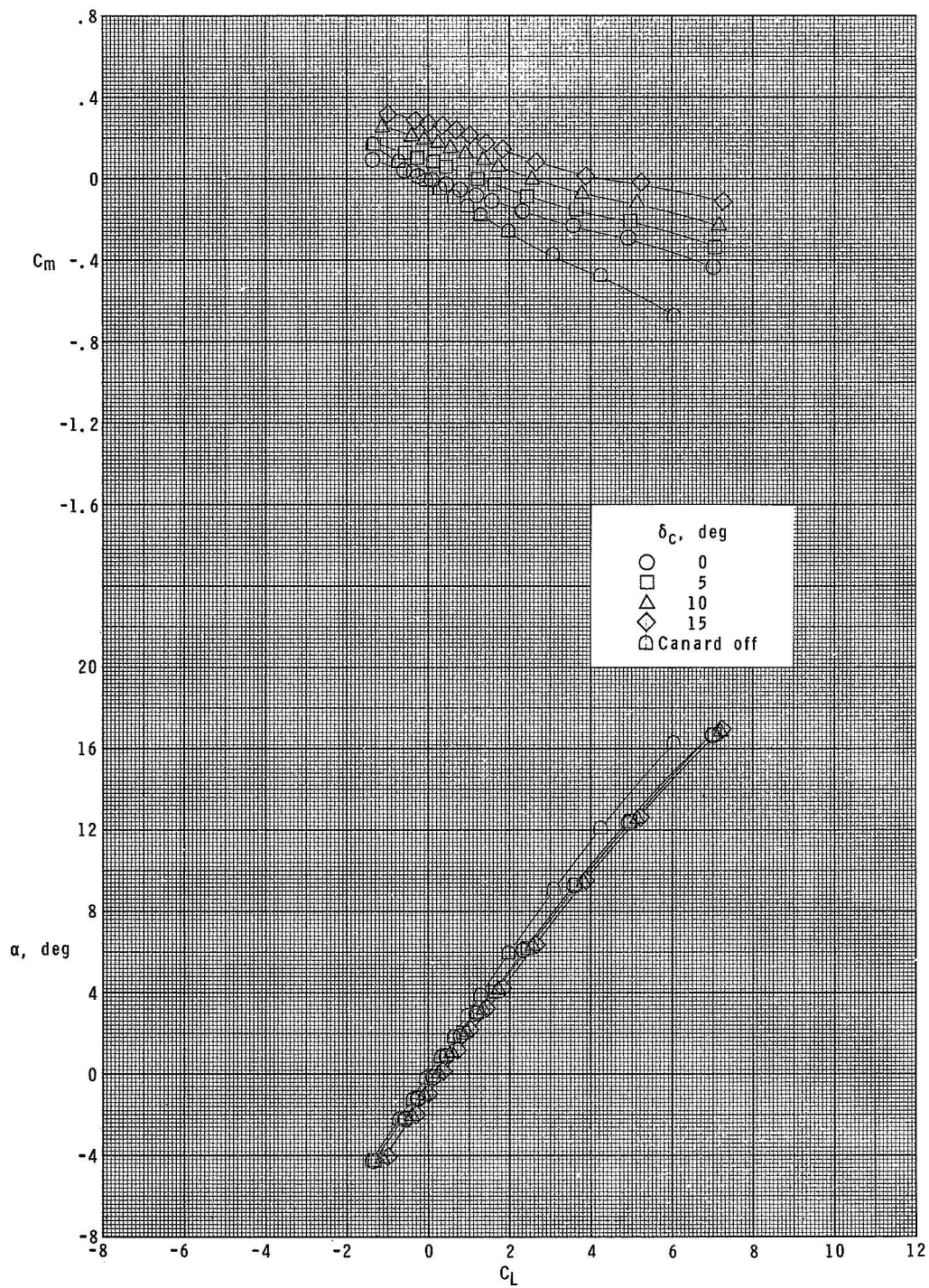
(c) $M = 2.86$.

Figure 7.- Continued.



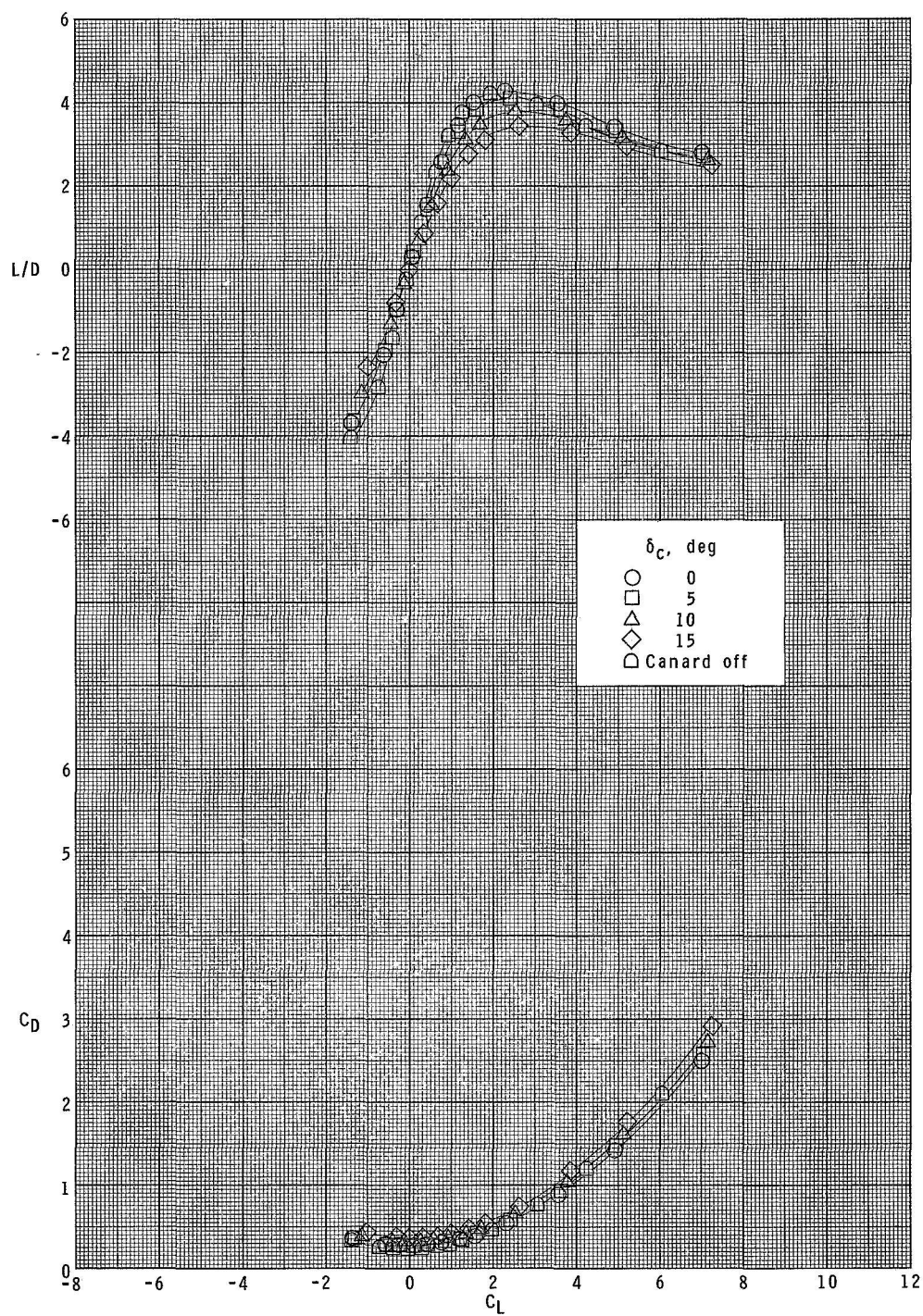
(c) Concluded.

Figure 7.- Continued.



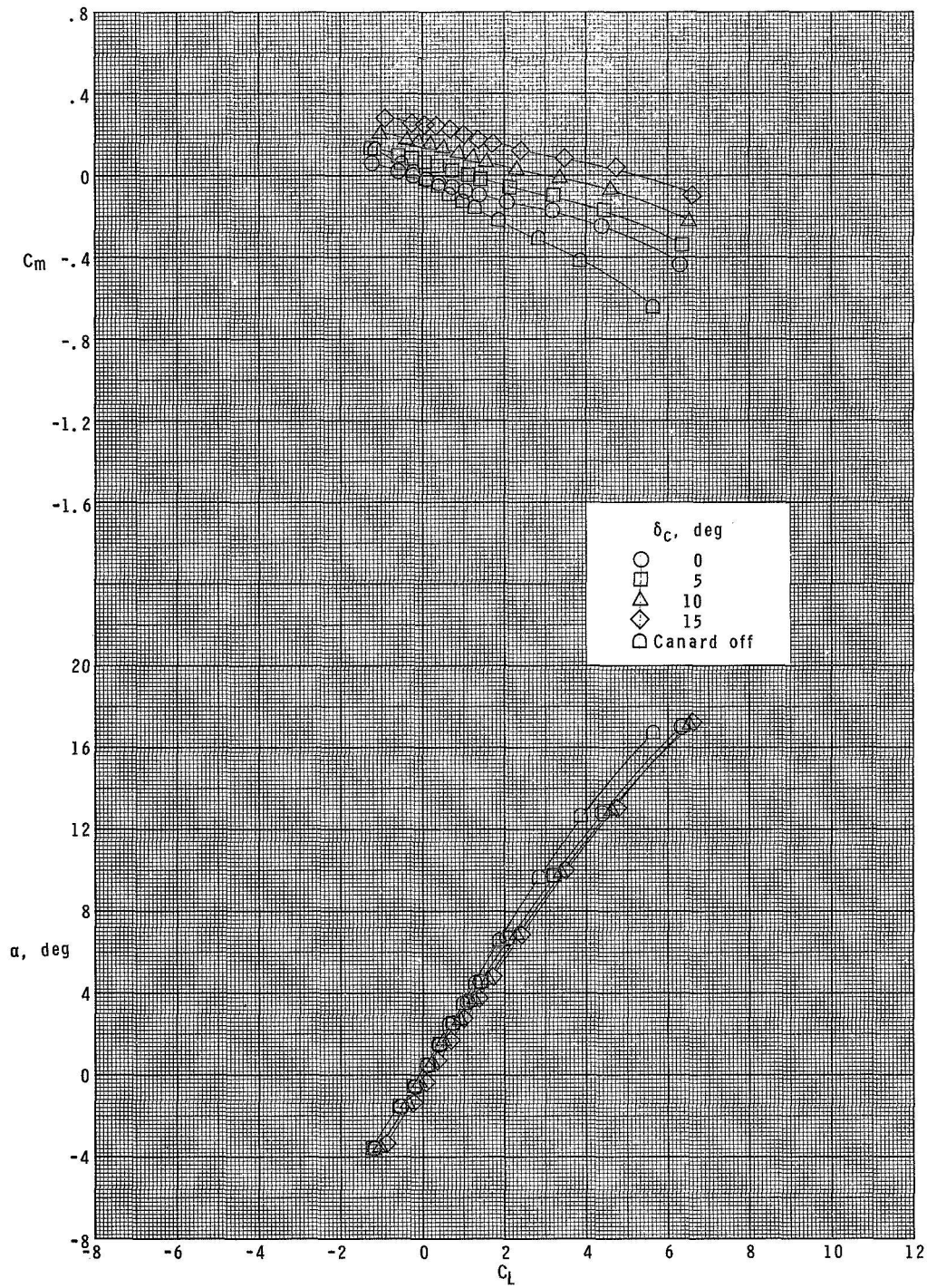
(d) $M = 3.95$.

Figure 7.- Continued.



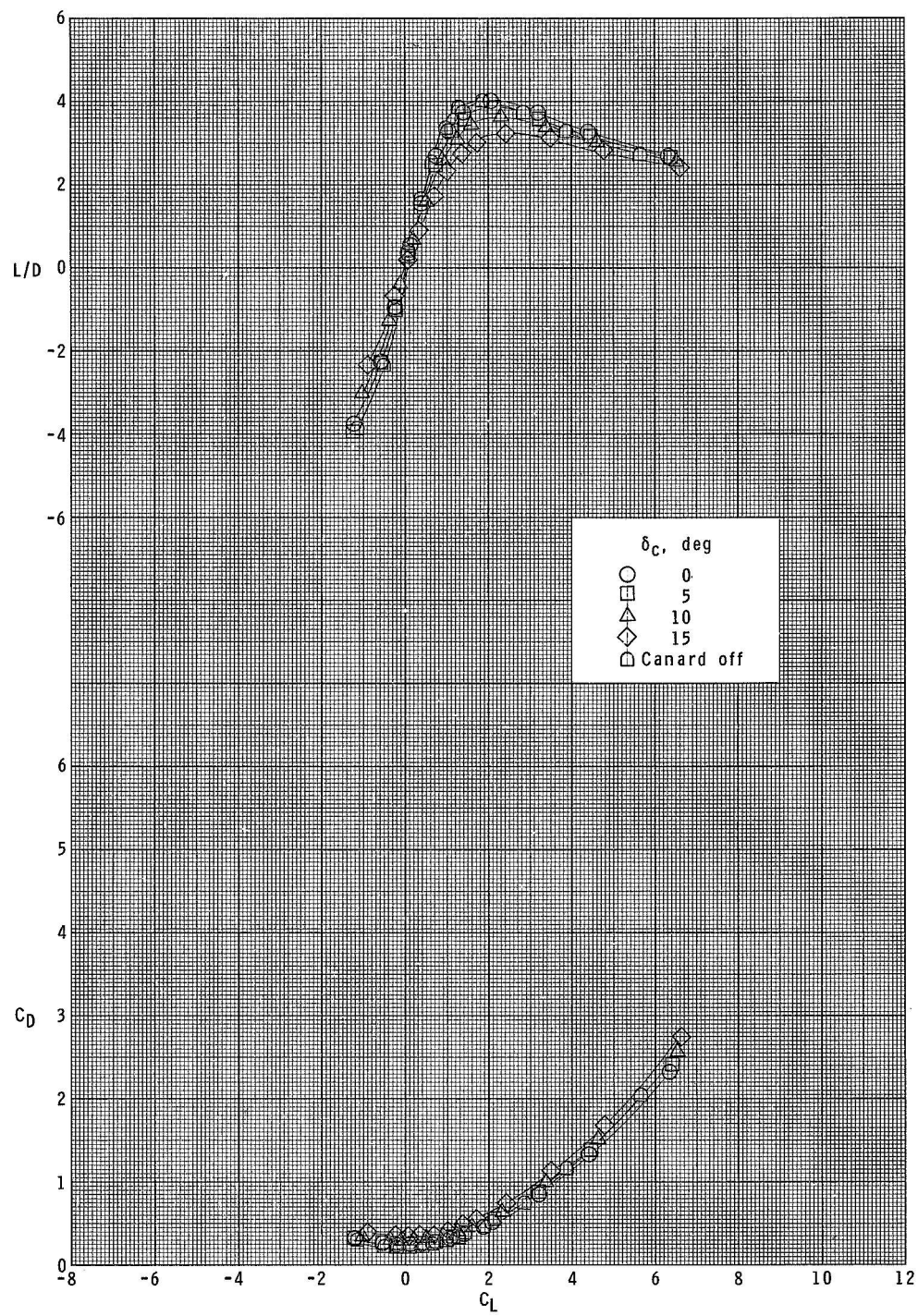
(d) Concluded.

Figure 7.- Continued.



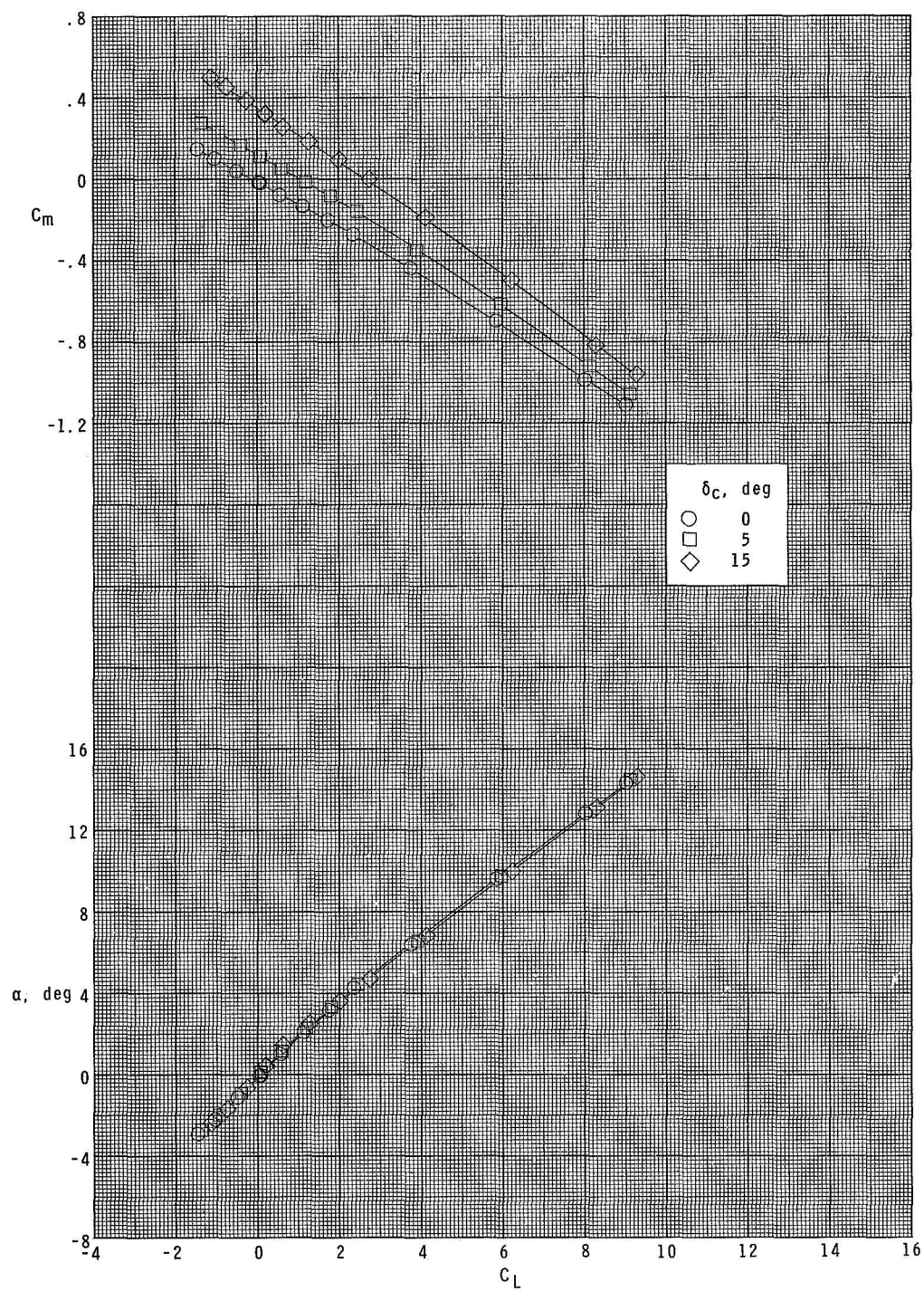
(e) $M = 4.63$.

Figure 7.- Continued.



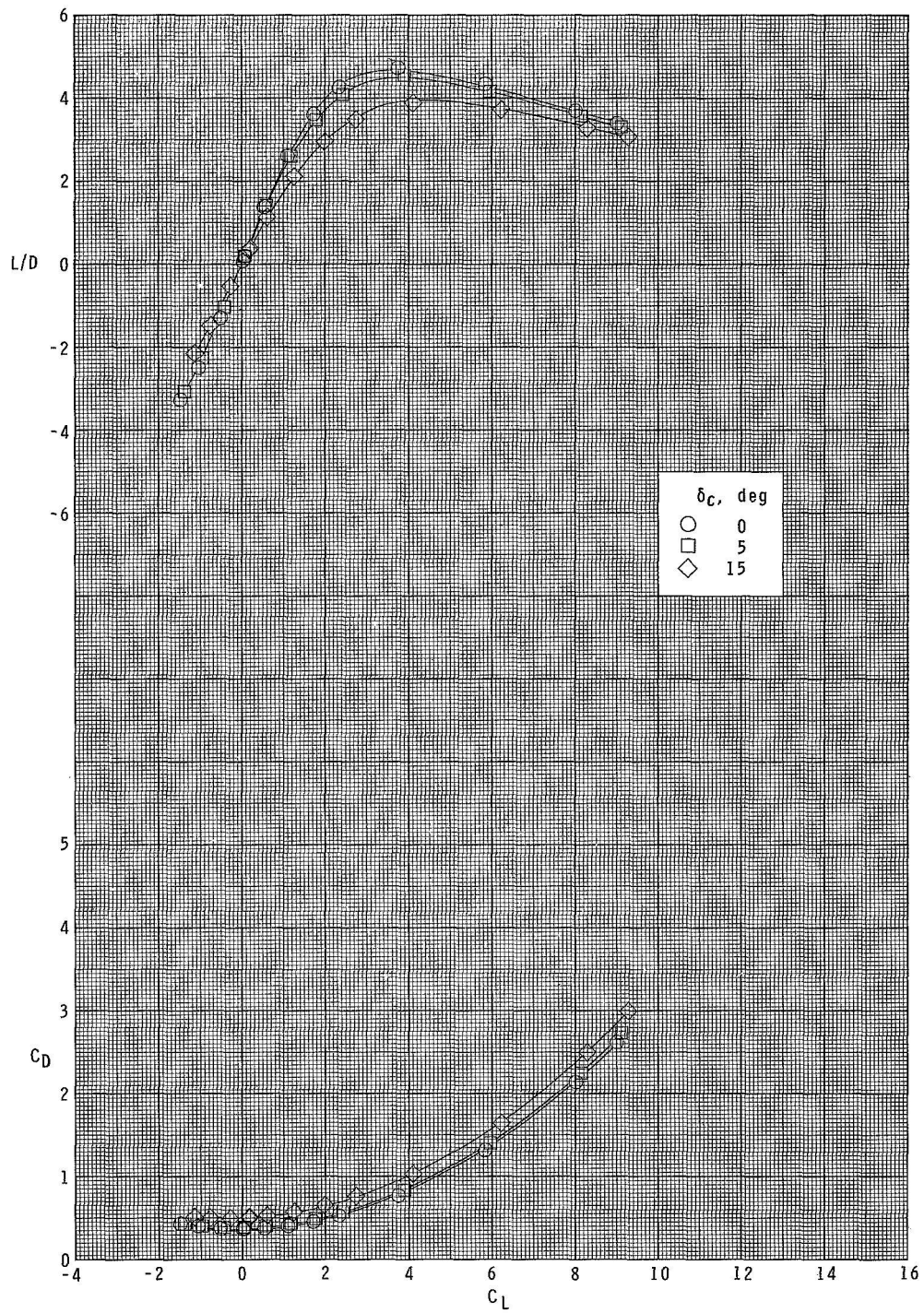
(e) Concluded.

Figure 7.- Concluded.



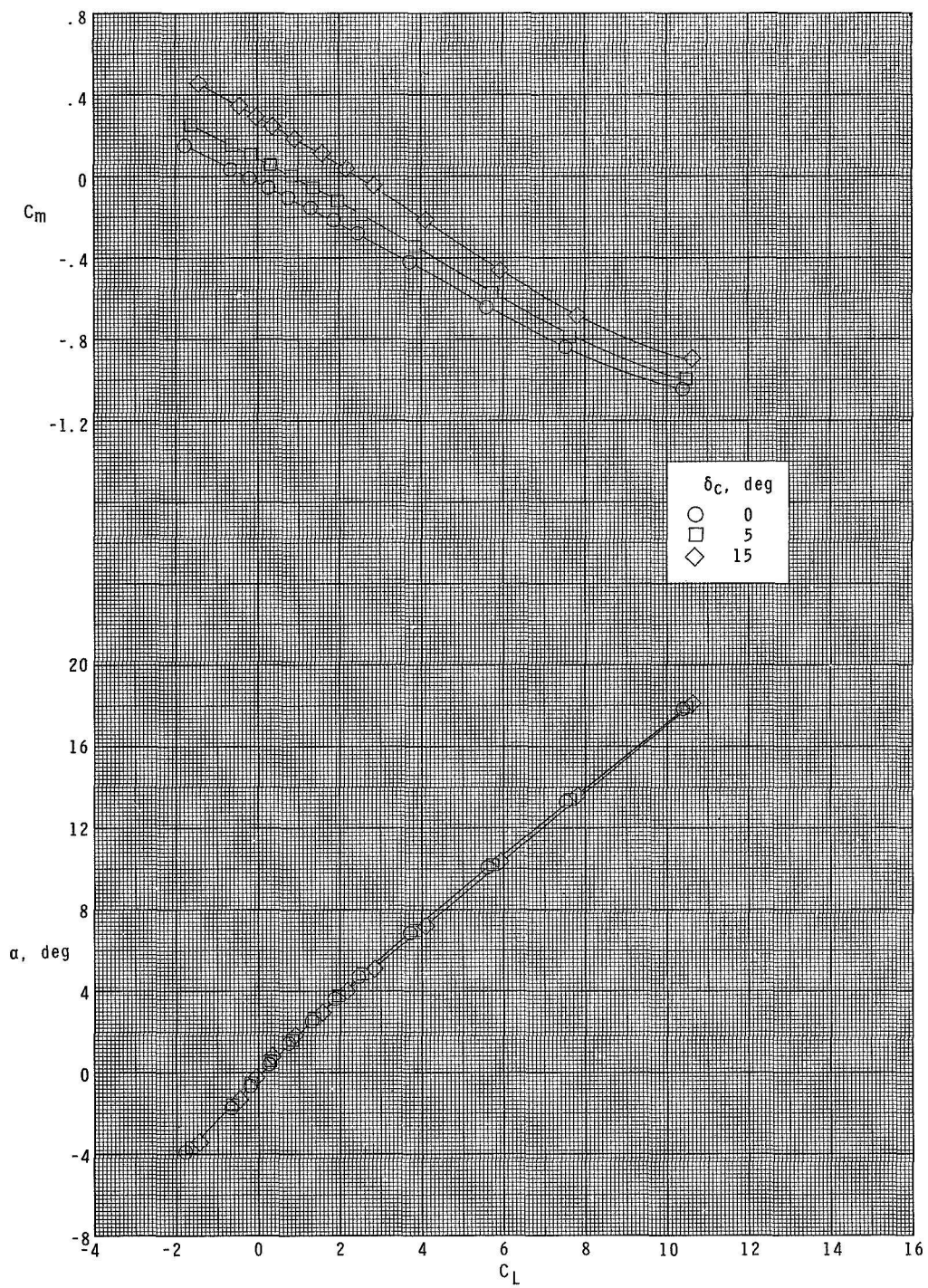
(a) $M = 1.70$.

Figure 8.- Longitudinal control characteristics of configuration B₁W₁F₁C₂.



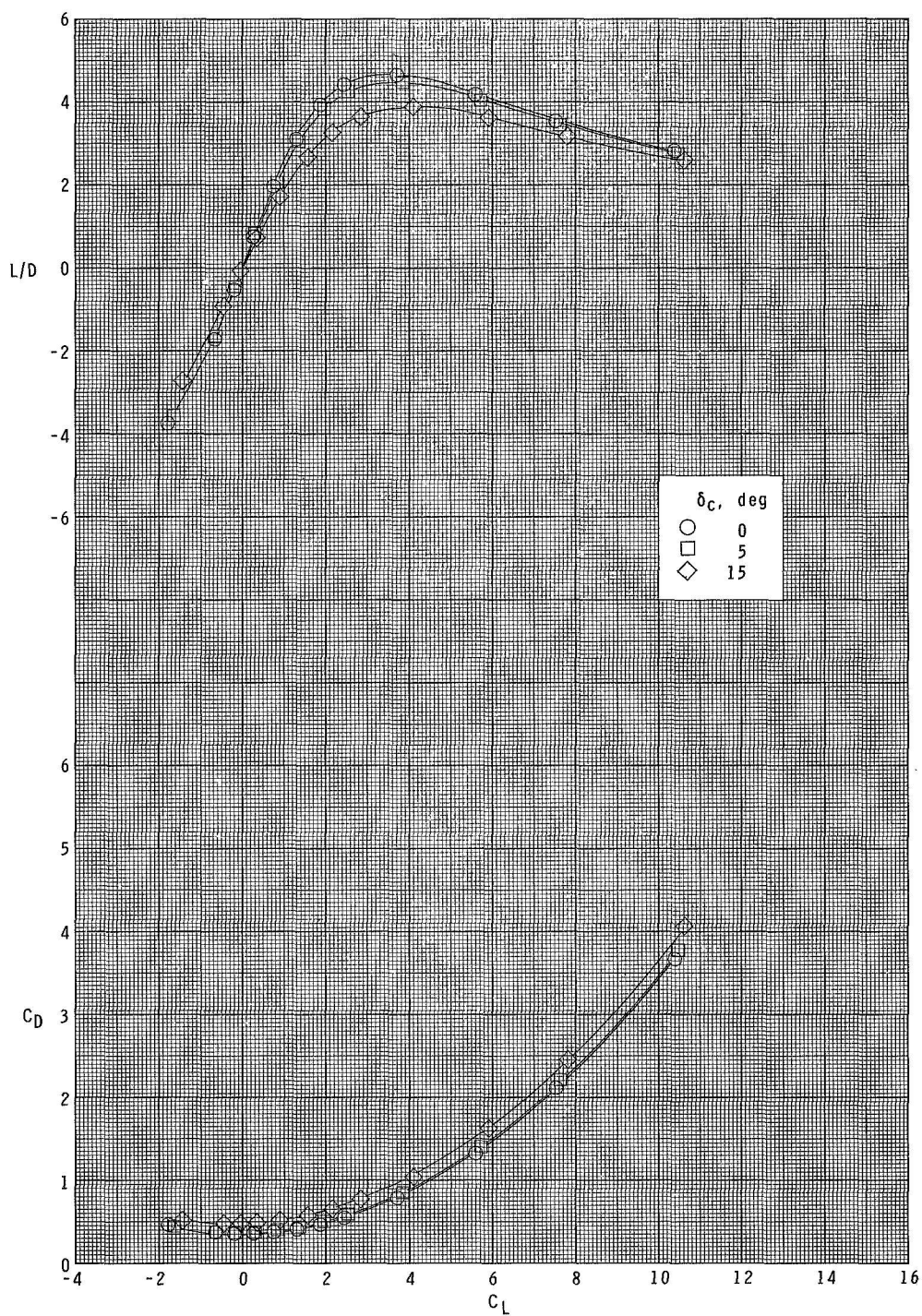
(a) Concluded.

Figure 8.- Continued.



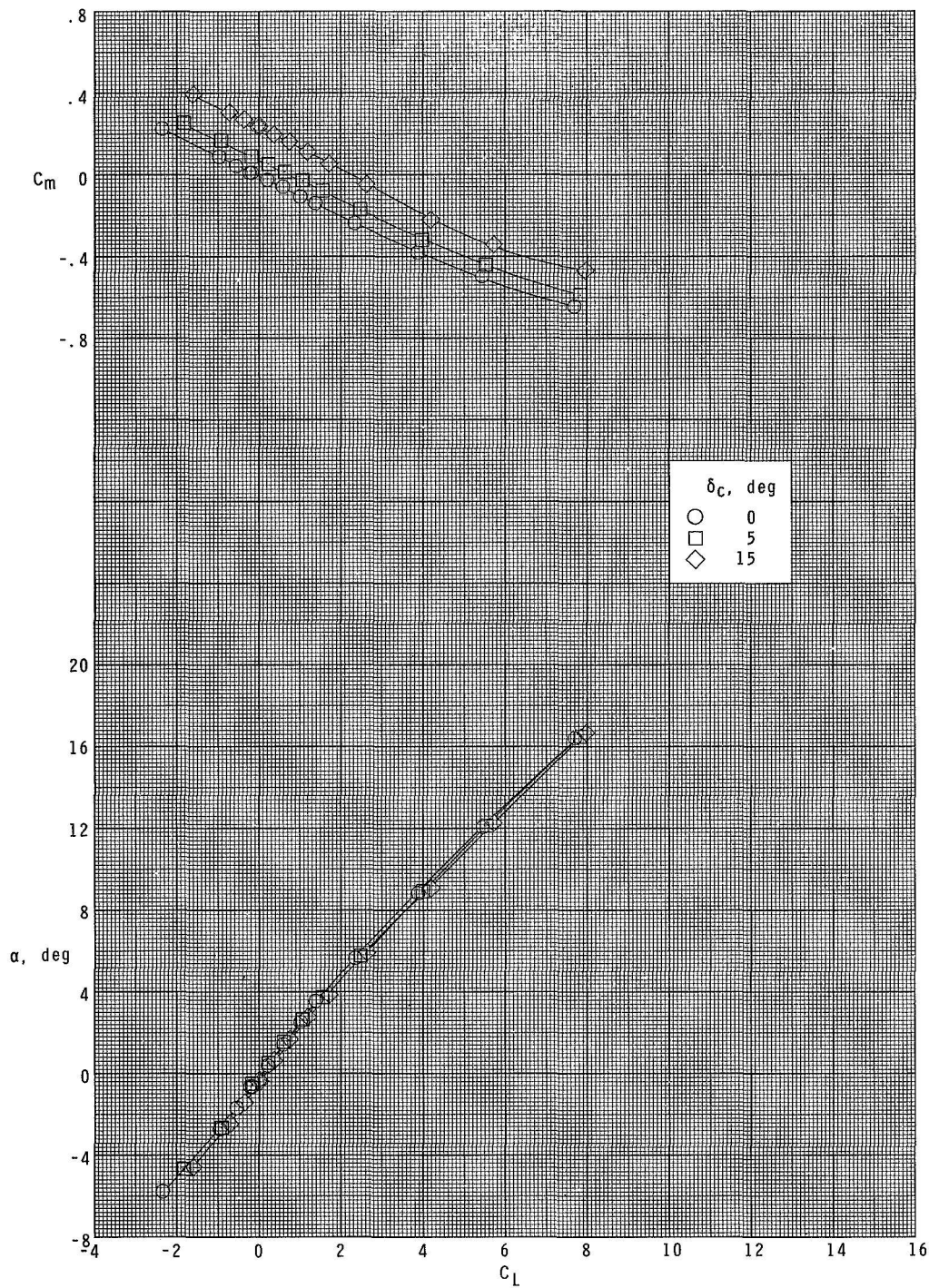
(b) $M = 2.00$.

Figure 8.- Continued.



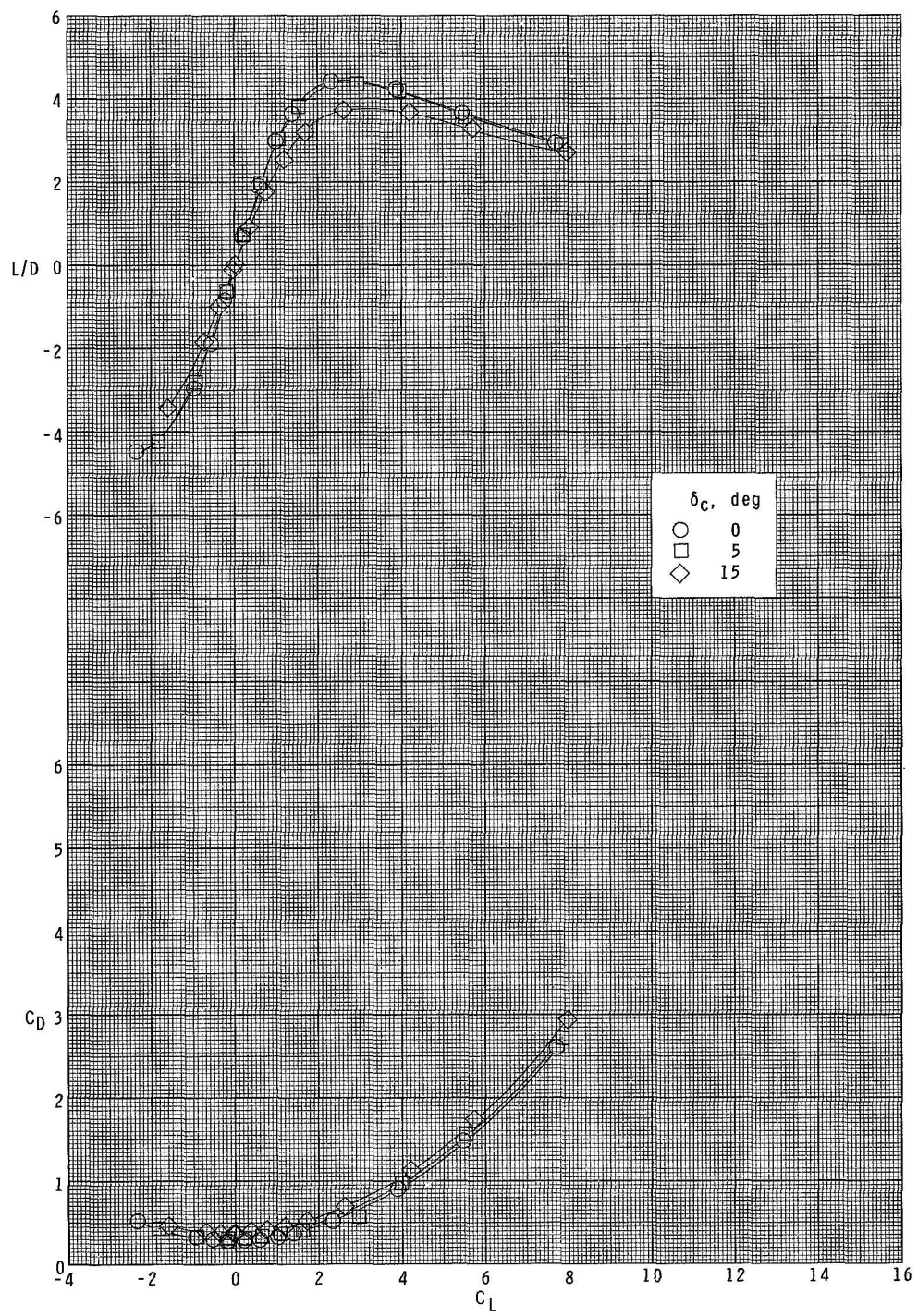
(b) Concluded.

Figure 8.- Continued.



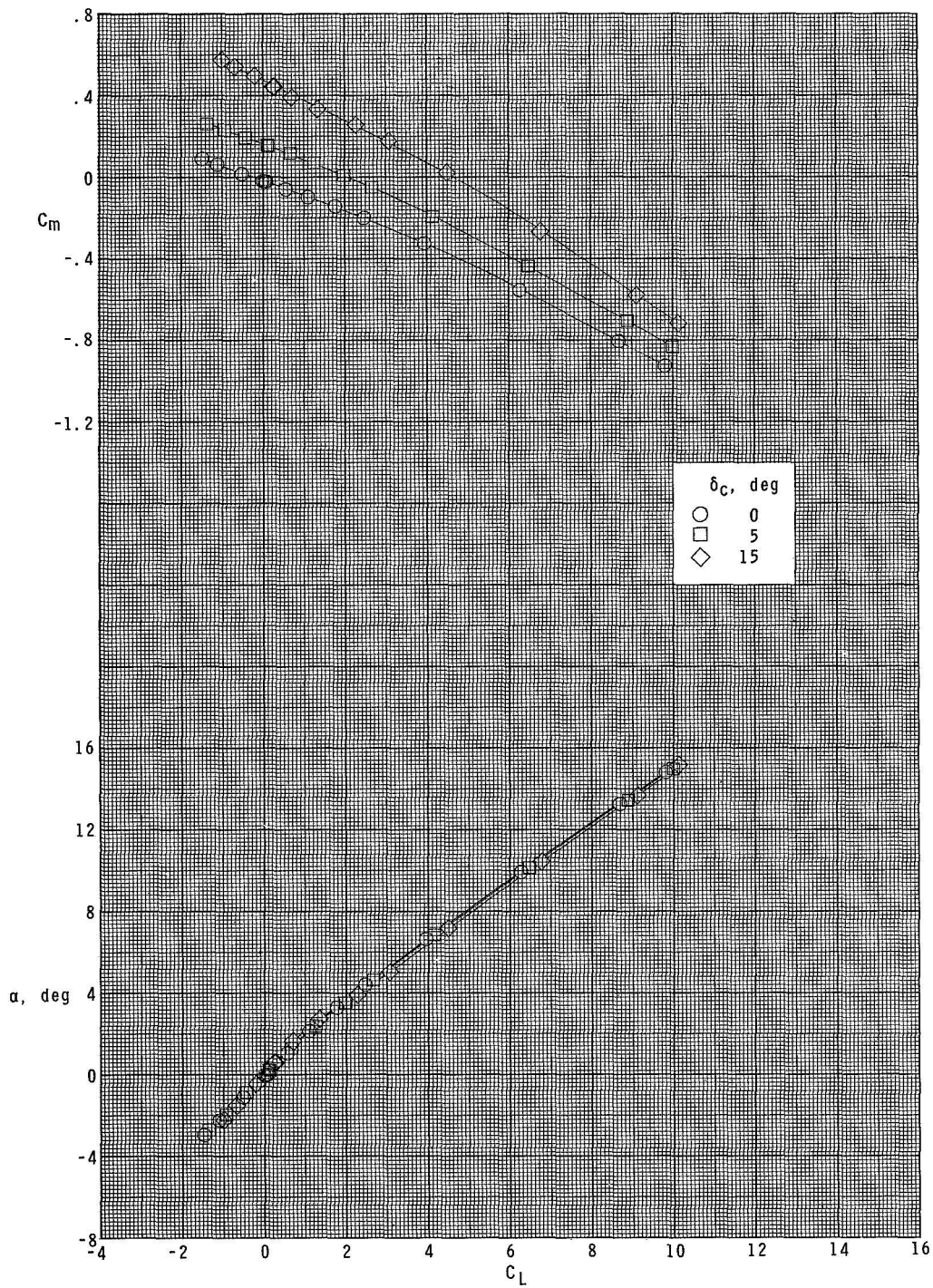
(c) $M = 2.86$.

Figure 8.- Continued.



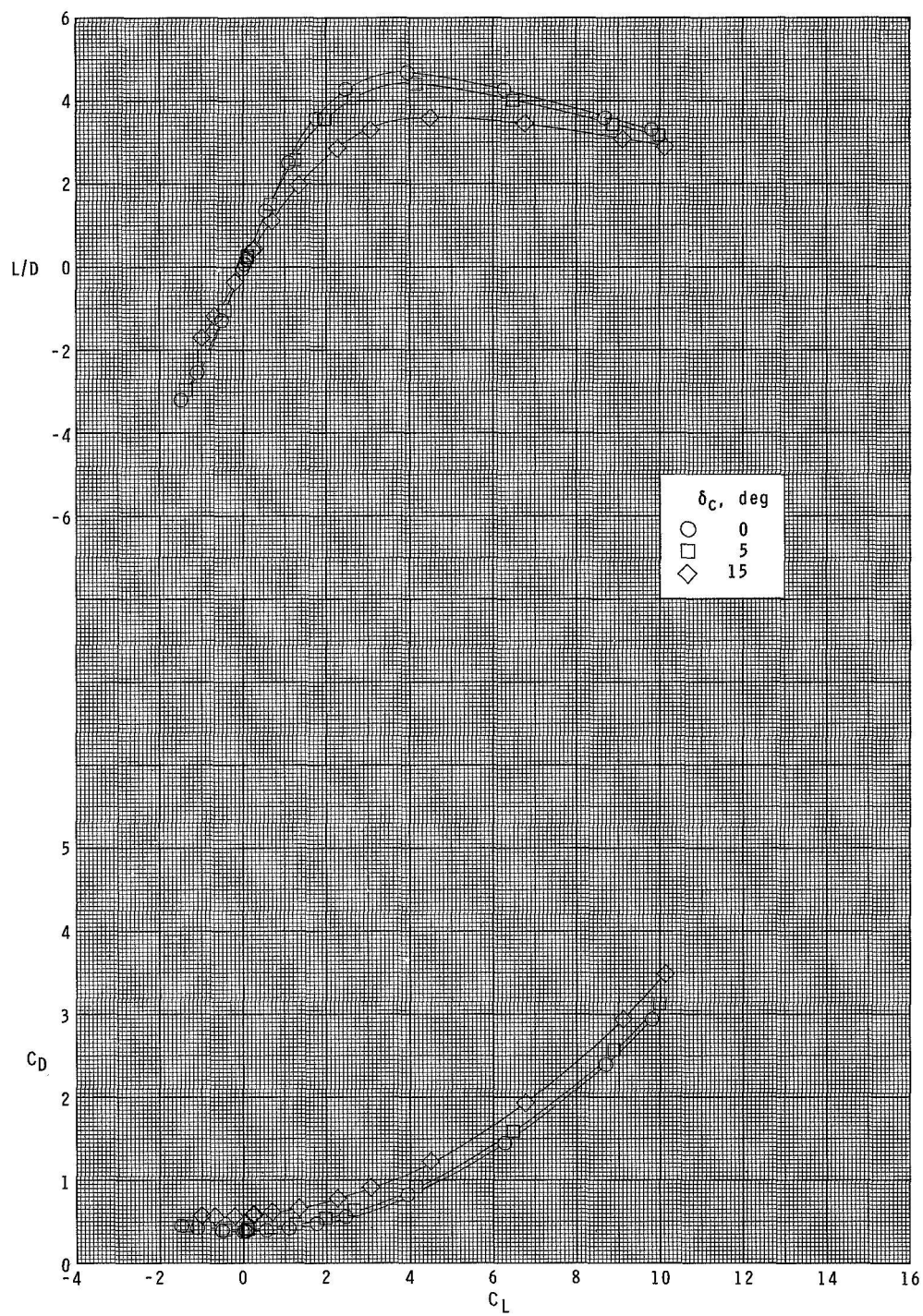
(c) Concluded.

Figure 8.- Concluded.



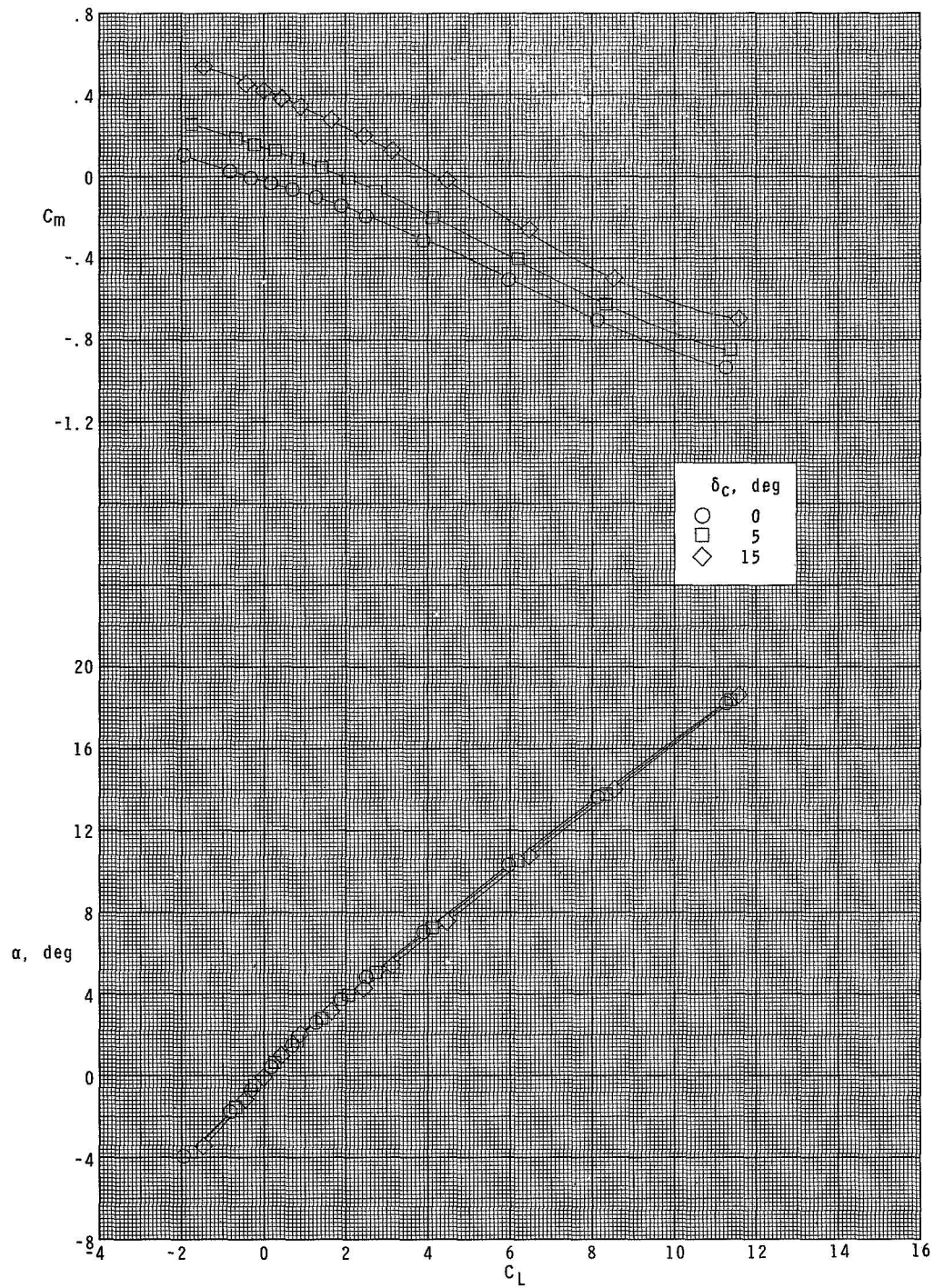
(a) $M = 1.70$.

Figure 9.- Longitudinal control characteristics of configuration $B_1W_2F_1C_1$.



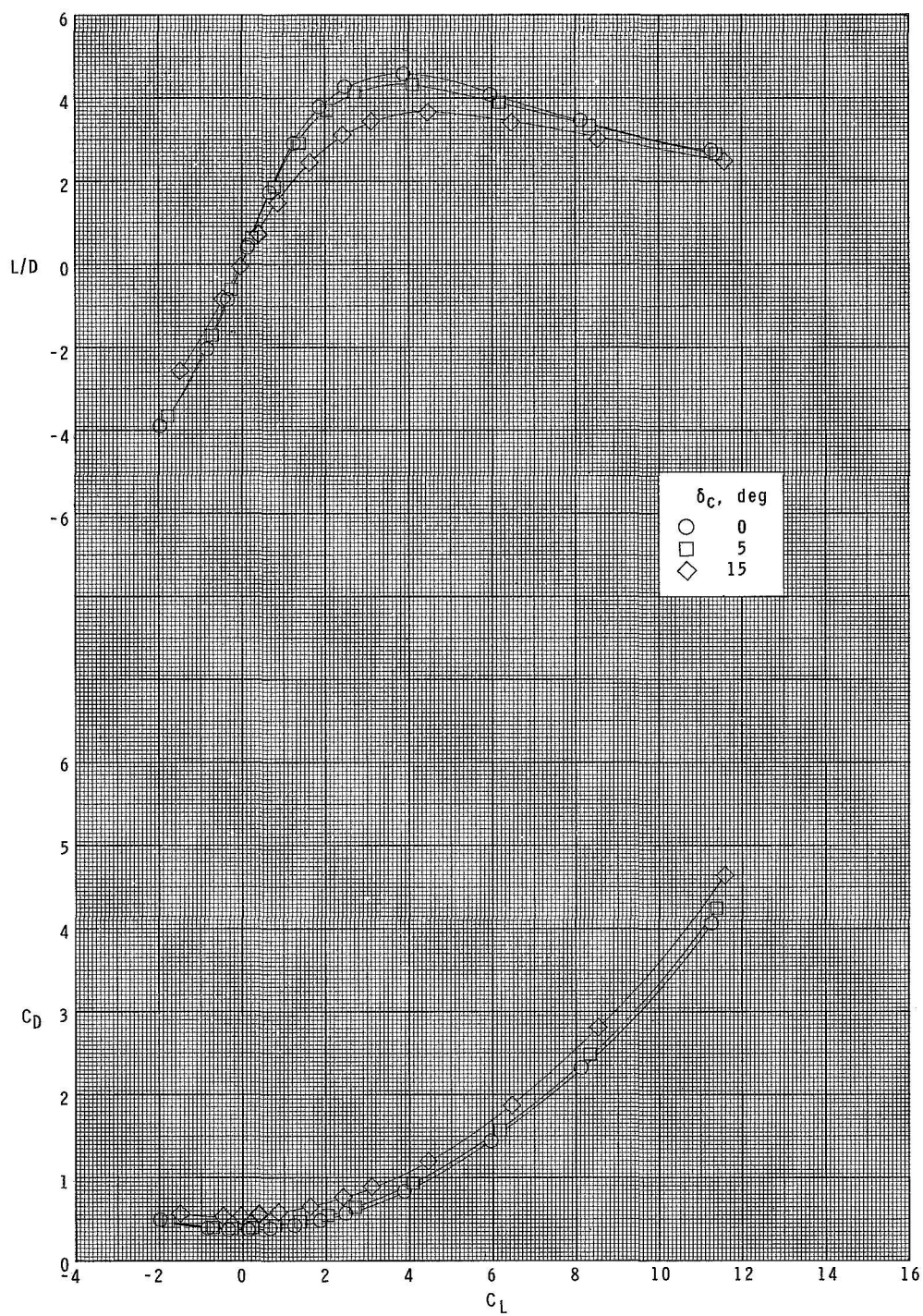
(a) Concluded.

Figure 9.- Continued.



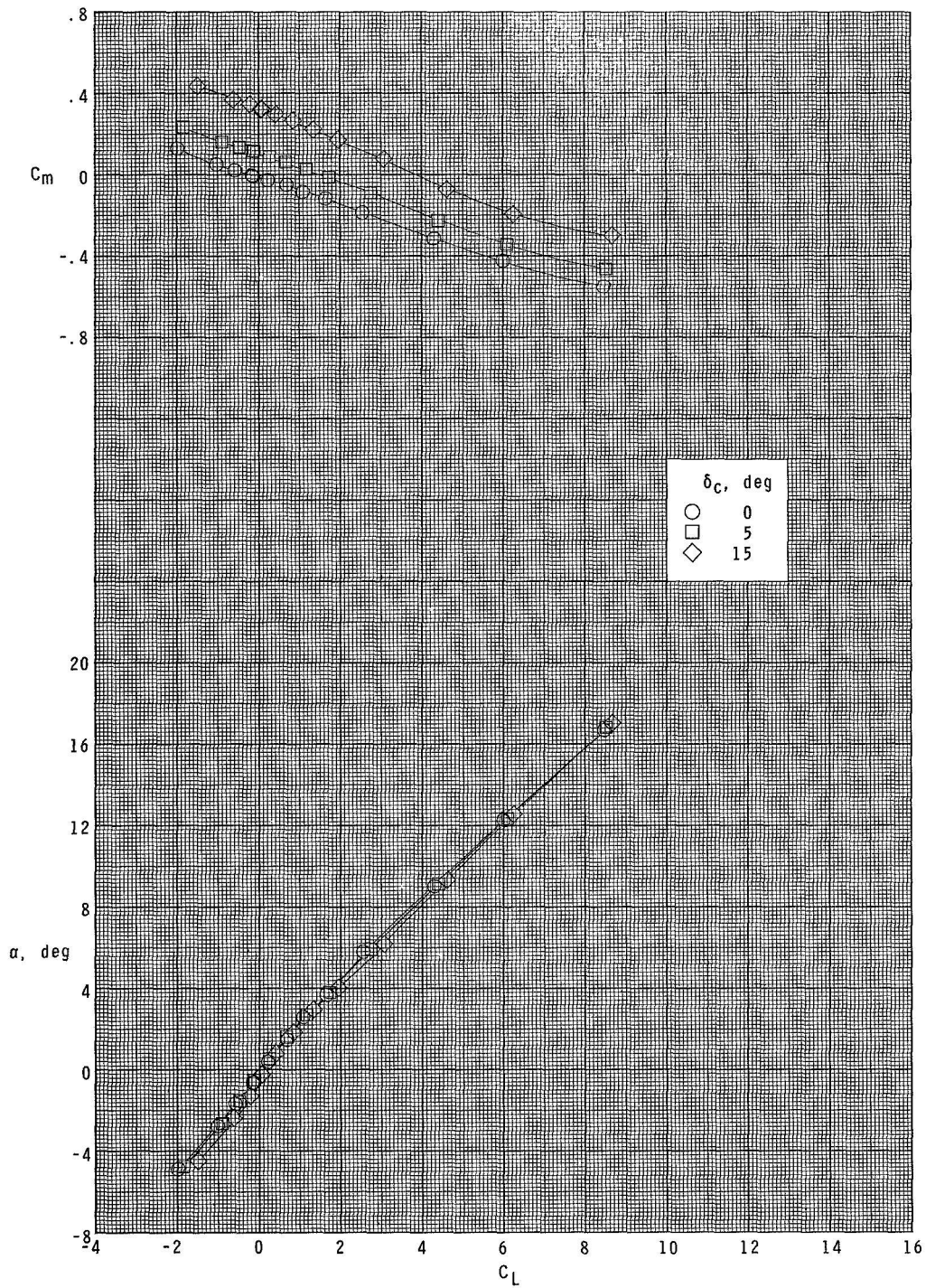
(b) $M = 2.00$.

Figure 9.- Continued.



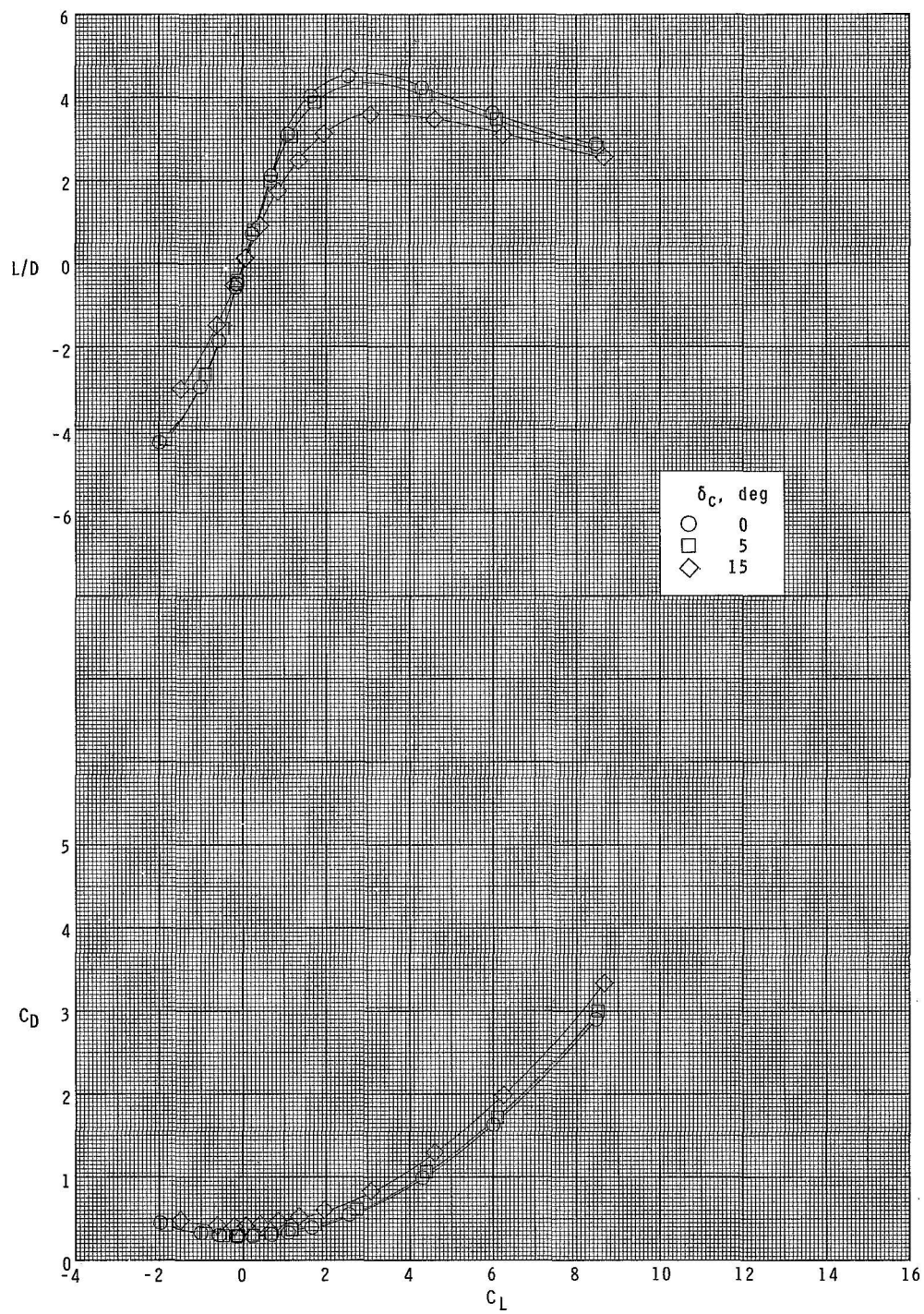
(b) Concluded.

Figure 9.- Continued.



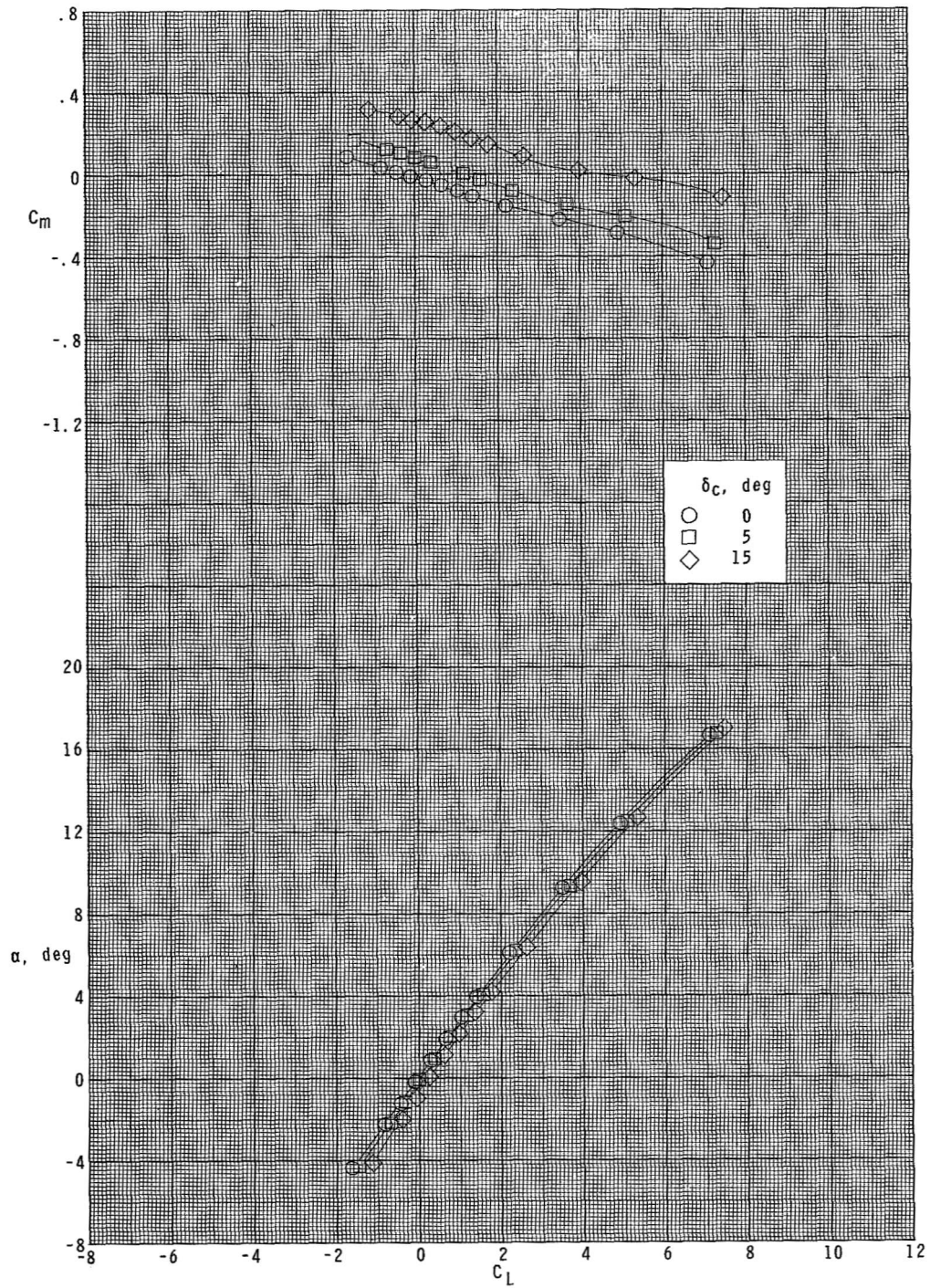
(c) $M = 2.86$.

Figure 9.- Continued.



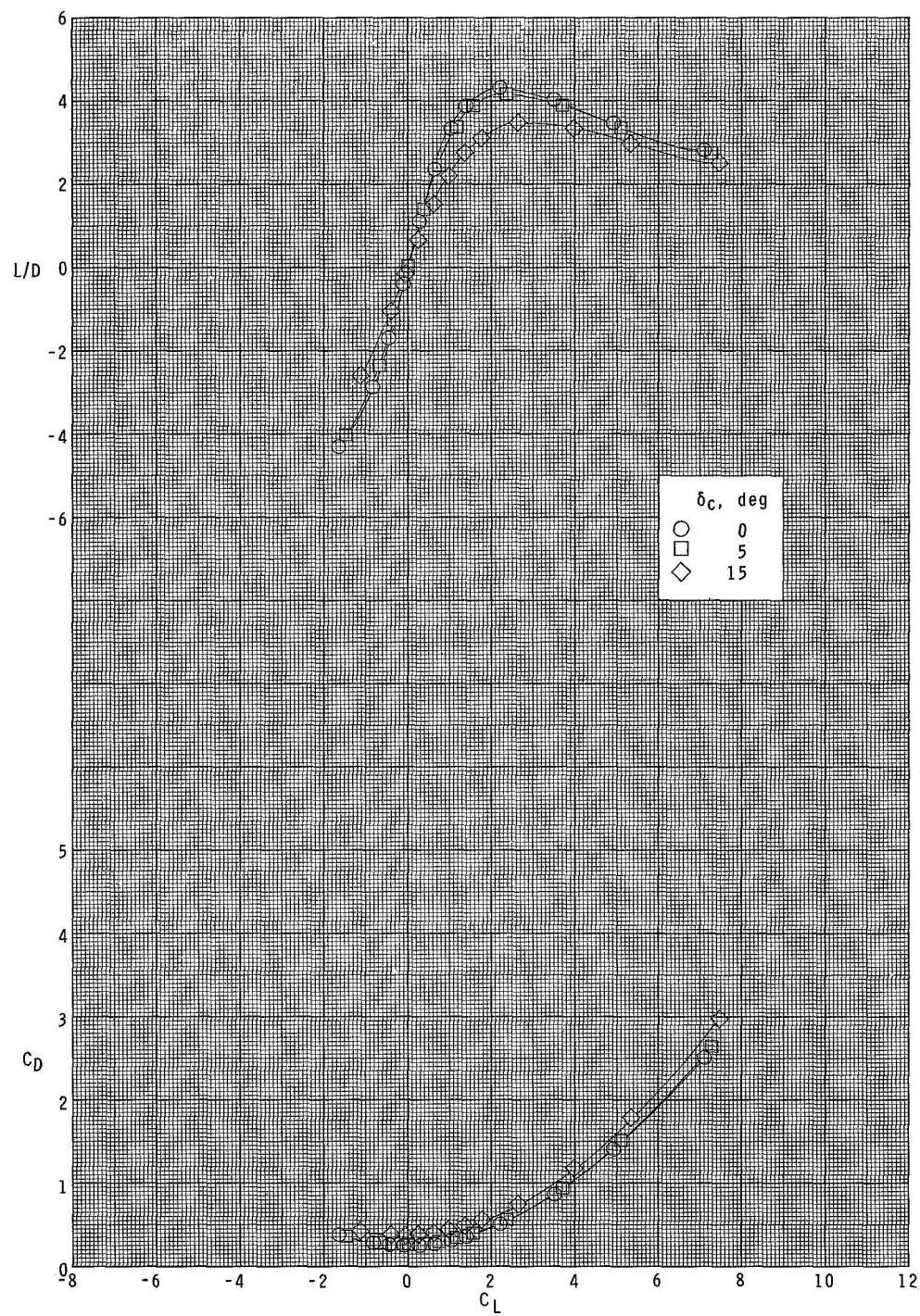
(c) Concluded.

Figure 9.- Continued.



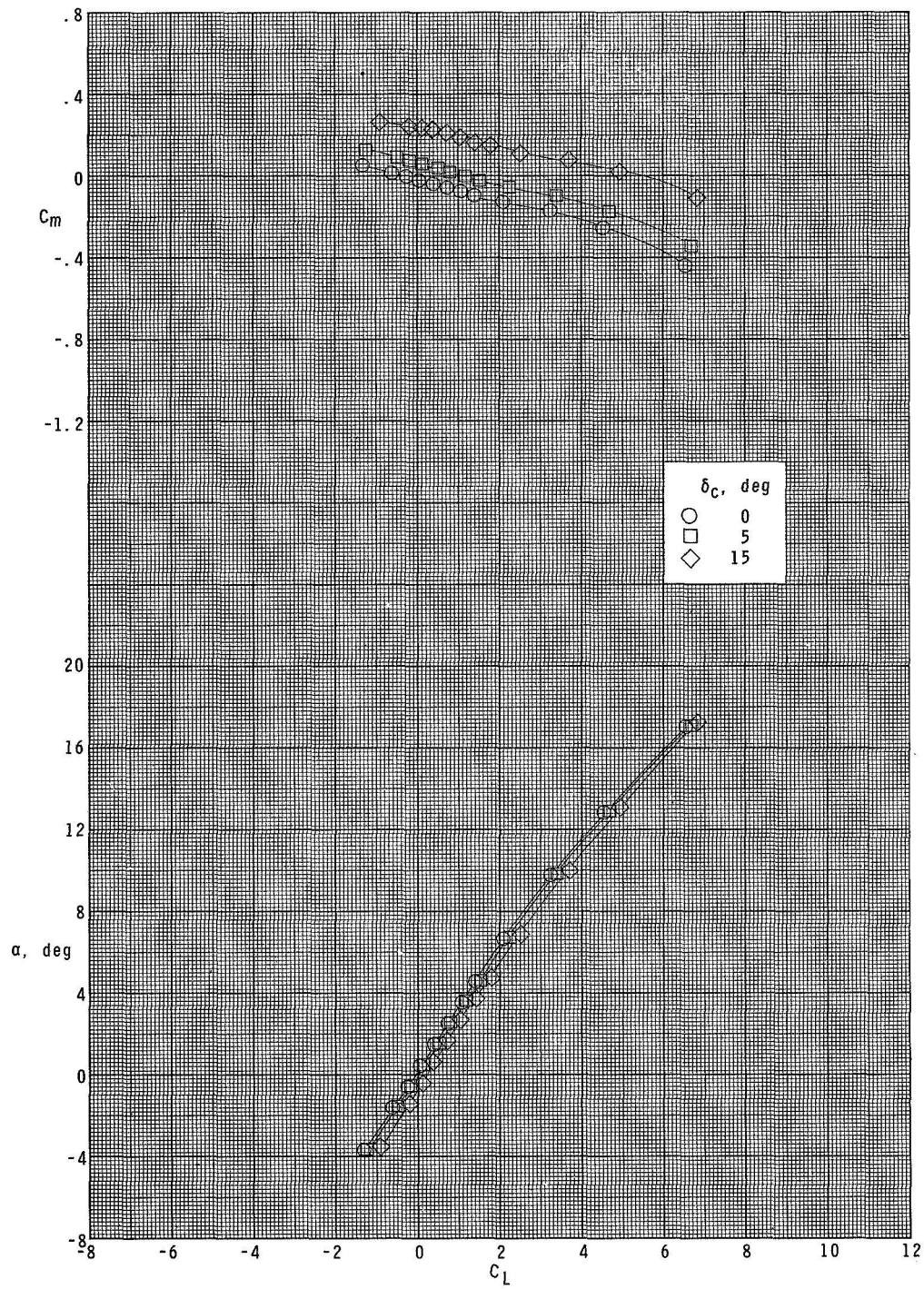
(d) $M = 3.95$.

Figure 9.- Continued.



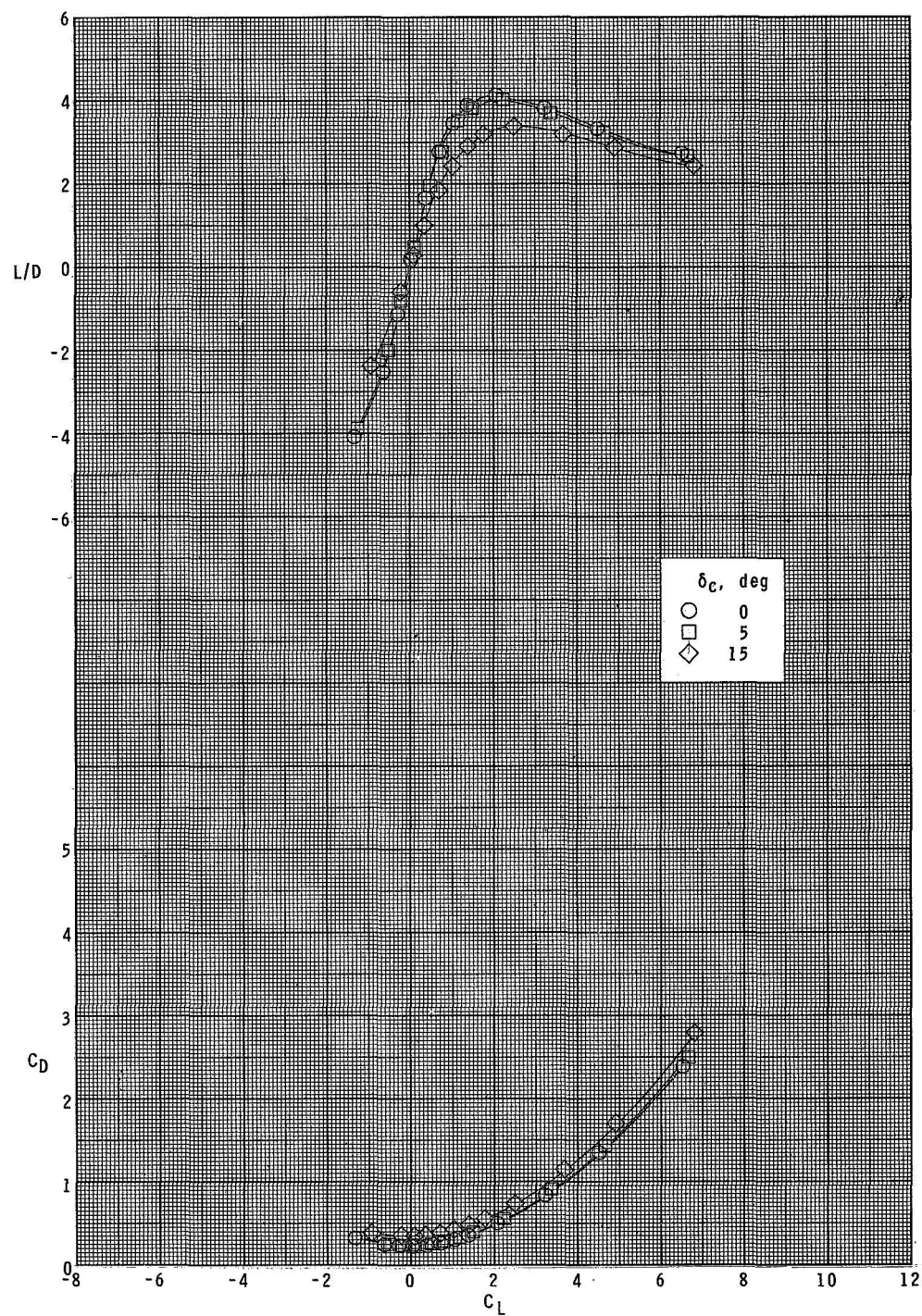
(d) Concluded.

Figure 9.- Continued.



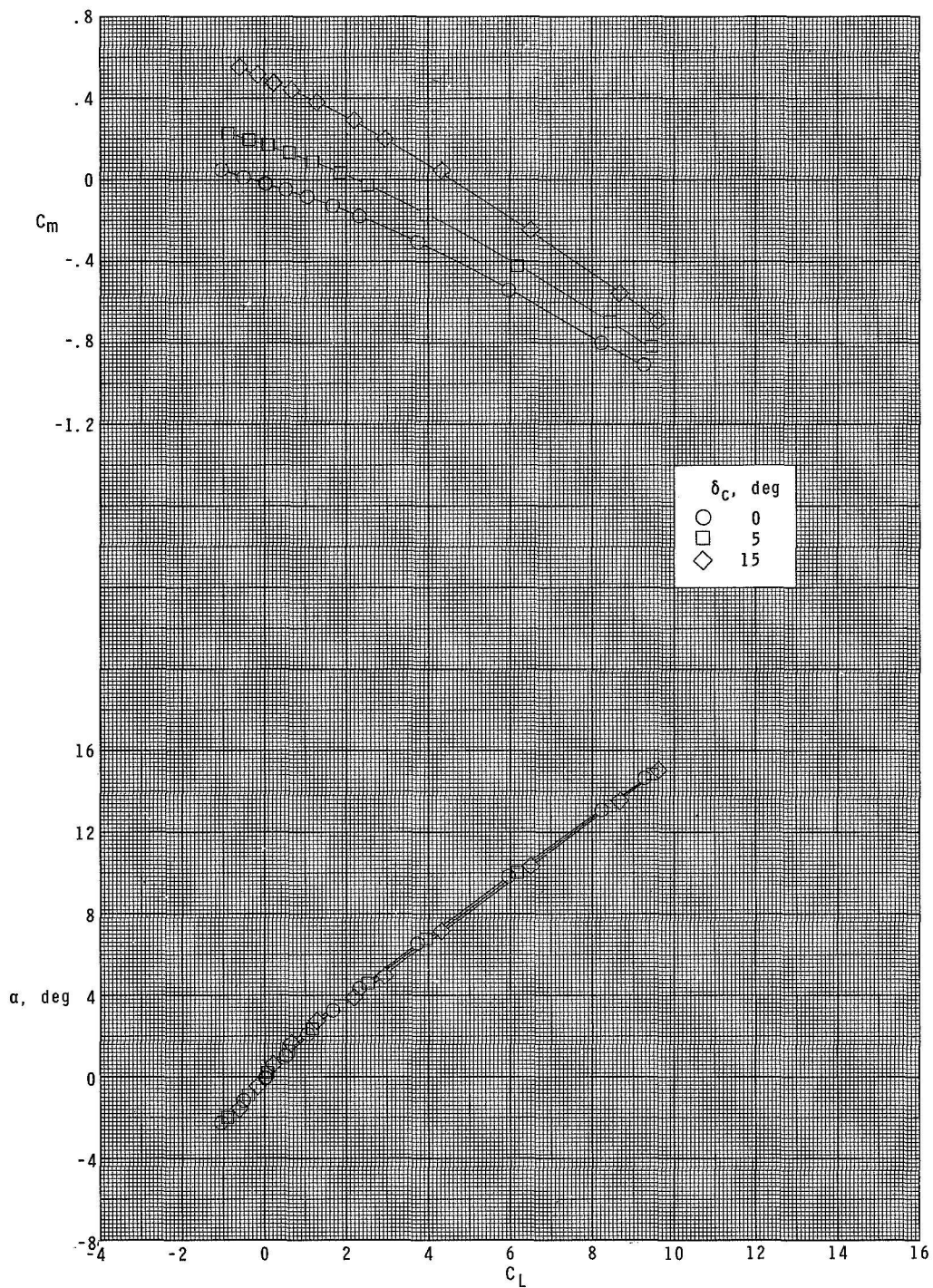
(e) $M = 4.63$.

Figure 9.- Continued.



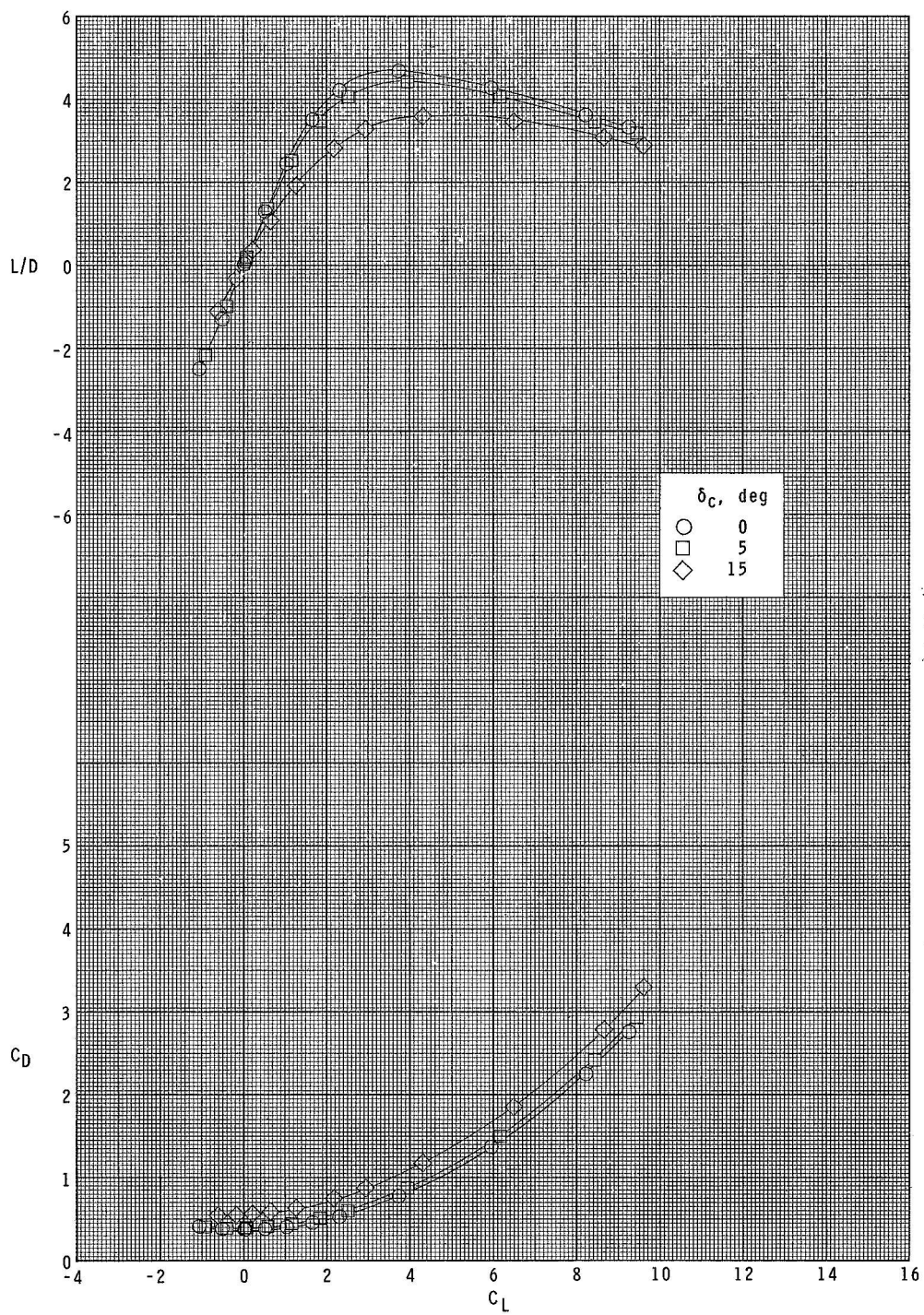
(e) Concluded.

Figure 9.- Concluded.



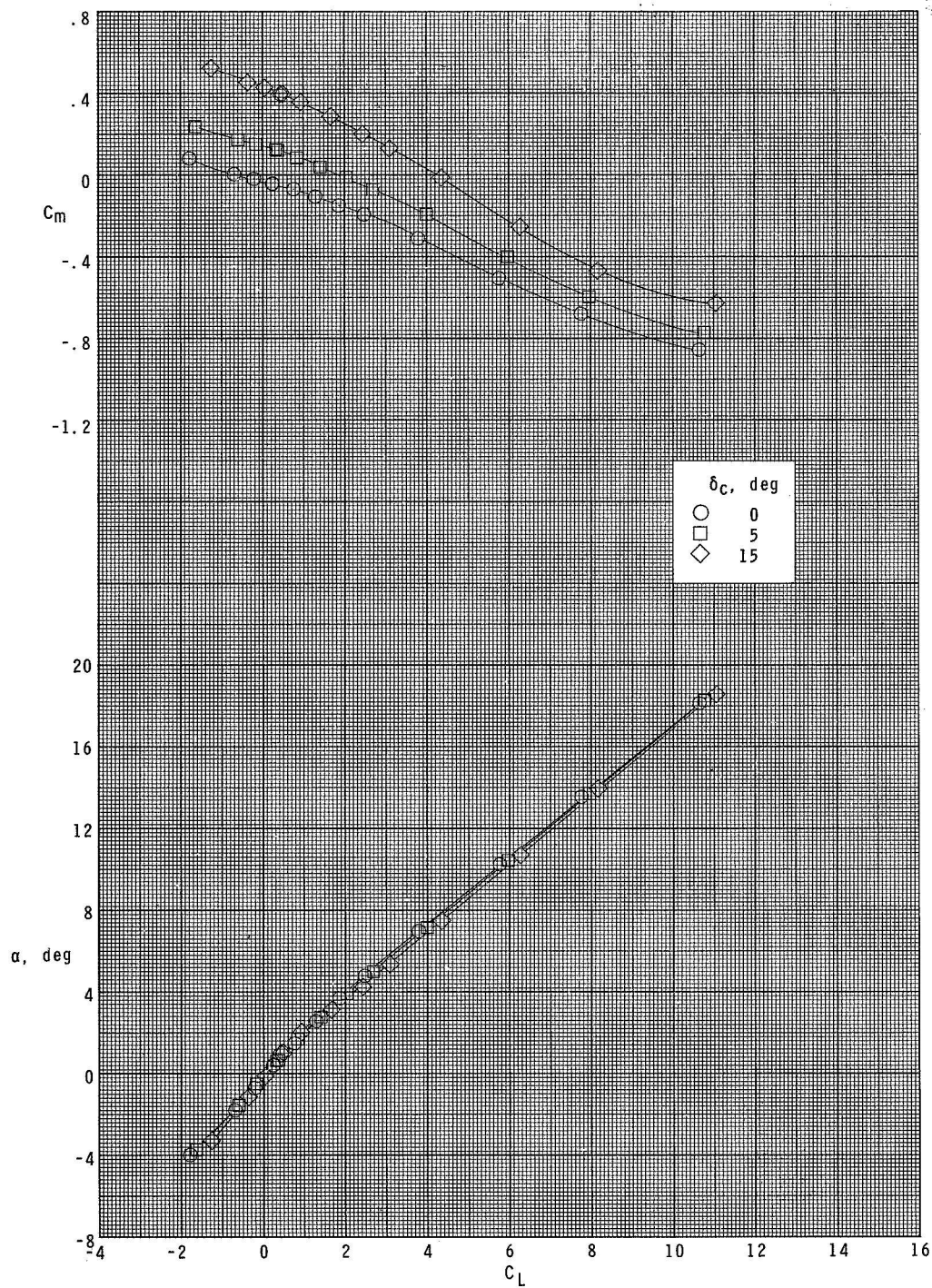
(a) $M = 1.70$.

Figure 10.- Longitudinal control characteristics of configuration $B_1W_1F_2C_1$.



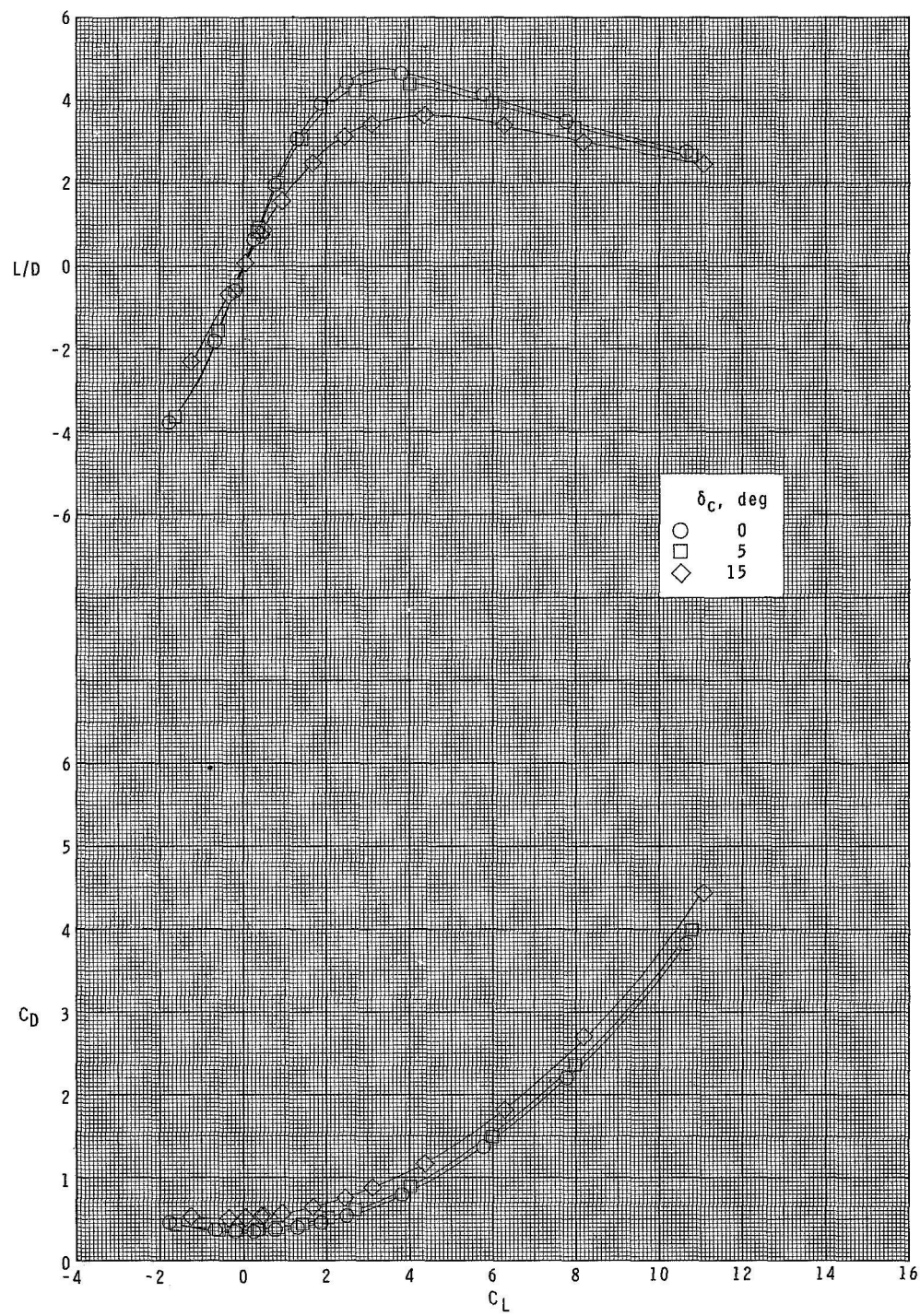
(a) Concluded.

Figure 10.- Continued.



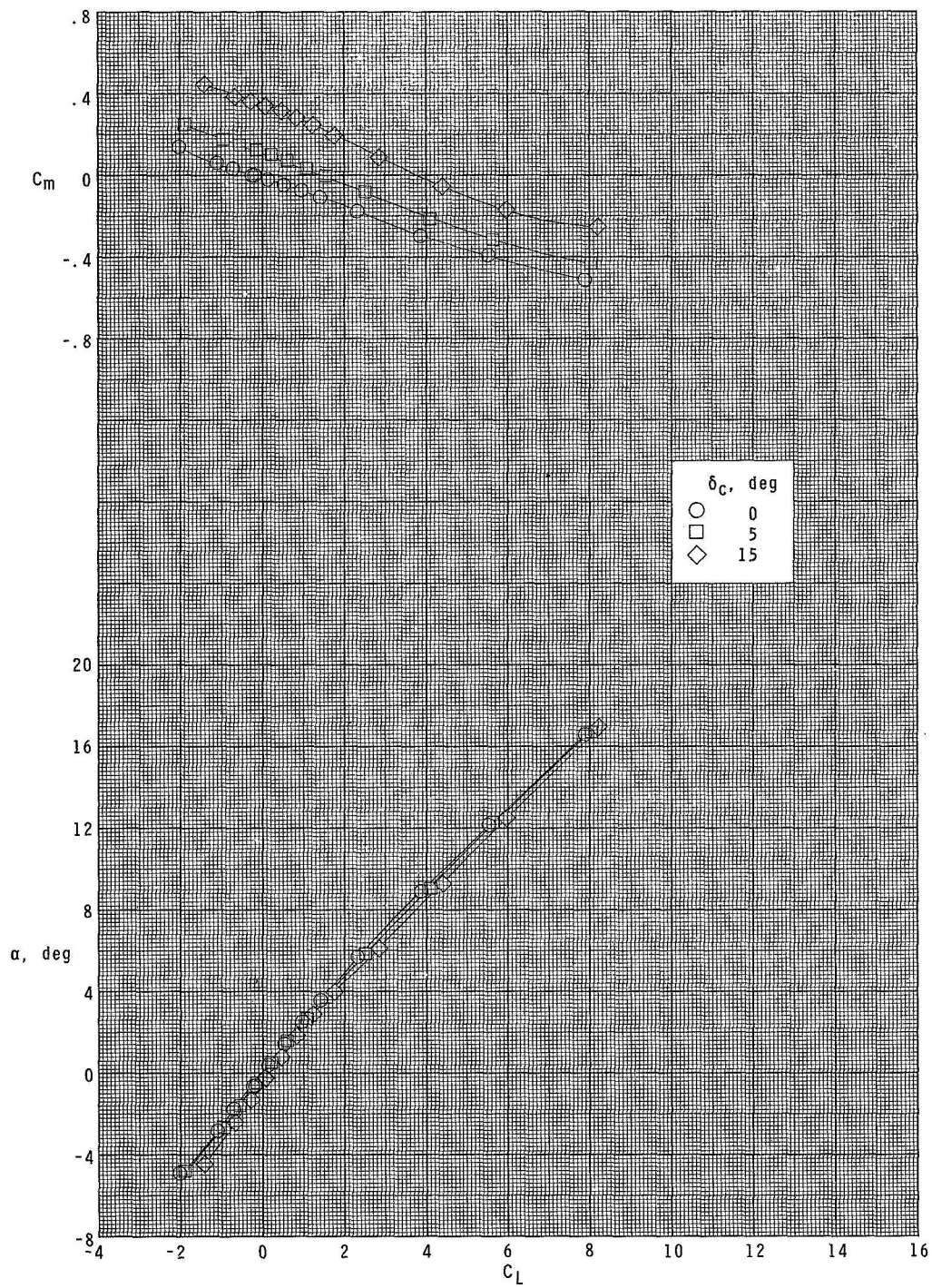
(b) $M = 2.00$.

Figure 10.- Continued.



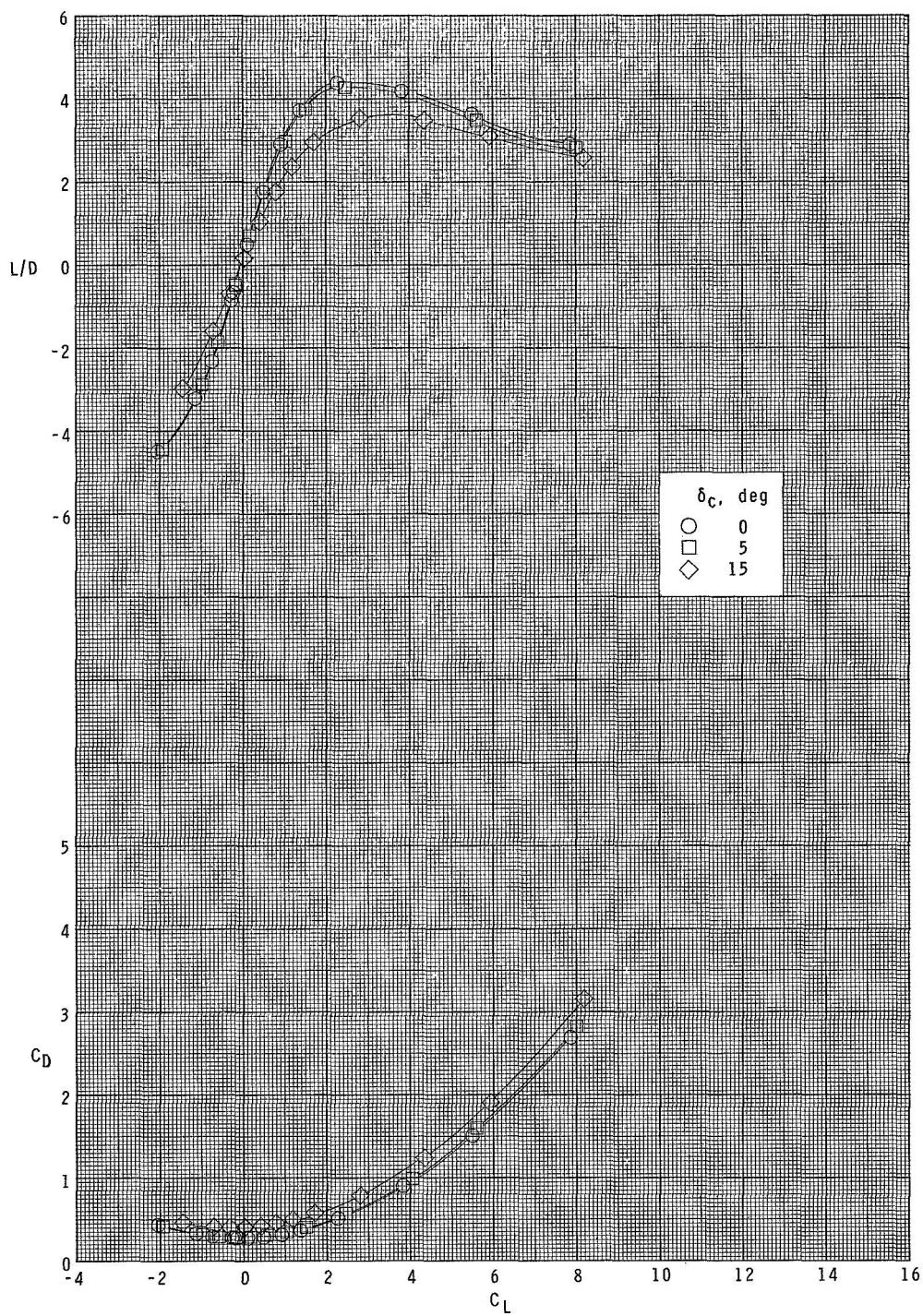
(b) Concluded.

Figure 10.- Continued.



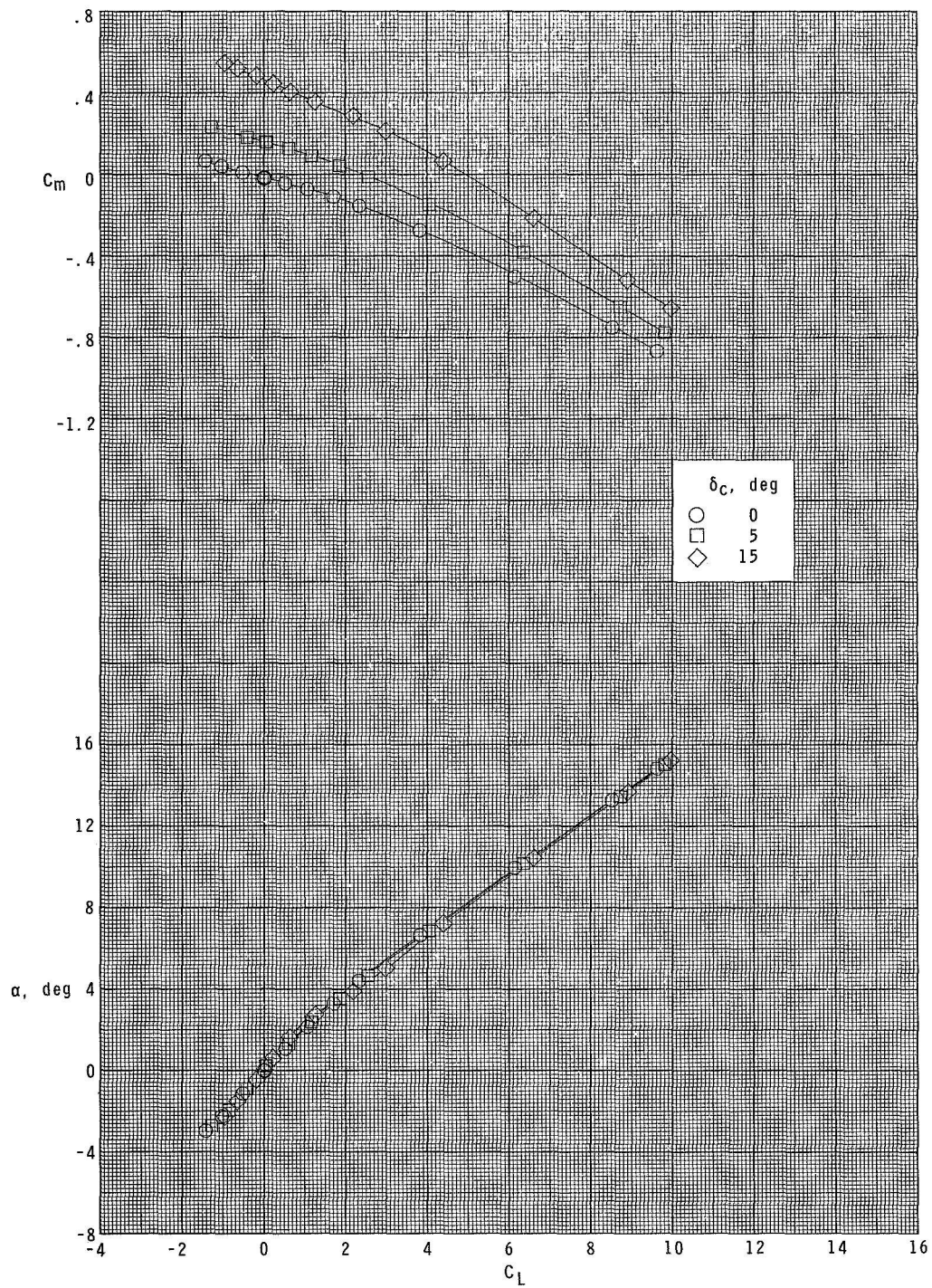
(c) $M = 2.86$.

Figure 10.- Continued.



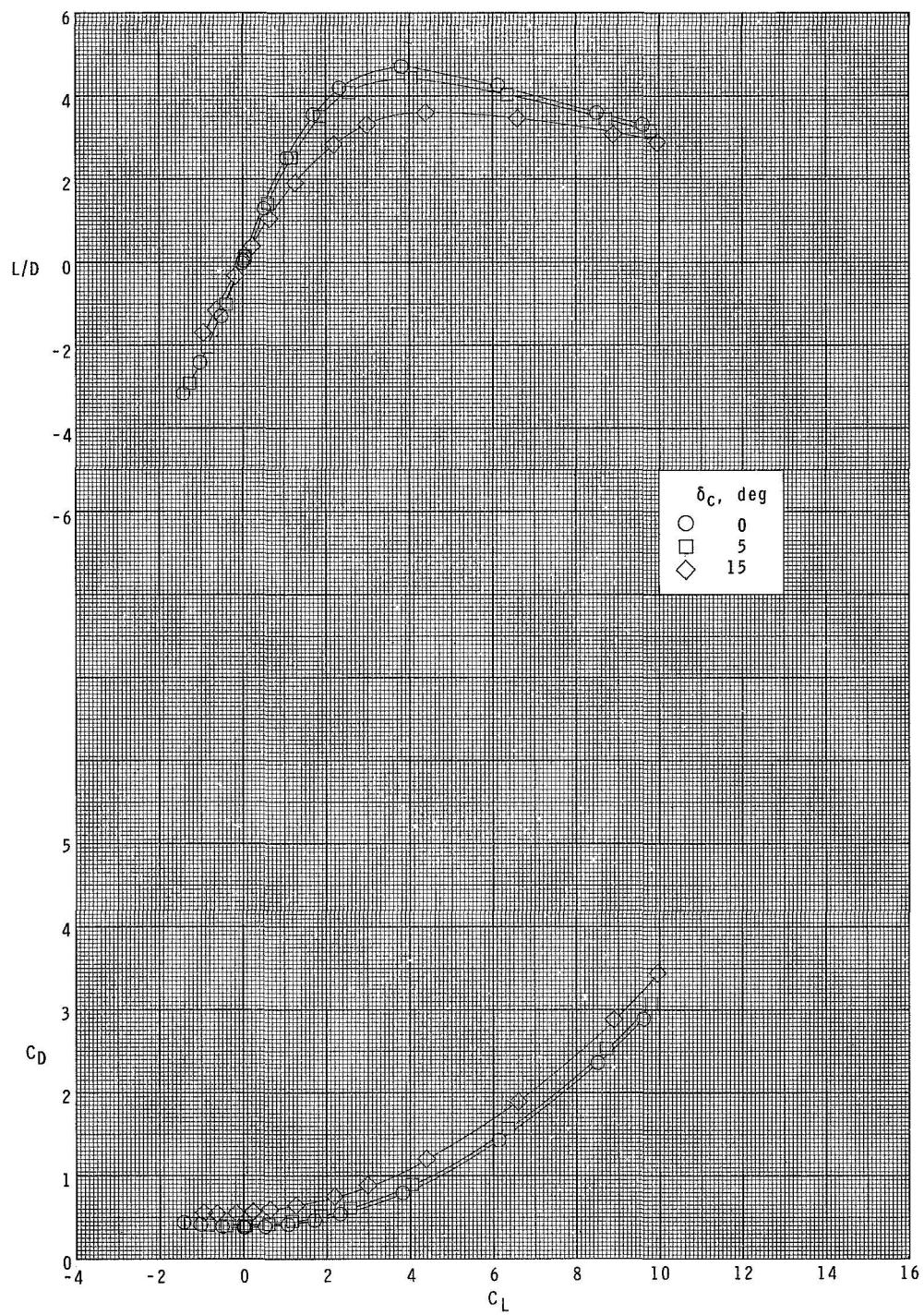
(c) Concluded.

Figure 10.- Concluded.



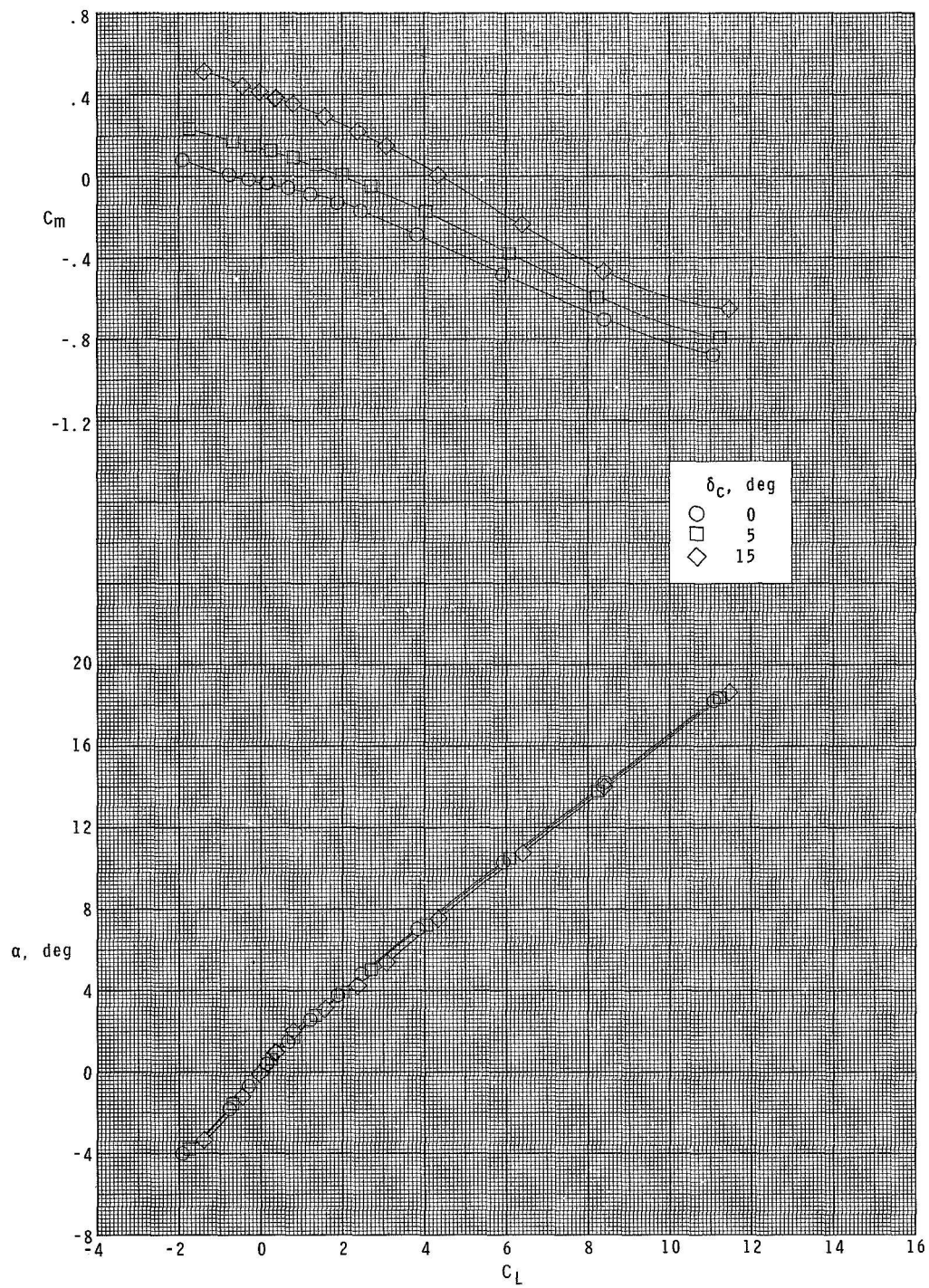
(a) $M \approx 1.70$.

Figure 11.- Longitudinal control characteristics of configuration $B_1W_2F_2C_1$.



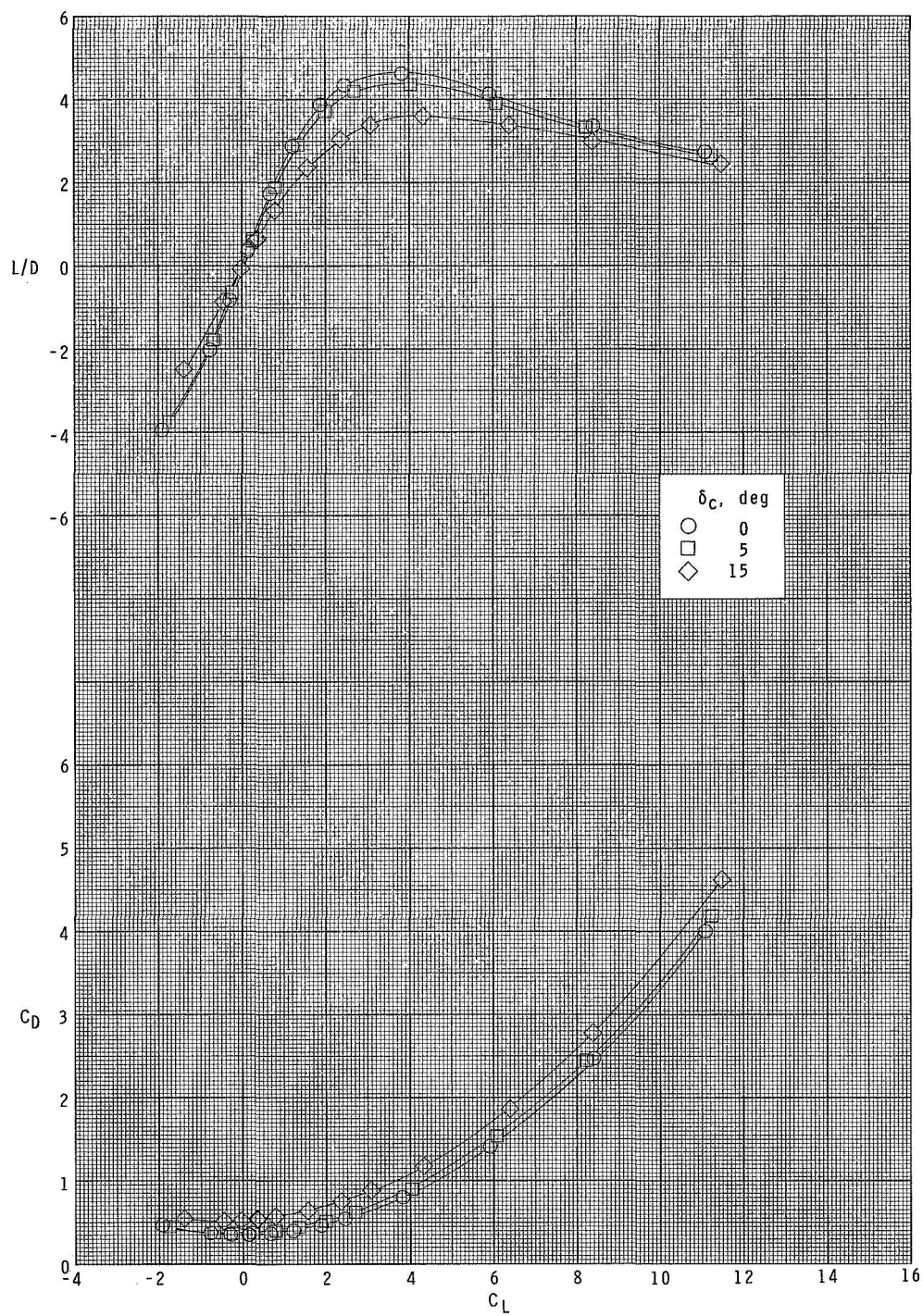
(a) Concluded.

Figure 11.- Continued.



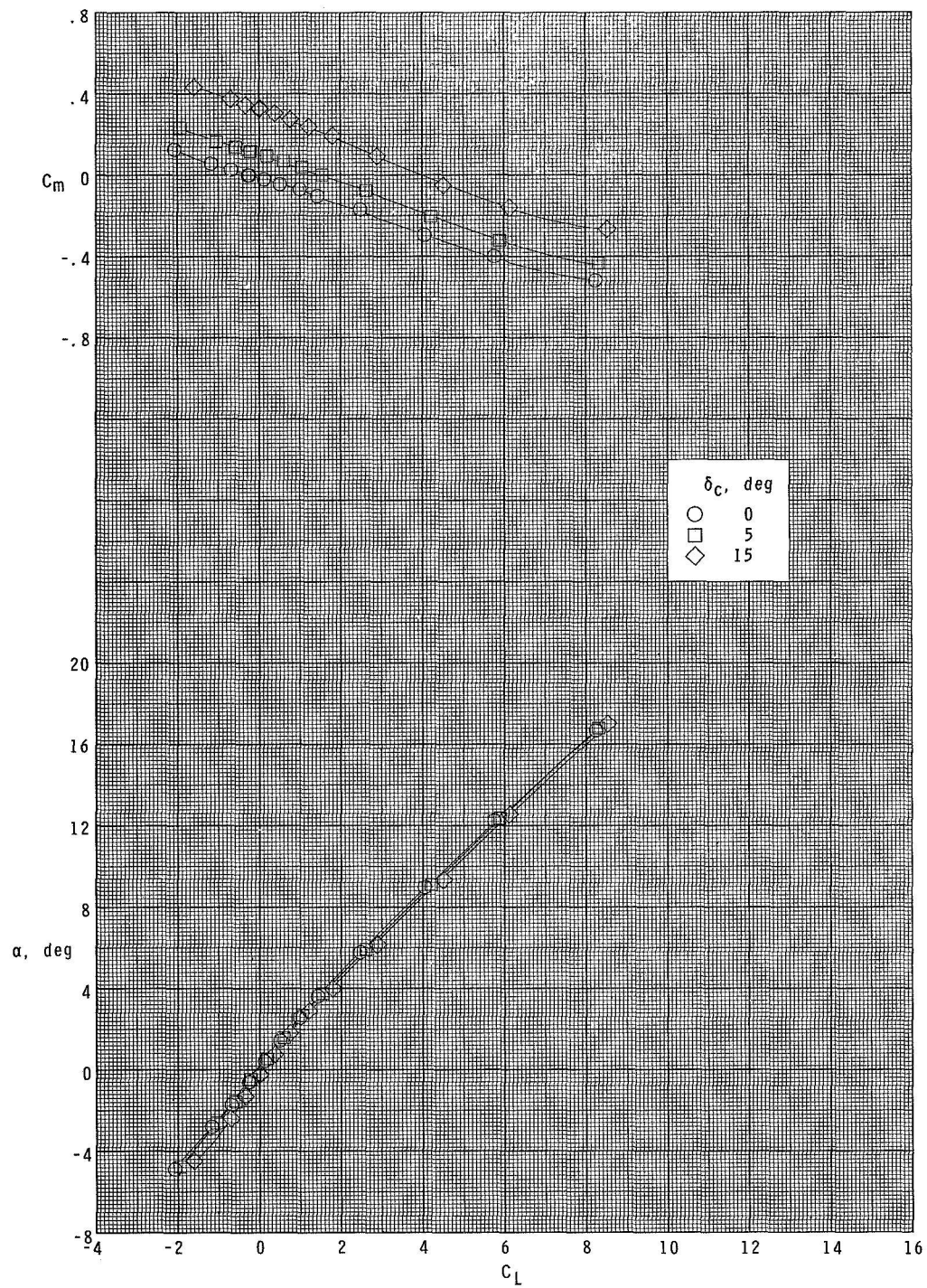
(b) $M = 2.00$.

Figure 11.- Continued.



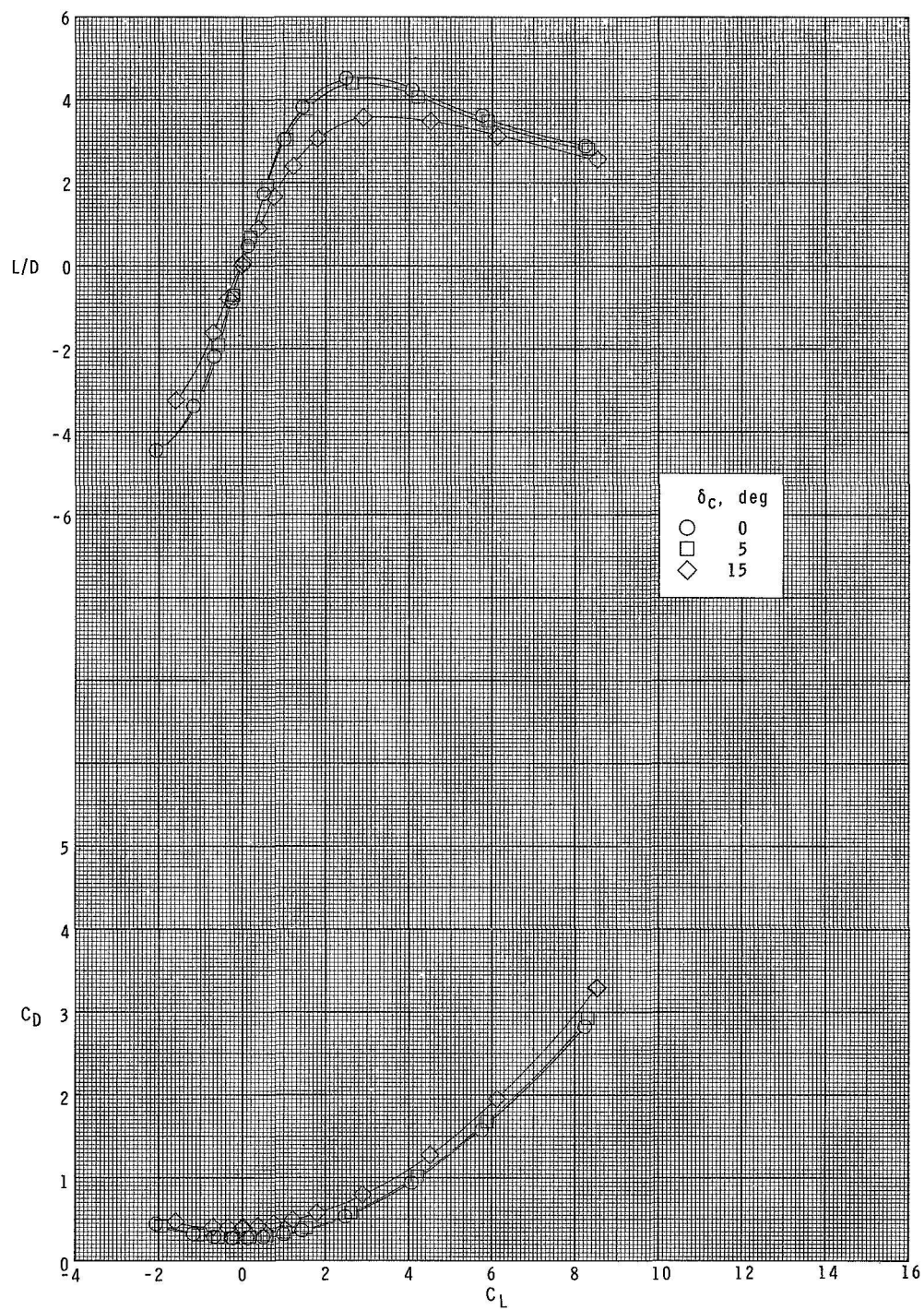
(b) Concluded.

Figure 11.- Continued.



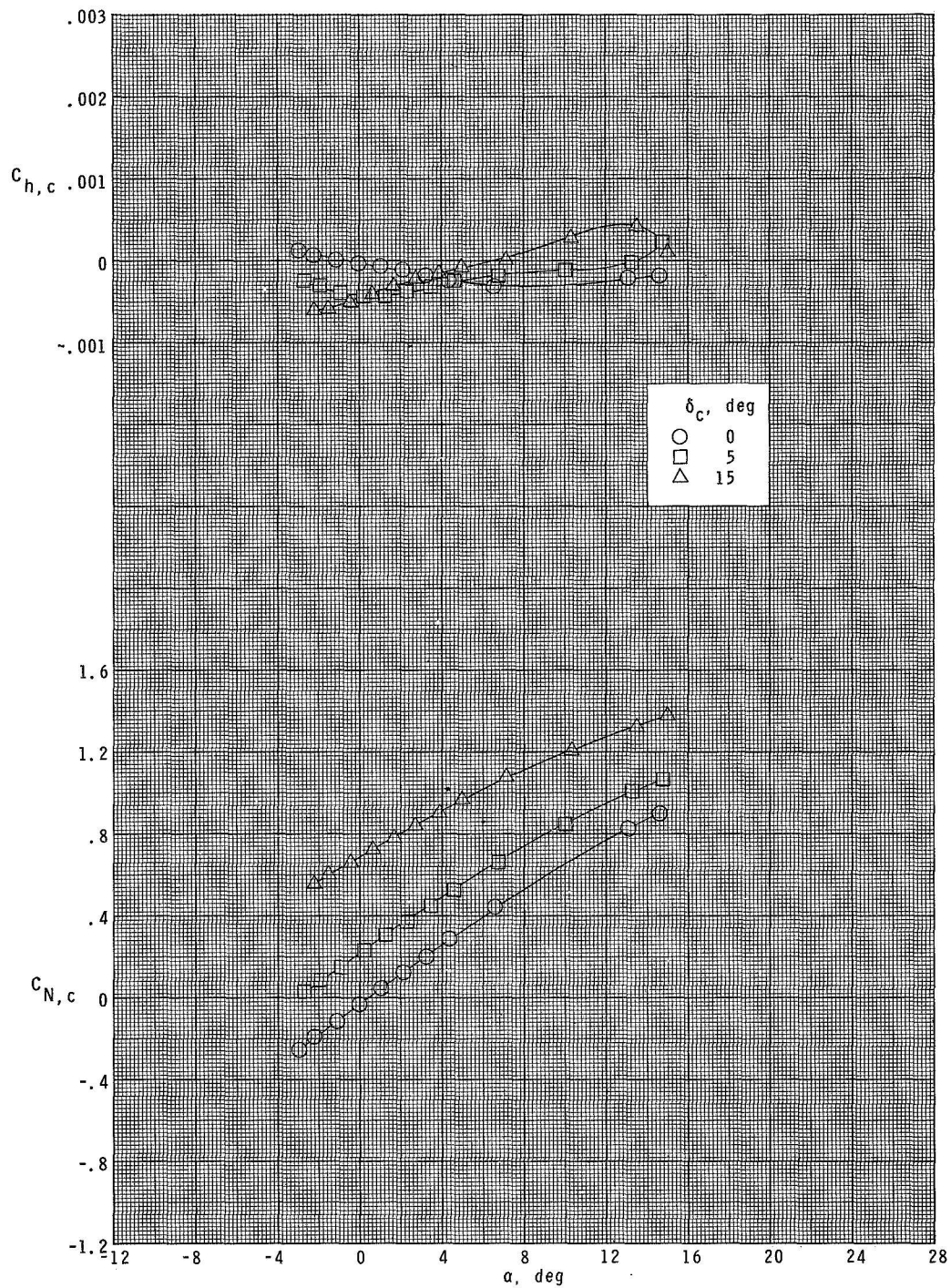
(c) $M = 2.86$.

Figure 11.- Continued.



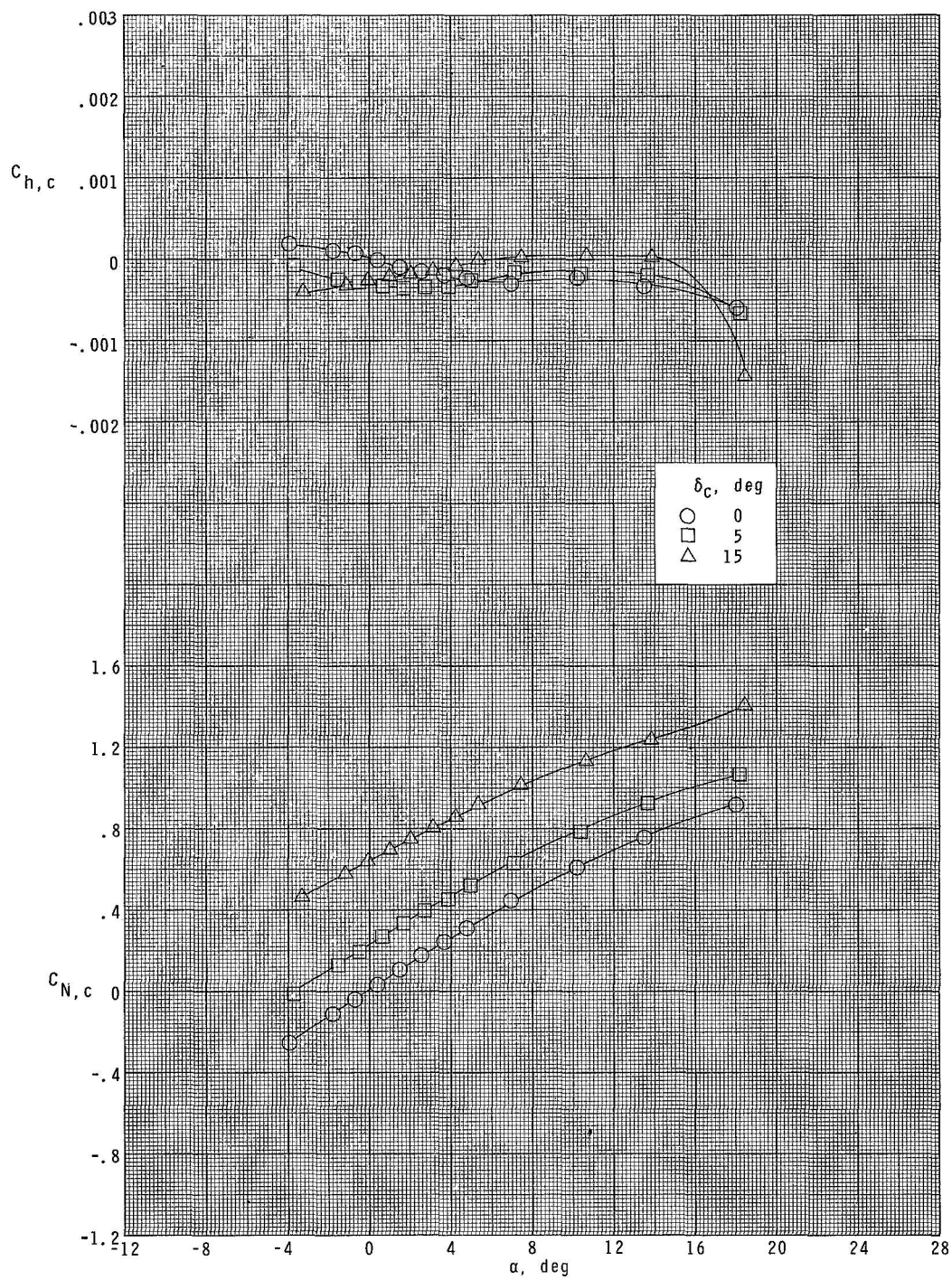
(c) Concluded.

Figure 11.- Concluded.



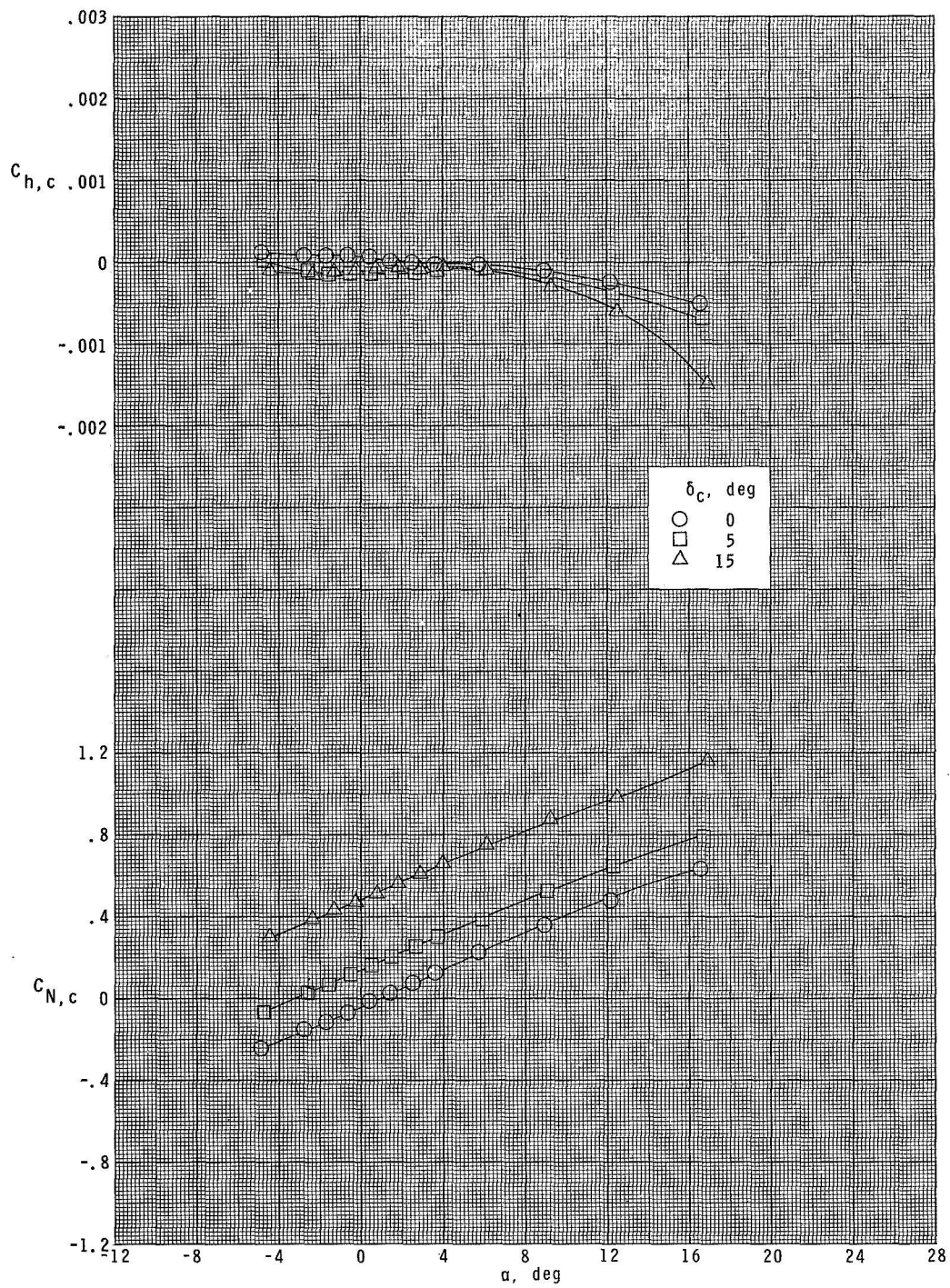
(a) $M = 1.70$.

Figure 12.- Canard normal-force and hinge-moment coefficients for configuration B₁W₁F₁C₁.



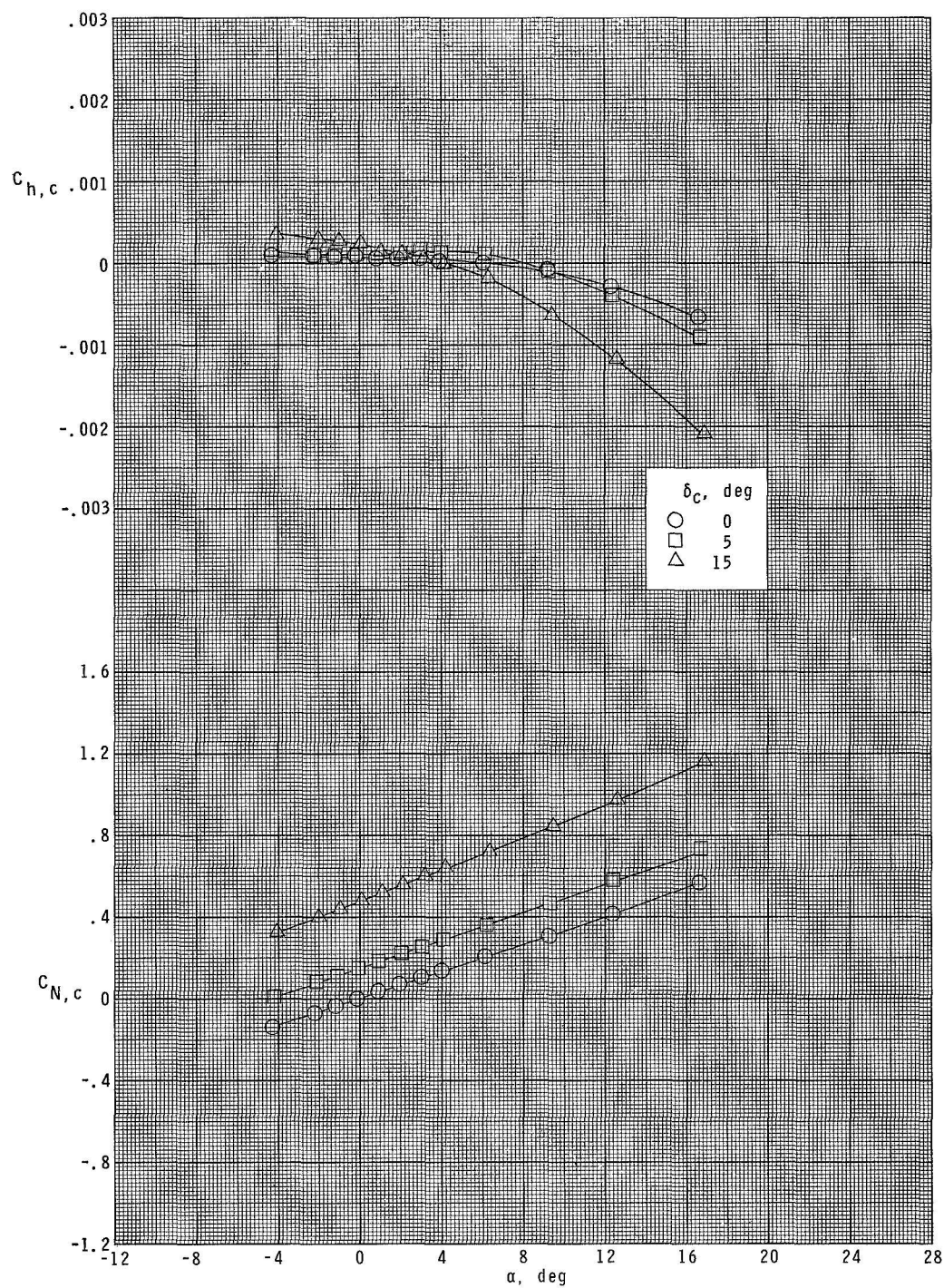
(b) $M = 2.00$.

Figure 12.- Continued.



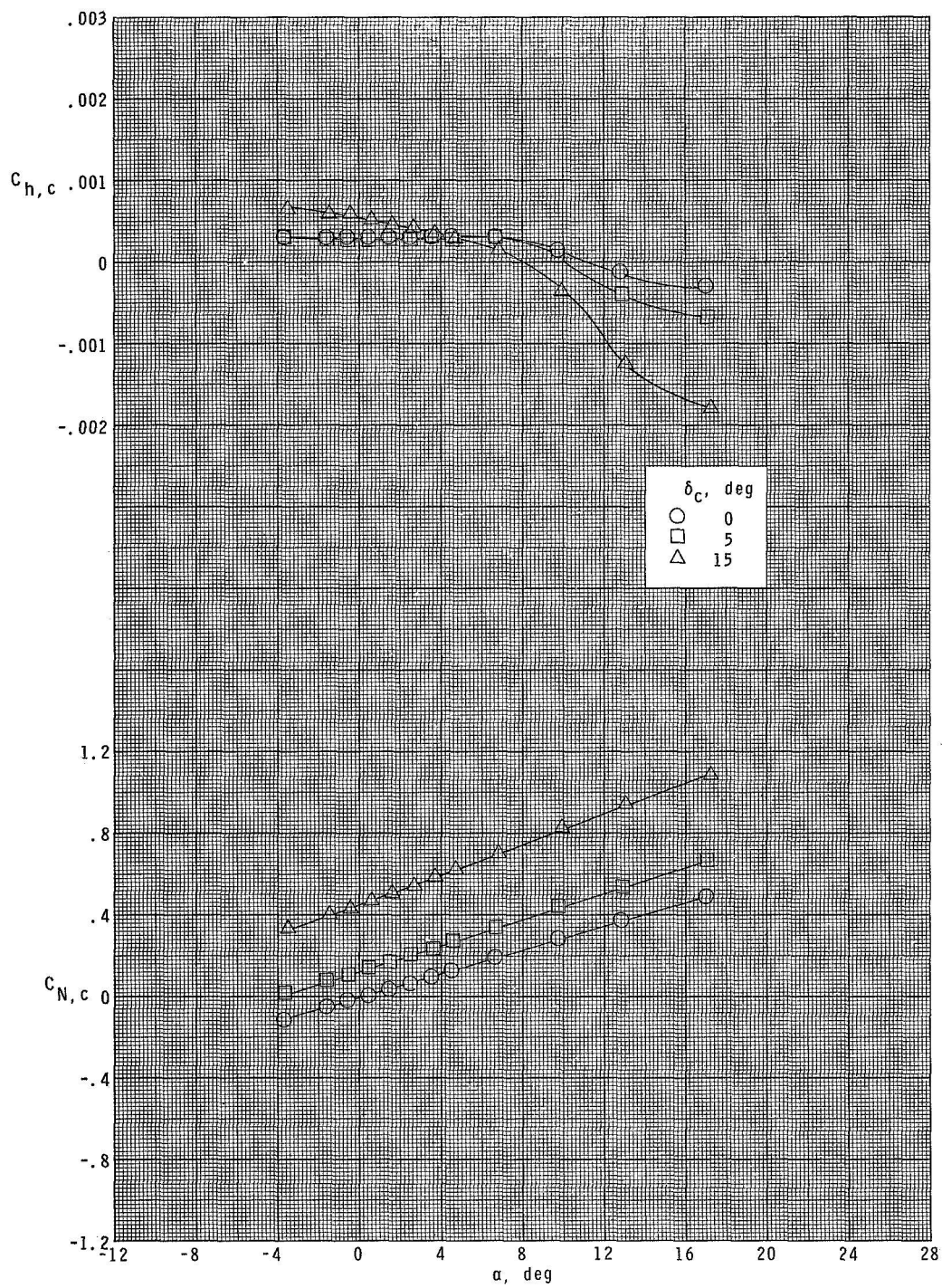
(c) $M = 2.86$.

Figure 12.- Continued.



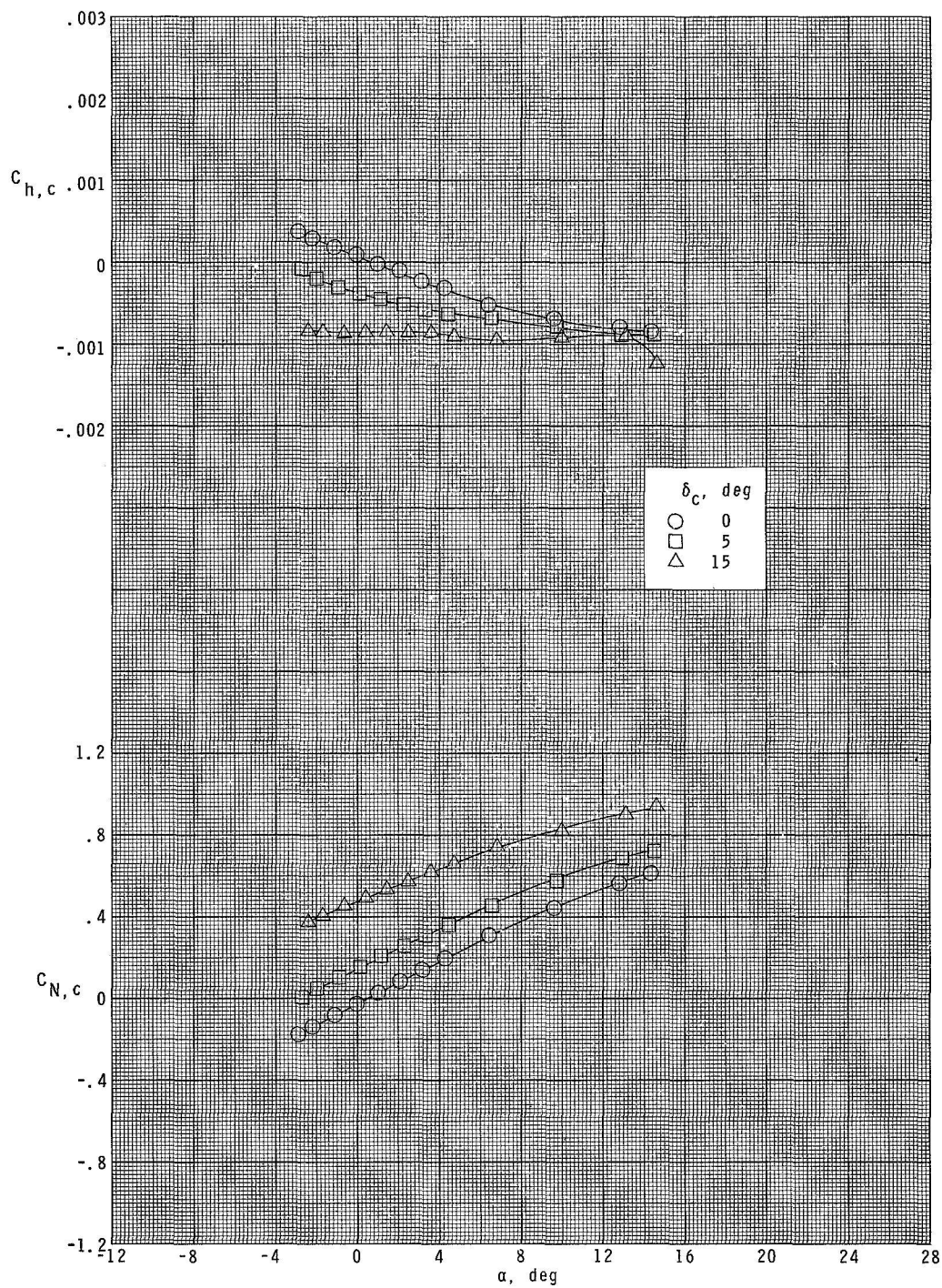
(d) $M = 3.95$.

Figure 12.- Continued.



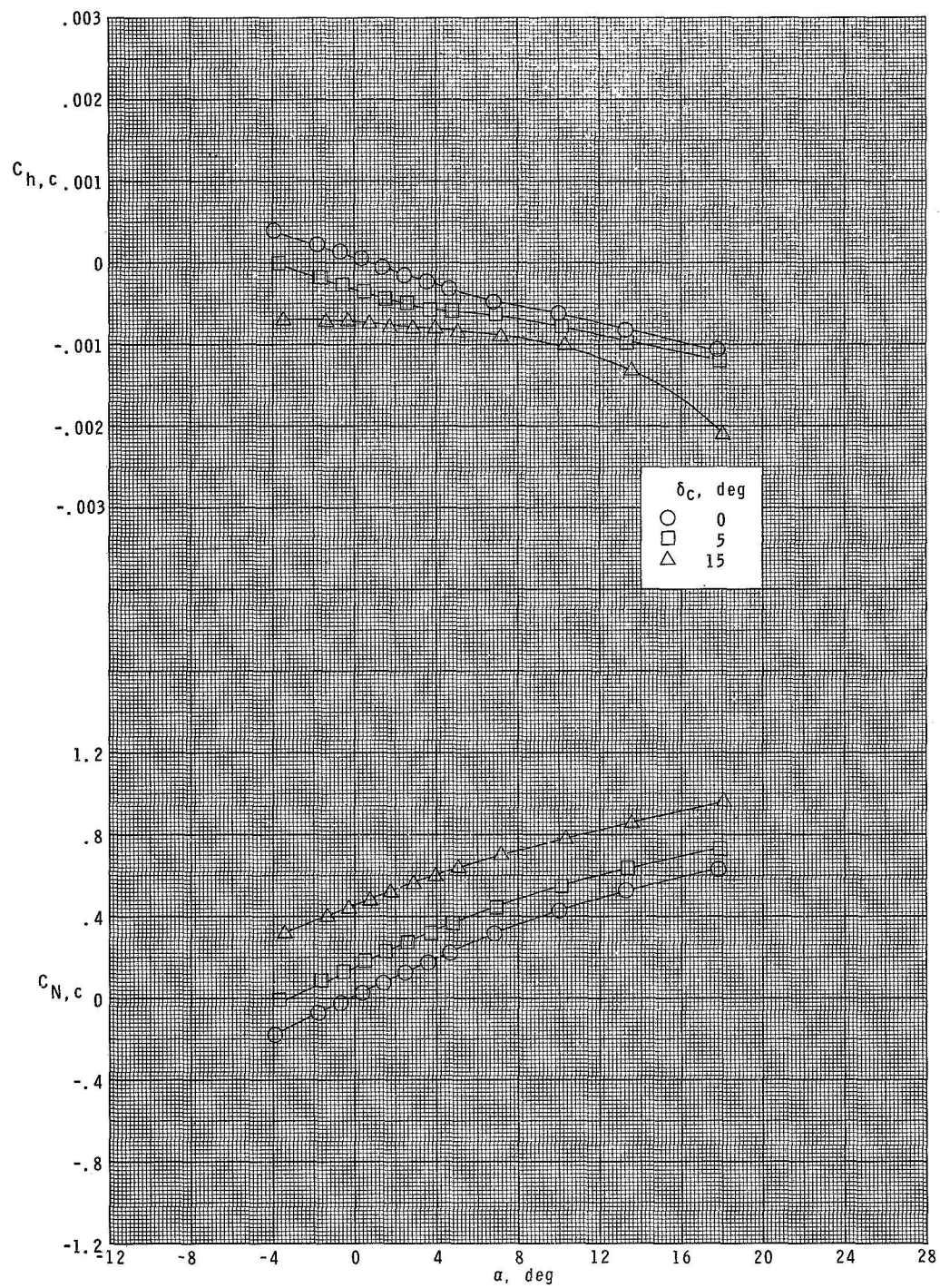
(e) $M = 4.63$.

Figure 12.- Concluded.



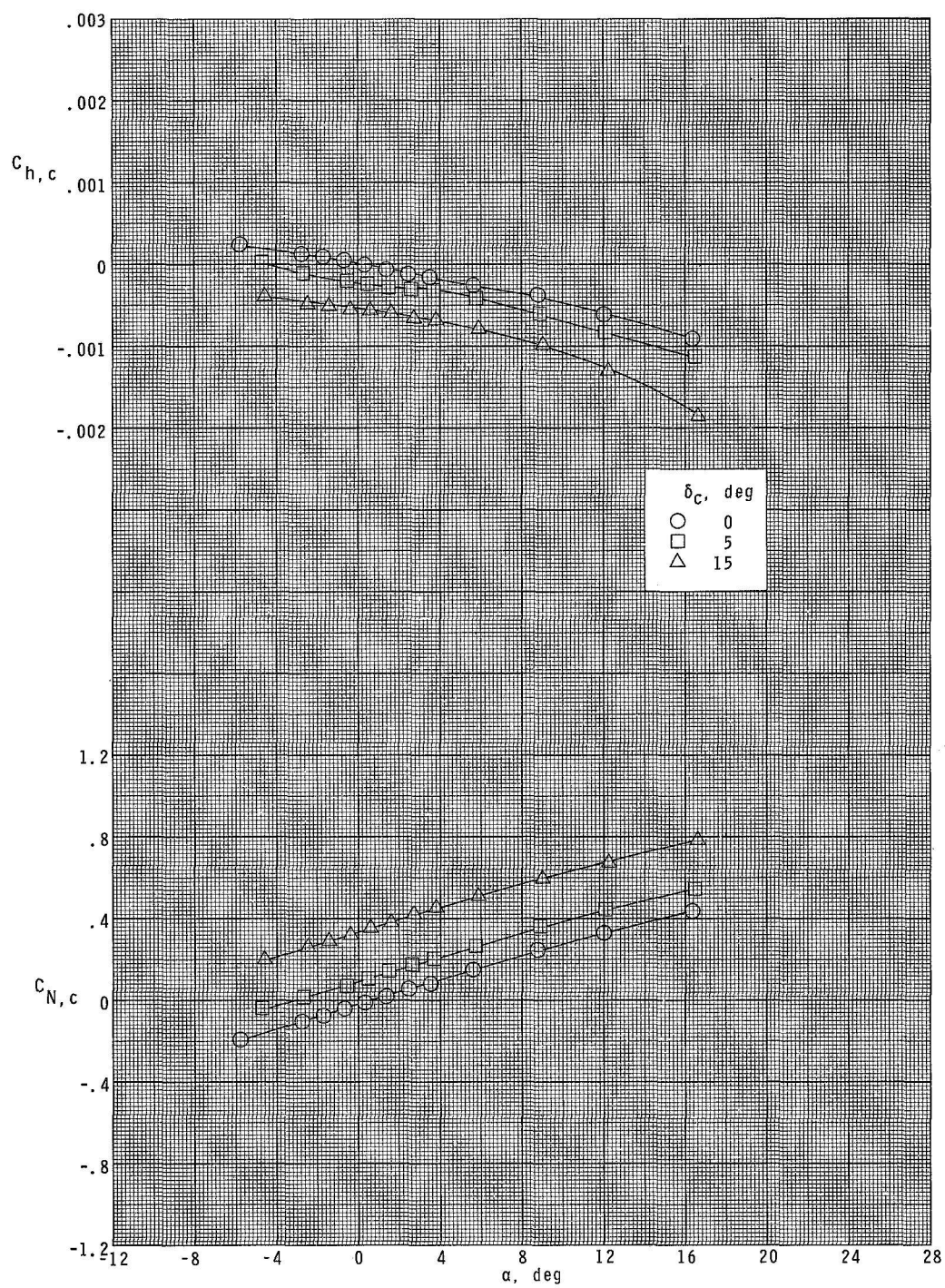
(a) $M = 1.70$.

Figure 13.- Canard normal-force and hinge-moment coefficients for configuration B₁W₁F₁C₂.



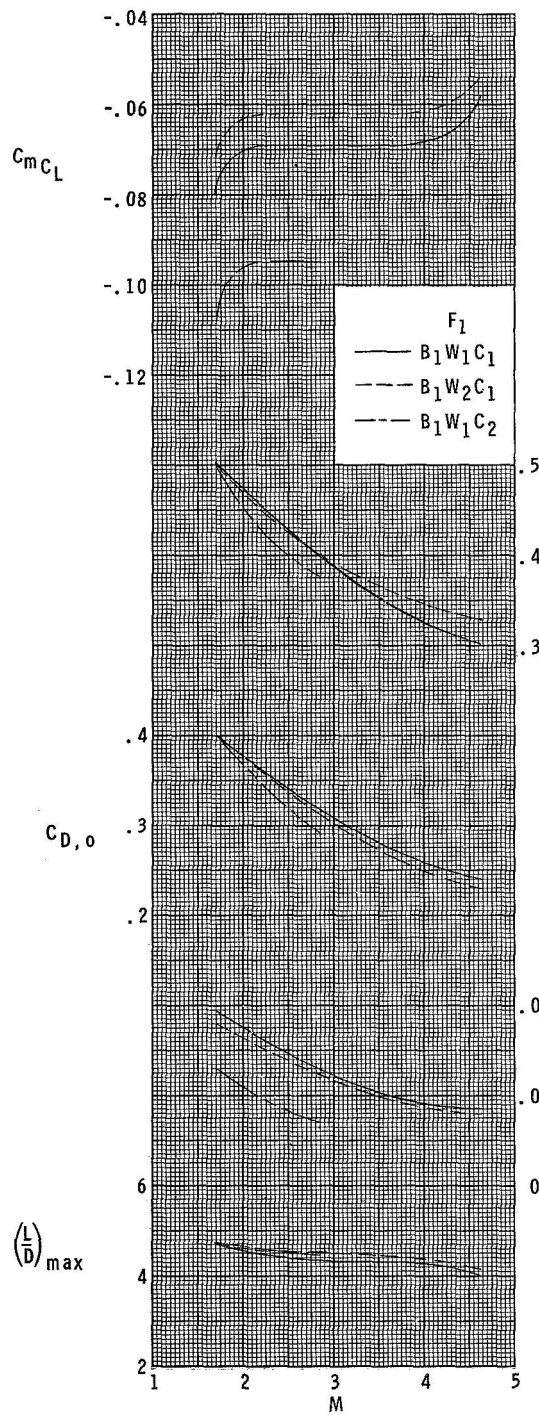
(b) $M = 2.00$.

Figure 13.- Continued.

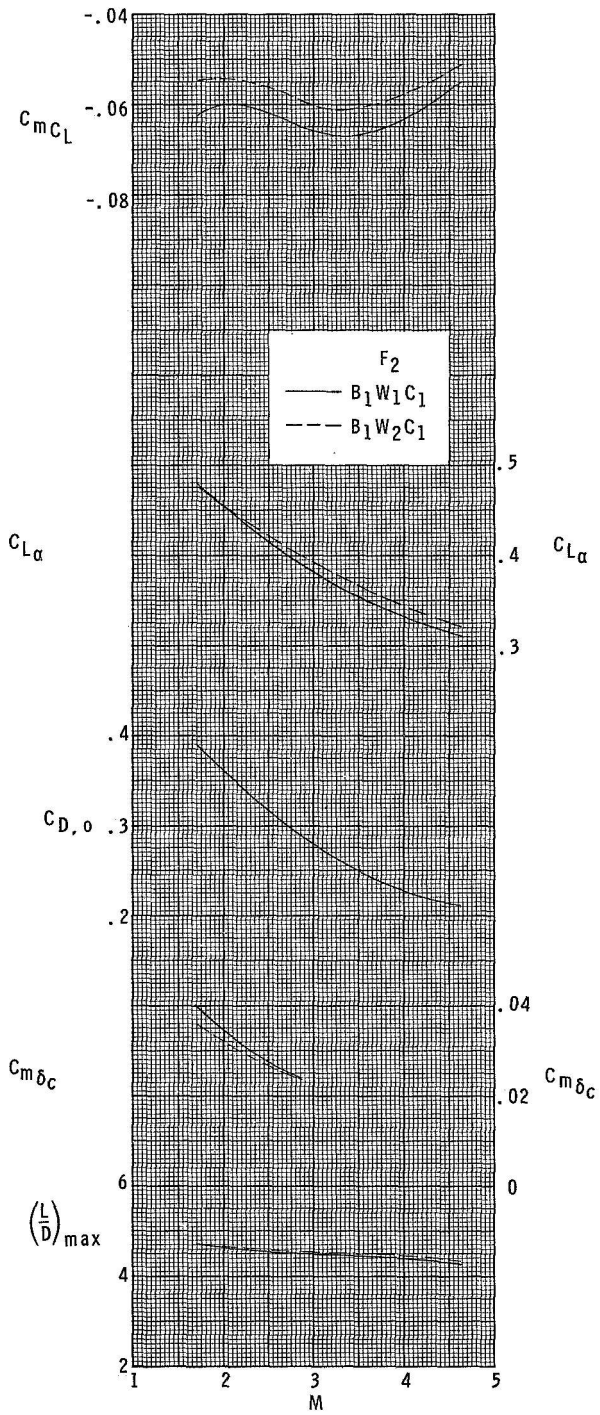


(c) $M = 2.86$.

Figure 13.- Concluded.

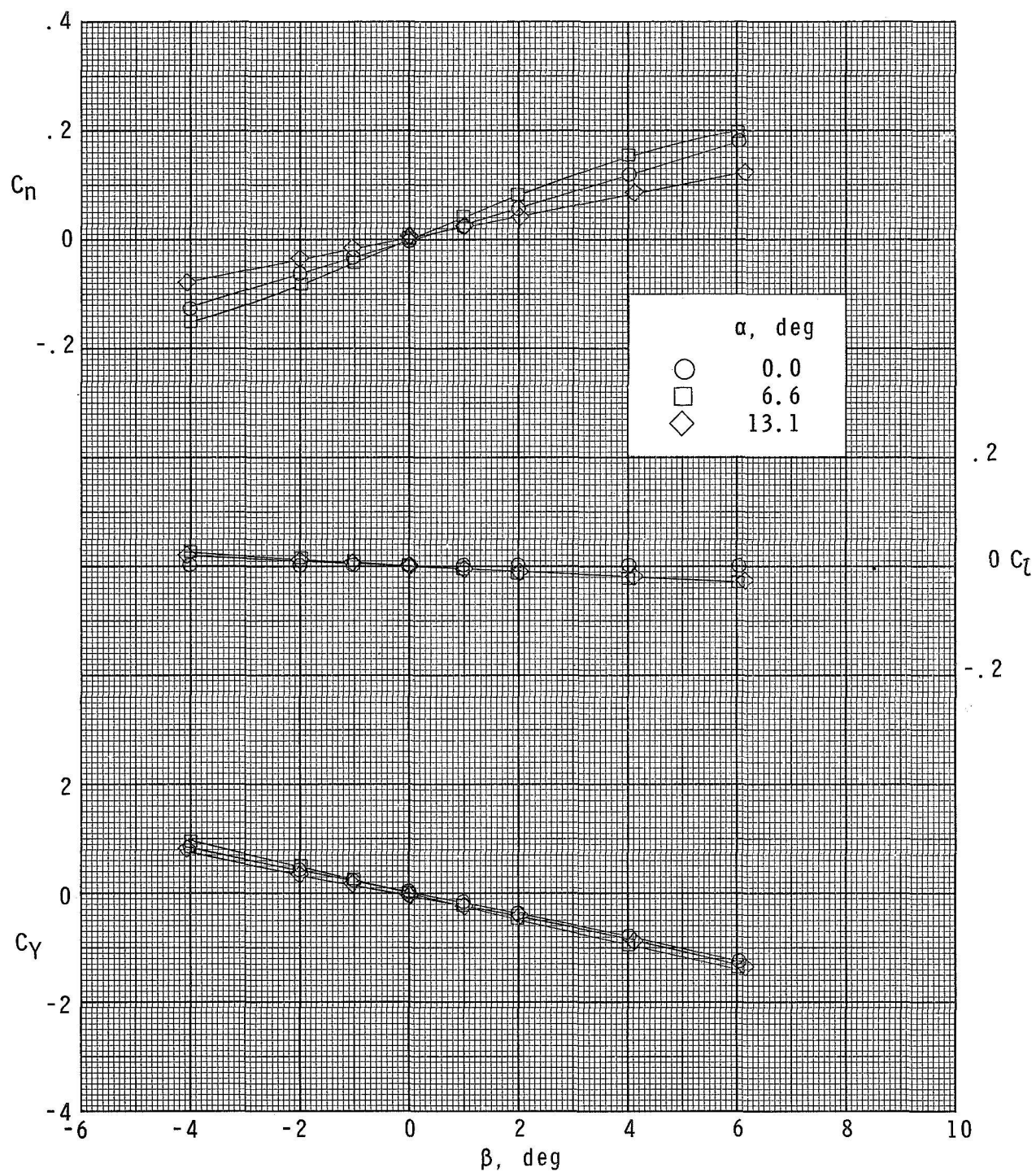


(a) Fin F_1 .



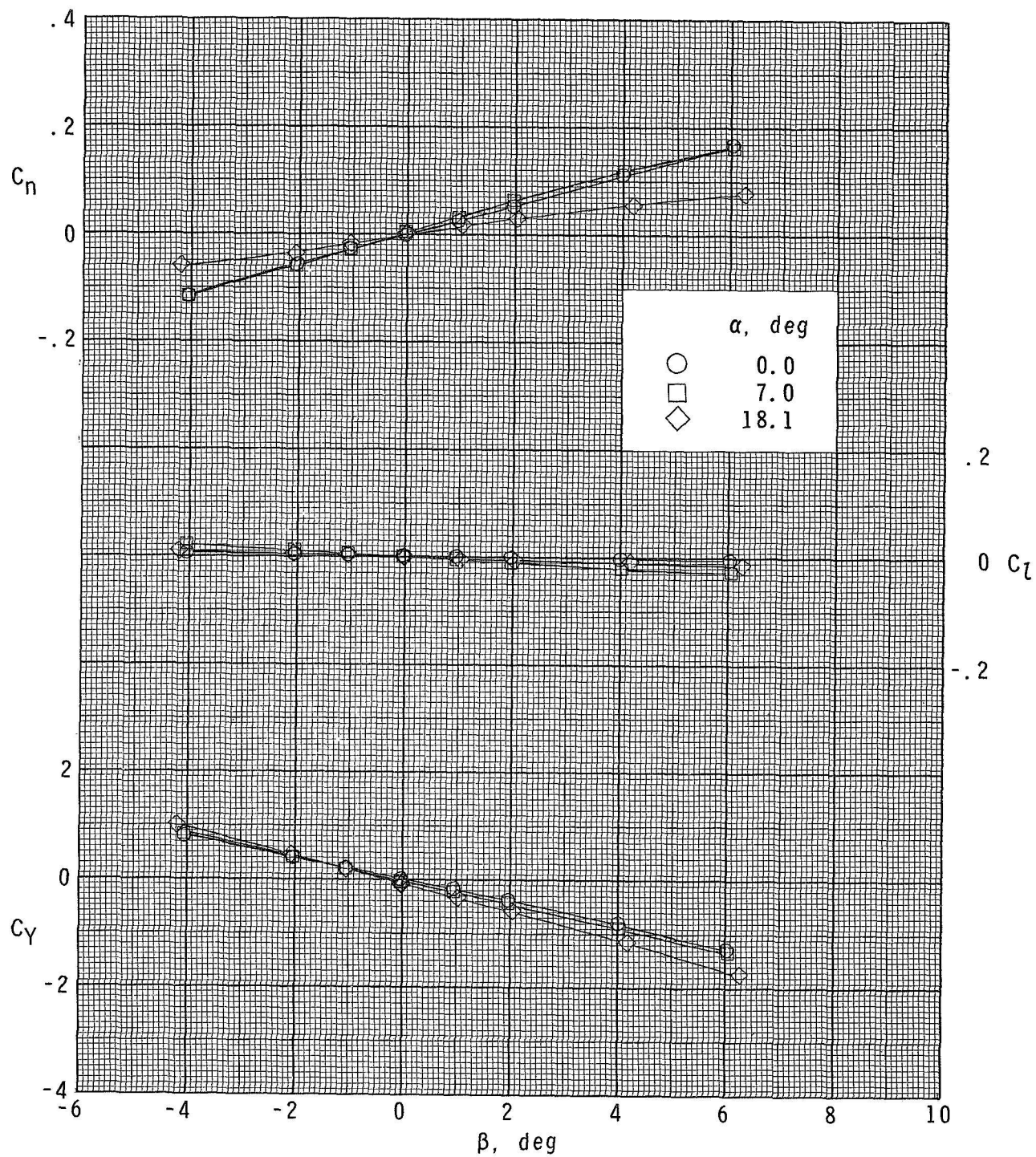
(b) Fin F_2 .

Figure 14.- Summary of longitudinal aerodynamic characteristics.



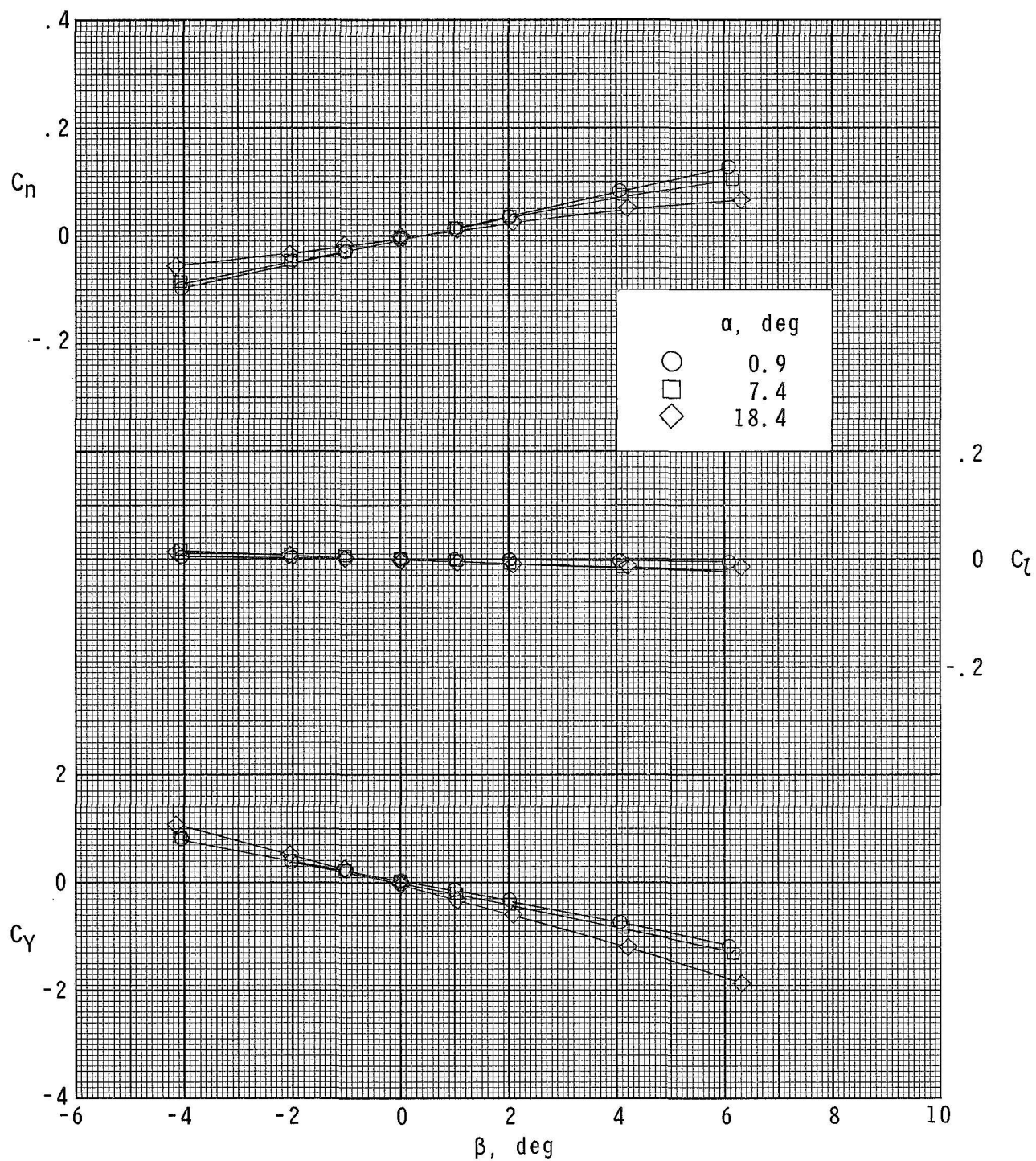
(a) $M = 1.70$.

Figure 15.- Lateral aerodynamic characteristics in sideslip for configuration B₁W₁F₁C₁.



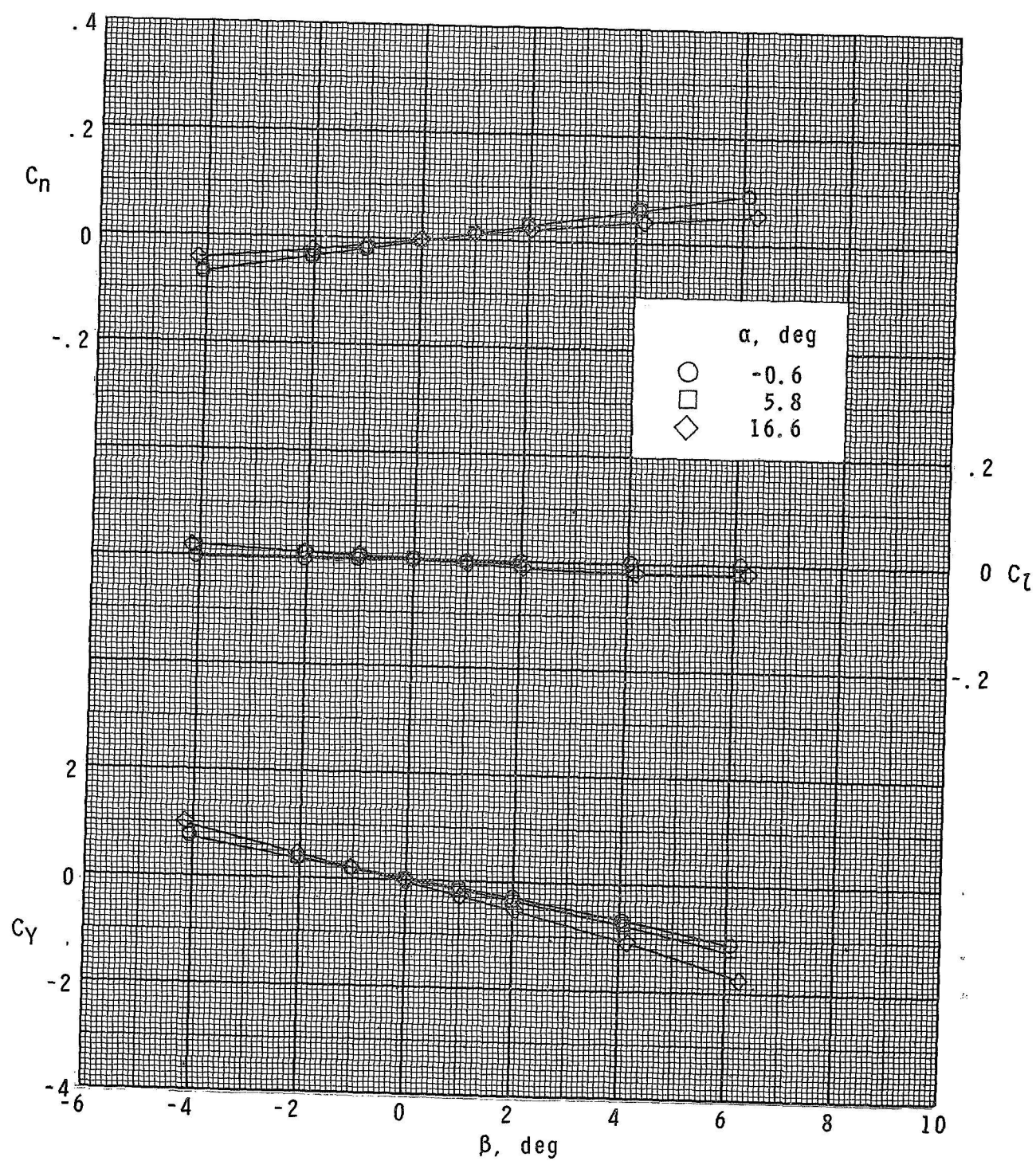
(b) $M = 2.00$.

Figure 15.- Continued.



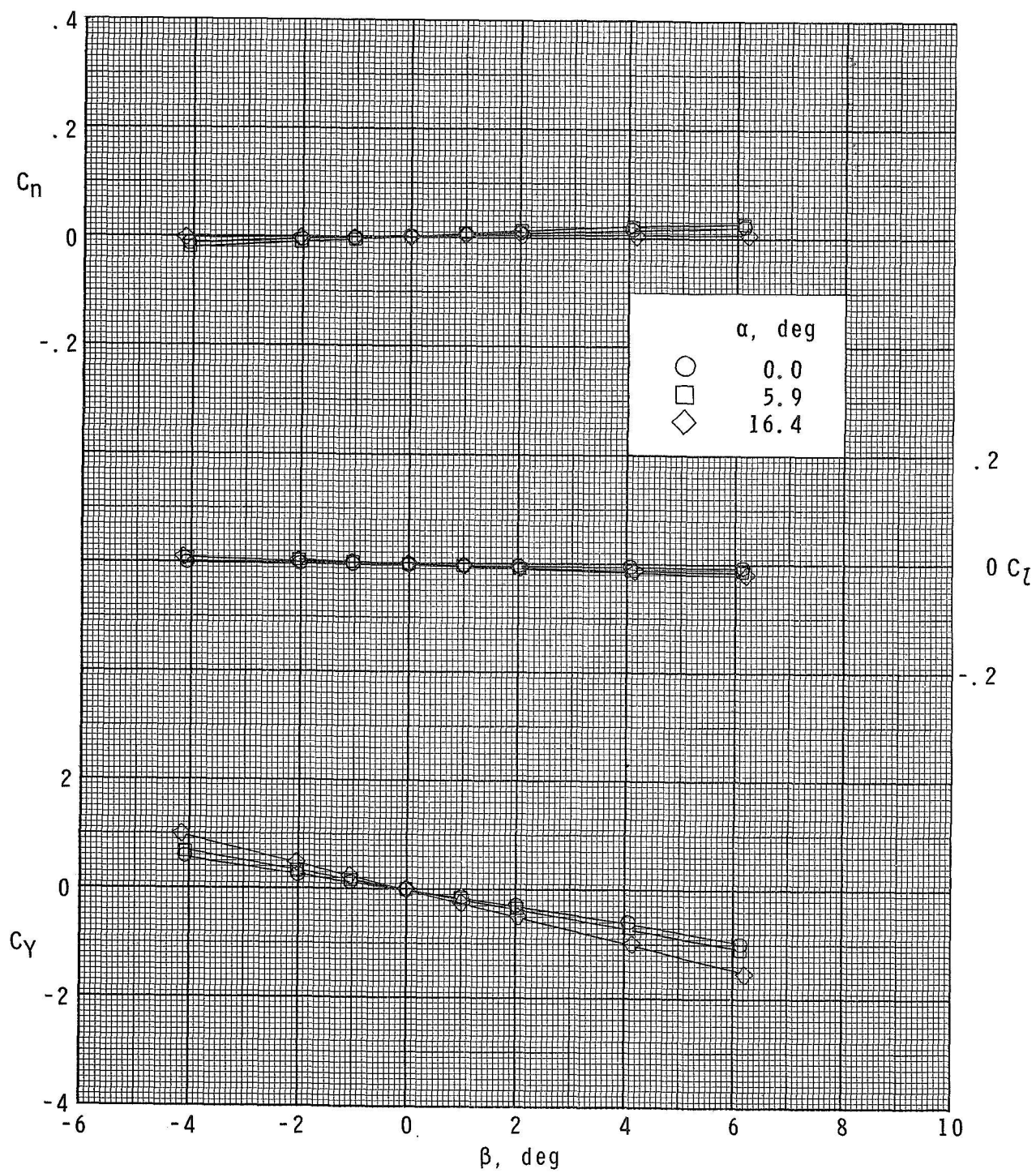
(c) $M = 2.36$.

Figure 15.- Continued.



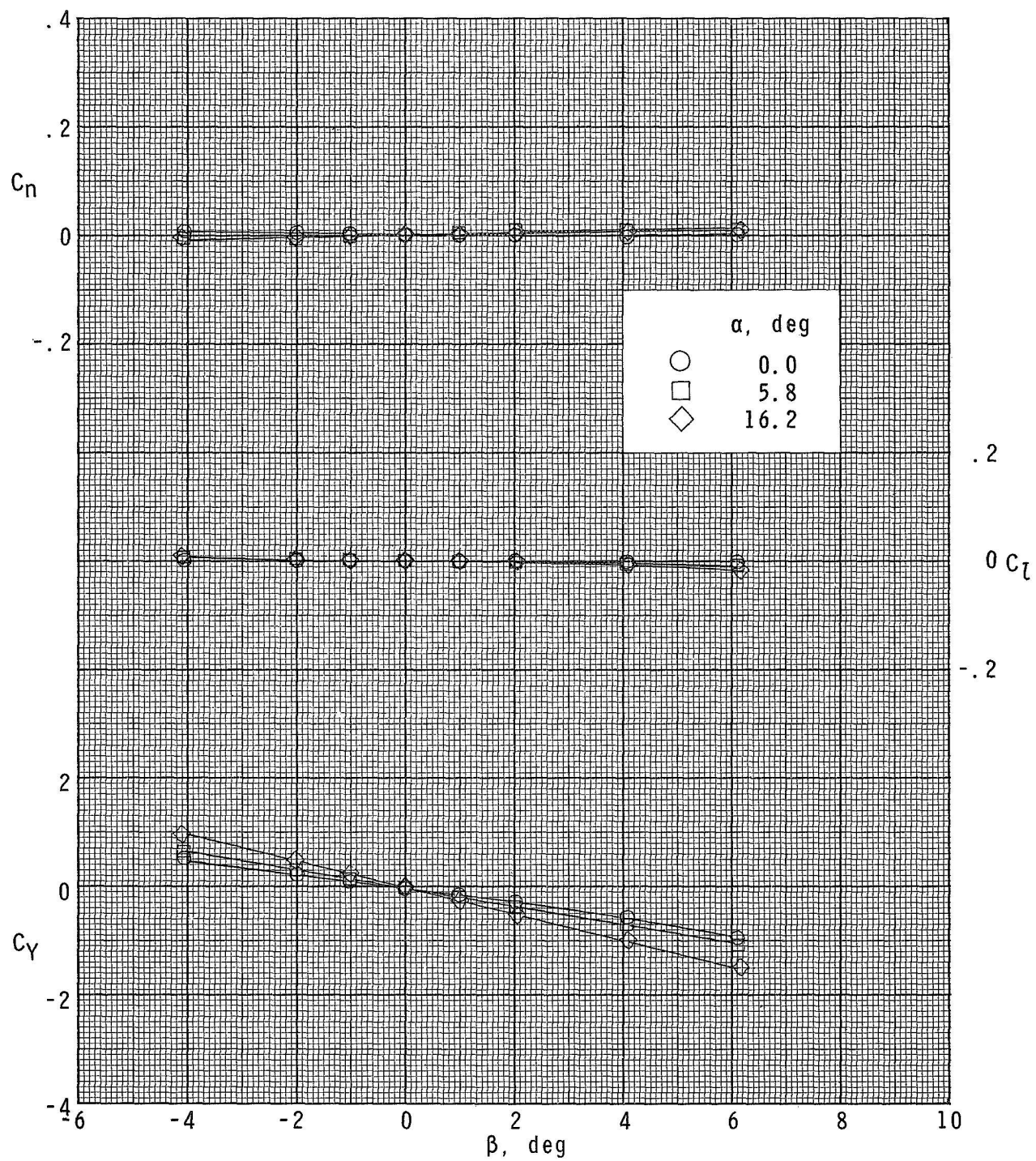
(d) $M = 2.86$.

Figure 15.- Continued.



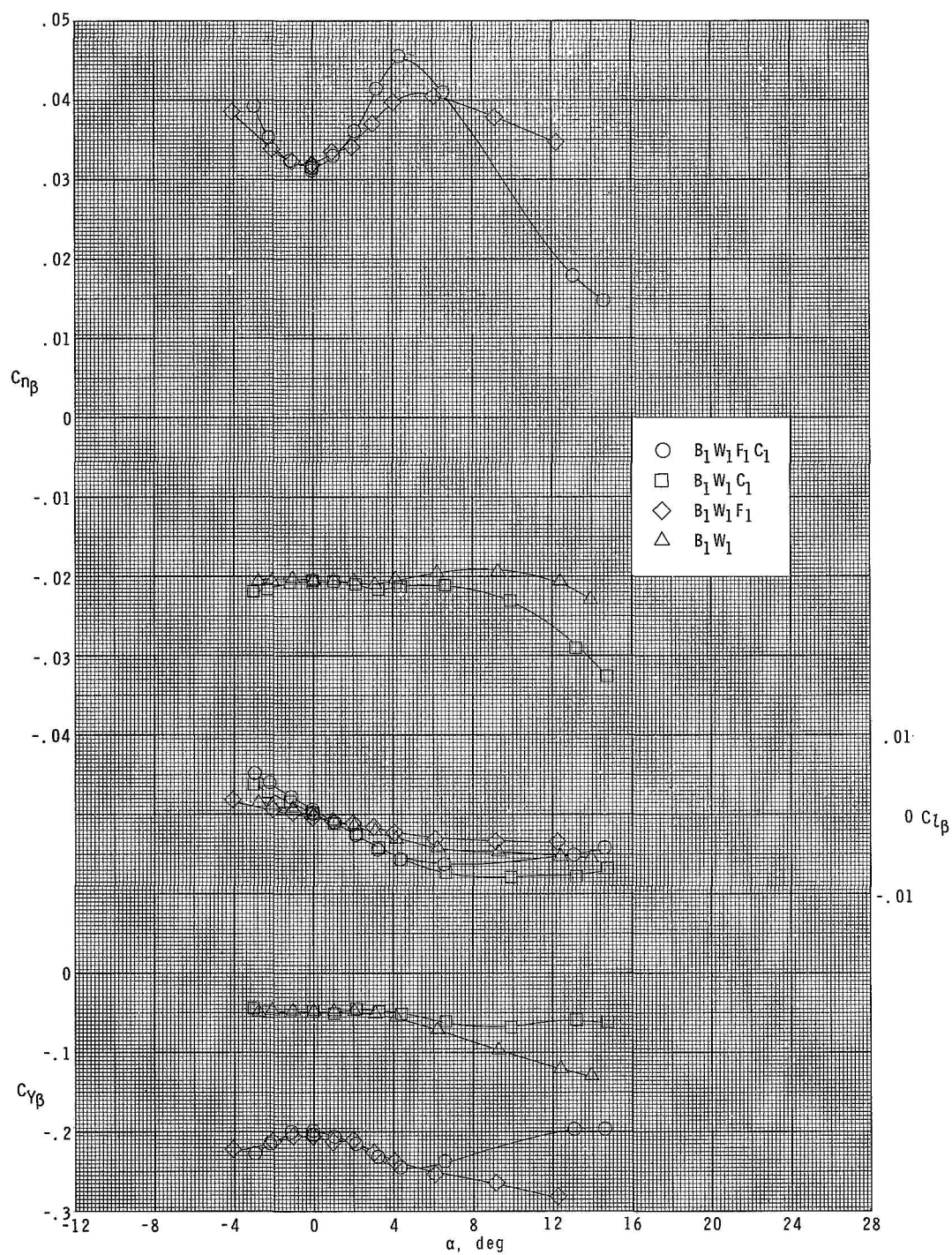
(e) $M = 3.95$.

Figure 15.- Continued.



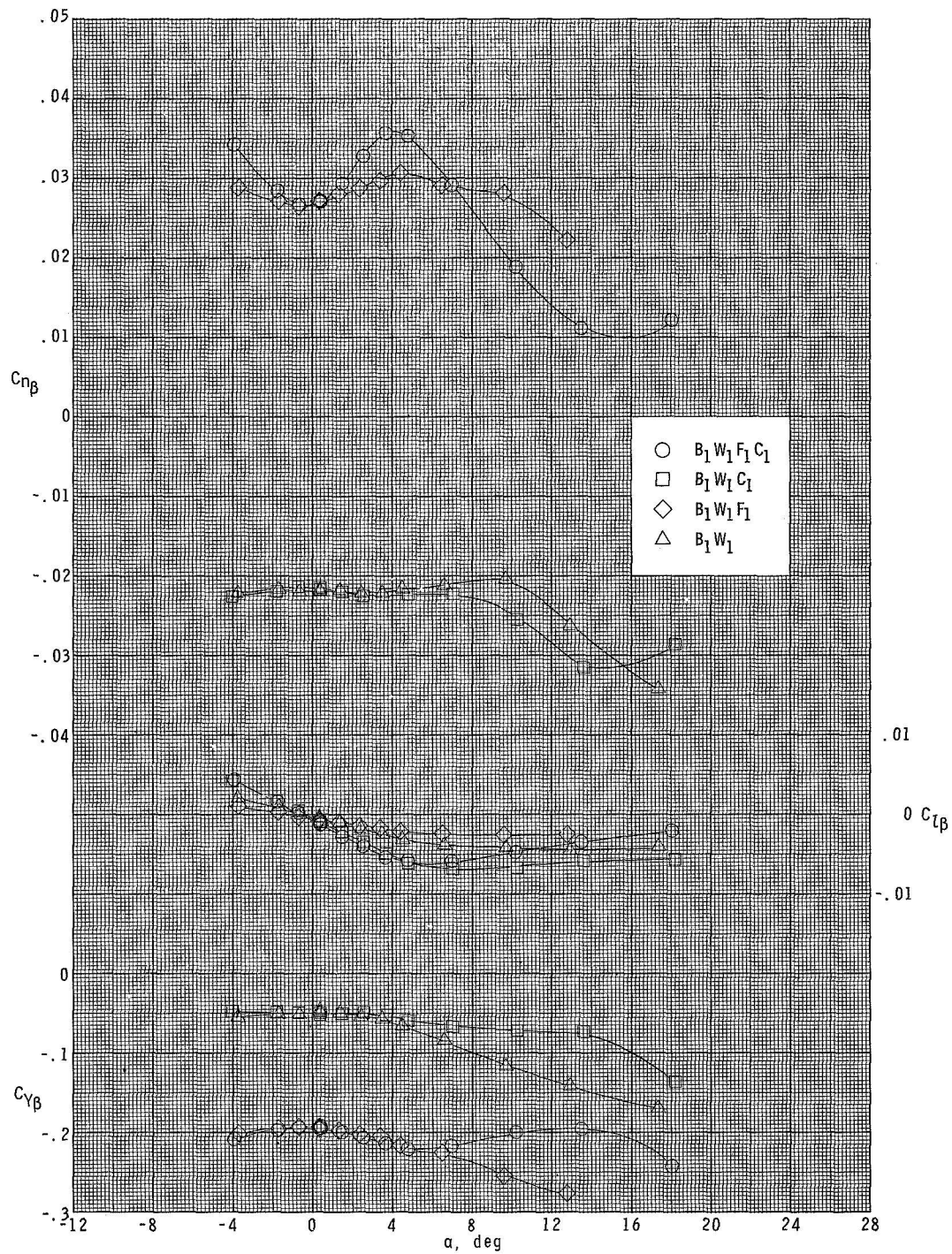
(f) $M = 4.63$.

Figure 15.- Concluded.



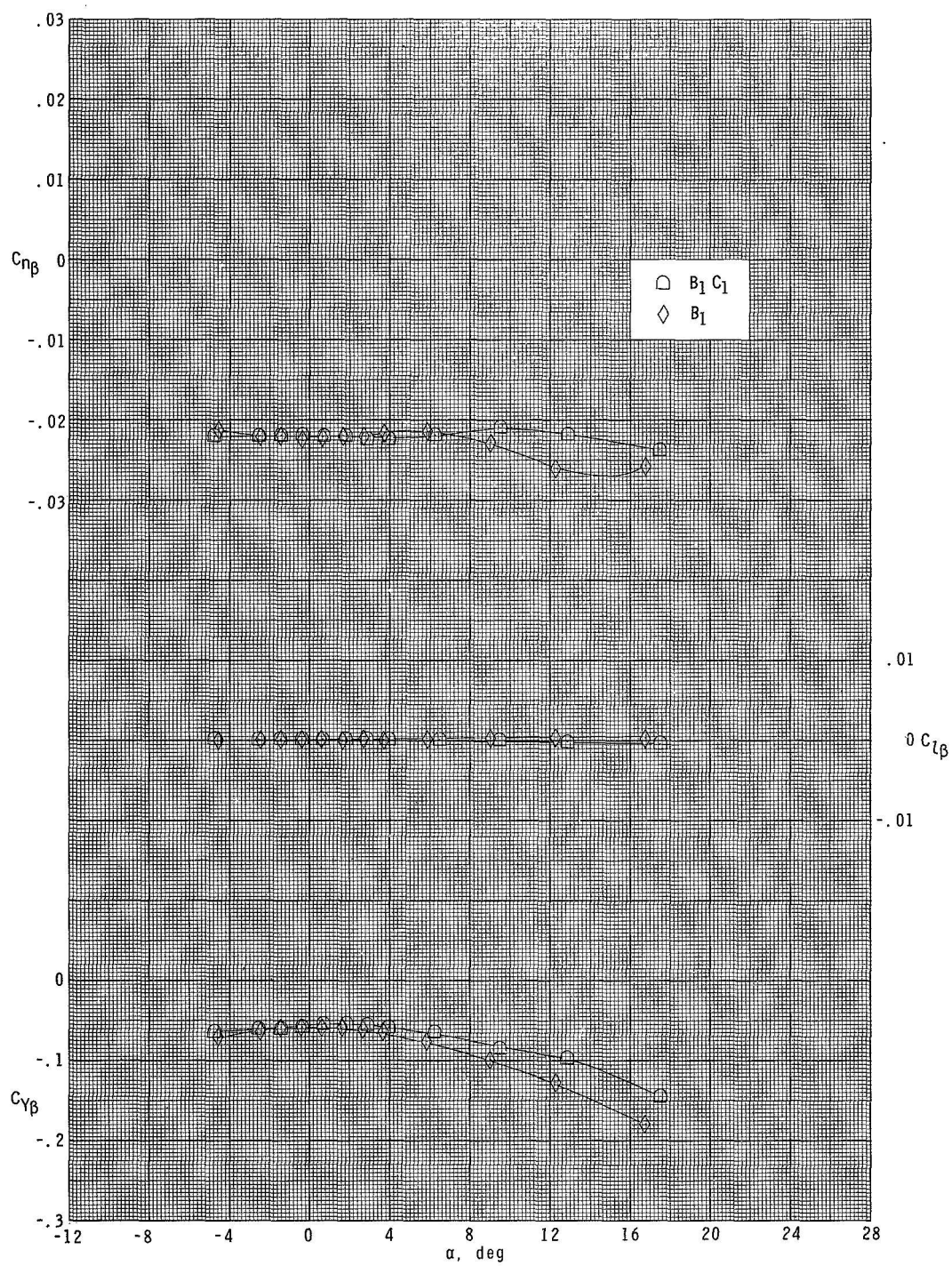
(a) $M = 1.70$.

Figure 16.- Effect of model components on lateral parameters.



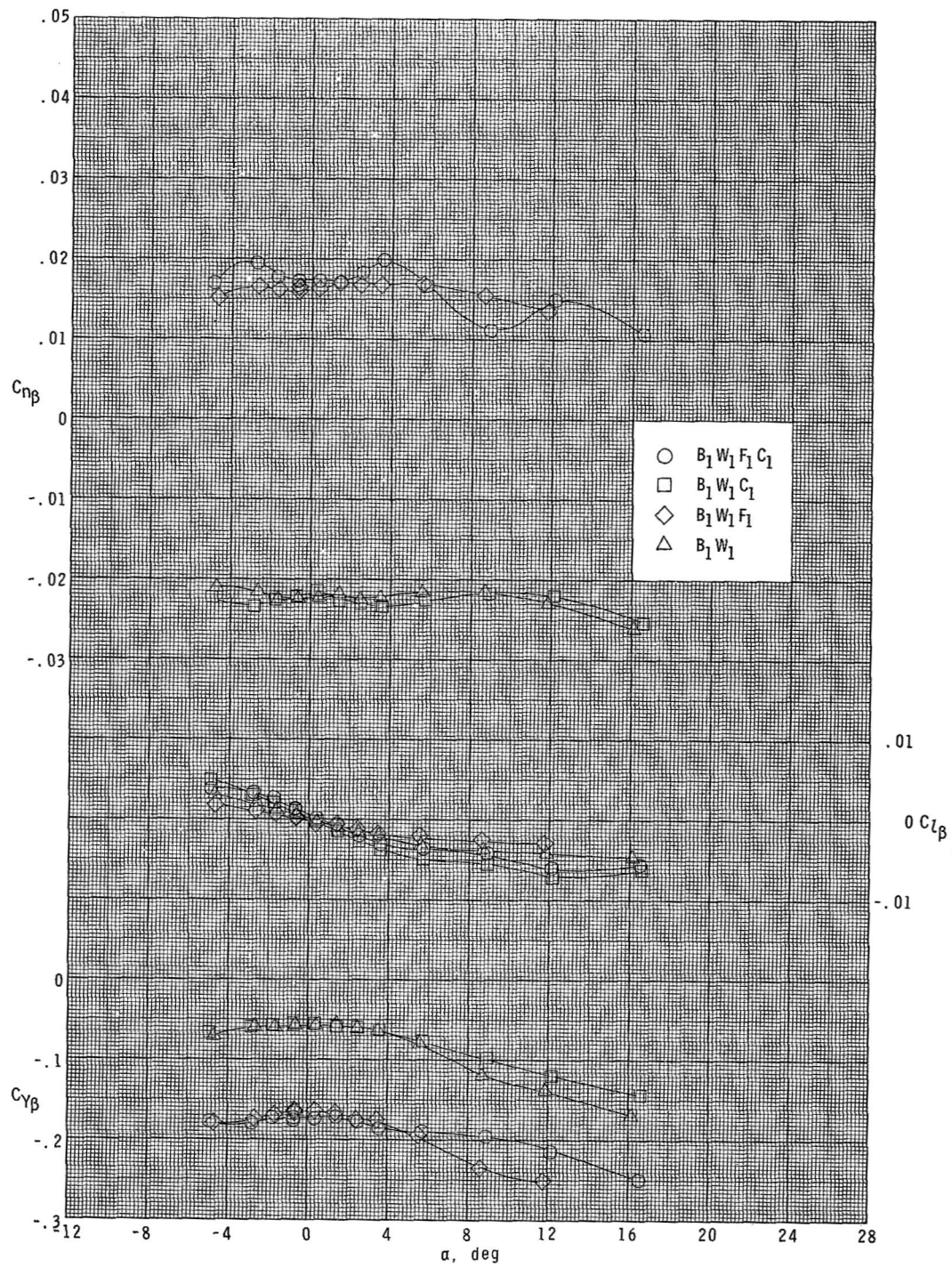
(b) $M = 2.00$.

Figure 16.- Continued.



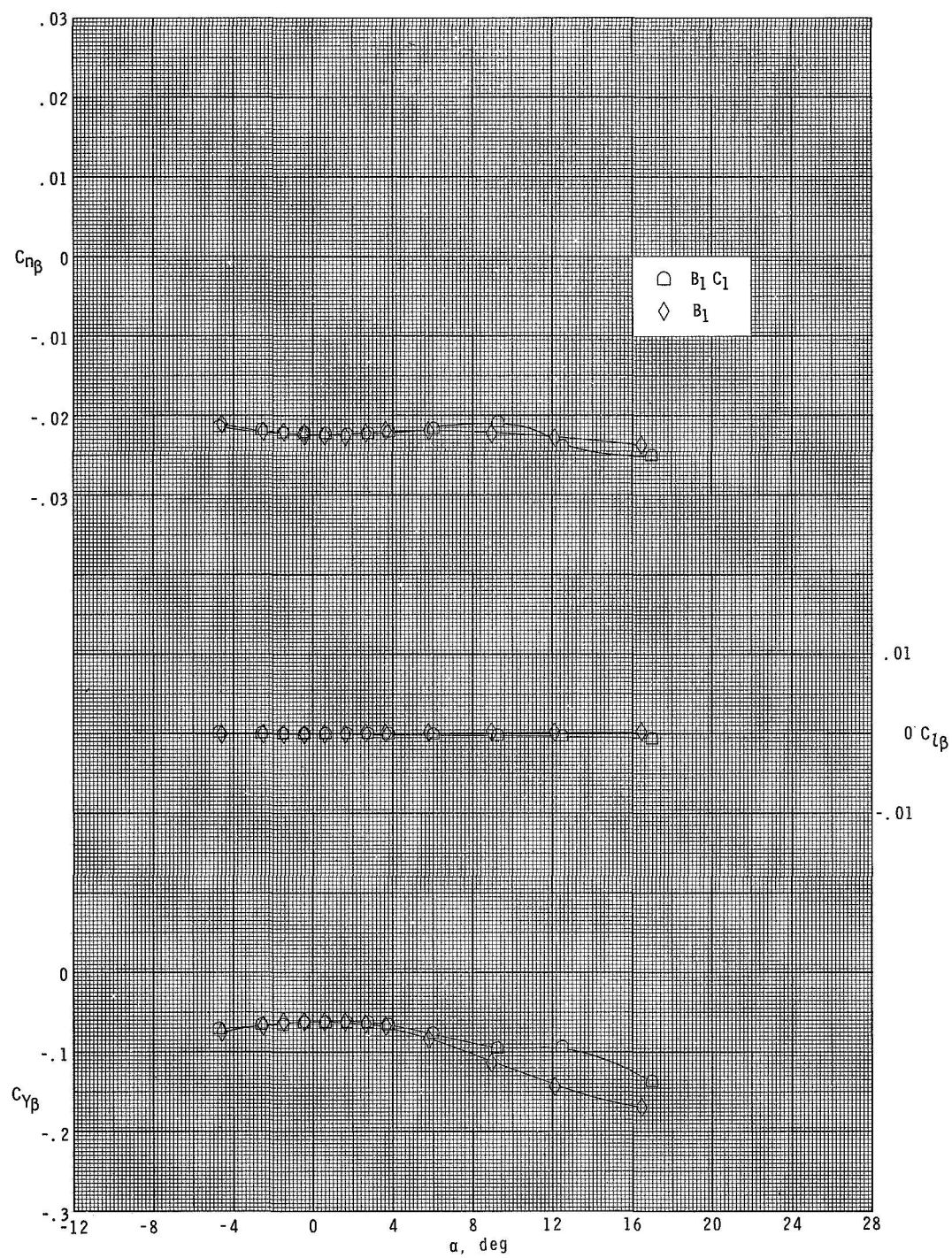
(c) $M = 2.30$.

Figure 16.- Continued.



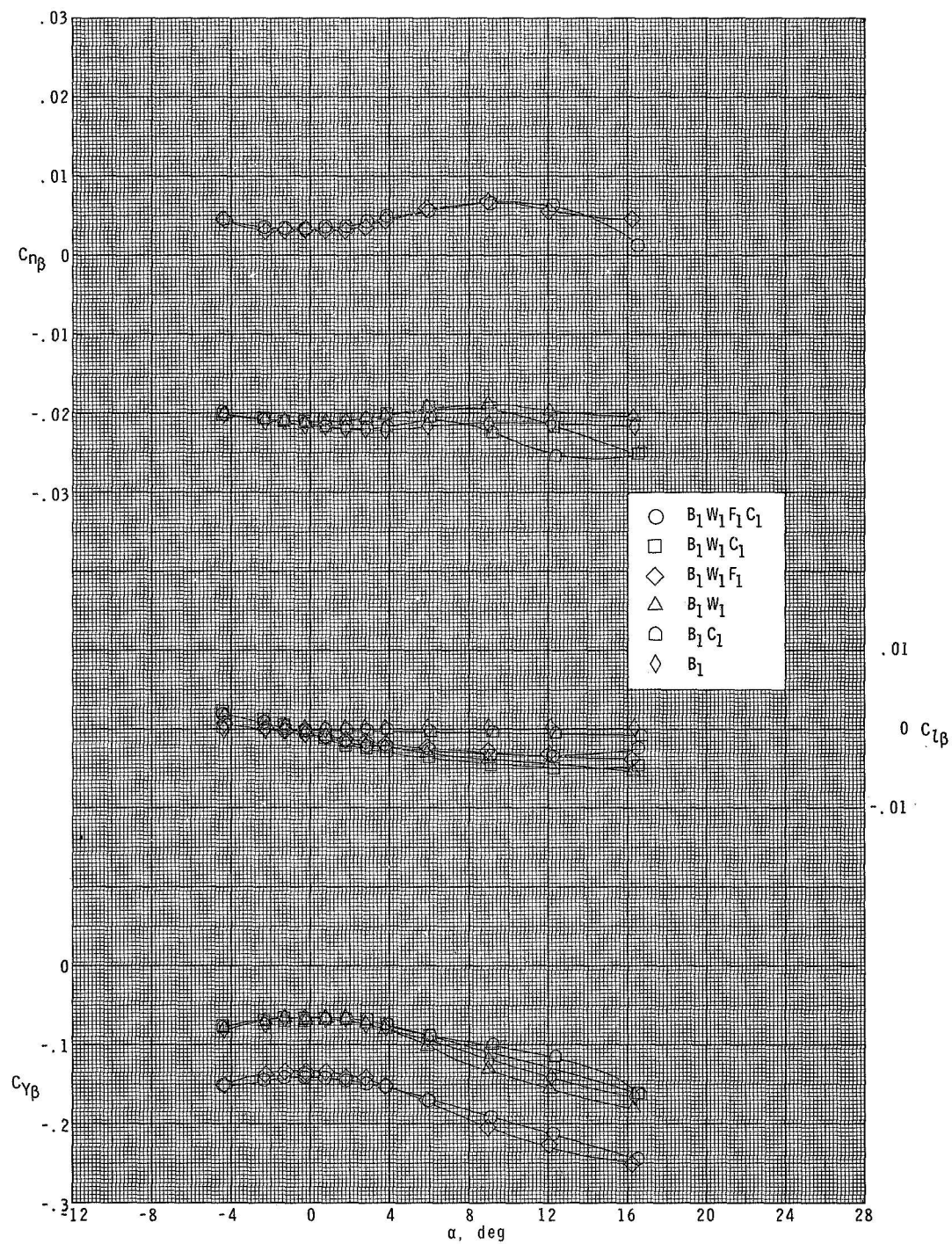
(d) $M = 2.86$.

Figure 16.- Continued.



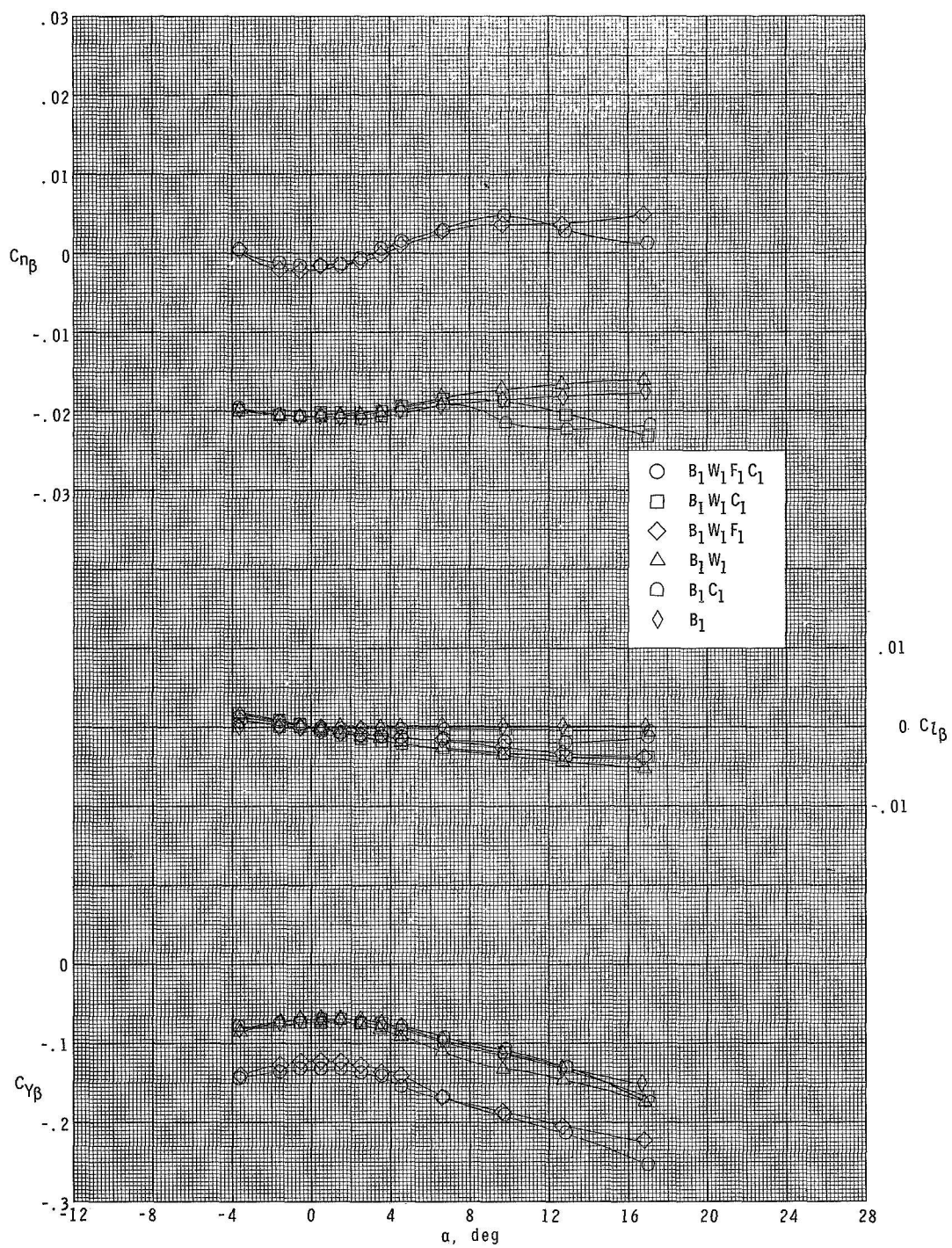
(e) $M = 2.96$.

Figure 16.- Continued.



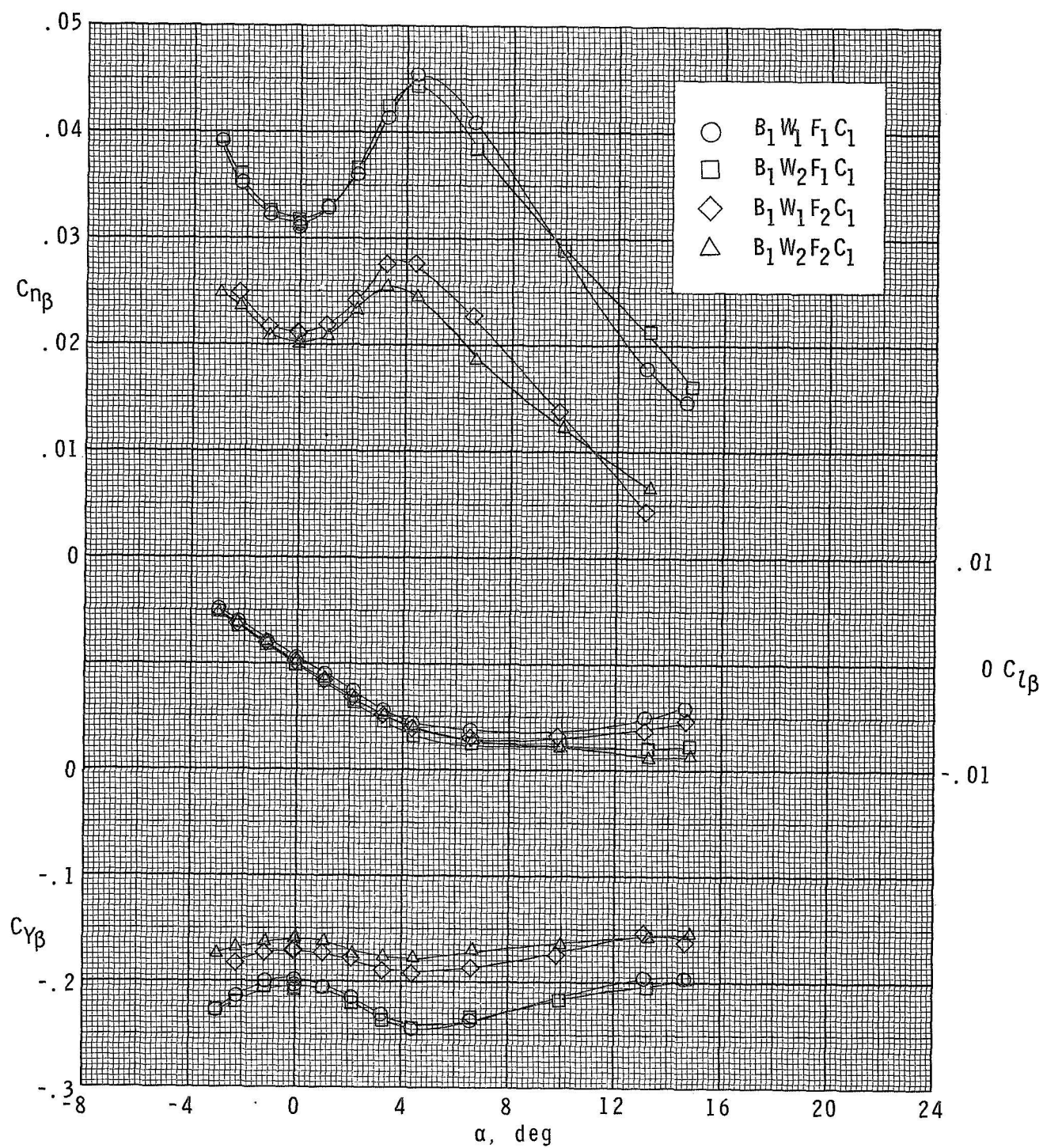
(f) $M = 3.95$.

Figure 16.- Continued.



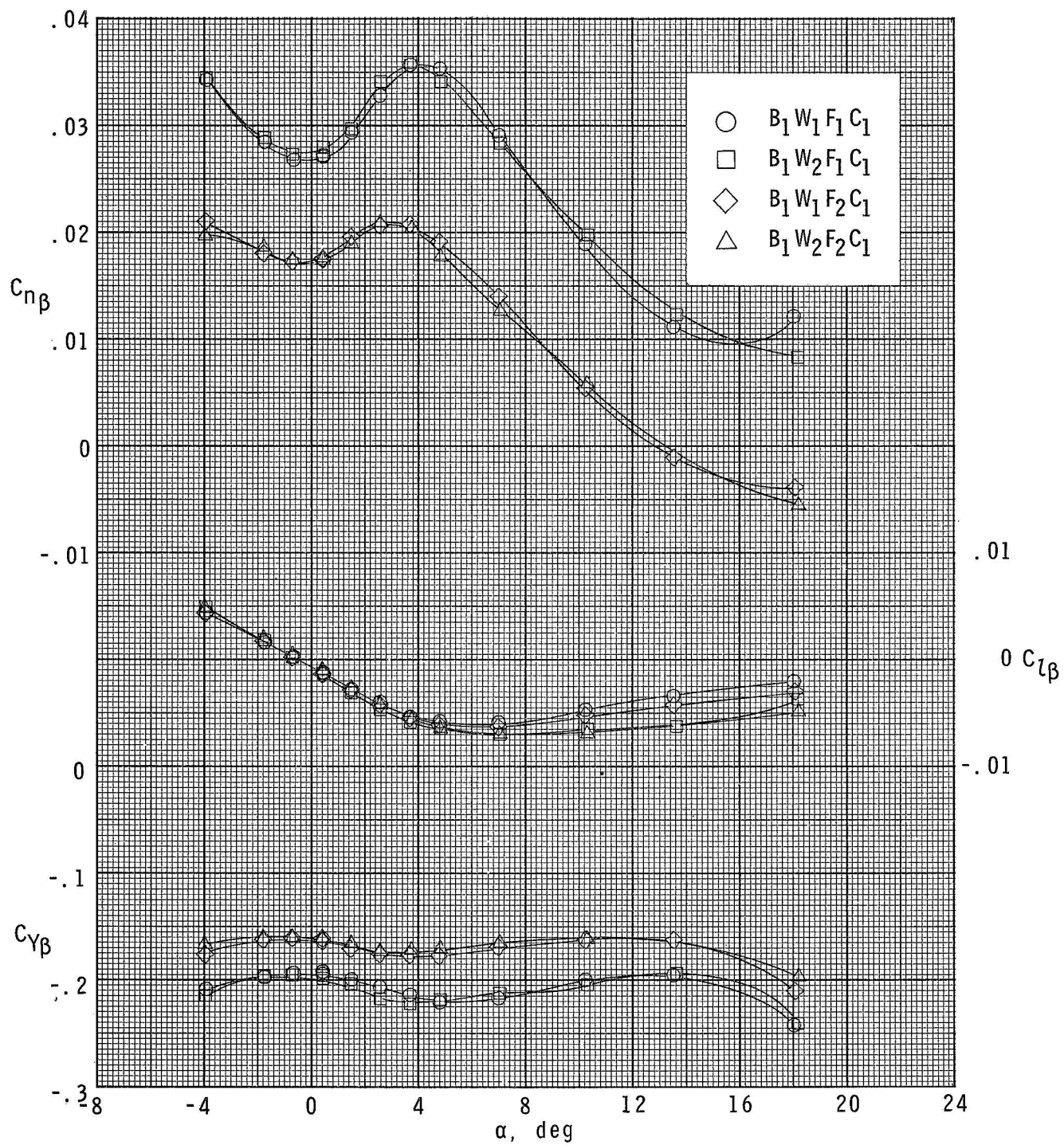
(g) $M = 4.63$.

Figure 16.- Concluded.



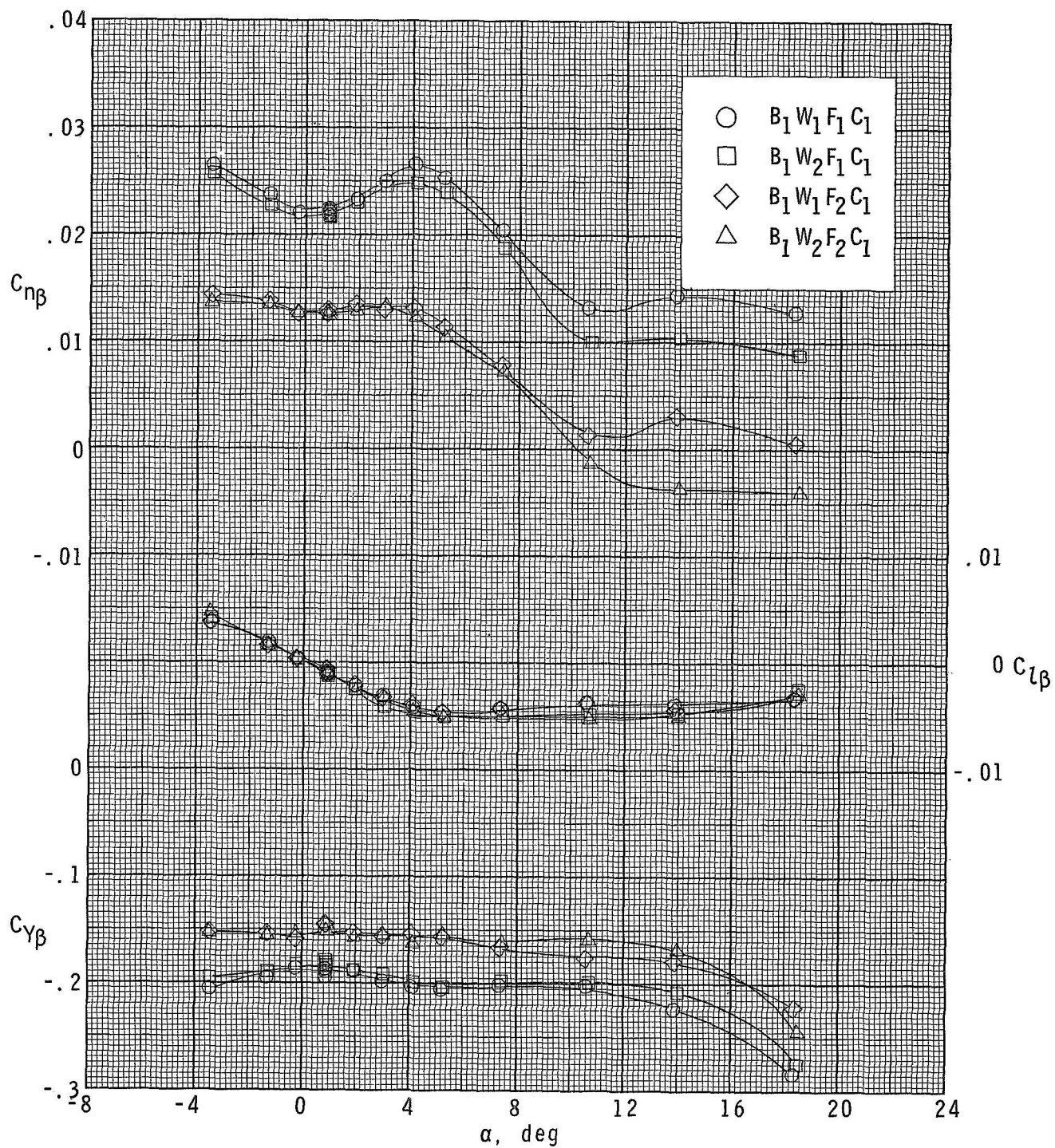
(a) $M \approx 1.70$.

Figure 17.- Effect of change in wing and/or vertical-fin planforms on lateral parameters.



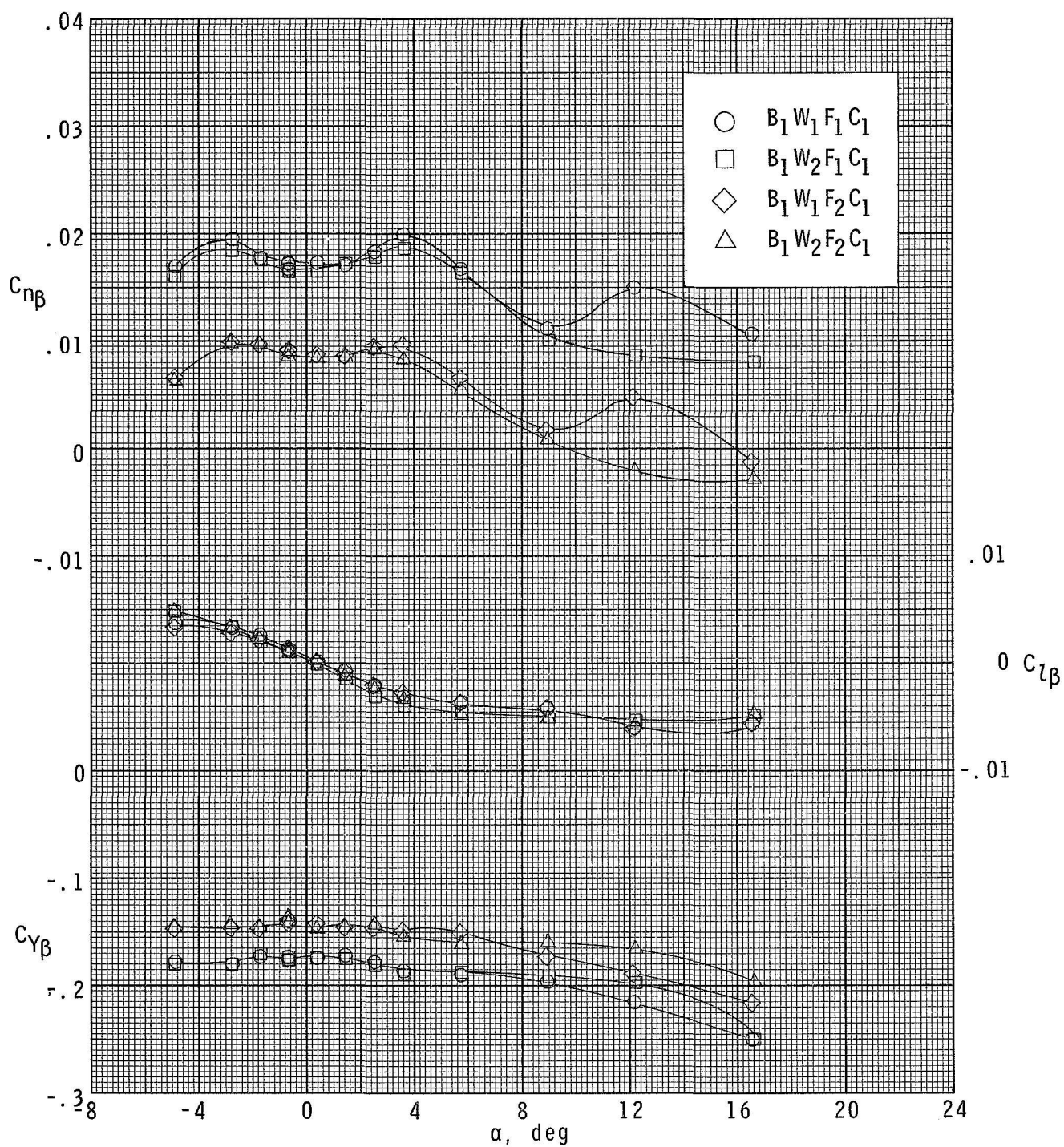
(b) $M = 2.00$.

Figure 17.- Continued.



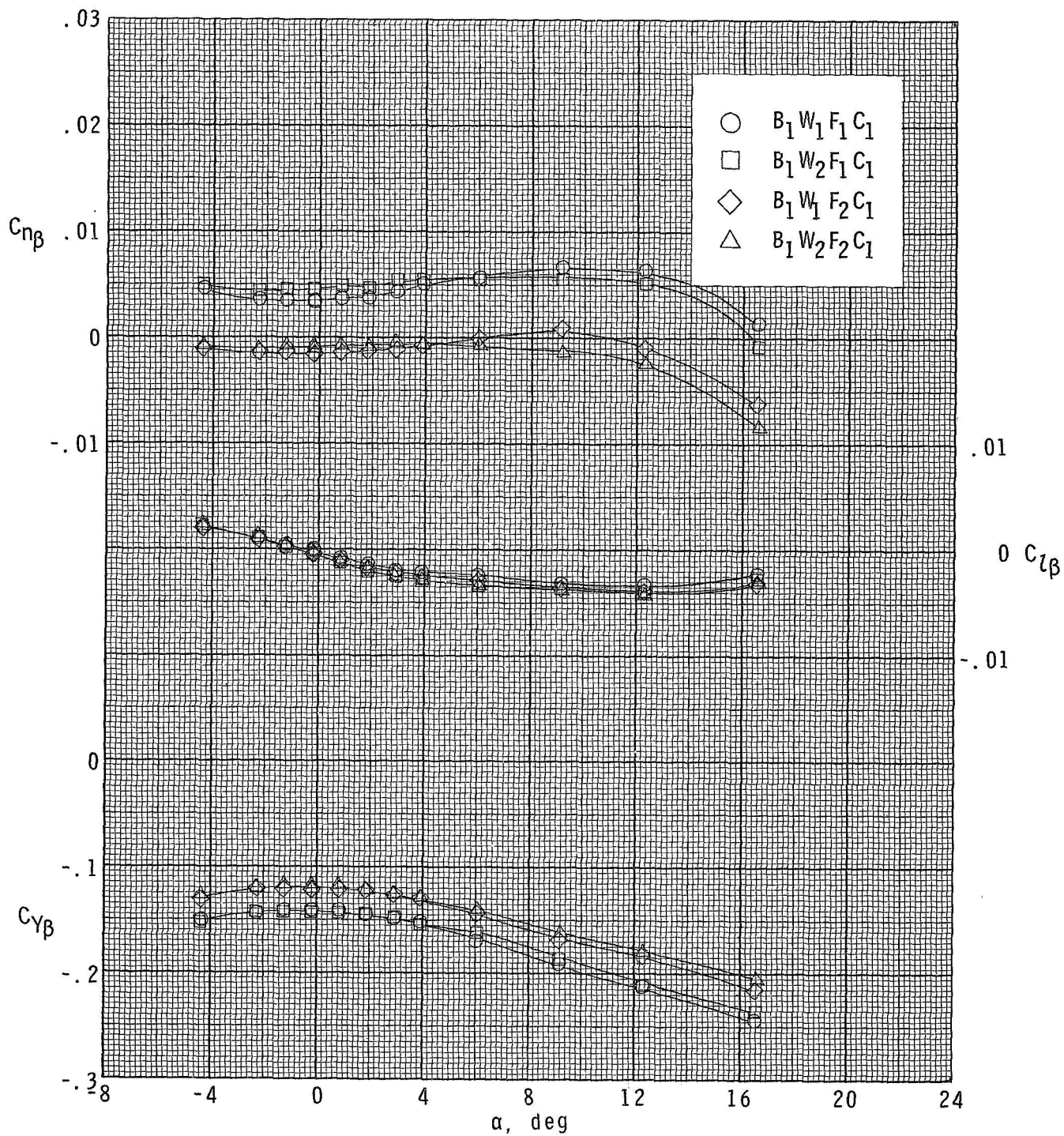
(c) $M = 2.36$.

Figure 17.- Continued.



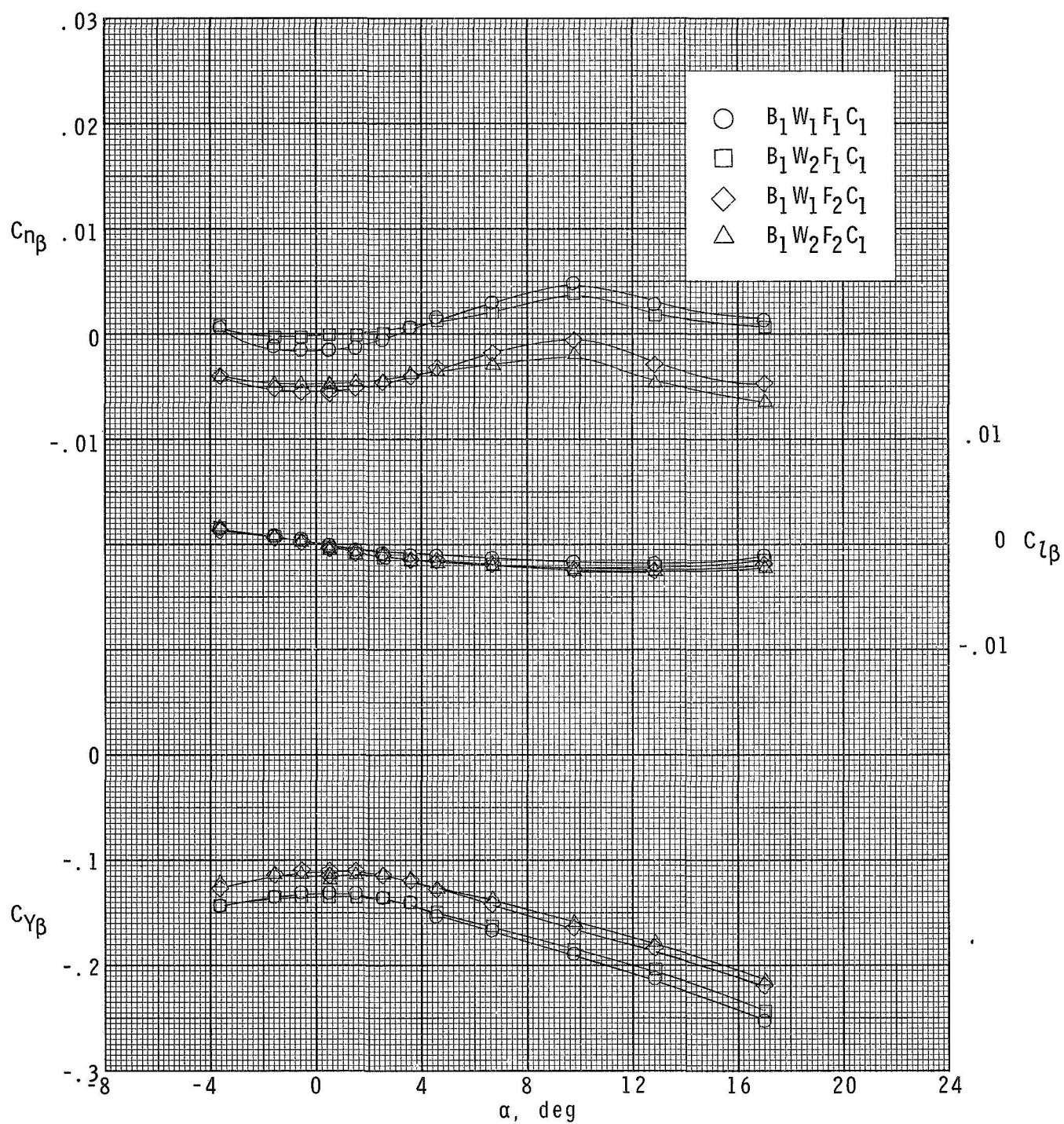
(d) $M = 2.86$.

Figure 17.- Continued.



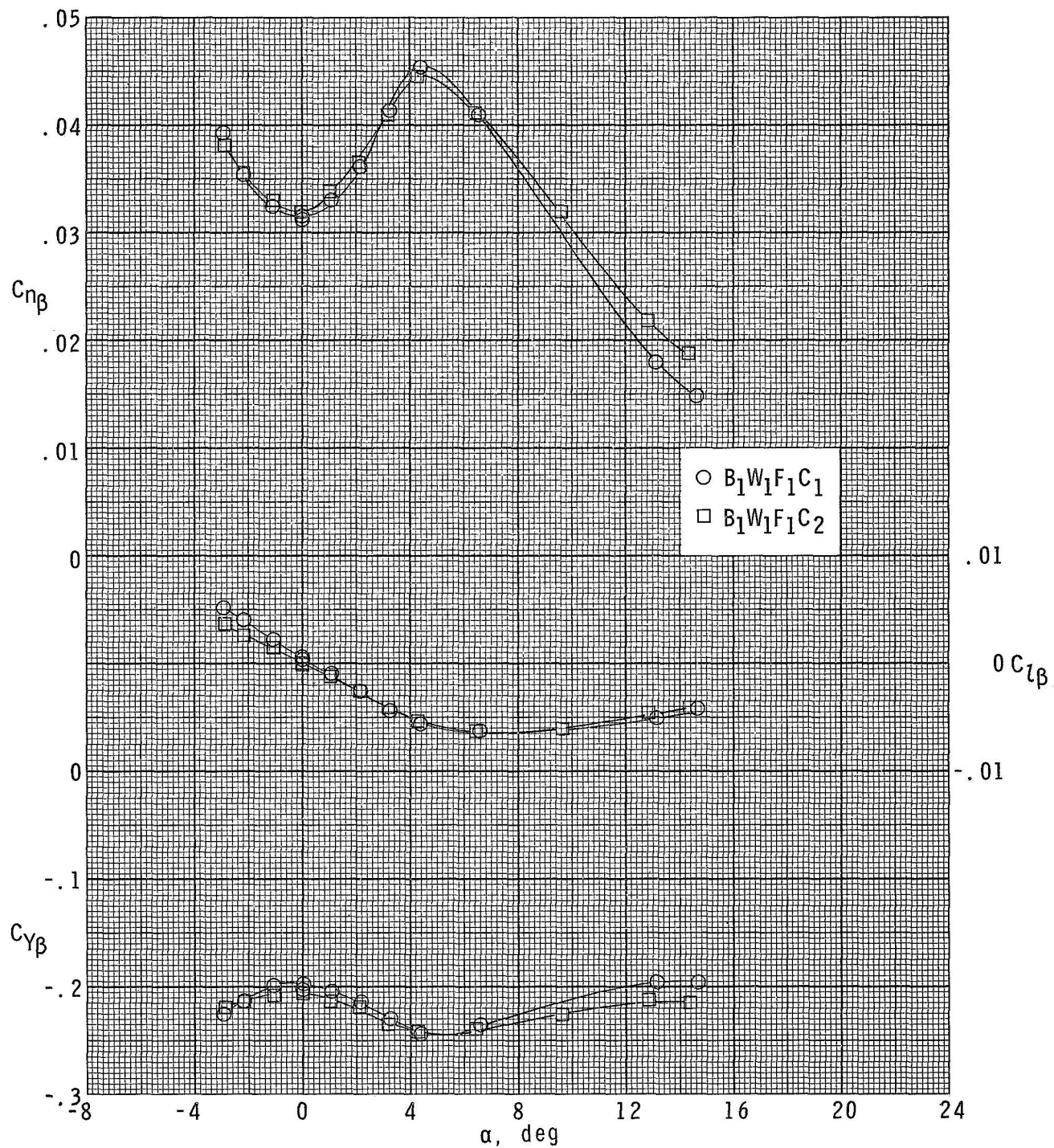
(e) $M = 3.95$.

Figure 17.- Continued.



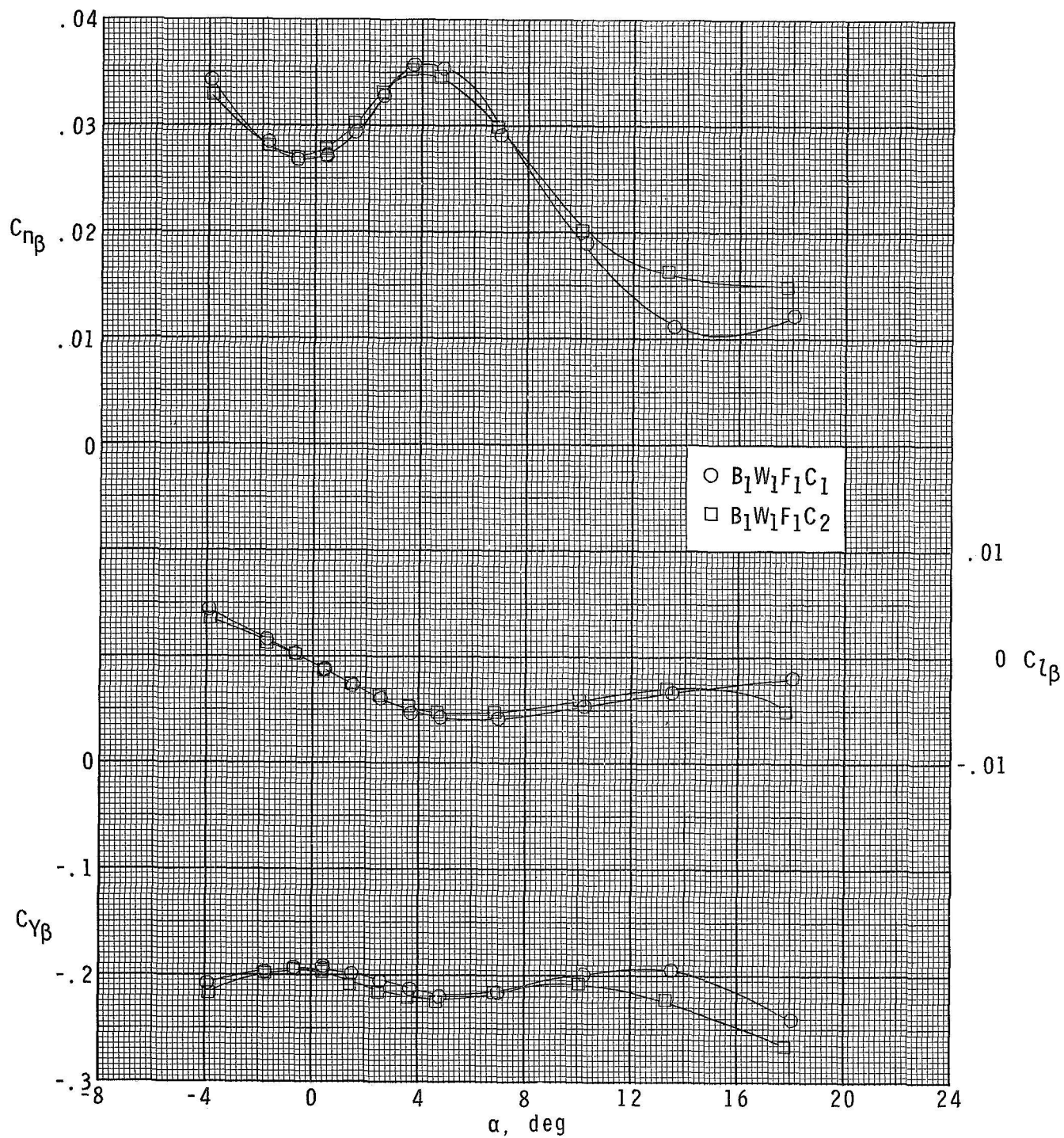
(f) $M = 4.63$.

Figure 17.- Concluded.



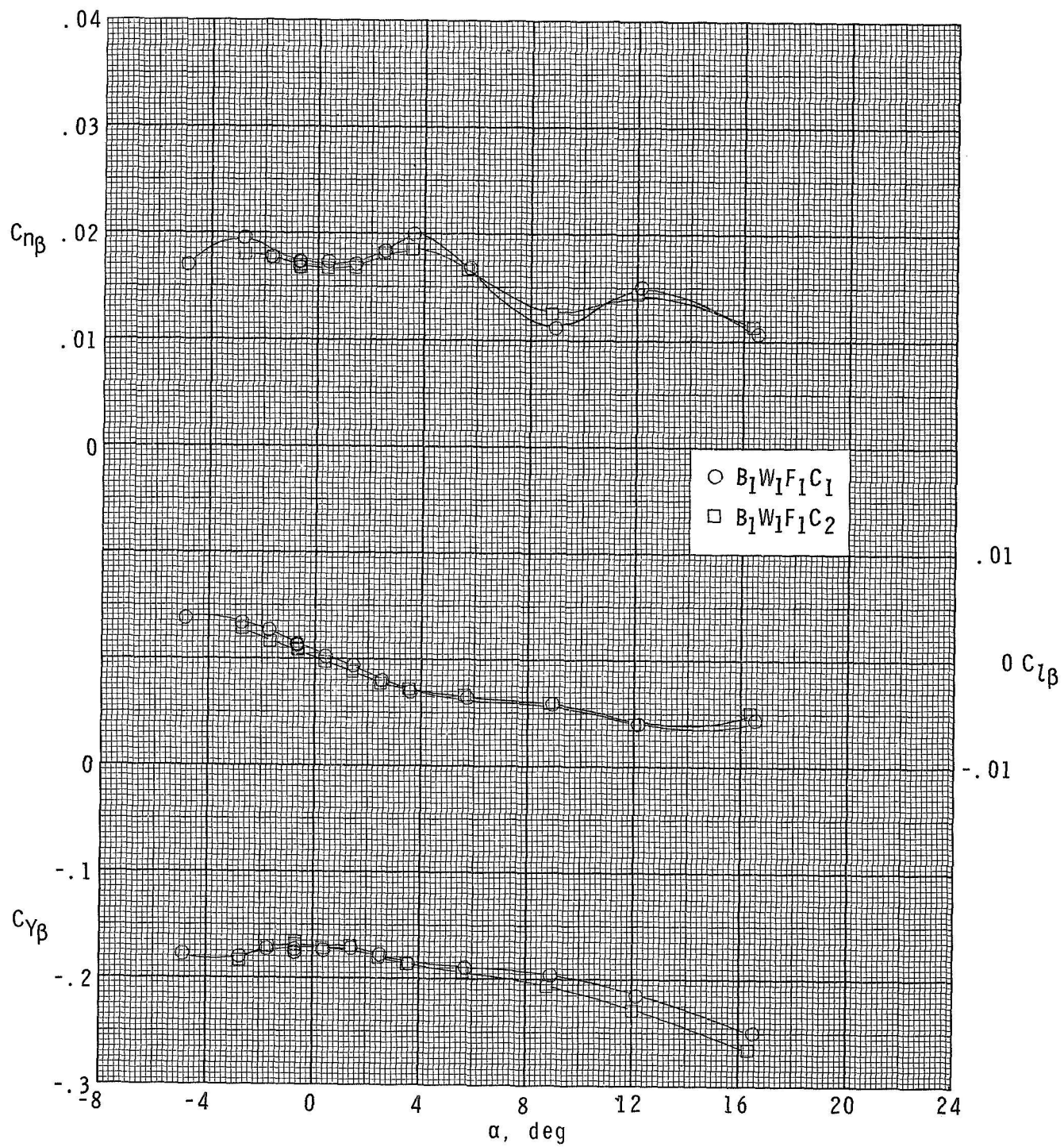
(a) $M = 1.70$.

Figure 18.- Effect of canard size on lateral parameters.



(b) $M = 2.00$.

Figure 18.- Continued.



(c) $M = 2.86$.

Figure 18.- Concluded.

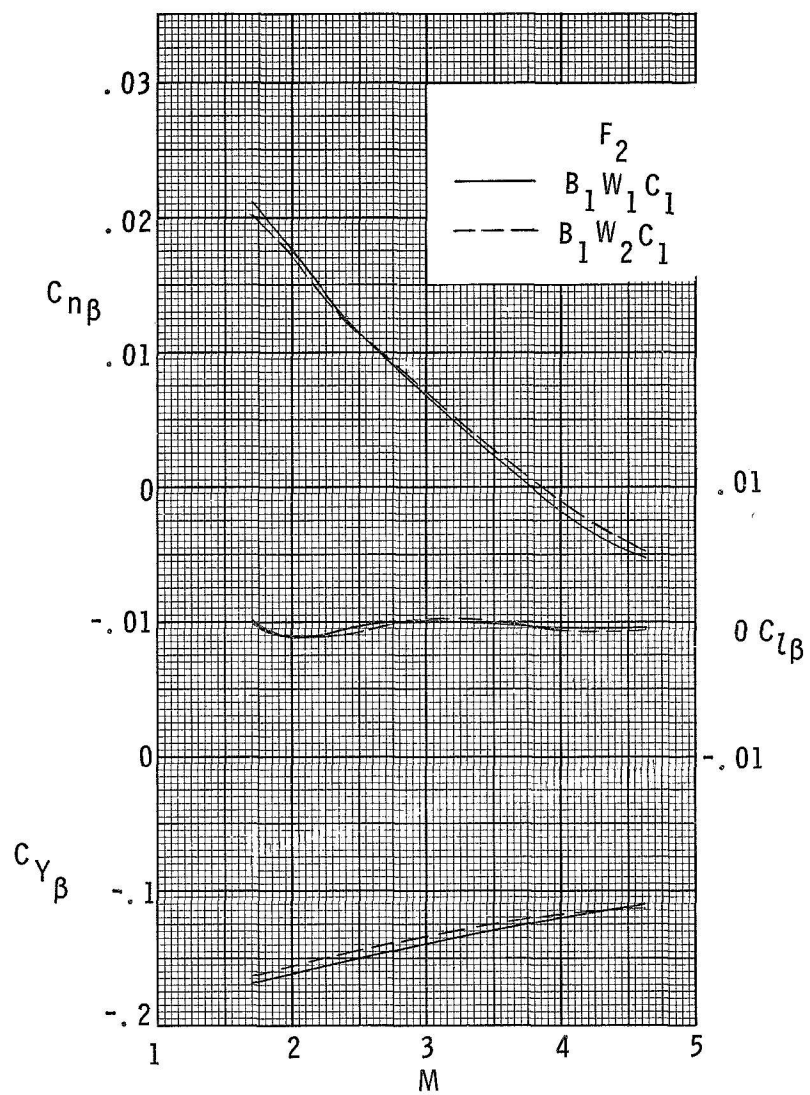
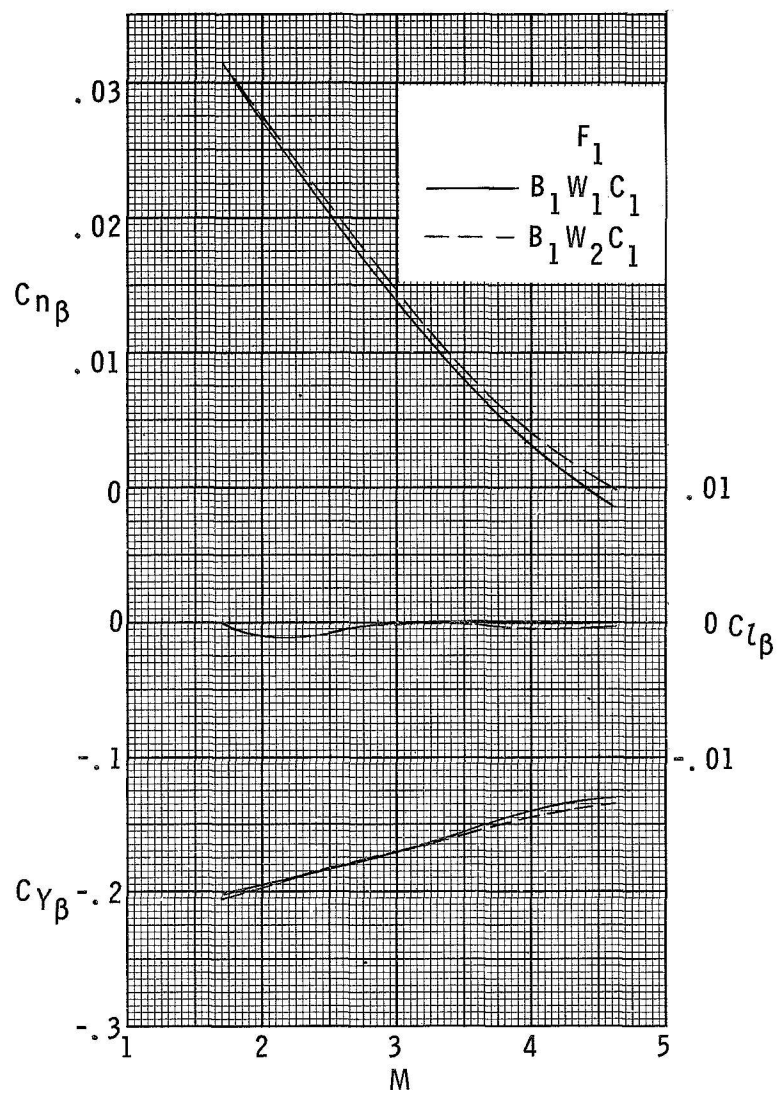
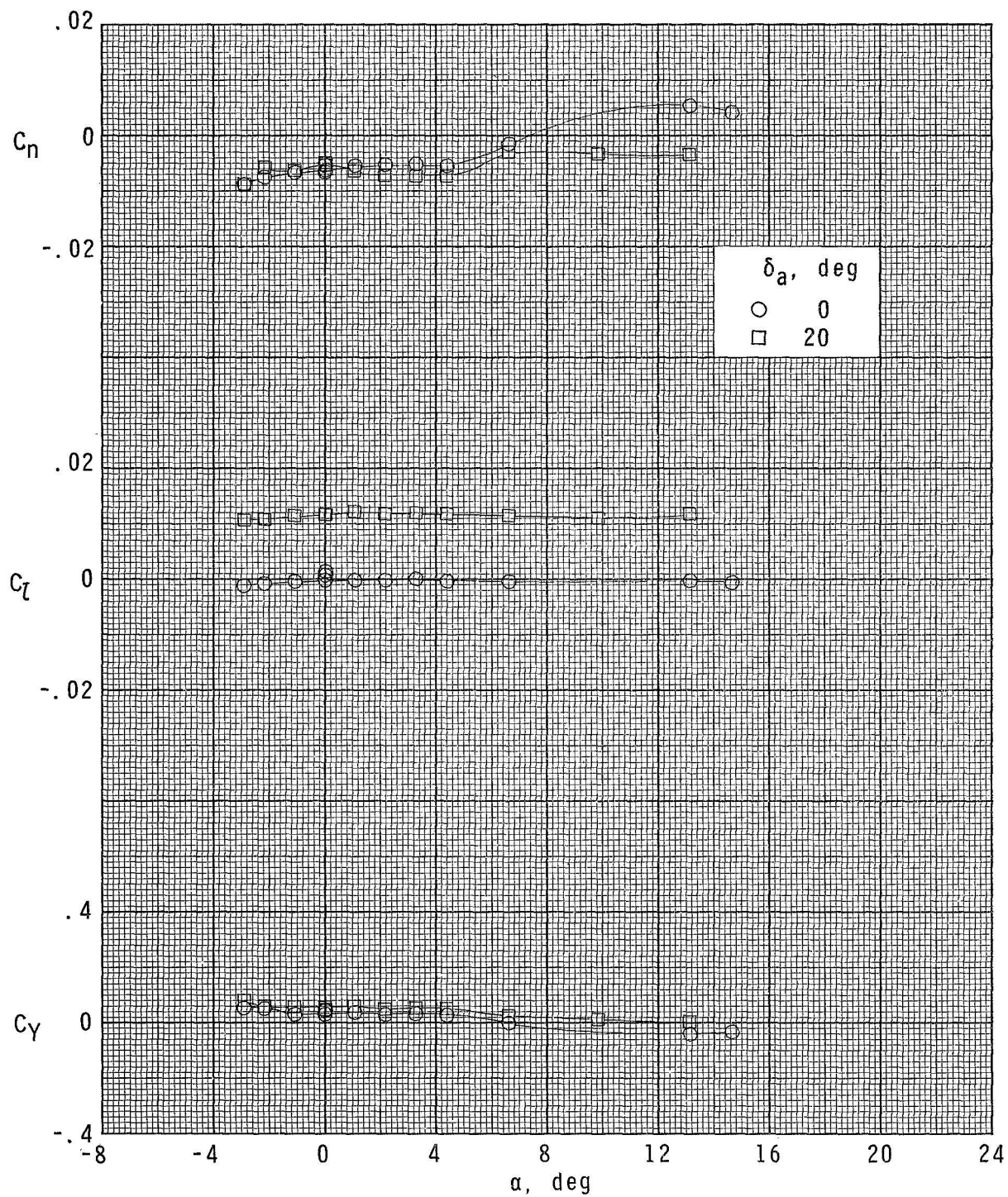
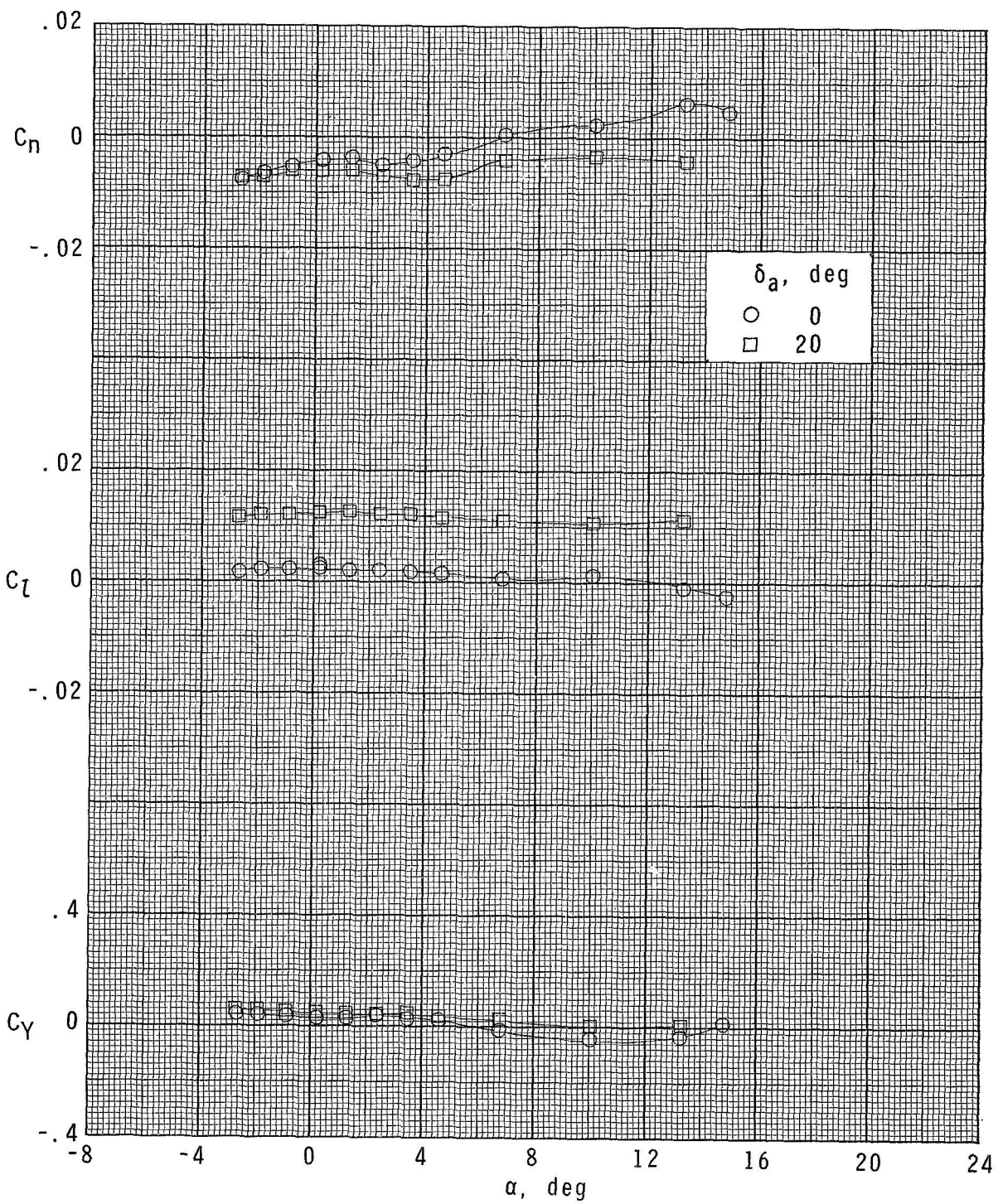


Figure 19.- Summary of lateral and directional stability parameters. $\alpha = 0^\circ$.



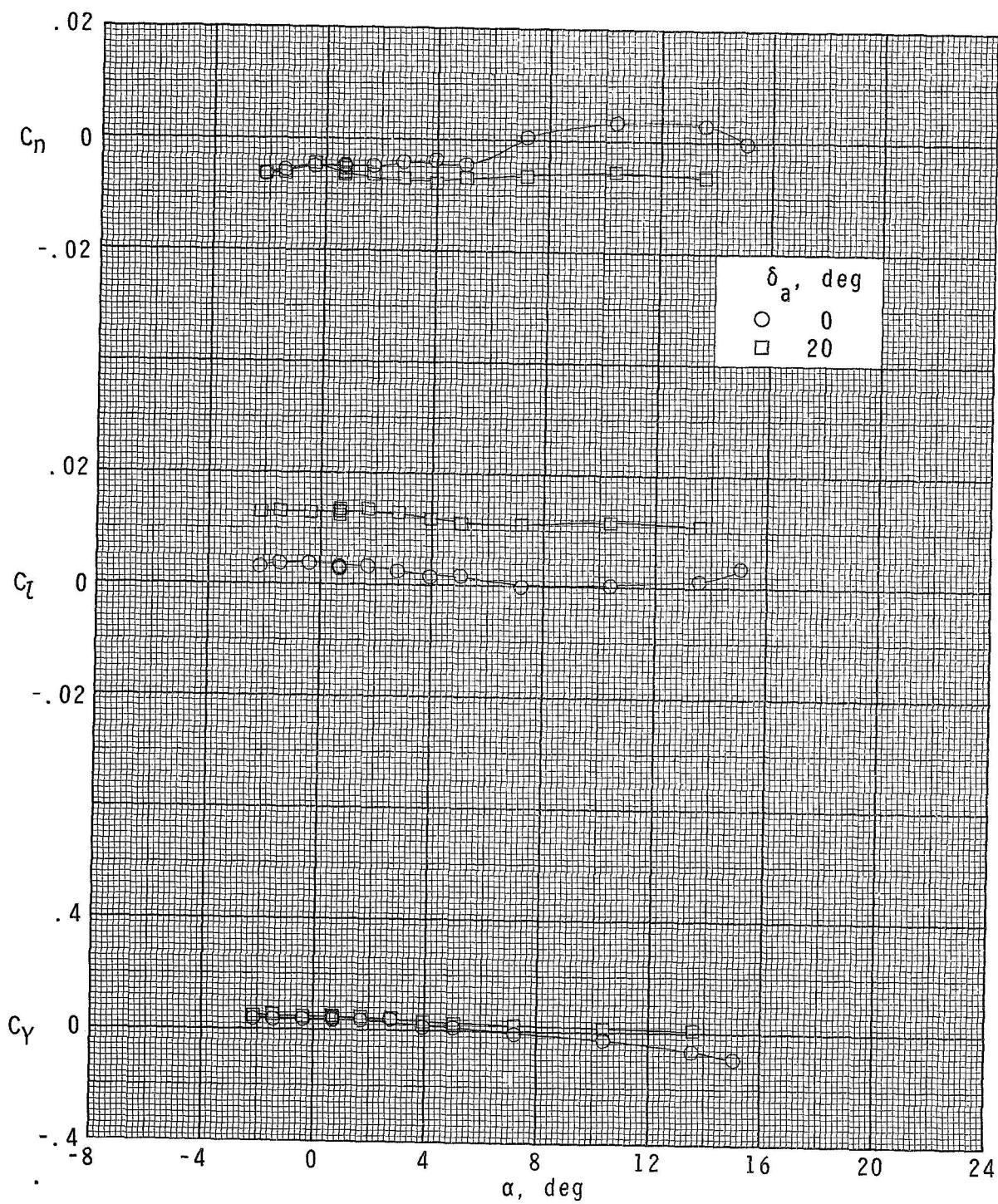
(a) $M = 1.70$; $\delta_c = 0^\circ$.

Figure 20.- Aileron-control effectiveness of configuration $B_1W_1F_1C_1$.



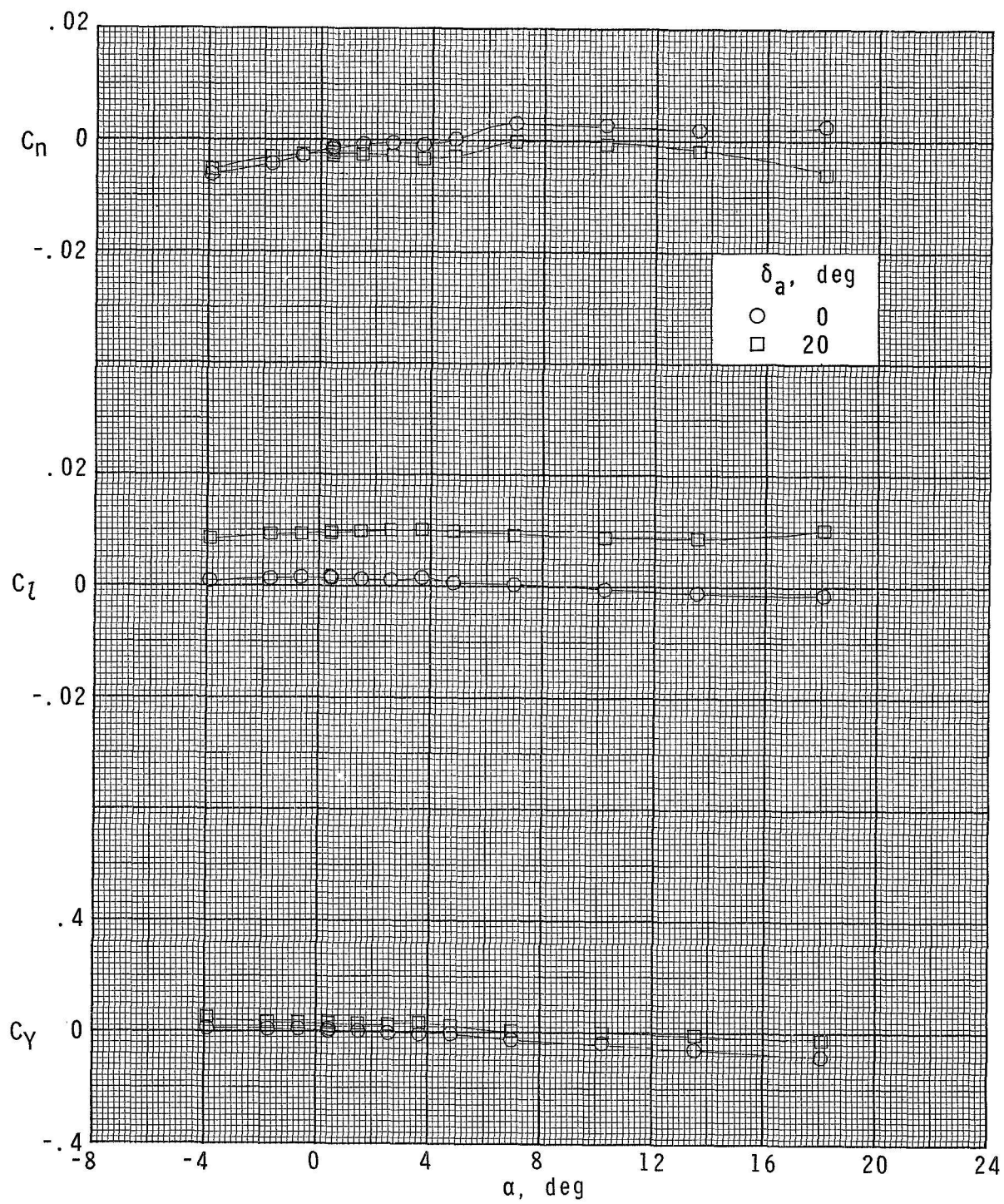
(b) $M = 1.70$; $\delta_c = 50^\circ$.

Figure 20.- Continued.



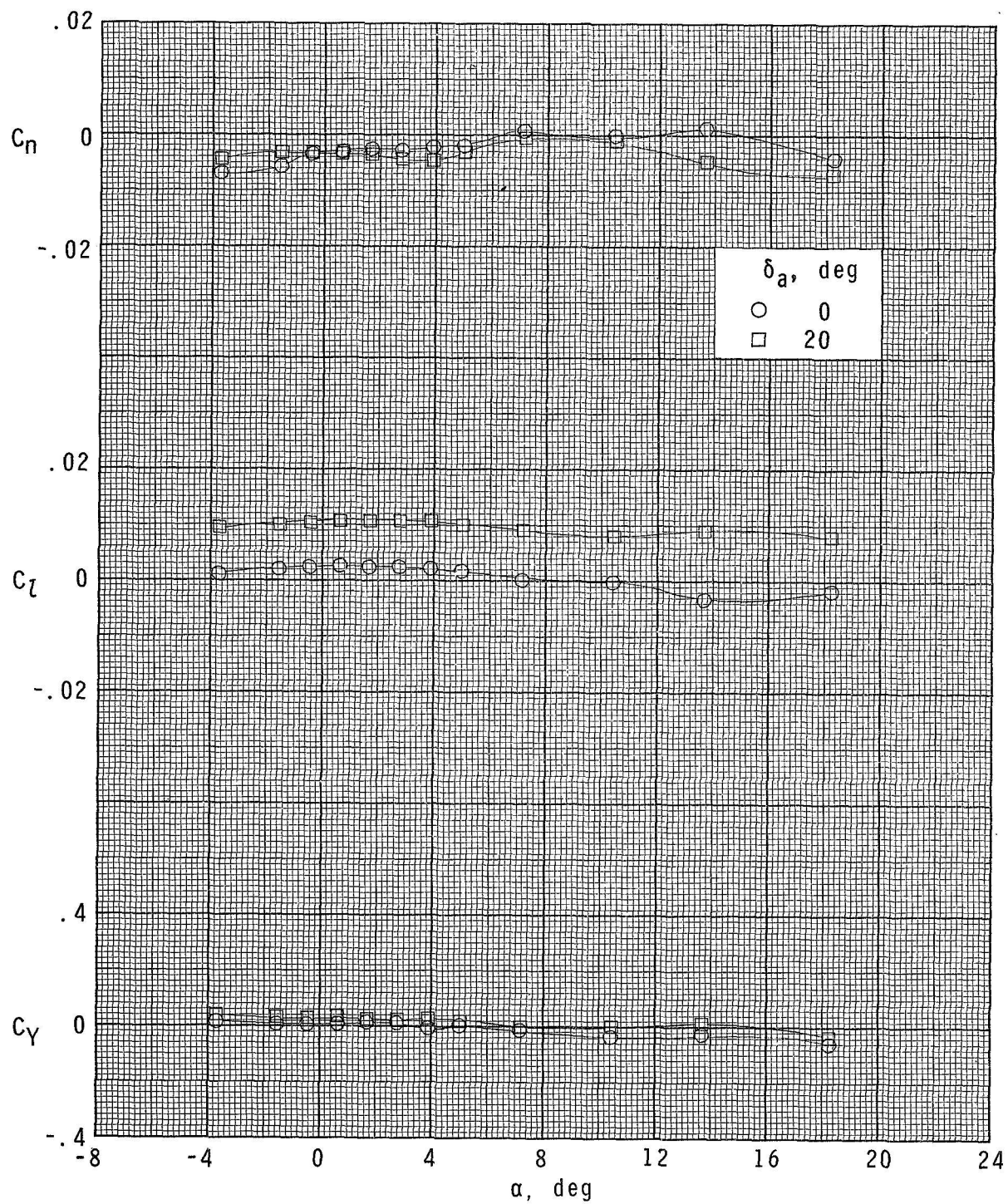
(c) $M = 1.70$; $\delta_c = 15^\circ$.

Figure 20.- Continued.



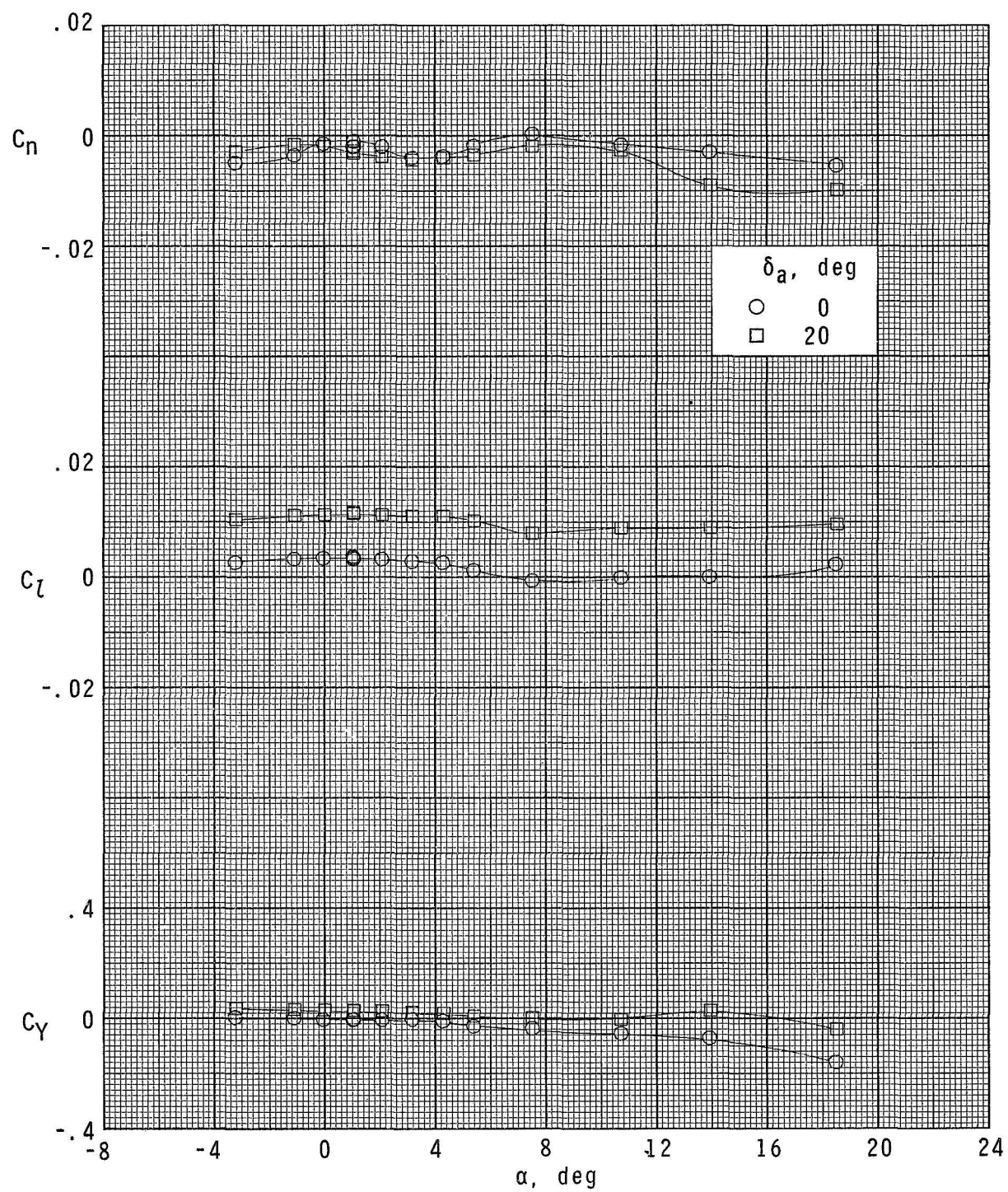
(d) $M = 2.00$; $\delta_c = 0^\circ$.

Figure 20.- Continued.



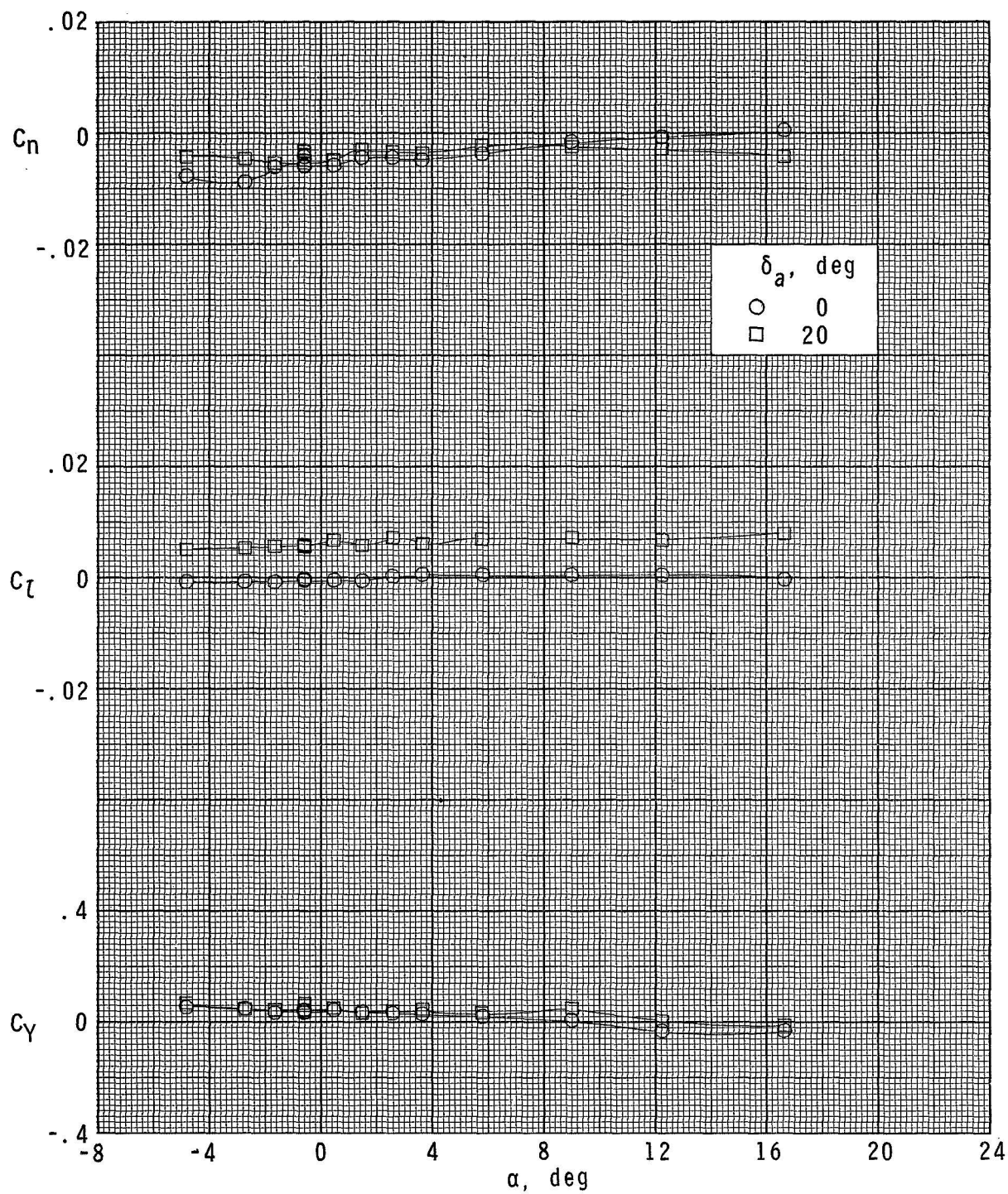
(e) $M = 2.00$; $\delta_c = 5^\circ$.

Figure 20.- Continued.



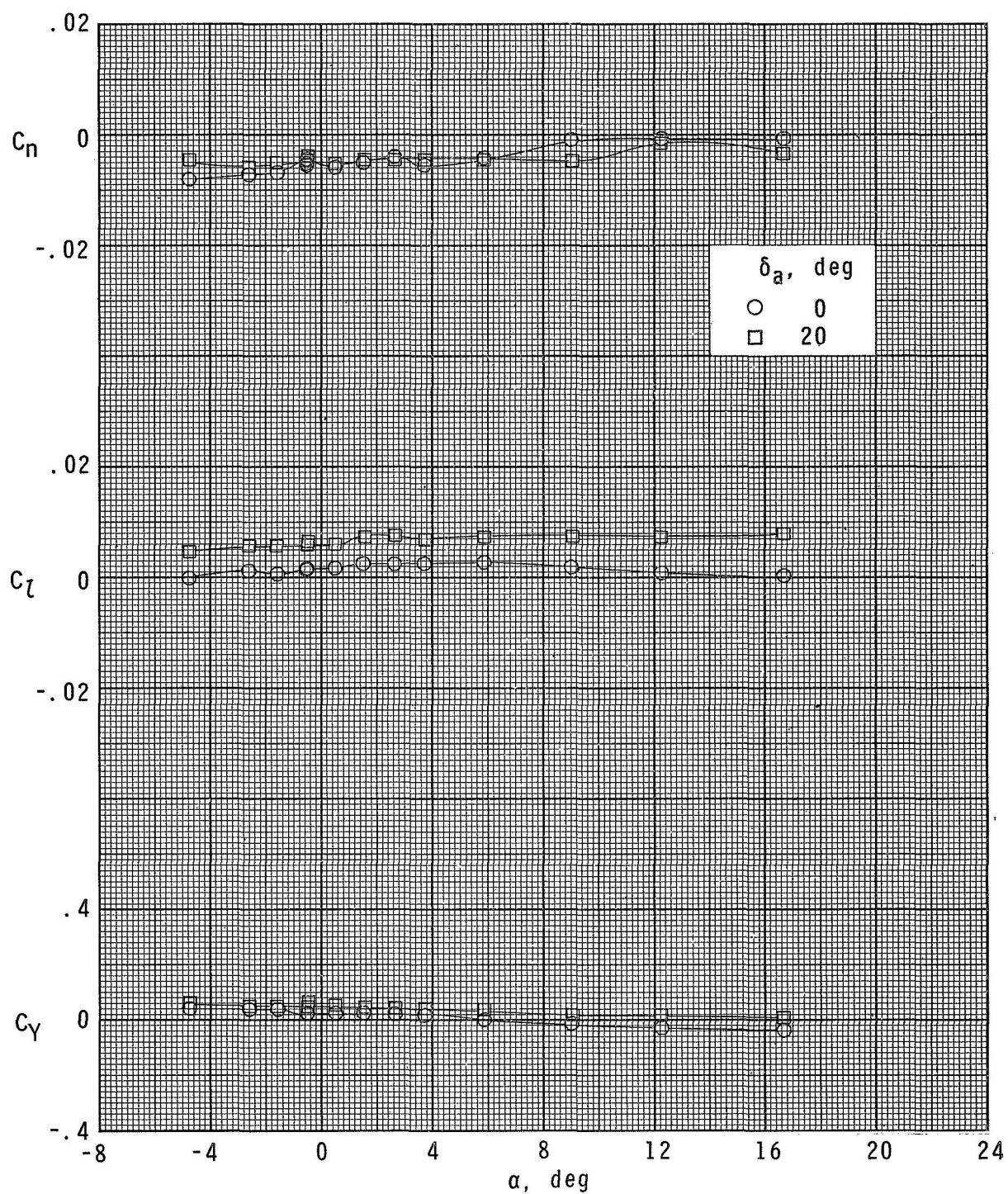
(f) $M = 2.00$; $\delta_c = 15^\circ$.

Figure 20.- Continued.



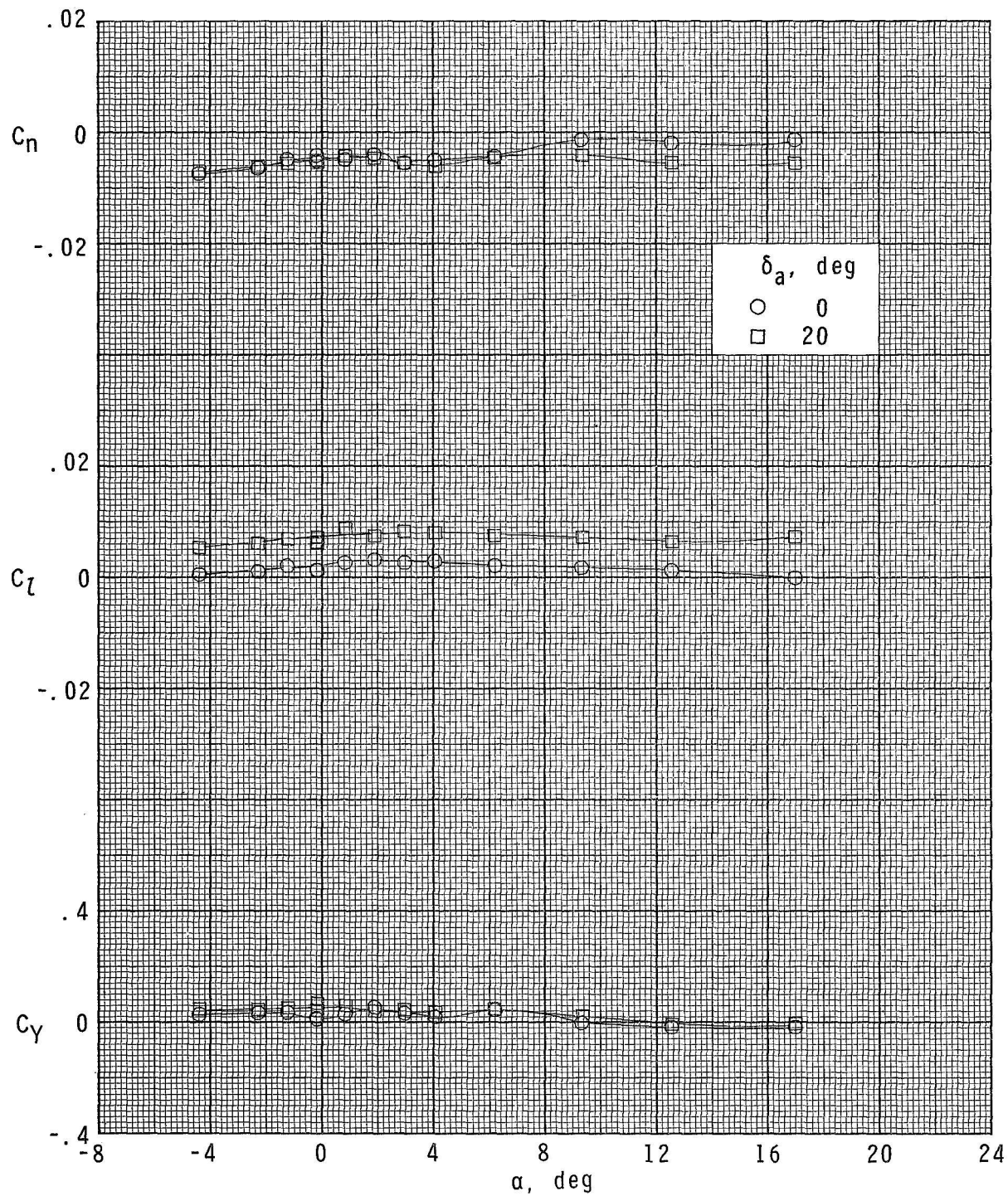
(g) $M = 2.86$; $\delta_c = 0^\circ$.

Figure 20.- Continued.



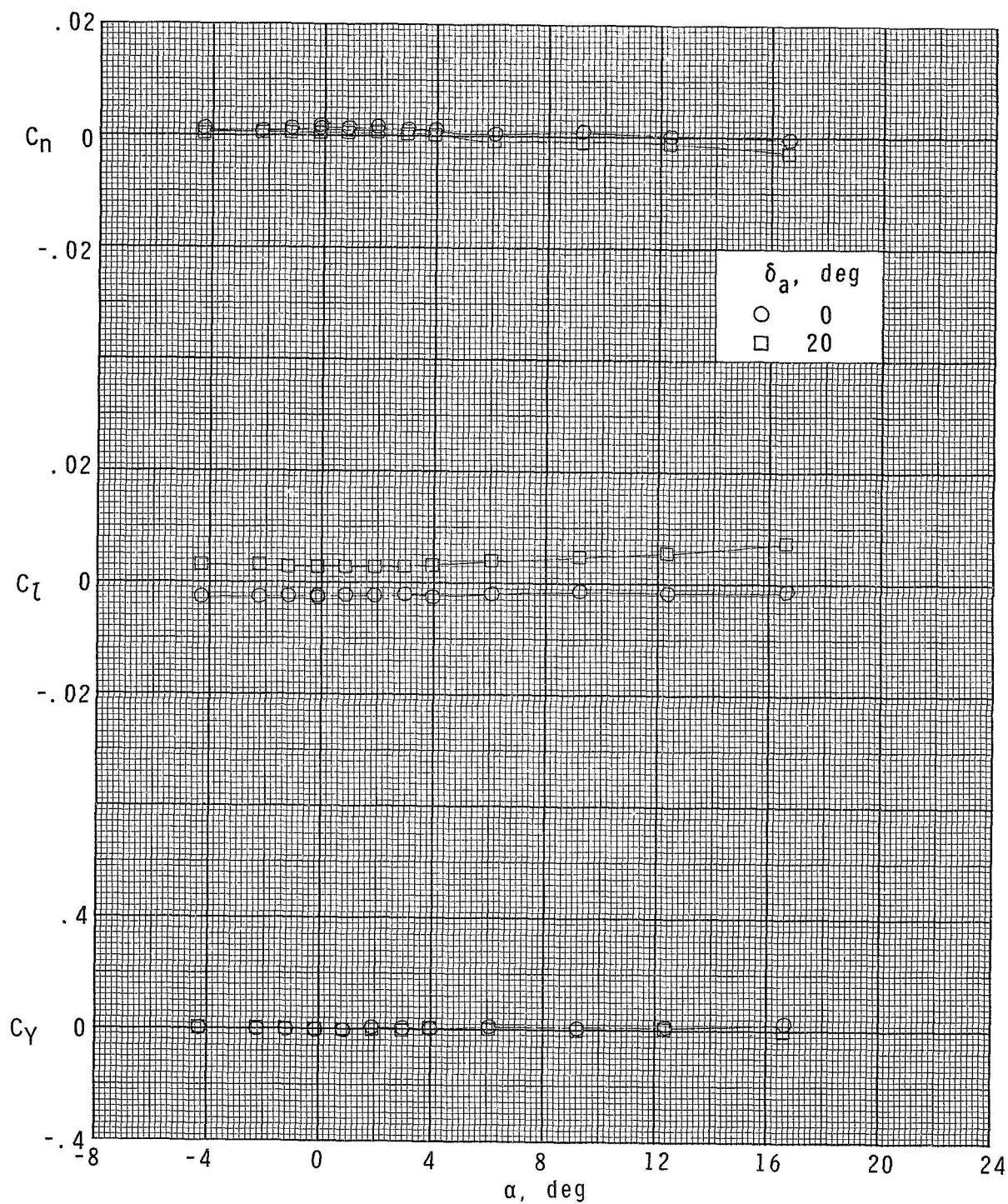
(h) $M = 2.86$; $\delta_c = 50^\circ$.

Figure 20.- Continued.



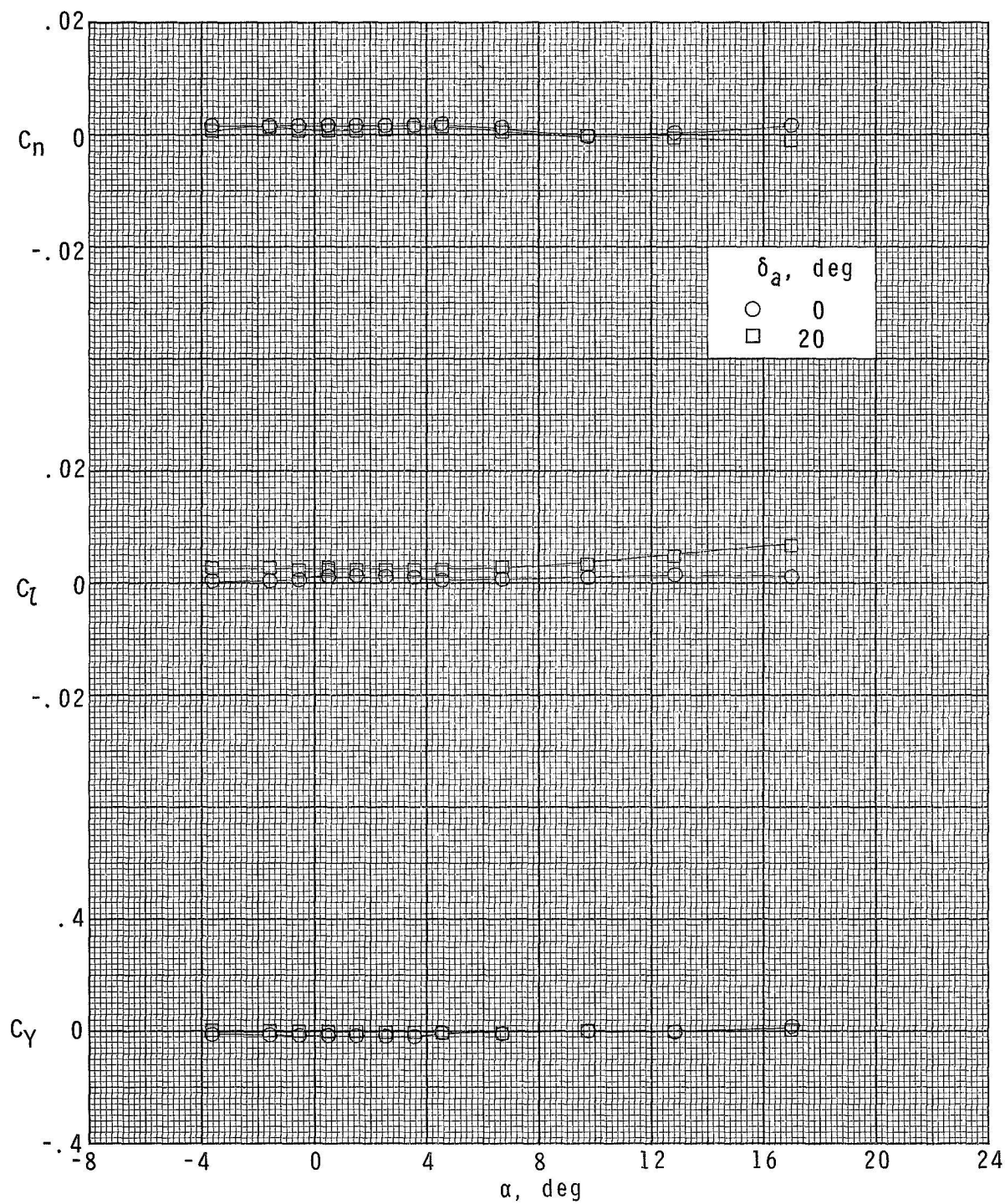
(i) $M = 2.86$; $\delta_c = 15^\circ$.

Figure 20.- Continued.



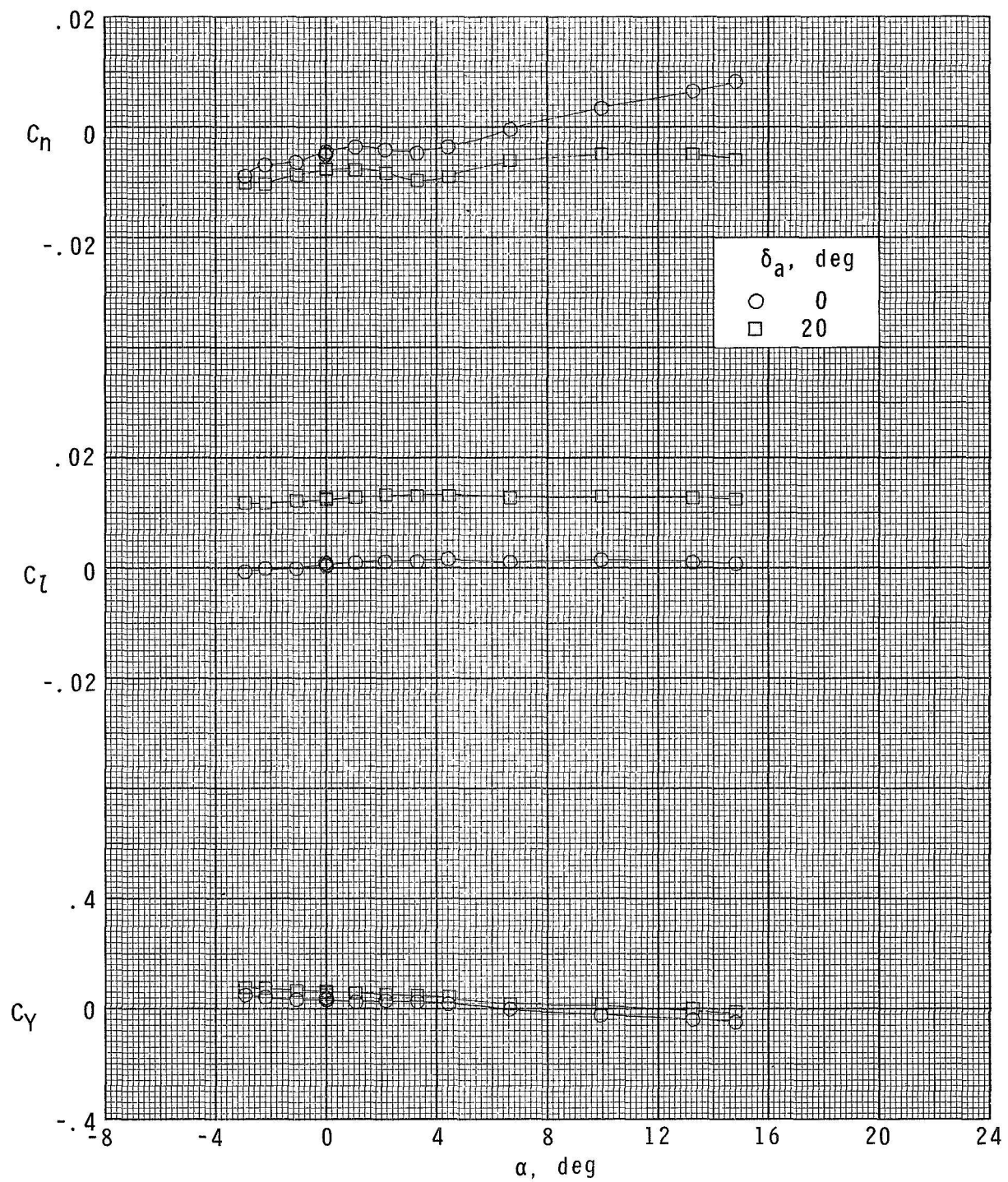
(j) $M \approx 3.95$; $\delta_c = 0^\circ$.

Figure 20.- Continued.



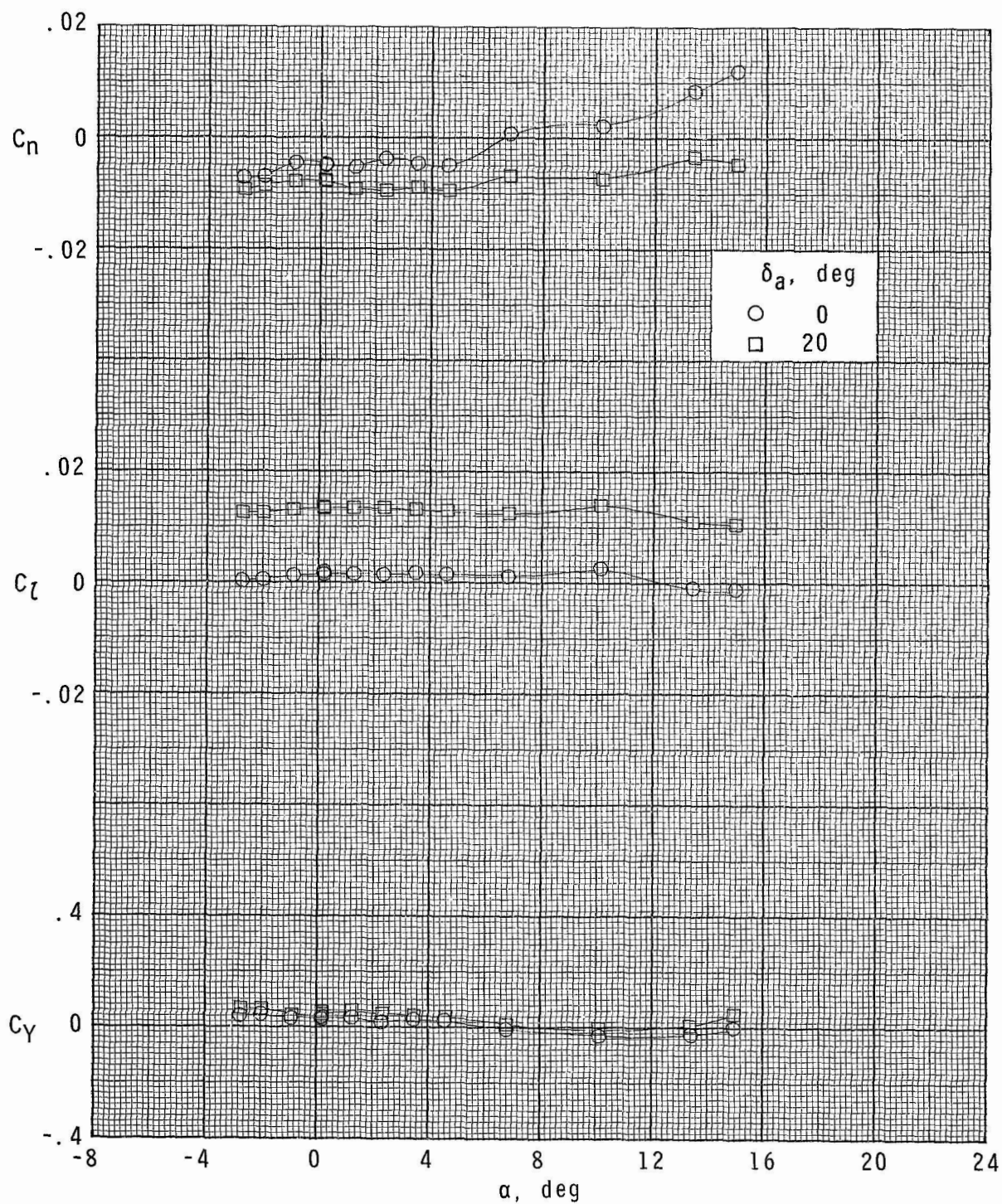
(k) $M = 4.63$; $\delta_c = 0^\circ$.

Figure 20.- Concluded.



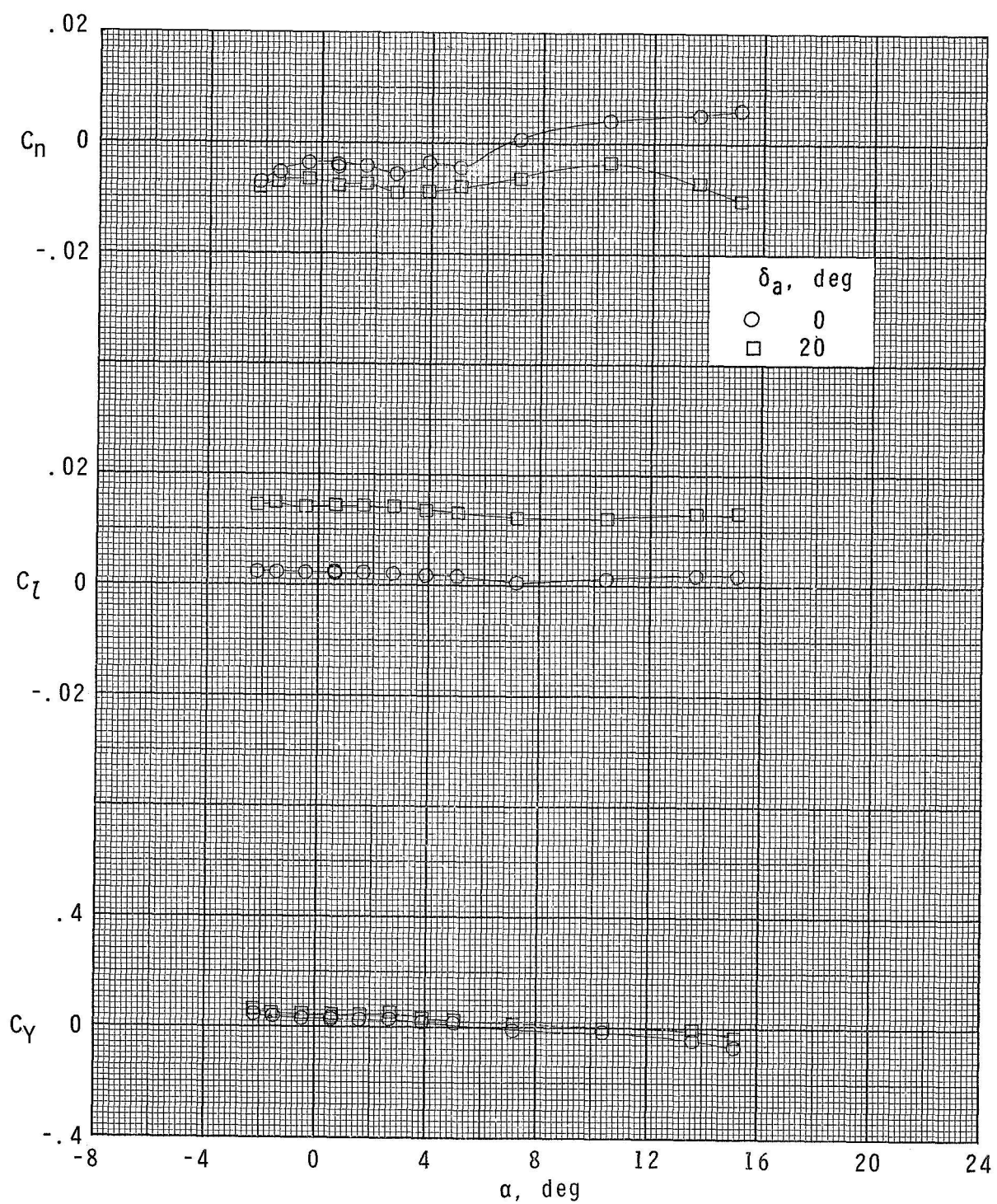
(a) $M = 1.70$; $\delta_c = 0^\circ$.

Figure 21.- Airleron-control effectiveness of configuration $B_1W_2F_1C_1$.



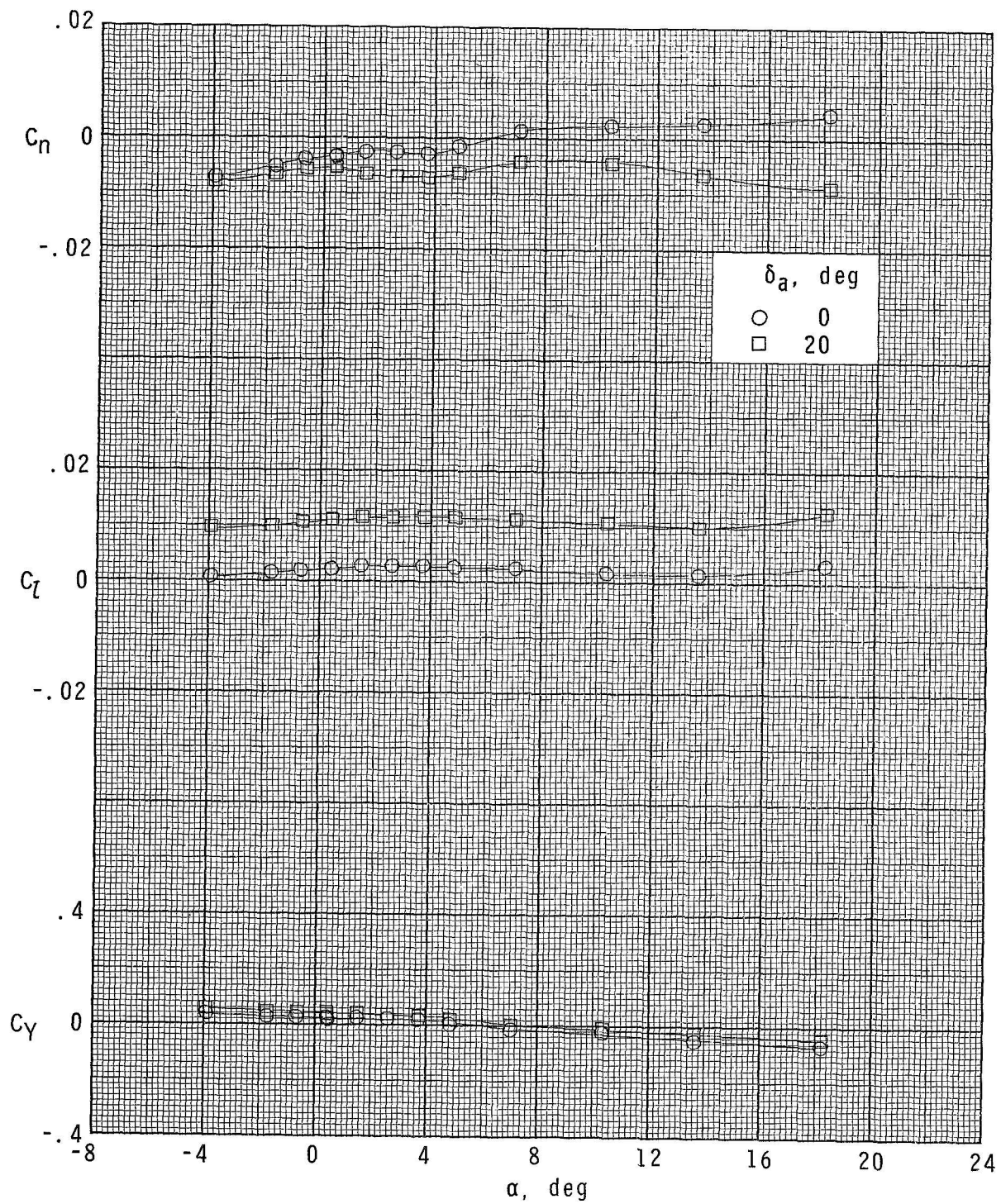
(b) $M = 1.70$; $\delta_c = 50^\circ$.

Figure 21.- Continued.



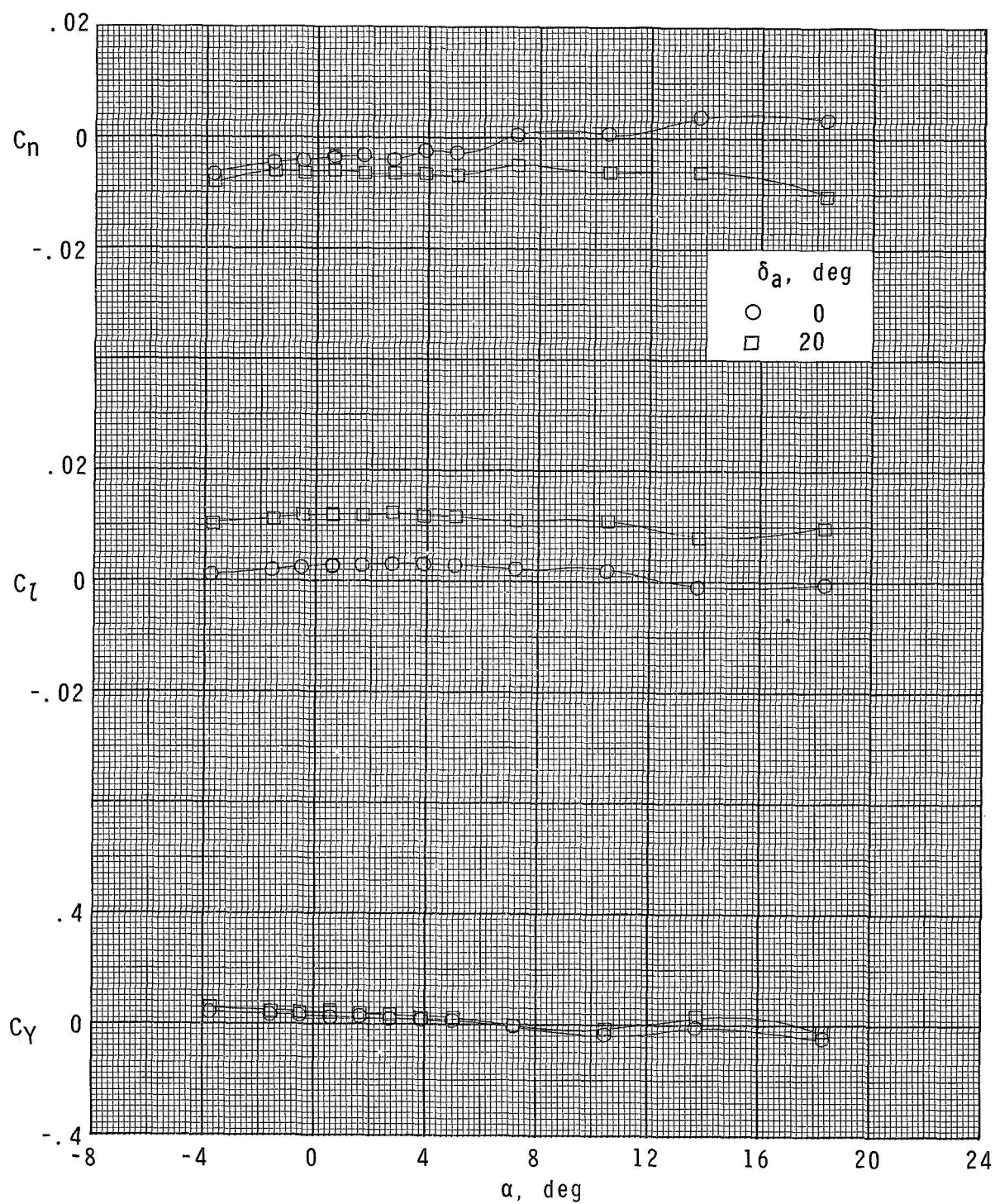
(c) $M = 1.70$; $\delta_c = 15^\circ$.

Figure 21.- Continued.



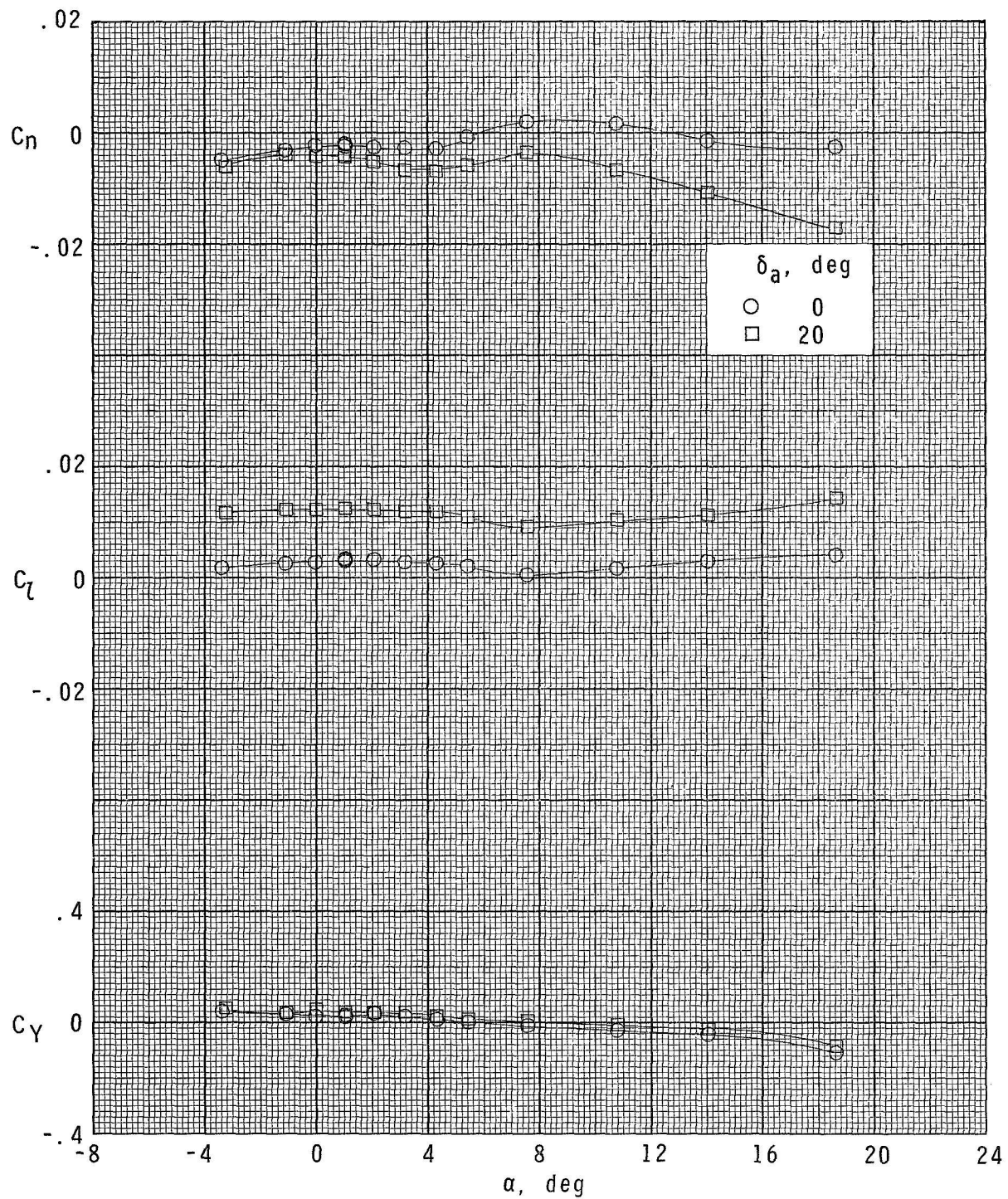
(d) $M = 2.00$; $\delta_c = 0^\circ$.

Figure 21.- Continued.



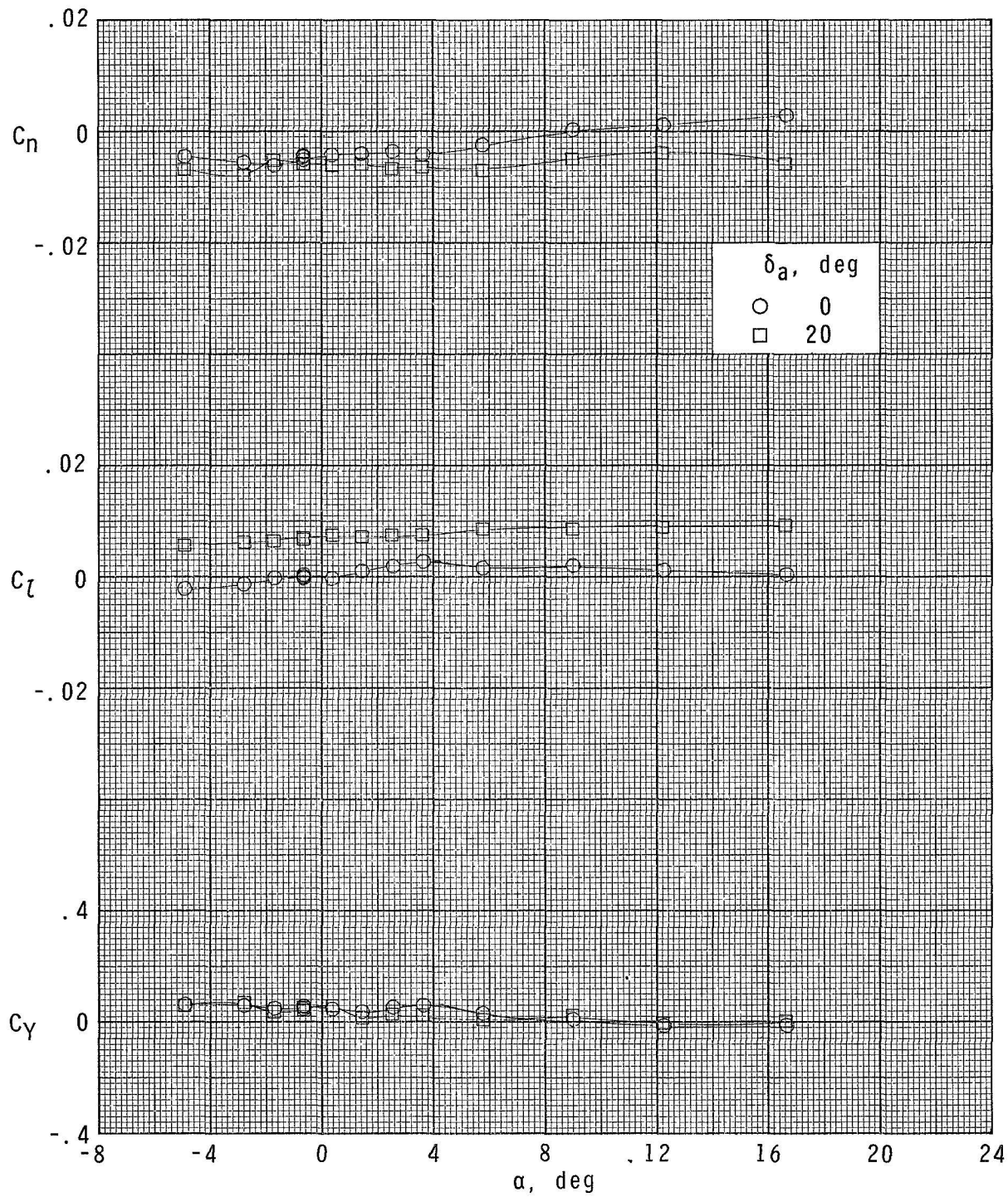
(e) $M = 2.00$; $\delta_c = 5^\circ$.

Figure 21.- Continued.



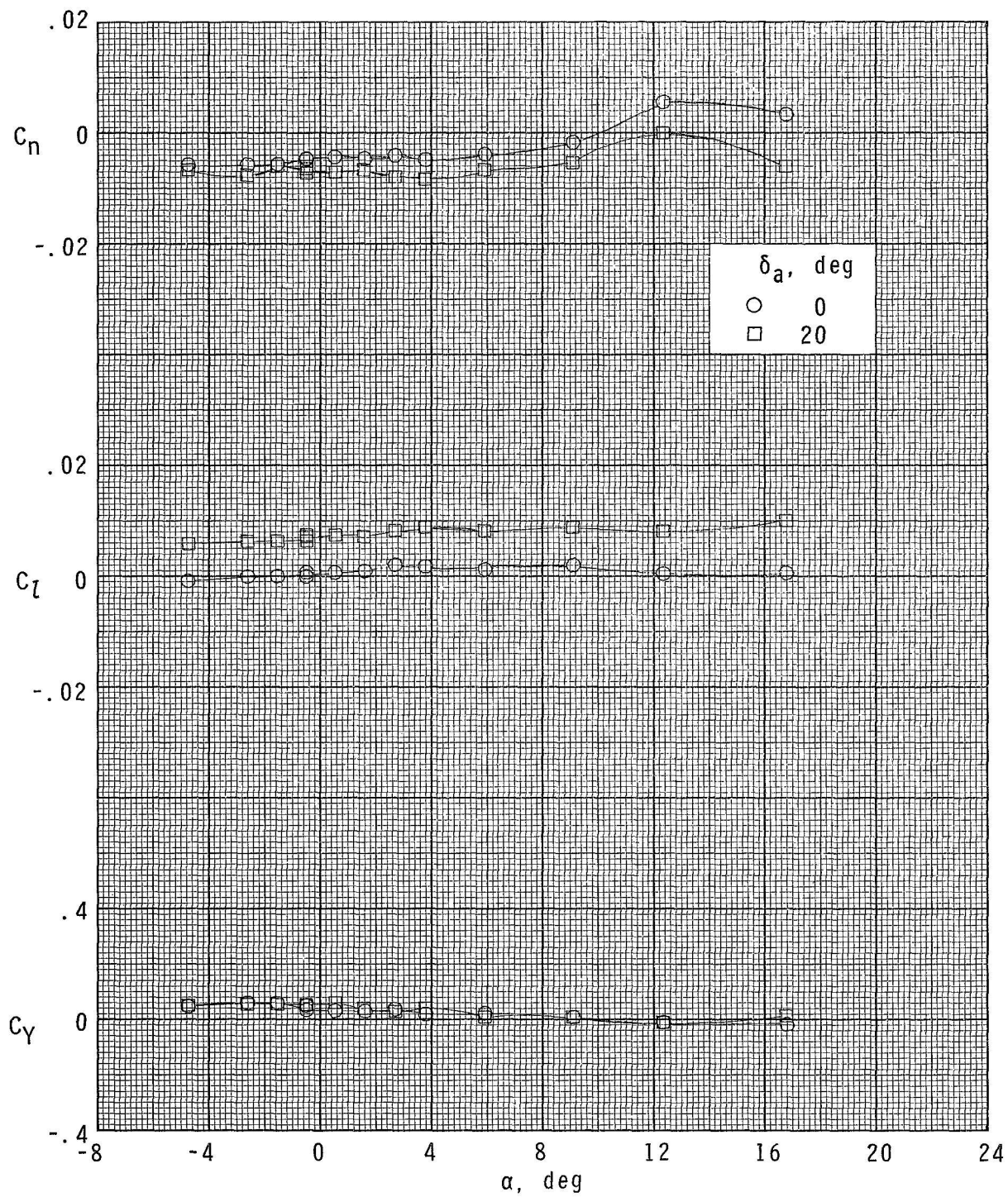
(f) $M = 2.00$; $\delta_c = 15^\circ$.

Figure 21.- Continued.



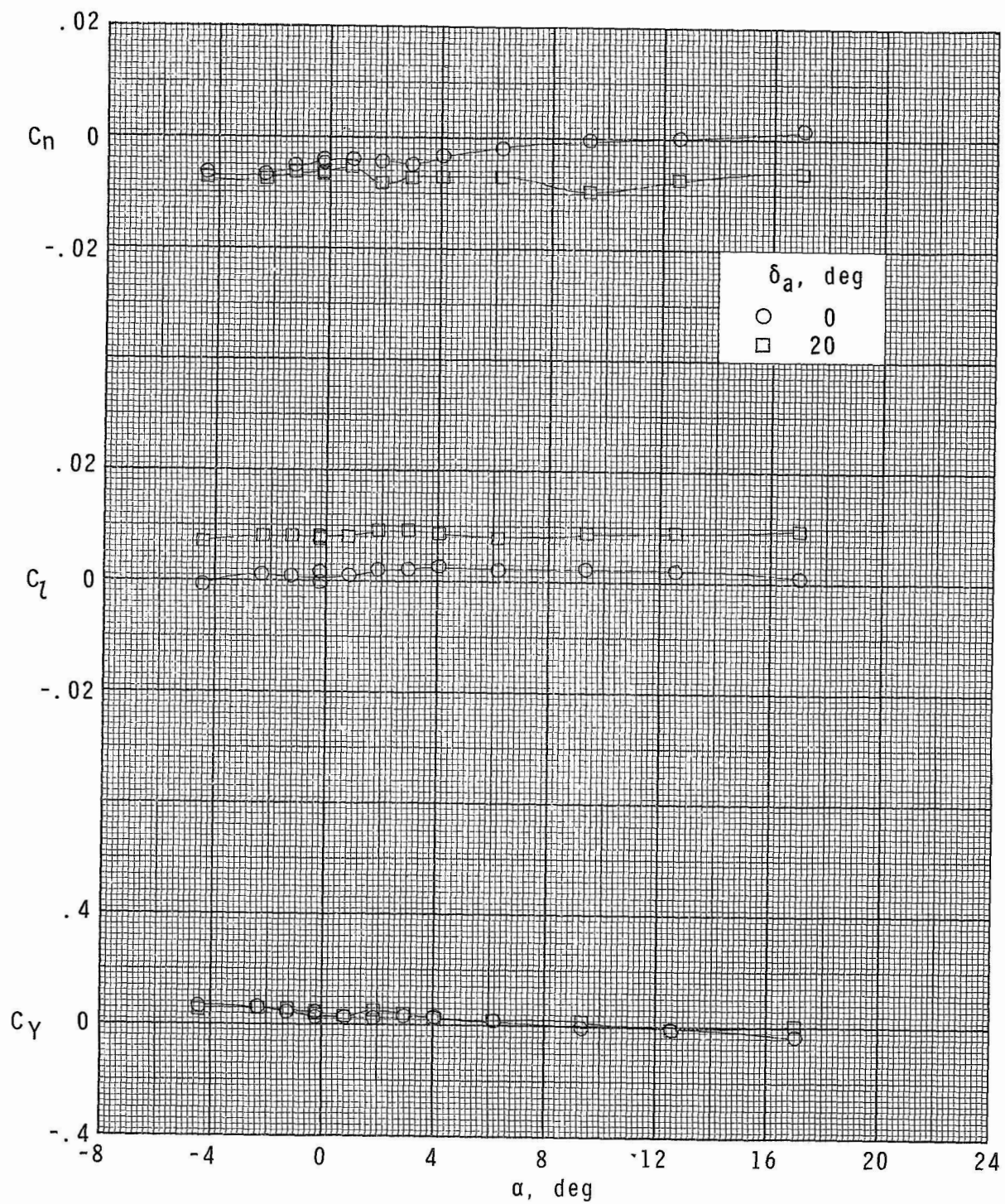
(g) $M = 2.86$; $\delta_c = 0^\circ$.

Figure 21.- Continued.



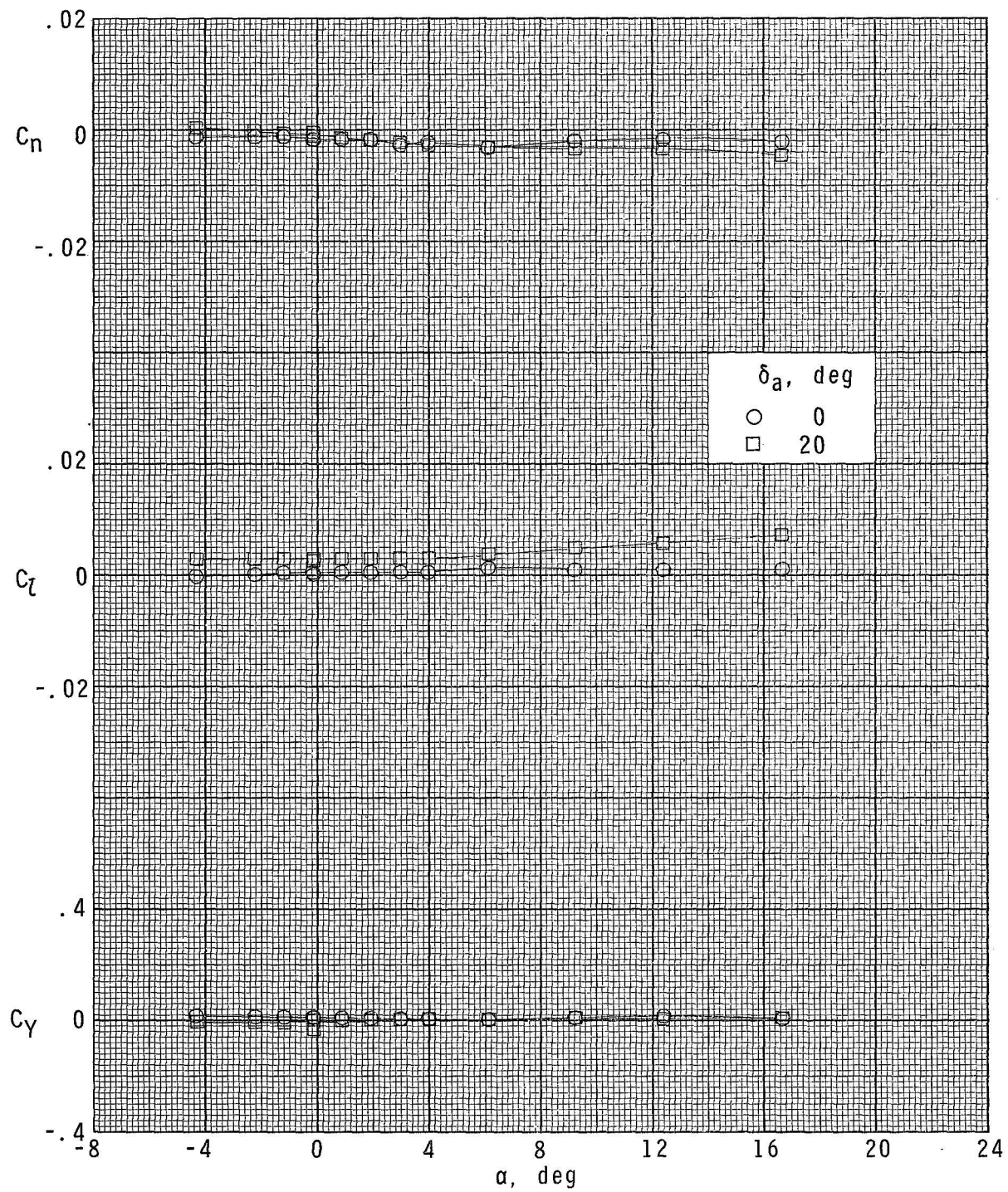
(h) $M = 2.86$; $\delta_c = 50^\circ$.

Figure 21.- Continued.



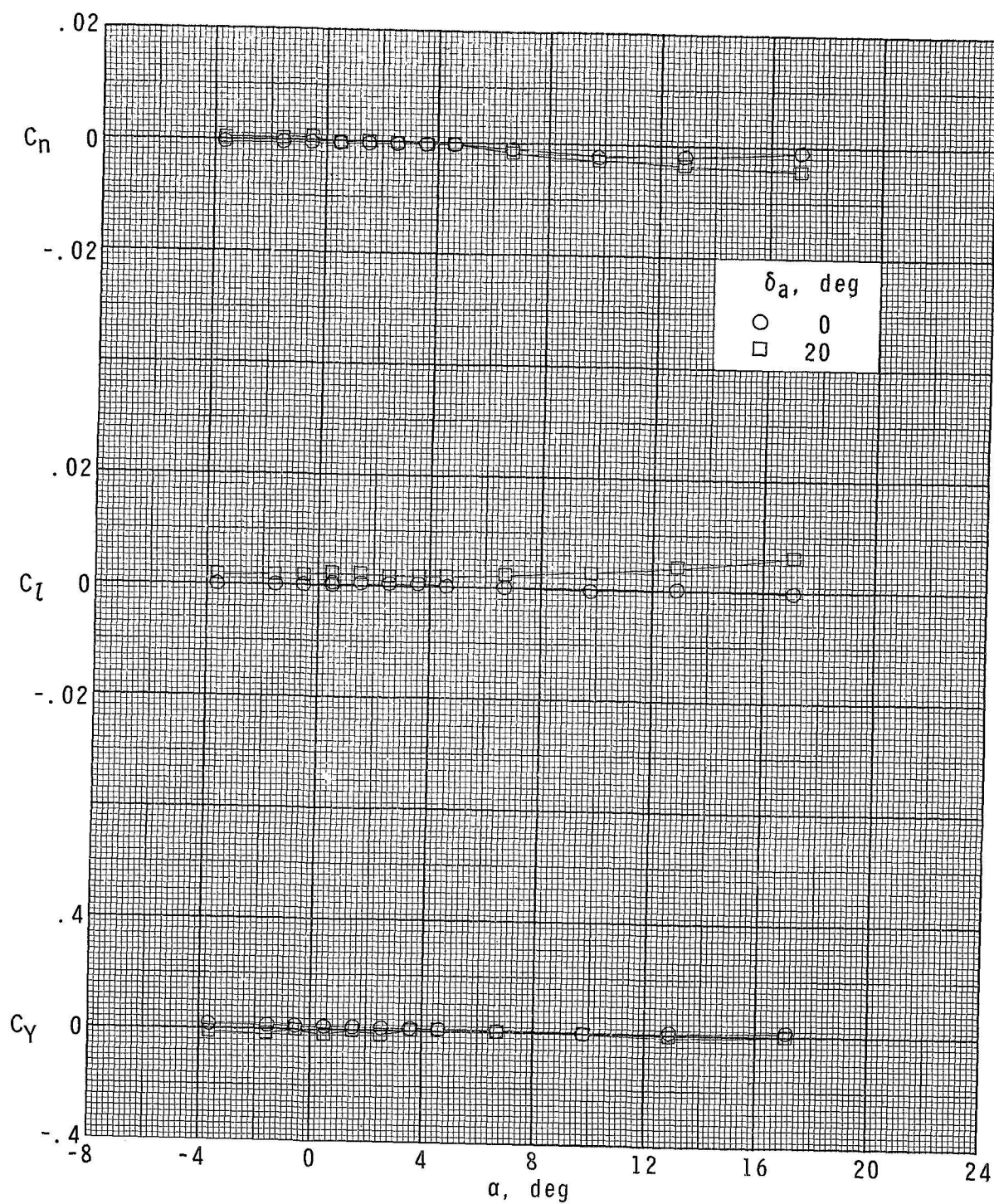
(i) $M = 2.86$; $\delta_c = 15^\circ$.

Figure 21.- Continued.



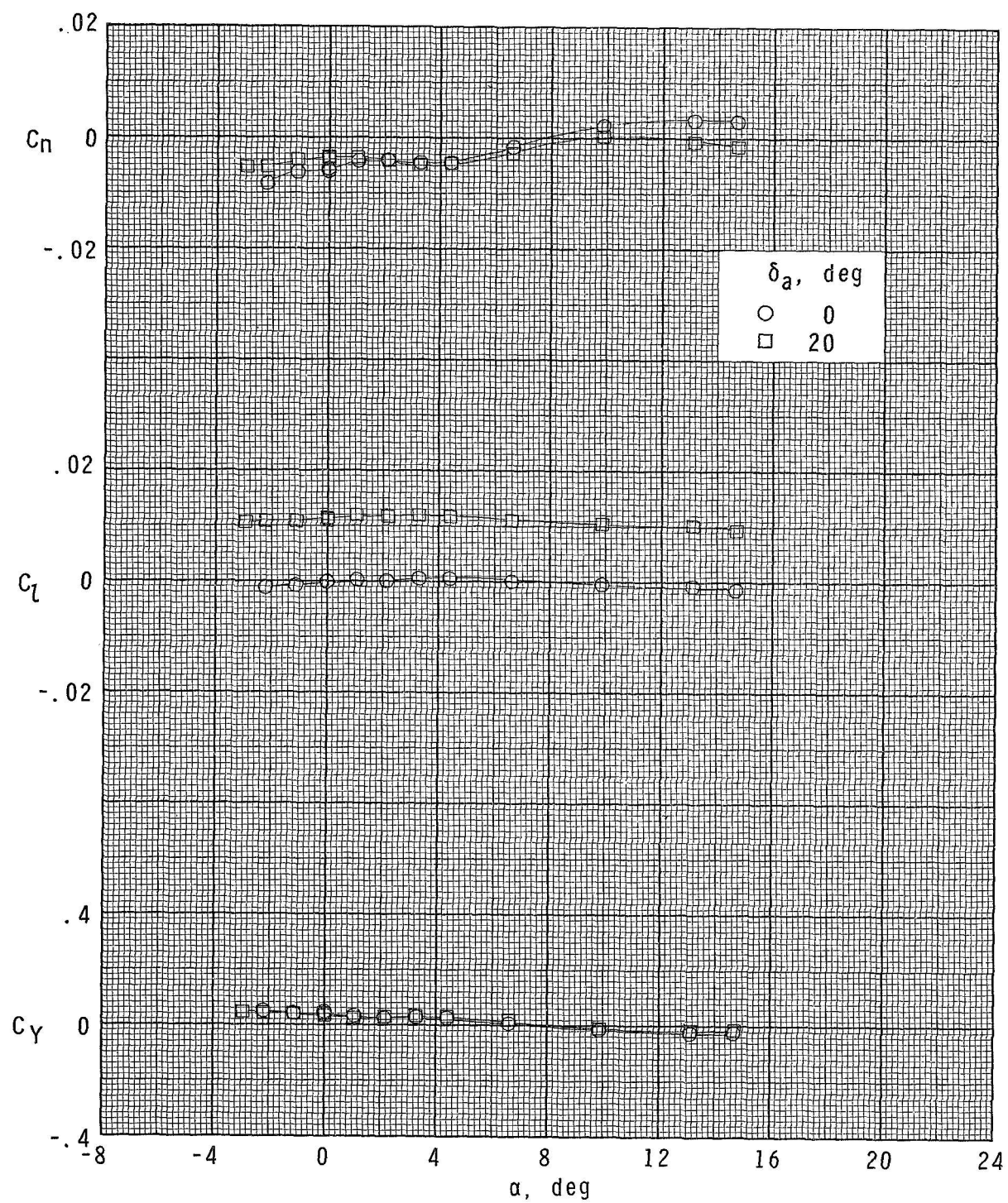
(j) $M = 3.95$; $\delta_c = 0^\circ$.

Figure 21.- Continued.



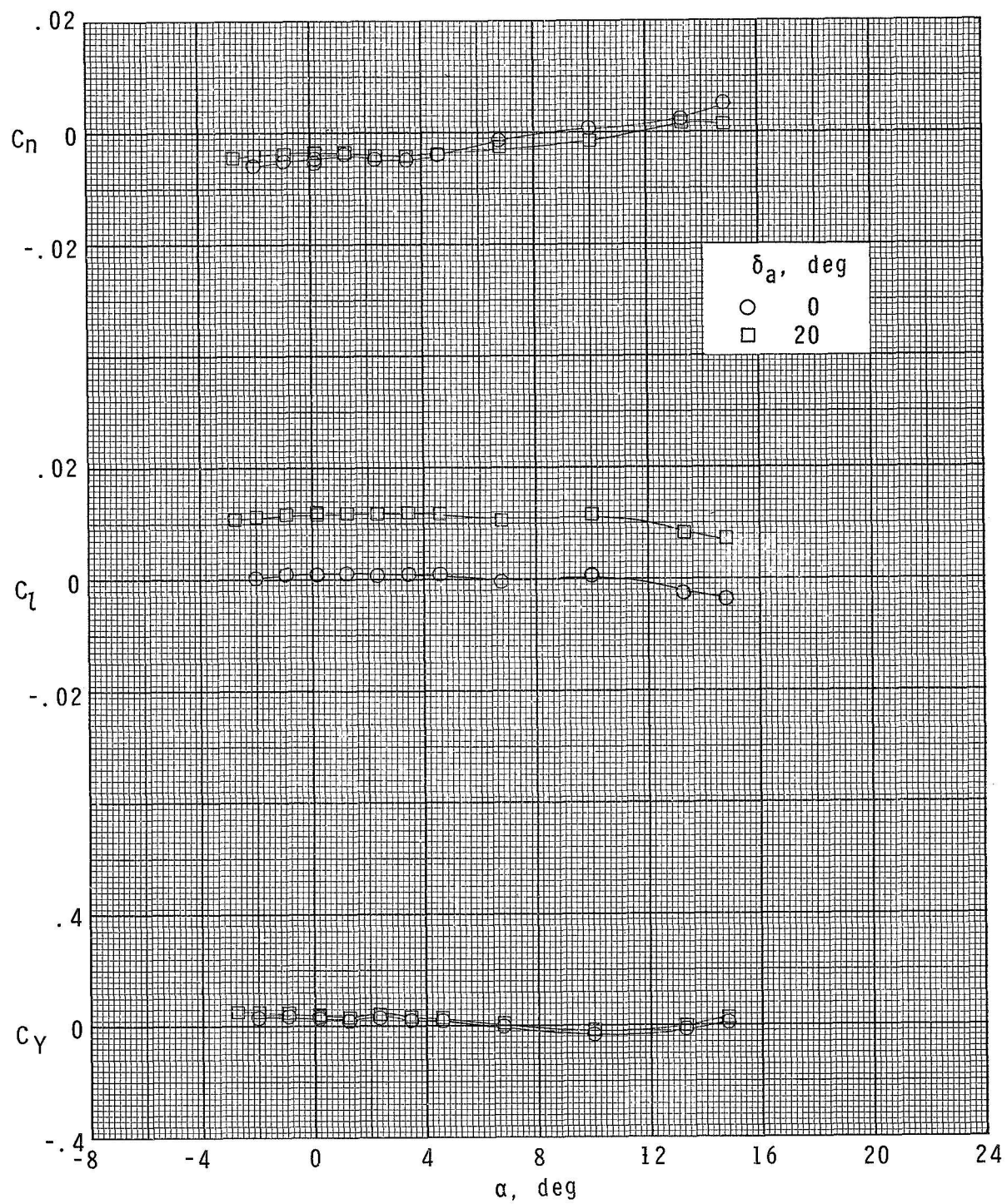
(k) $M = 4.63$; $\delta_c = 0^\circ$.

Figure 21.- Concluded.



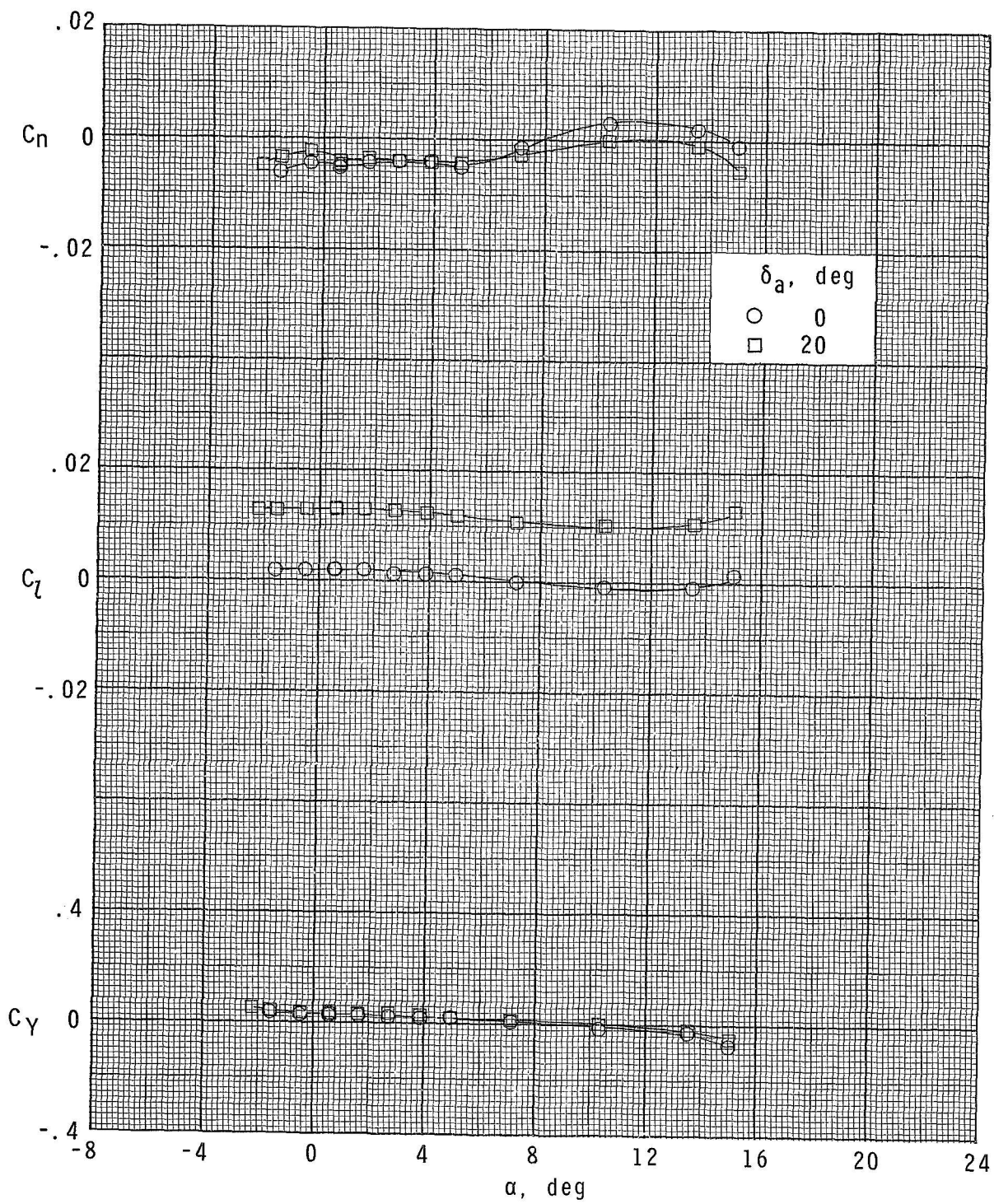
(a) $M = 1.70$; $\delta_c = 0^\circ$.

Figure 22.- Aileron-control effectiveness of configuration $B_1W_1F_2C_1$.



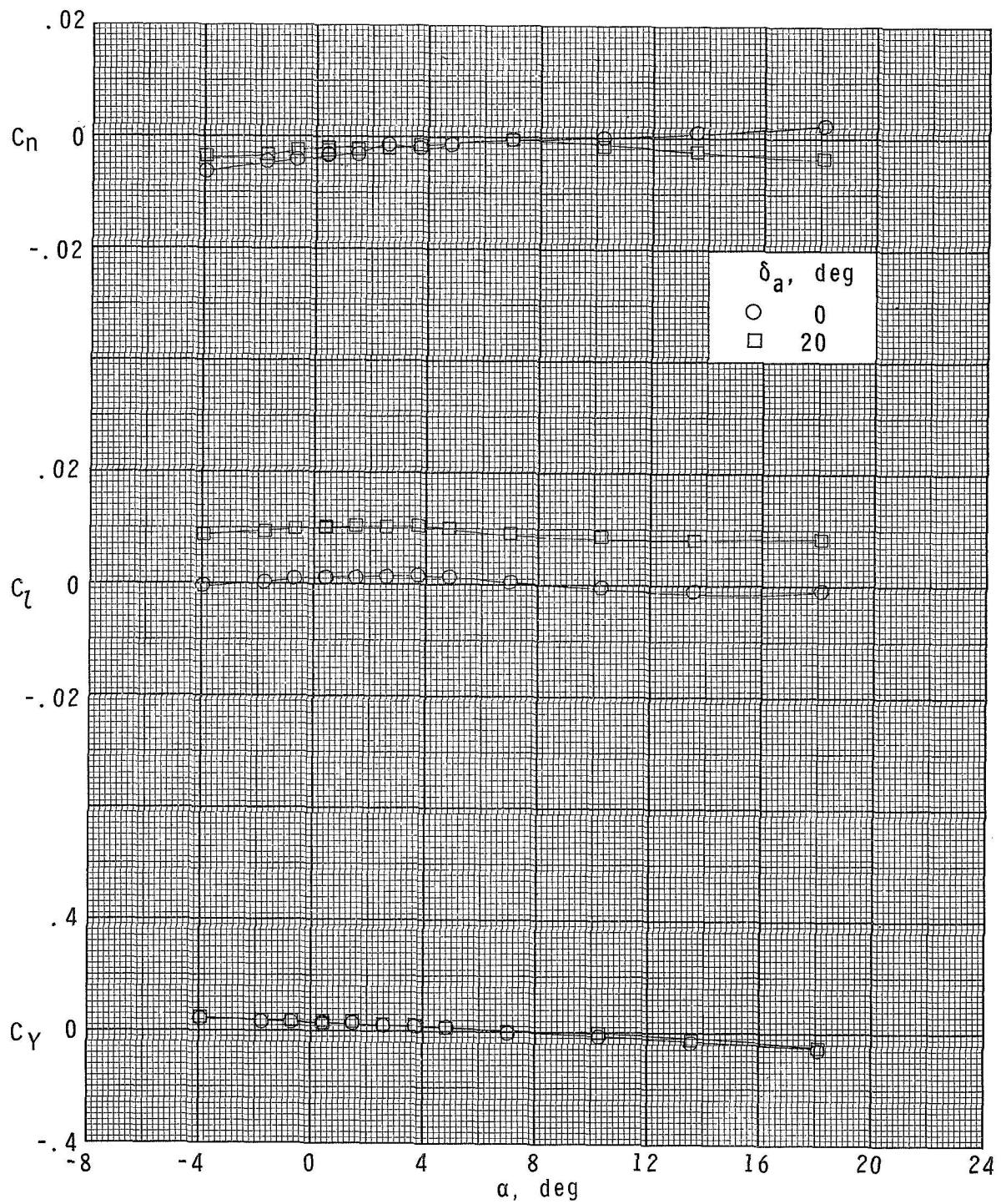
(b) $M = 1.70$; $\delta_c = 5^\circ$.

Figure 22.- Continued.



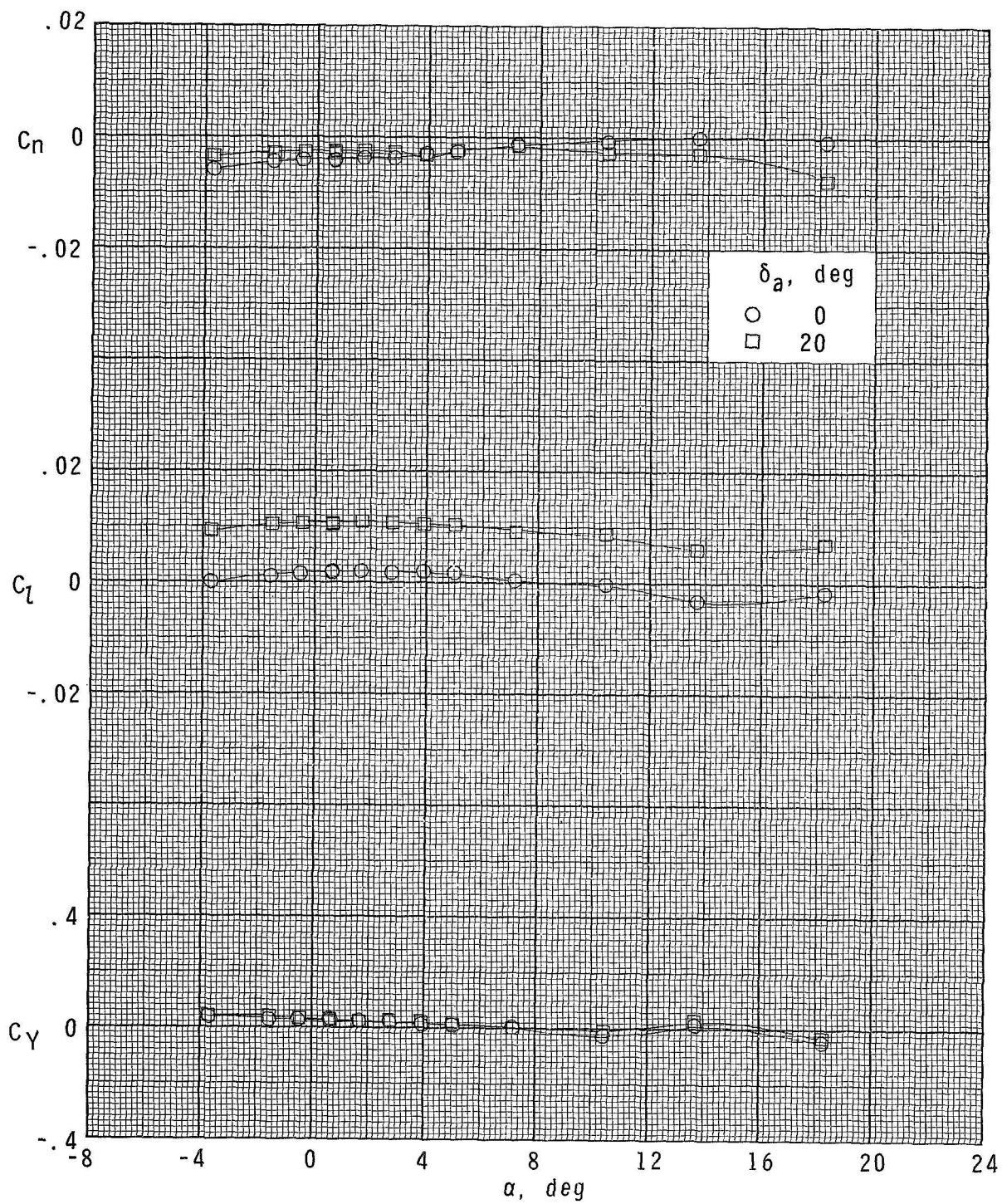
(c) $M = 1.70$; $\delta_c = 15^\circ$.

Figure 22.- Continued.



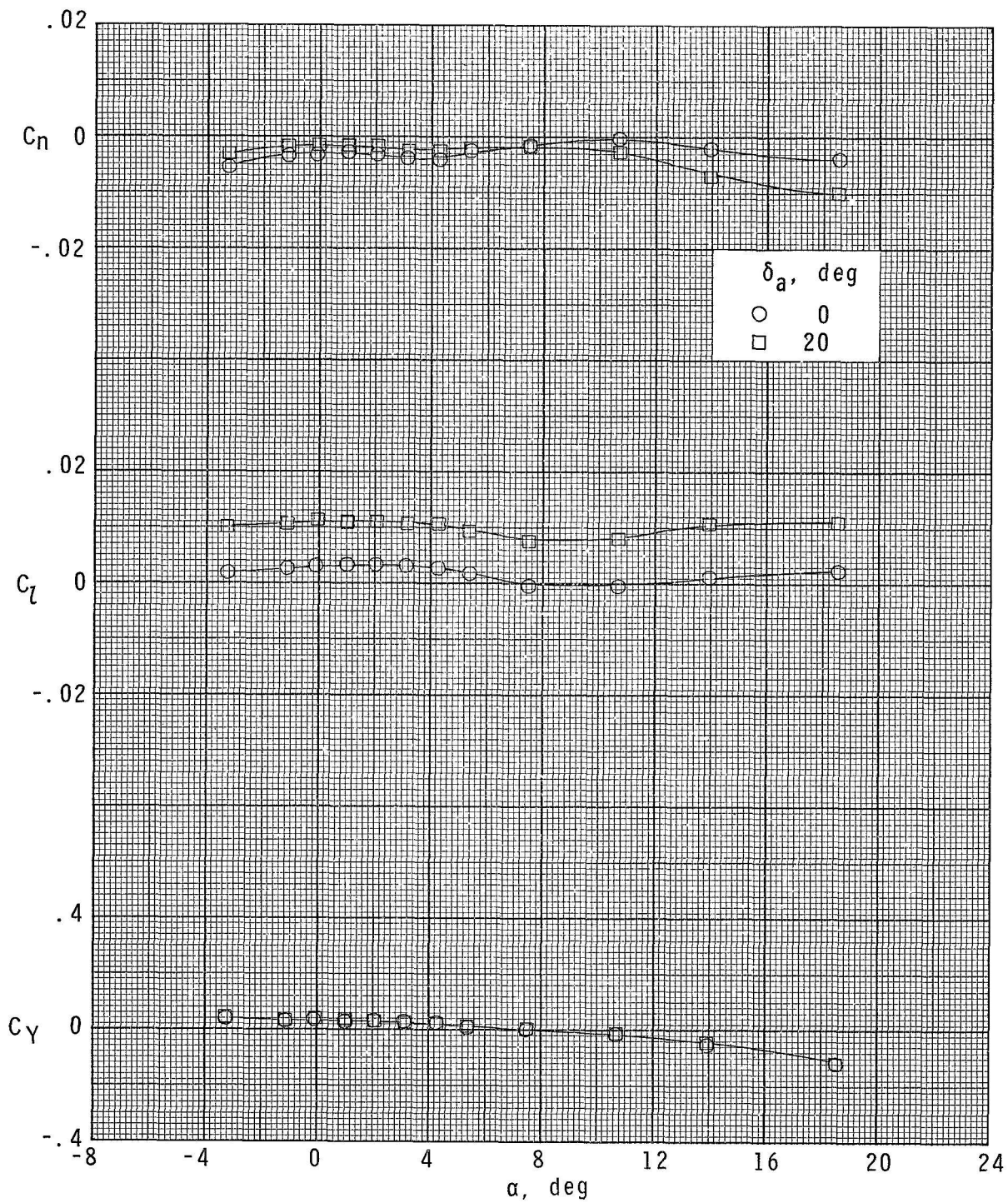
(d) $M = 2.00$; $\delta_c = 0^\circ$.

Figure 22.- Continued.



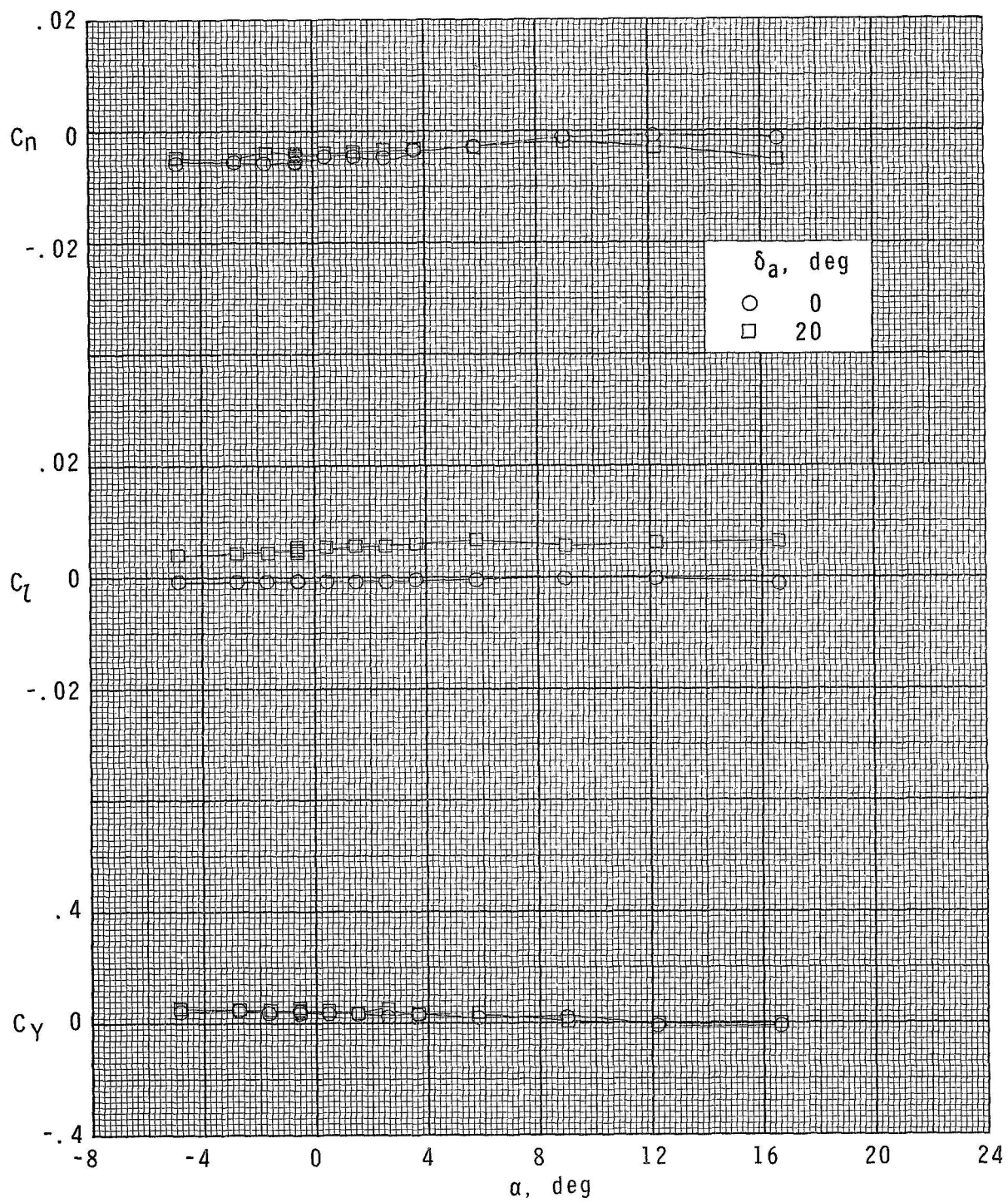
(e) $M = 2.00$; $\delta_c = 5^\circ$.

Figure 22.- Continued.



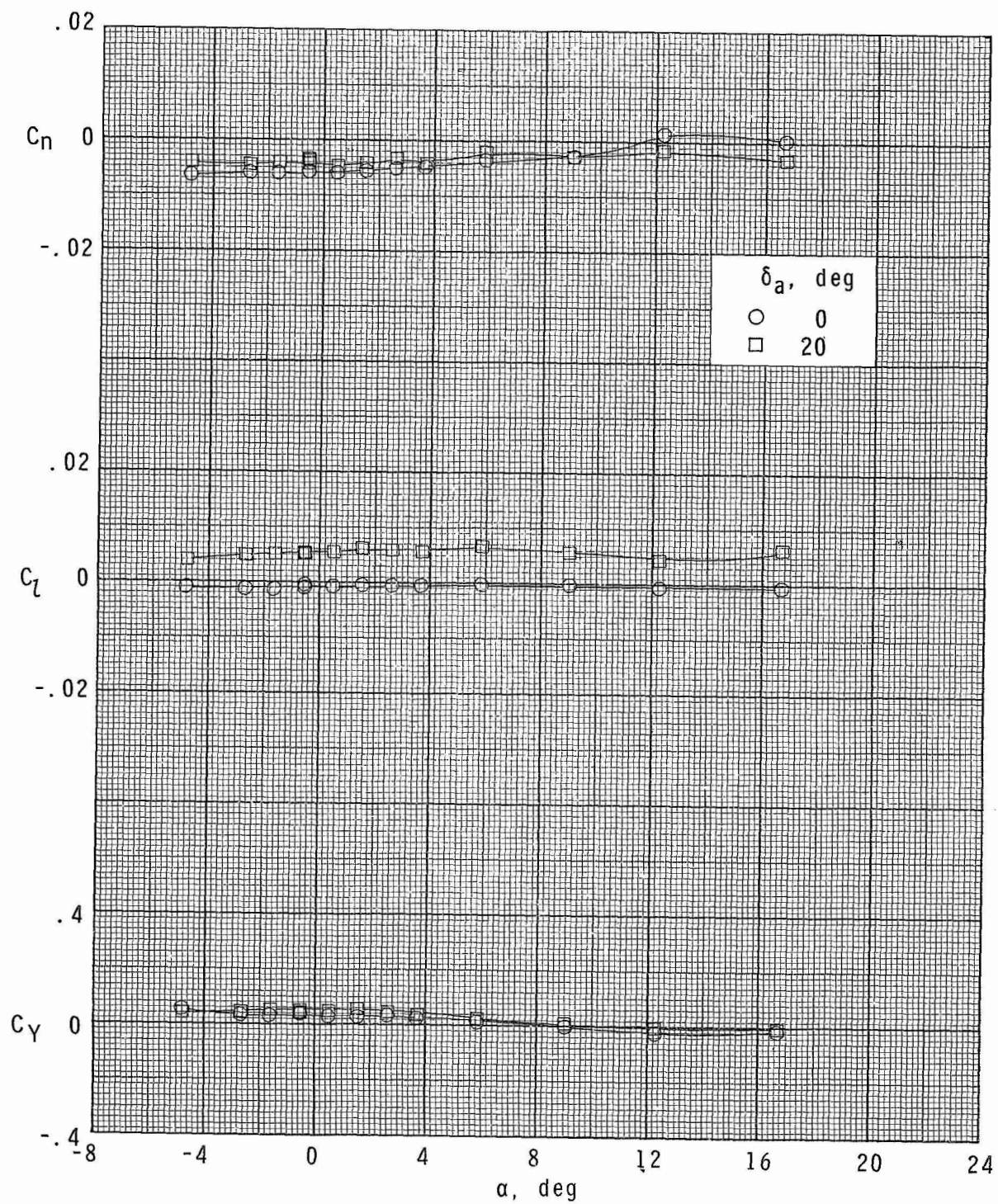
(f) $M = 2.00$; $\delta_c = 15^\circ$.

Figure 22.- Continued.



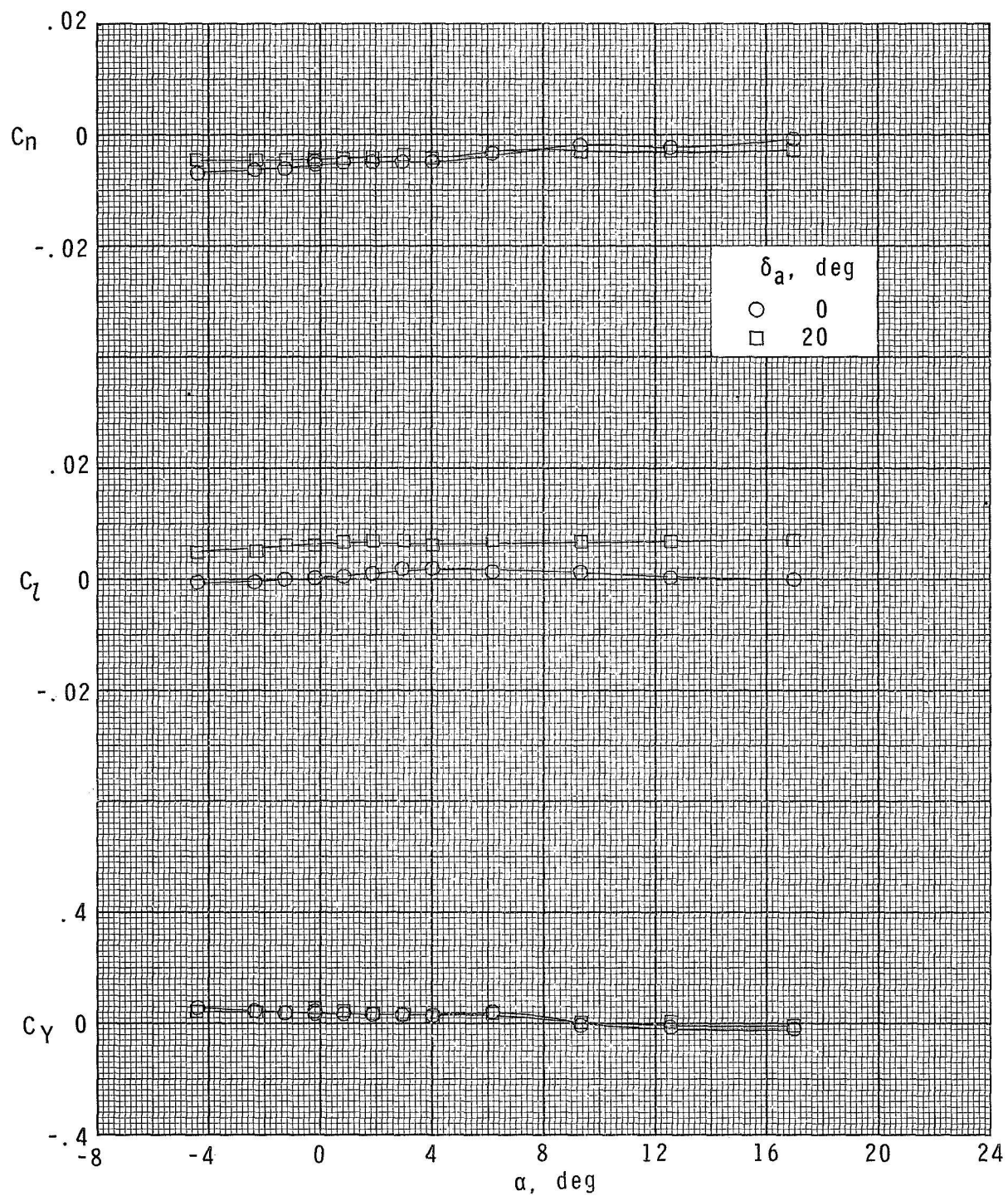
(g) $M = 2.86$; $\delta_c = 0^\circ$.

Figure 22.- Continued.



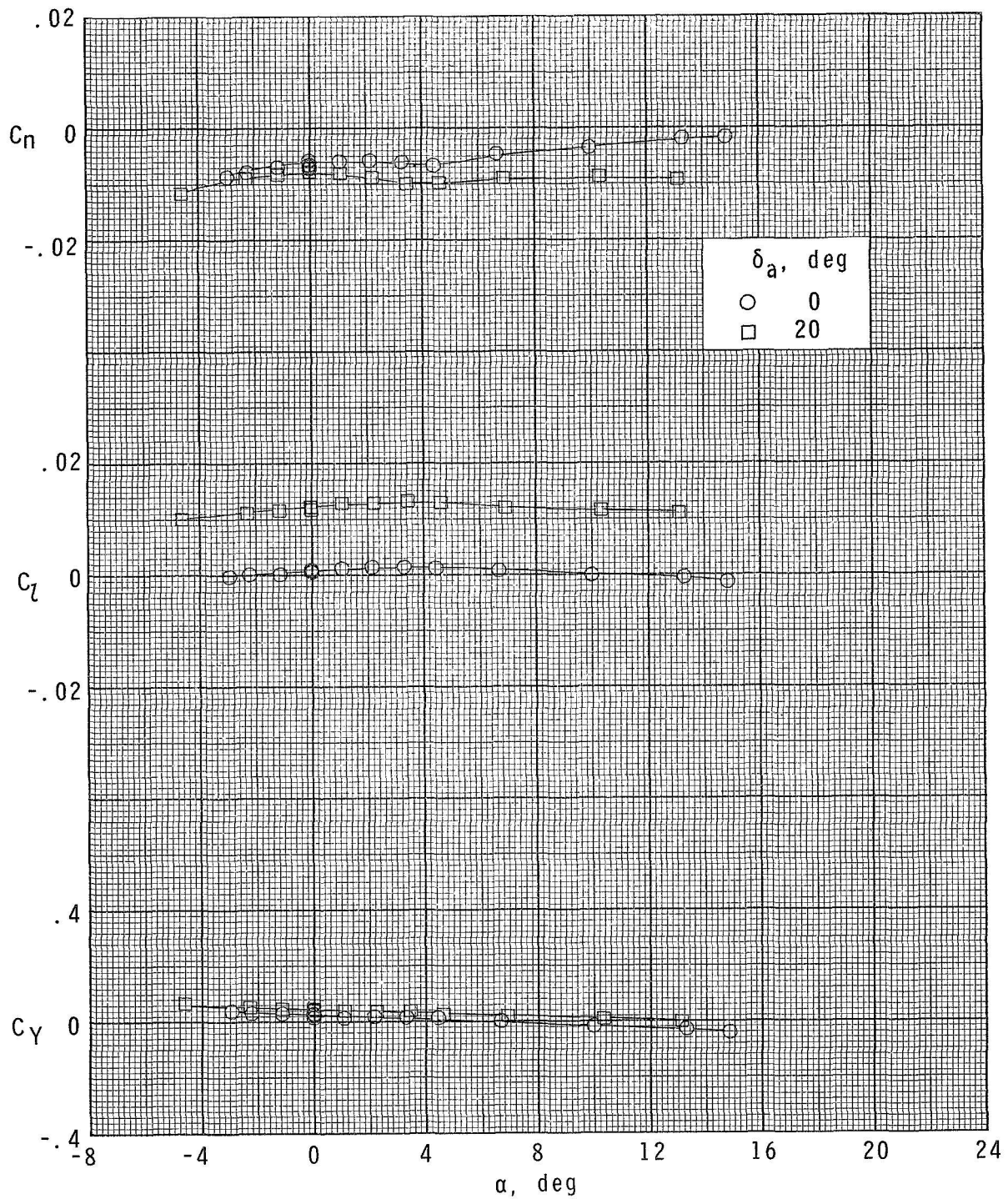
(h) $M = 2.86$; $\delta_c = 50^\circ$.

Figure 22.- Continued.



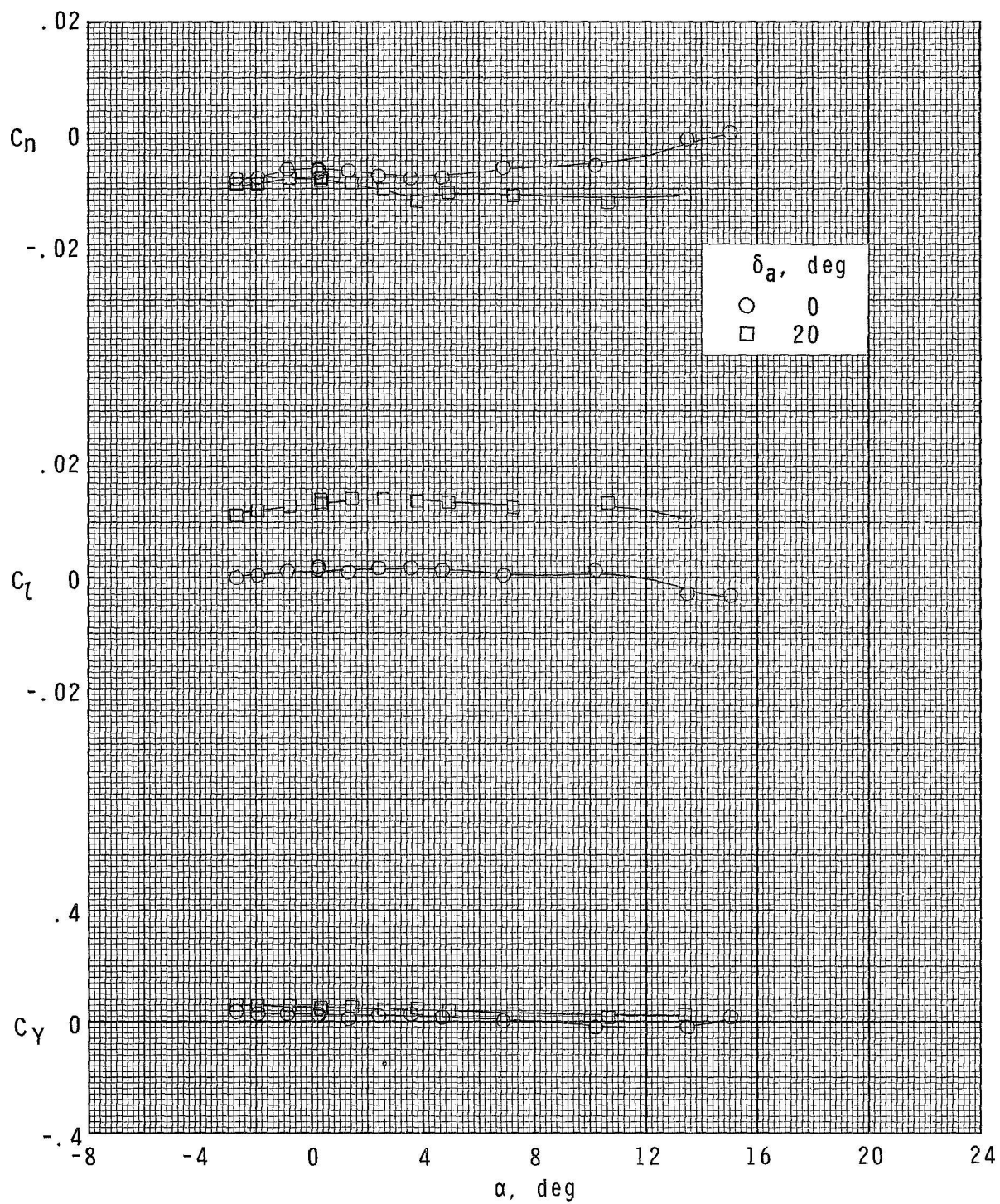
(i) $M = 2.86$; $\delta_c = 15^\circ$.

Figure 22.- Concluded.



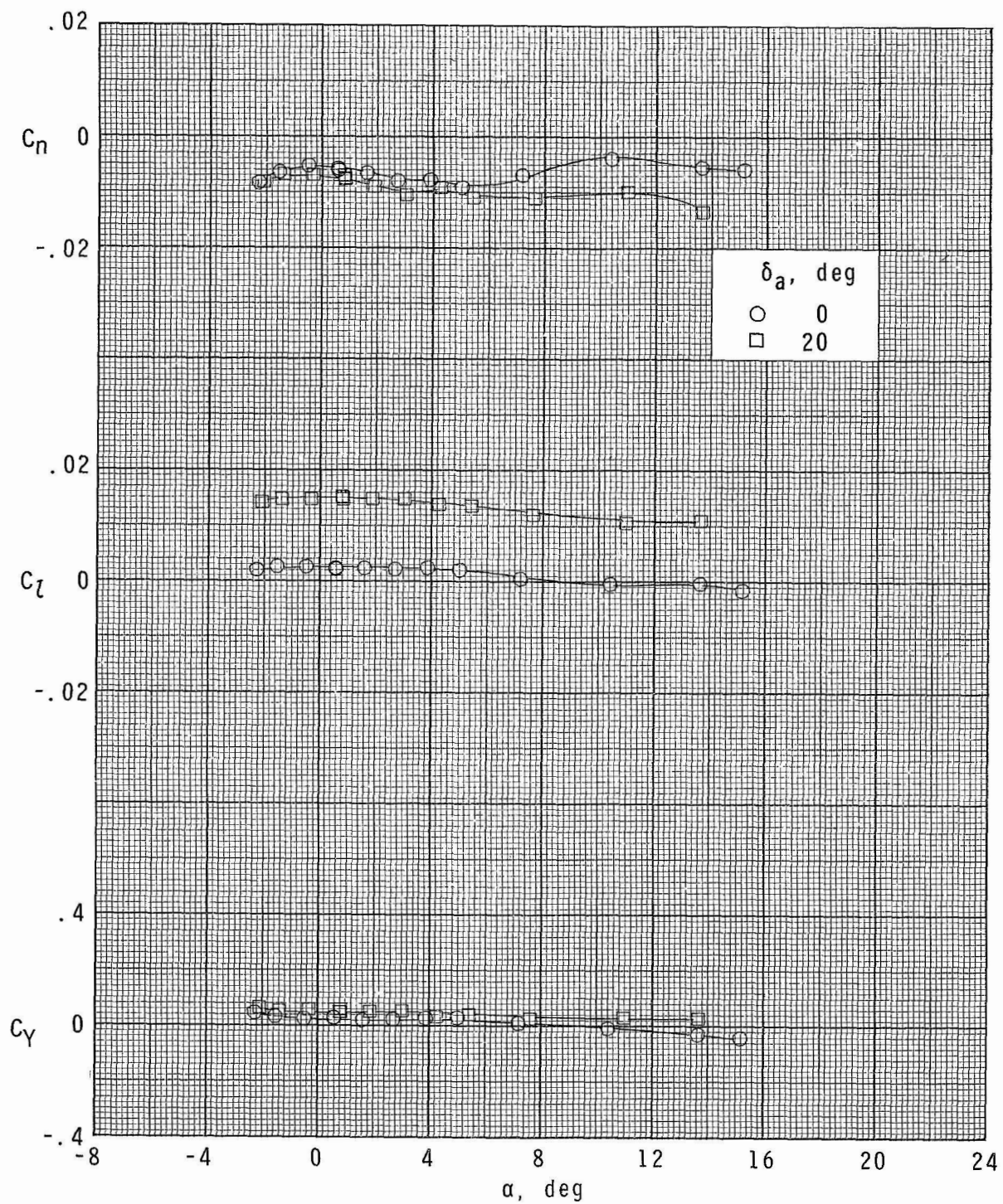
(a) $M = 1.70$; $\delta_c = 0^\circ$.

Figure 23.- Aileron-control effectiveness of configuration $B_1W_2F_2C_1$.



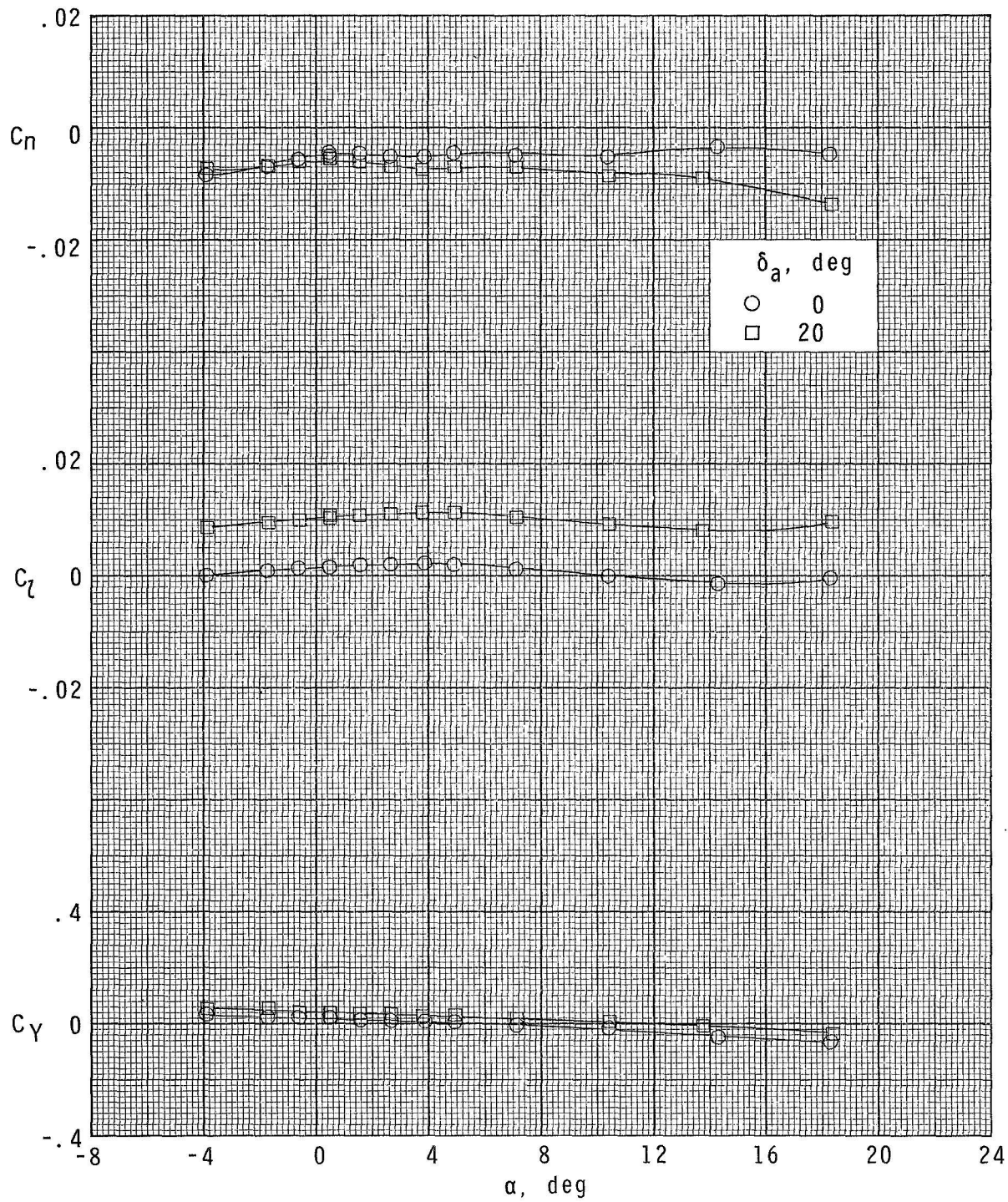
(b) $M = 1.70$; $\delta_c = 5^\circ$.

Figure 23.- Continued.



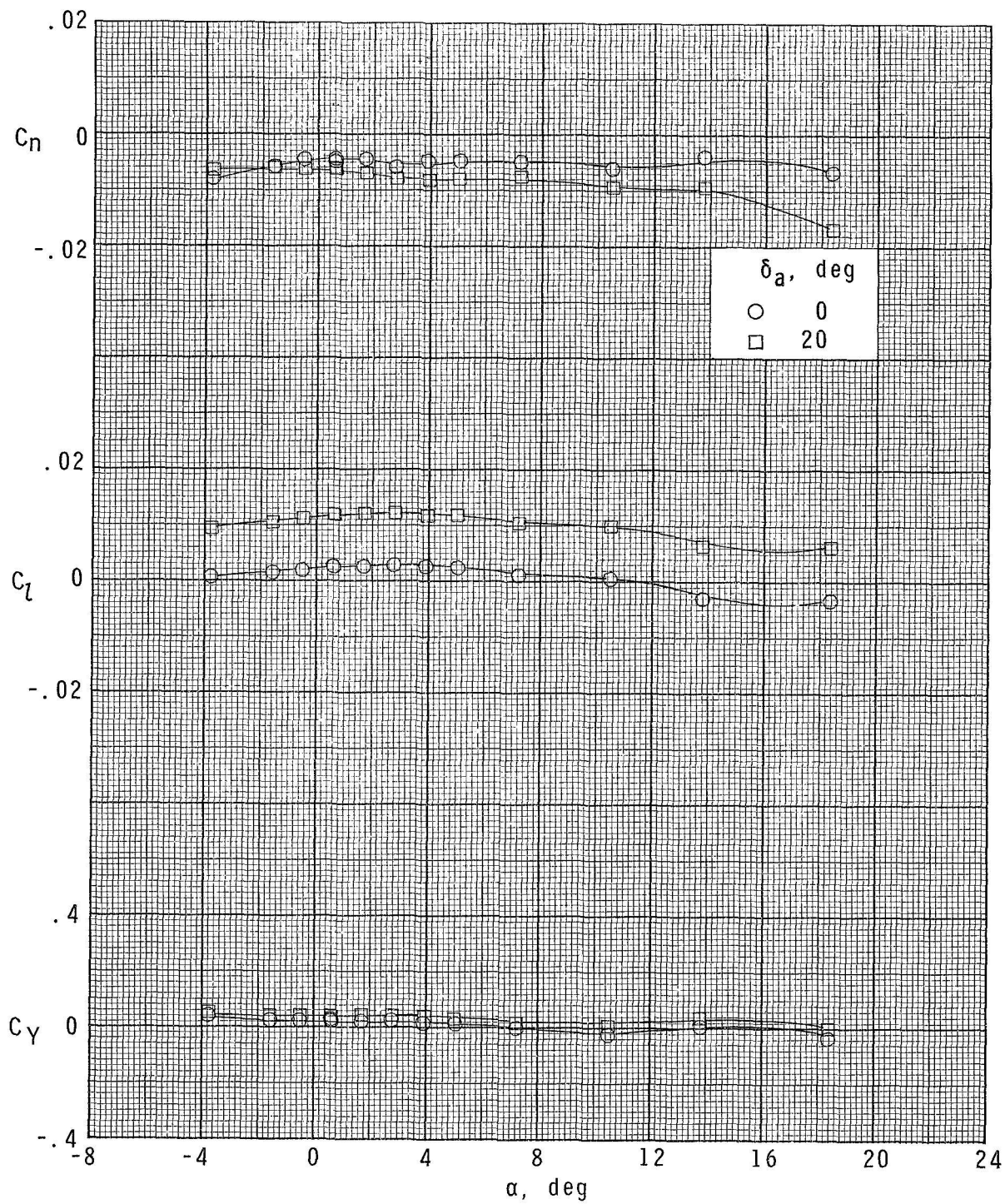
(c) $M = 1.70$; $\delta_c = 15^\circ$.

Figure 23.- Continued.



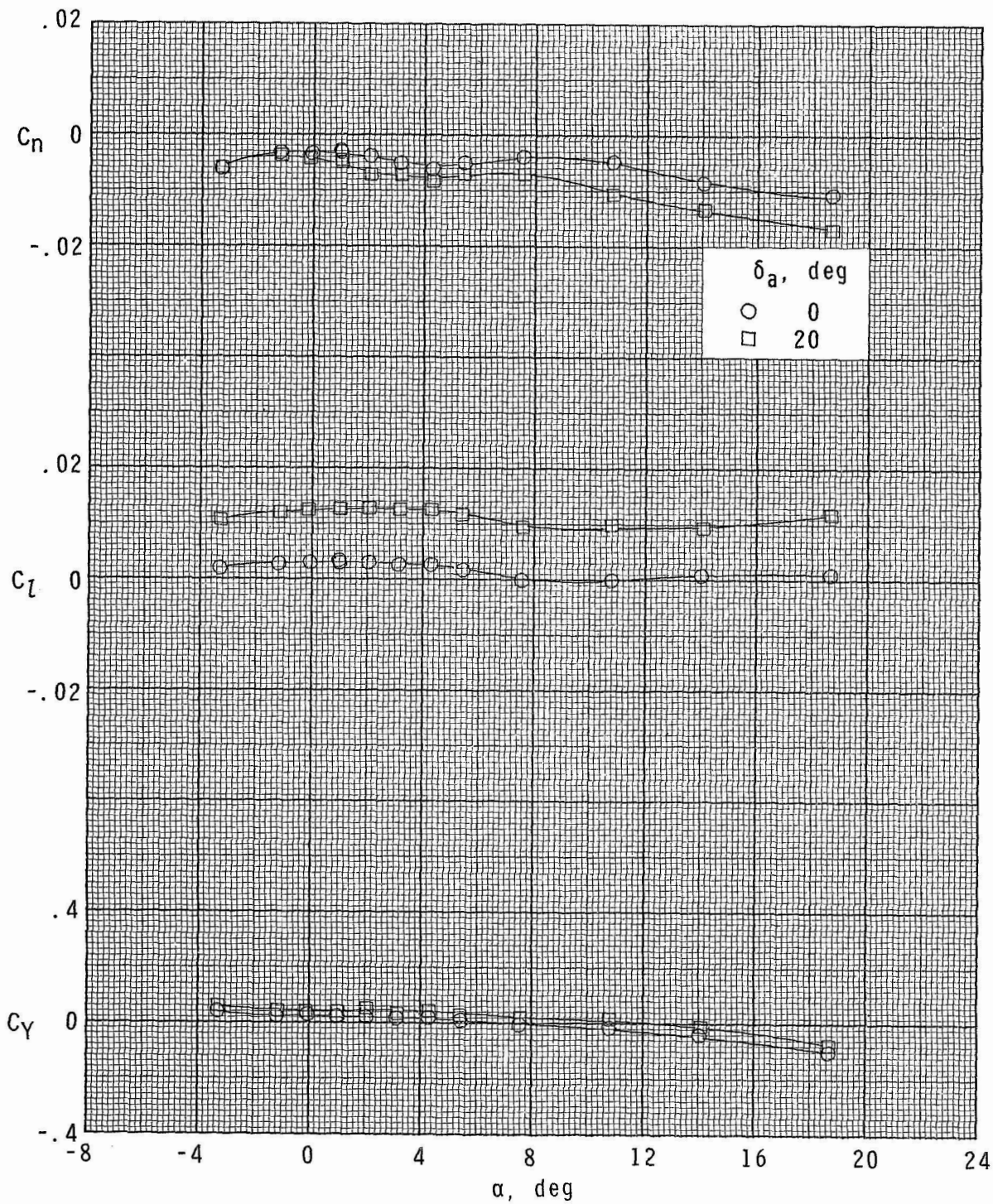
(d) $M = 2.00$; $\delta_c = 0^\circ$.

Figure 23.- Continued.



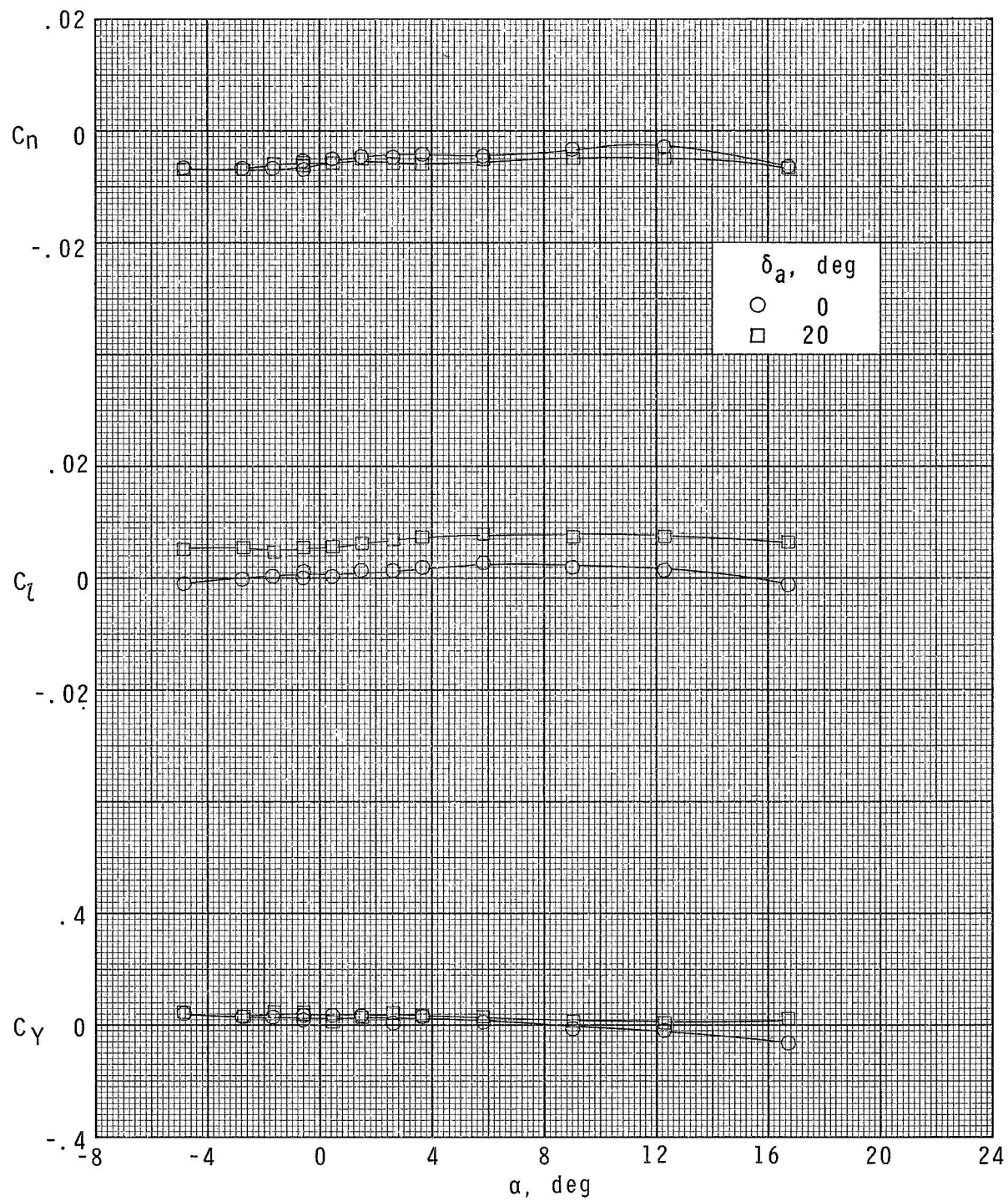
(e) $M = 2.00$; $\delta_c = 5^\circ$.

Figure 23.- Continued.



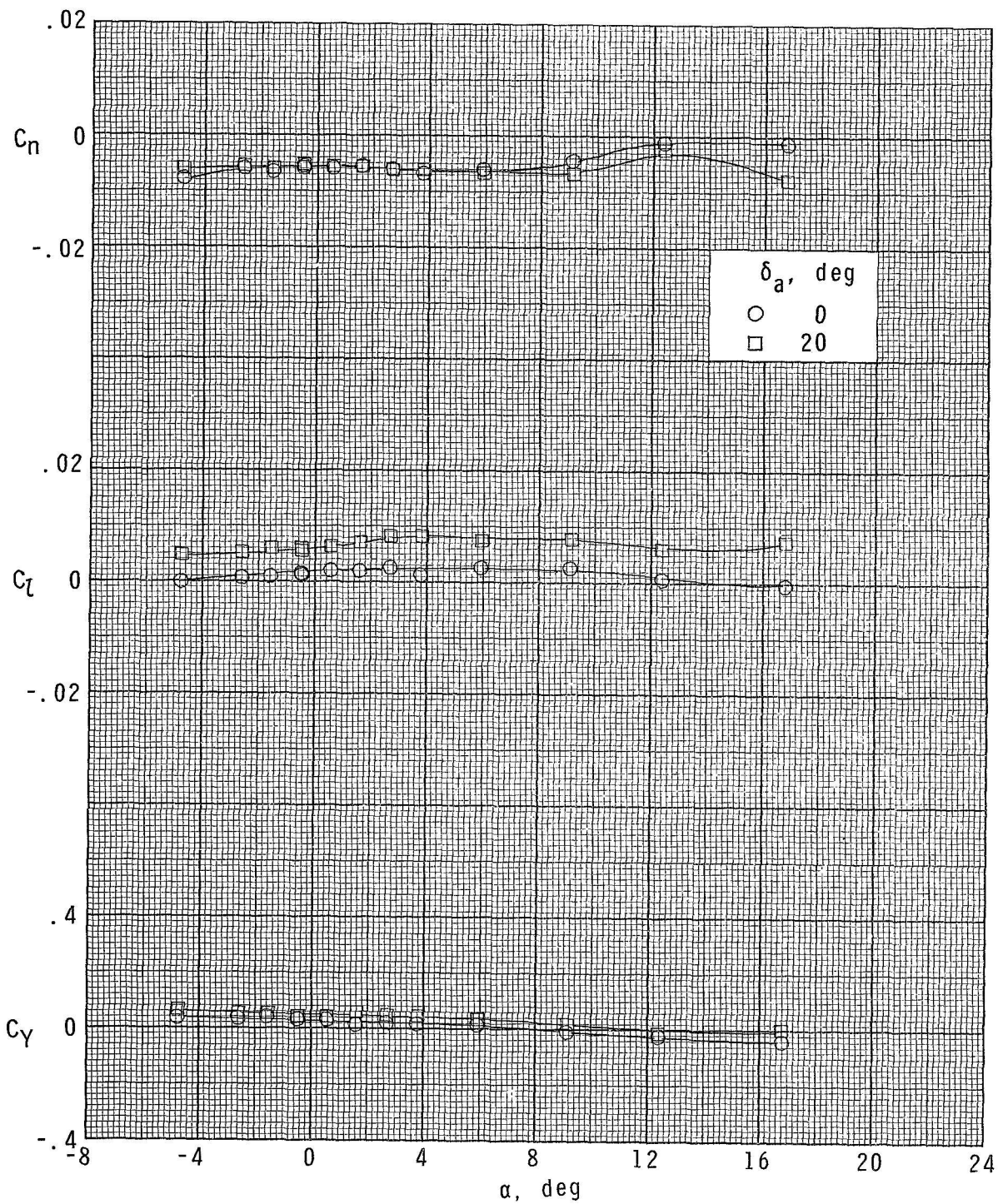
(f) $M = 2.00$; $\delta_c = 15^\circ$.

Figure 23.- Continued.



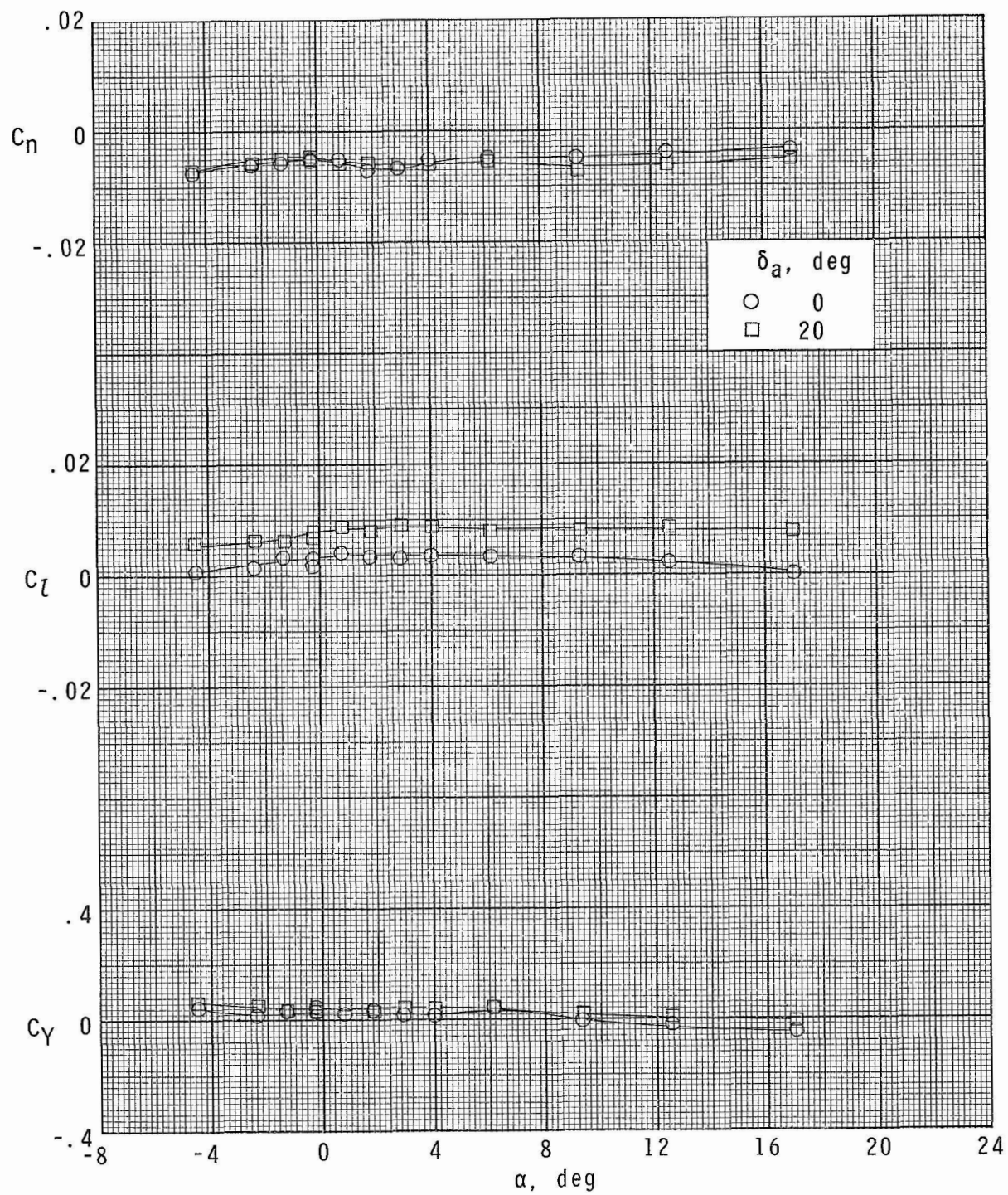
(g) $M = 2.86$; $\delta_c = 0^\circ$.

Figure 23.- Continued.



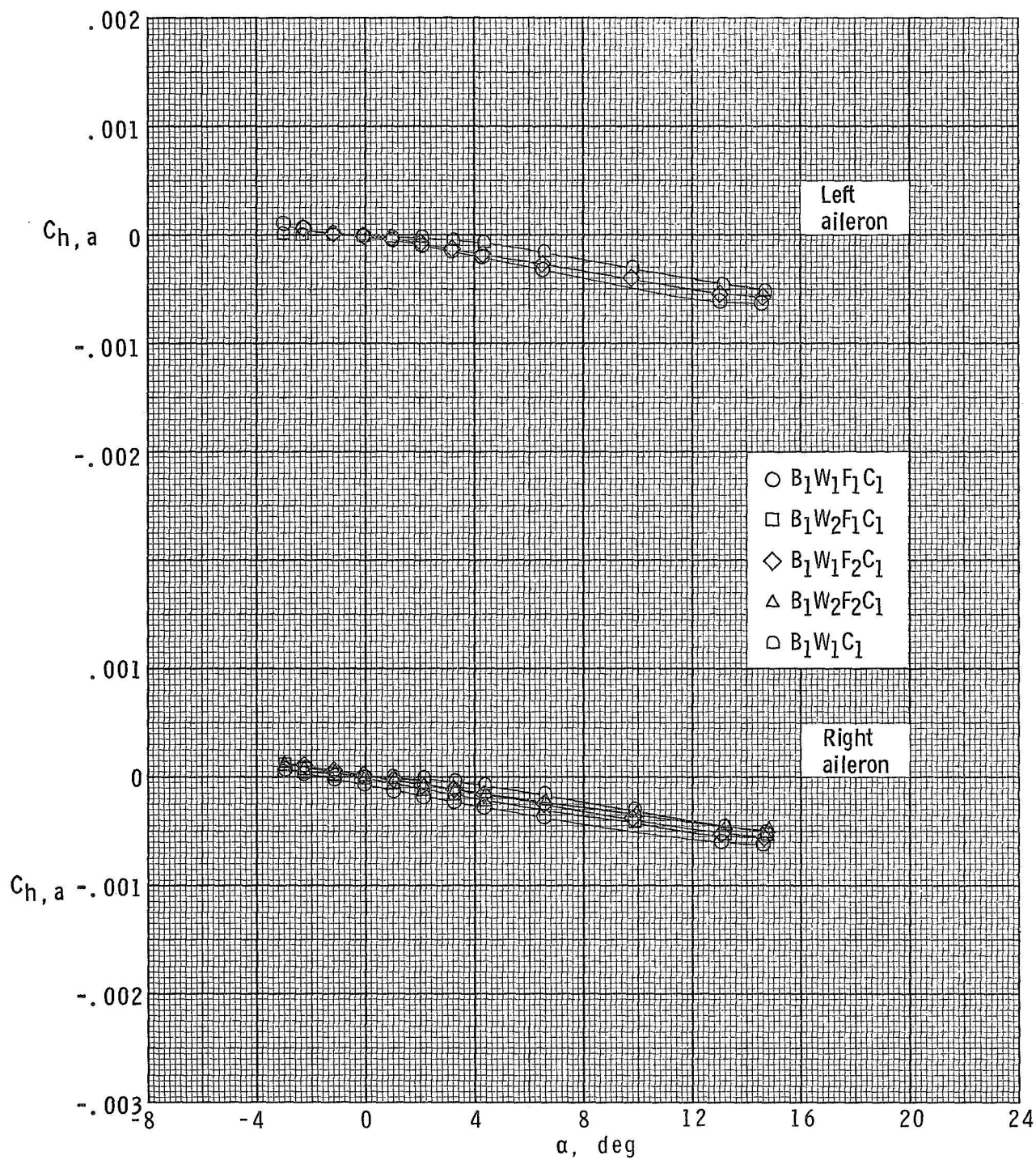
(h) $M = 2.86$; $\delta_c = 5^\circ$.

Figure 23.- Continued.



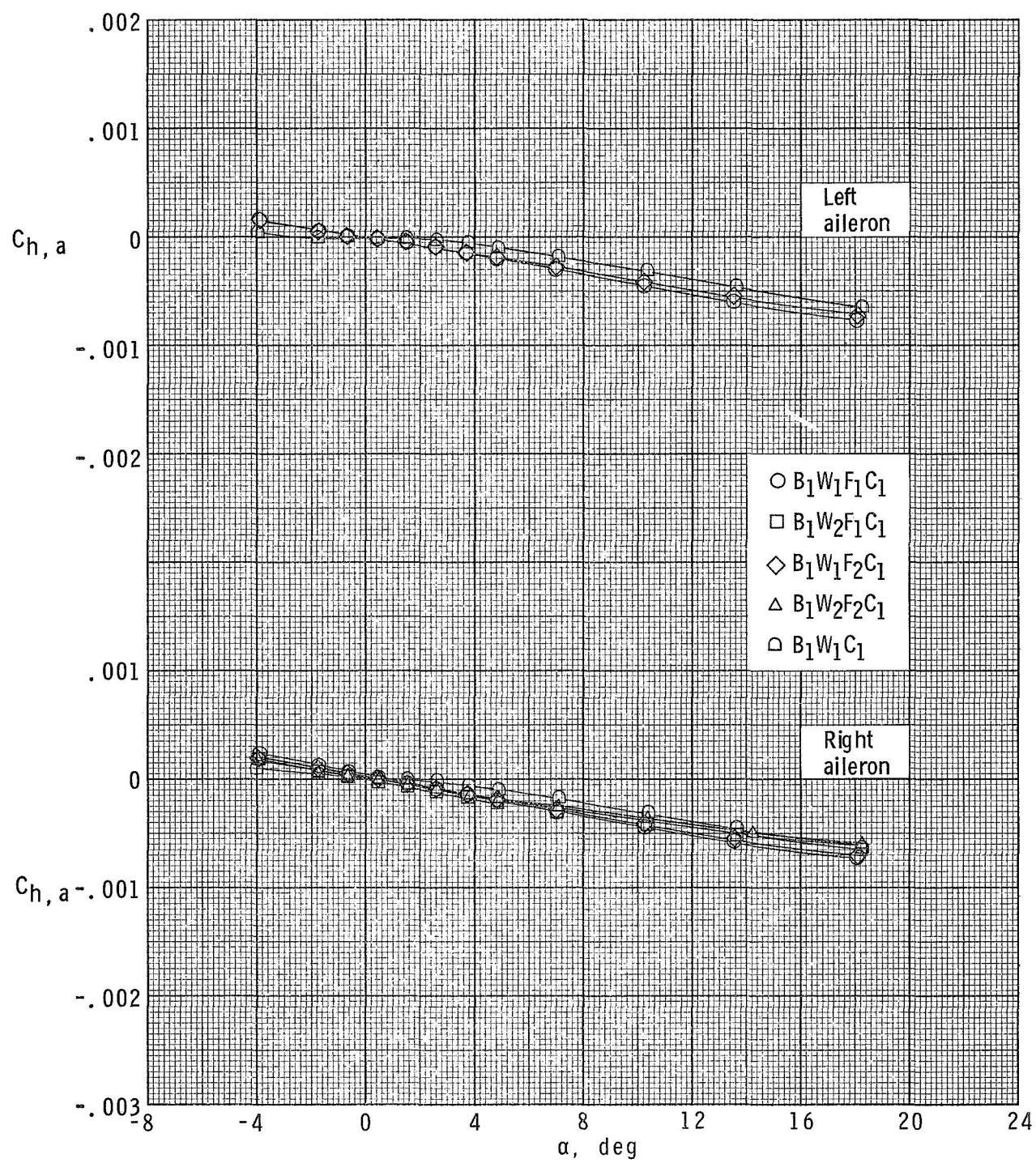
(i) $M = 2.86$; $\delta_c = 15^\circ$.

Figure 23.- Concluded.



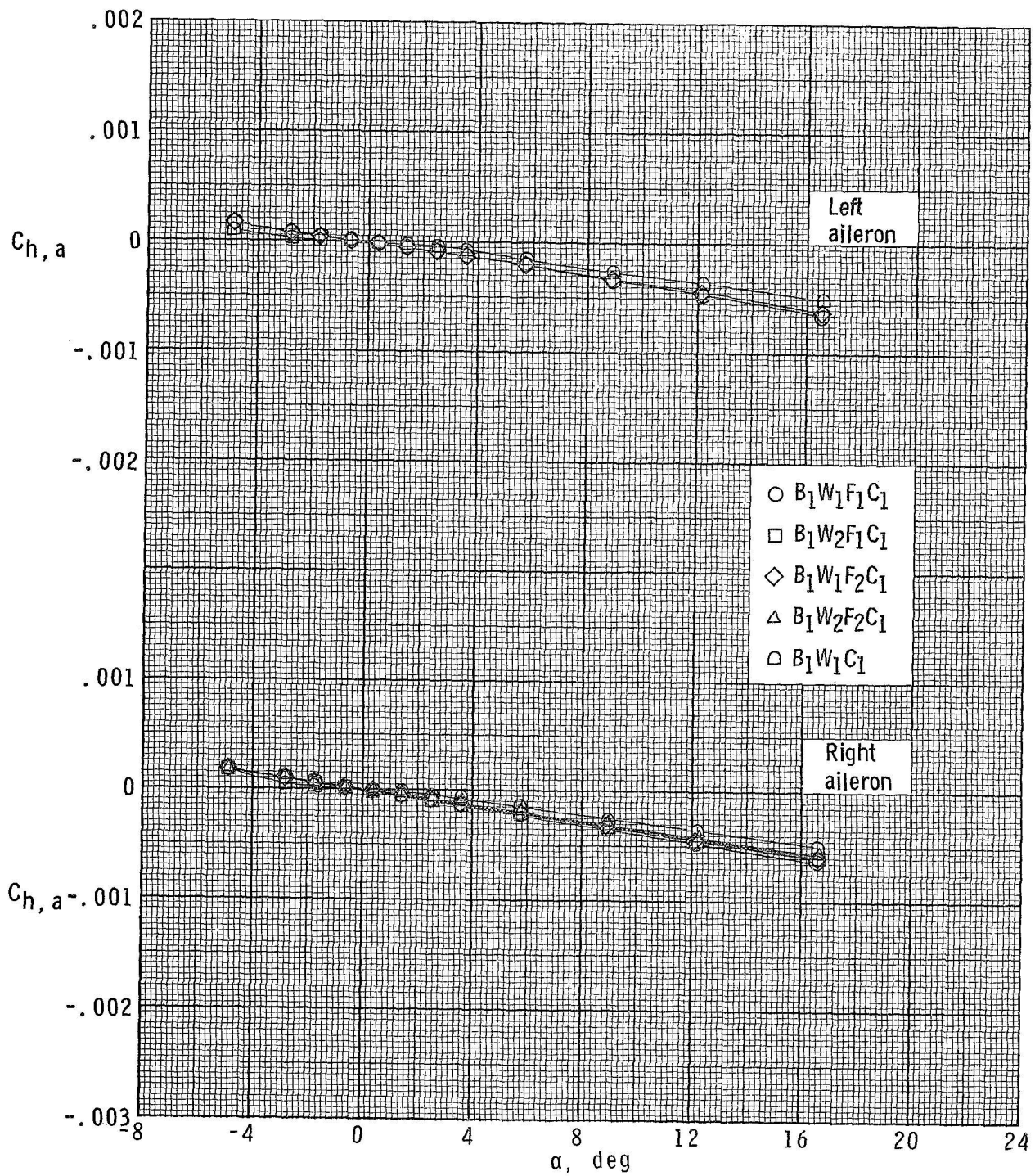
(a) $M = 1.70$.

Figure 24.- Aileron hinge-moment coefficients for $\delta_c = 0^\circ$ and $\delta_a = 0^\circ$.



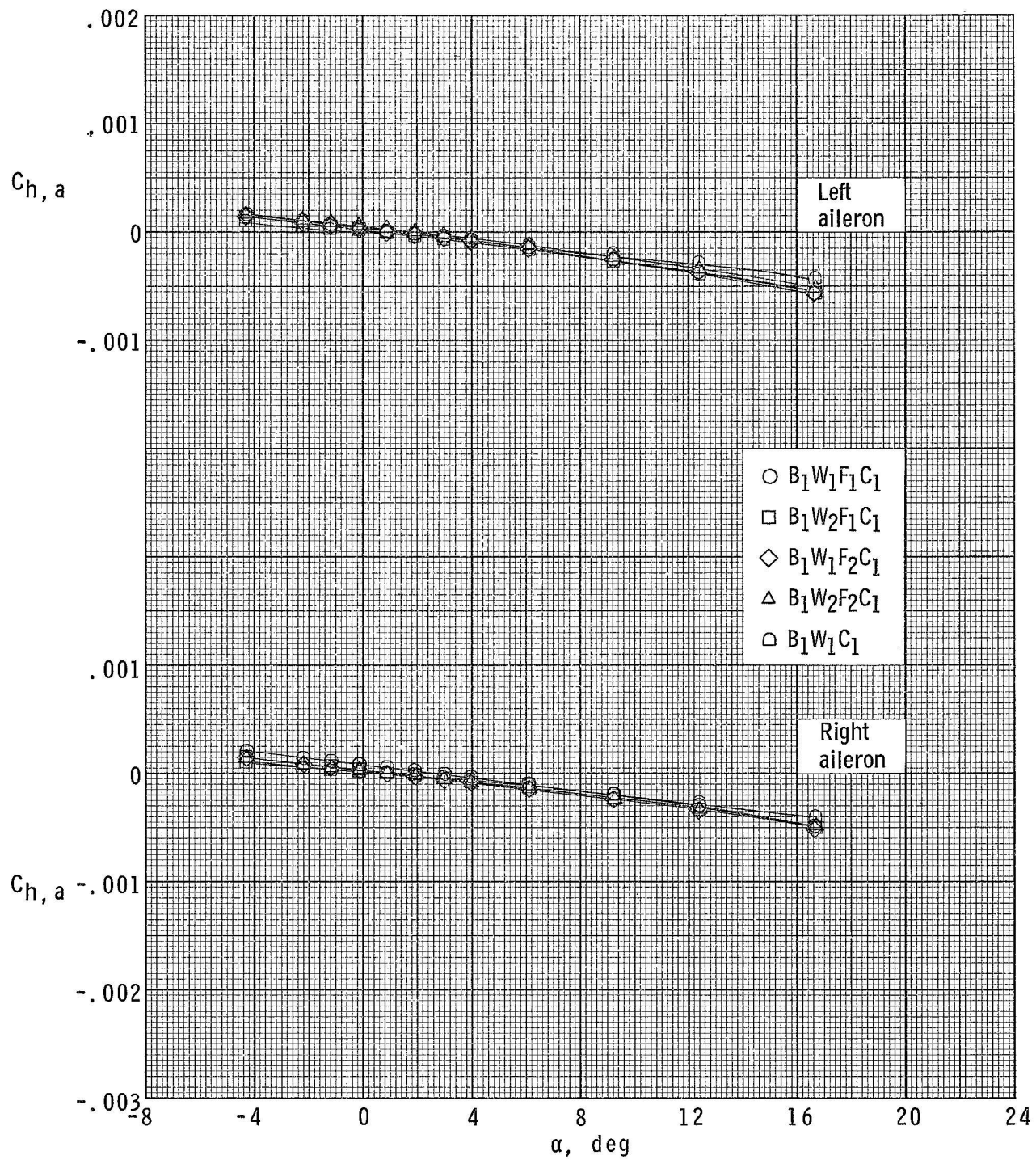
(b) $M = 2.00$.

Figure 24.- Continued.



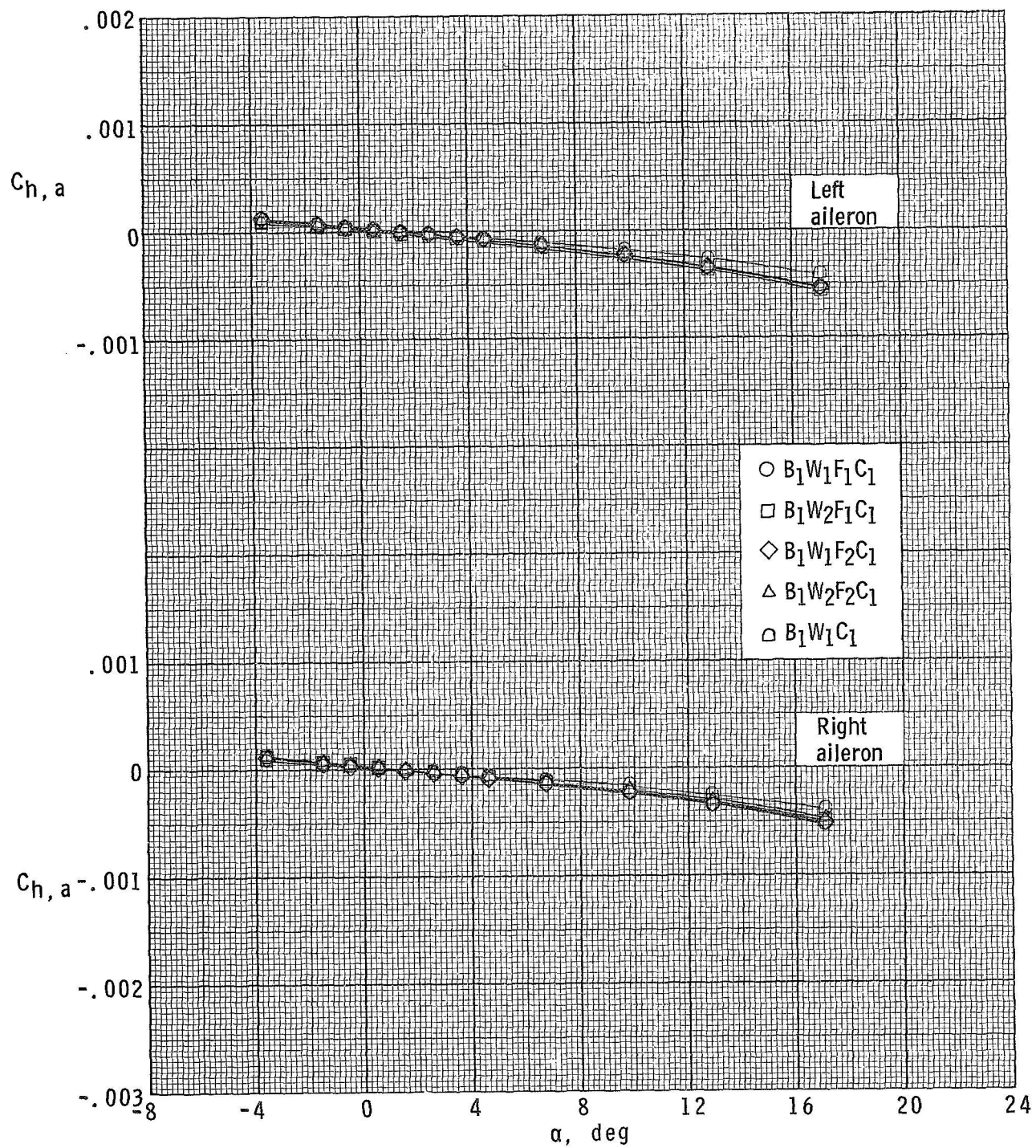
(c) $M = 2.86$.

Figure 24.- Continued.



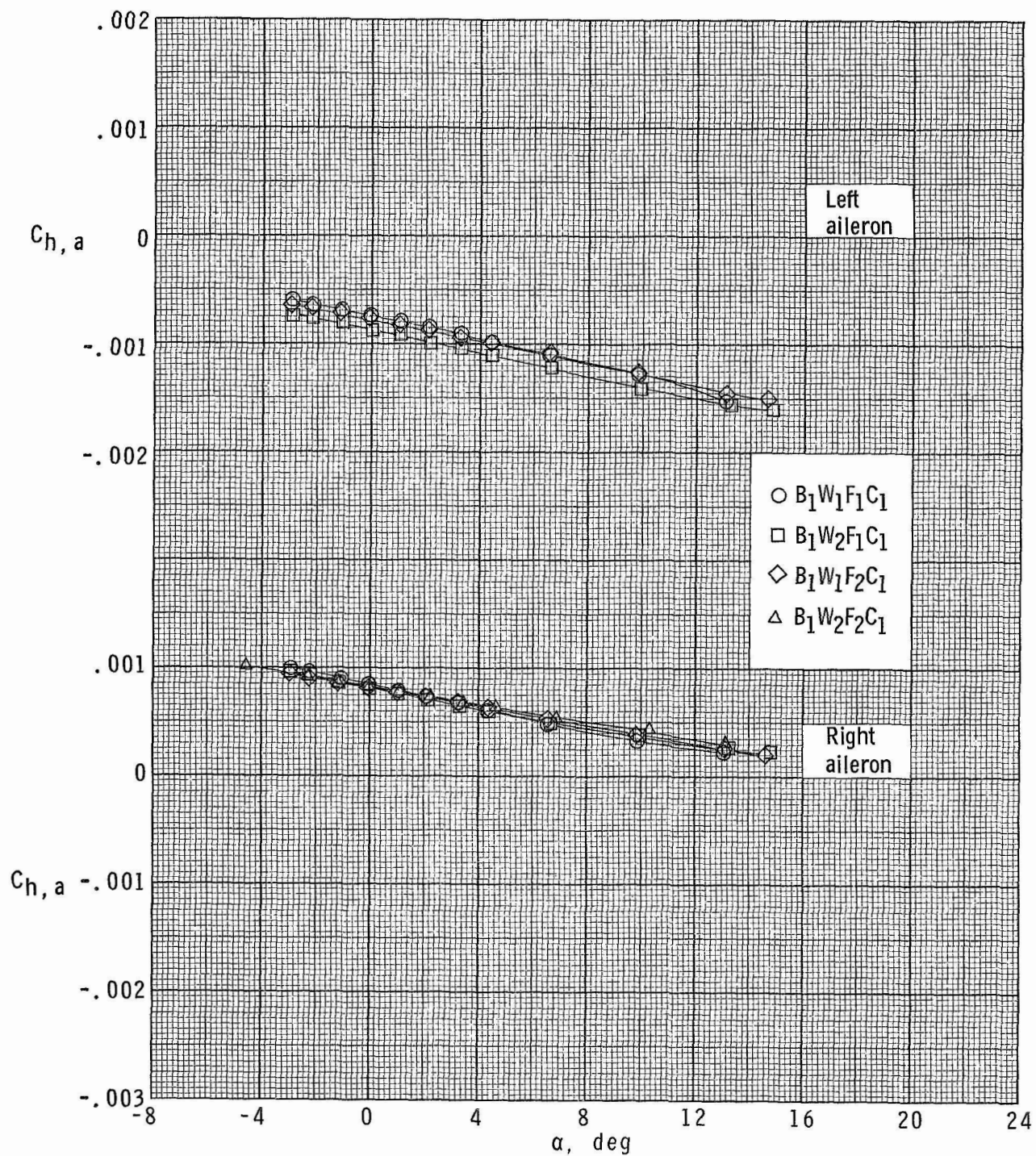
(d) $M = 3.95$.

Figure 24.- Continued.



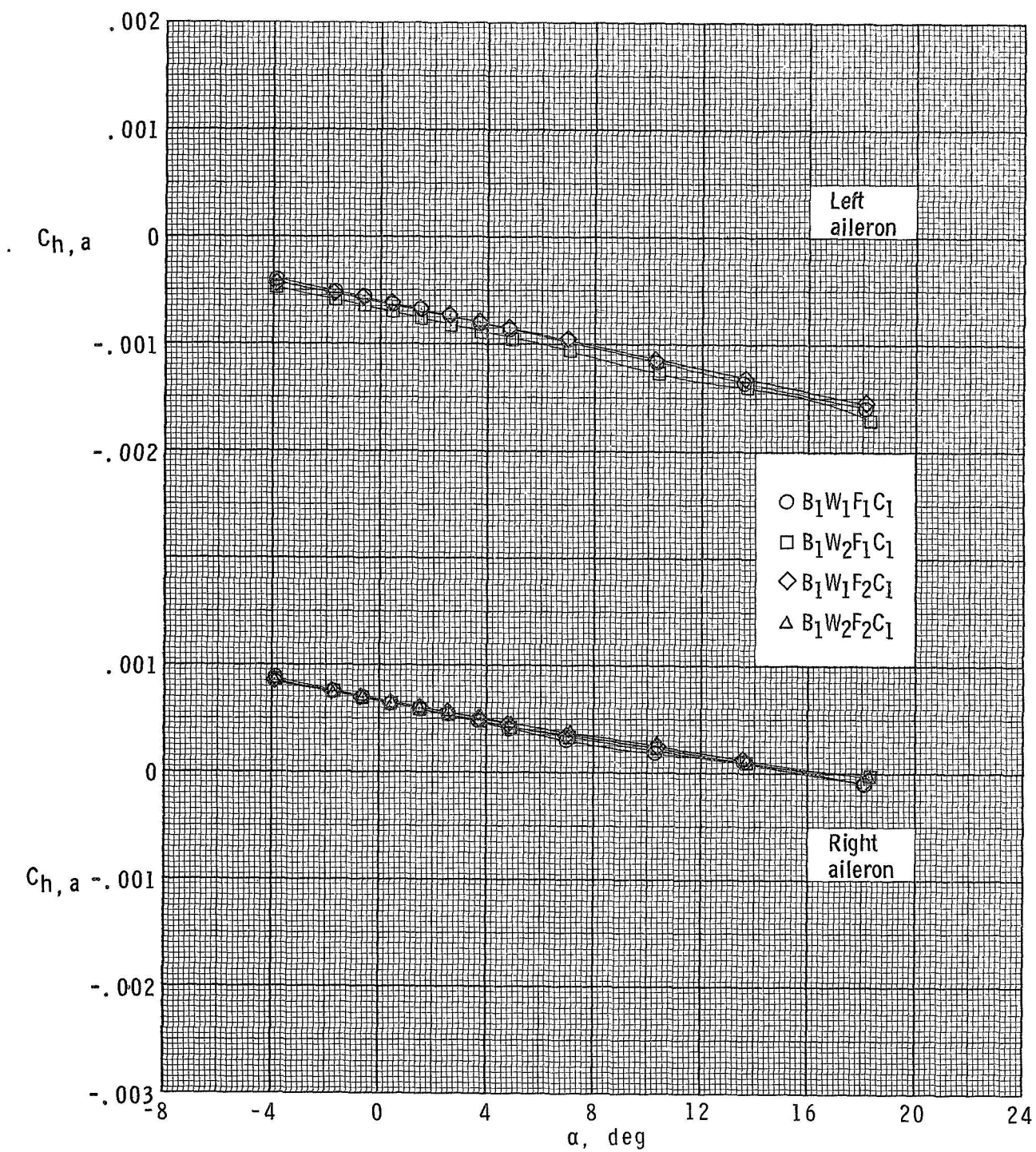
(e) $M = 4.63$.

Figure 24.- Concluded.



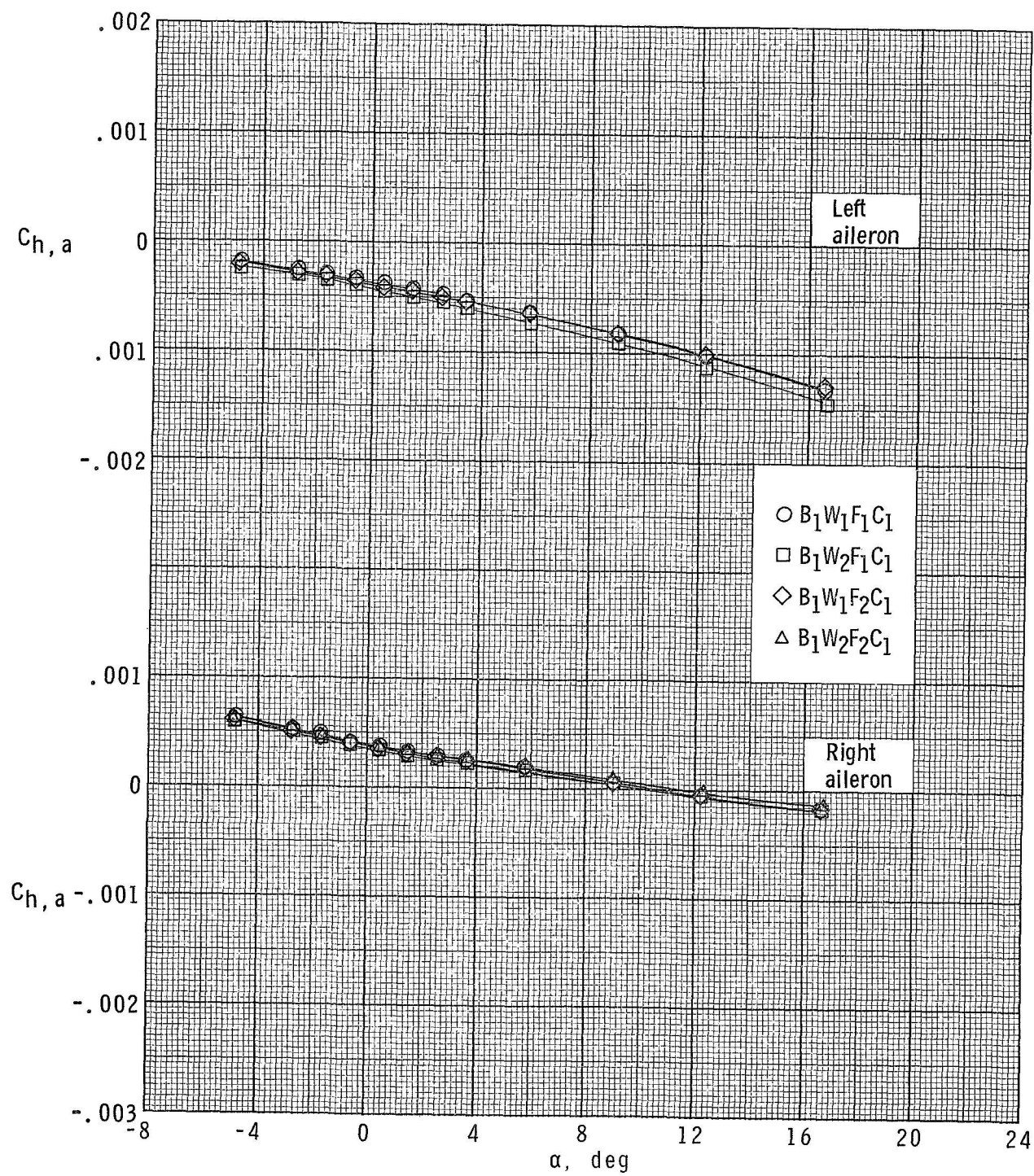
(a) $M = 1.70$.

Figure 25.- Aileron hinge-moment coefficients for $\delta_c = 0^\circ$ and $\delta_a = 20^\circ$.



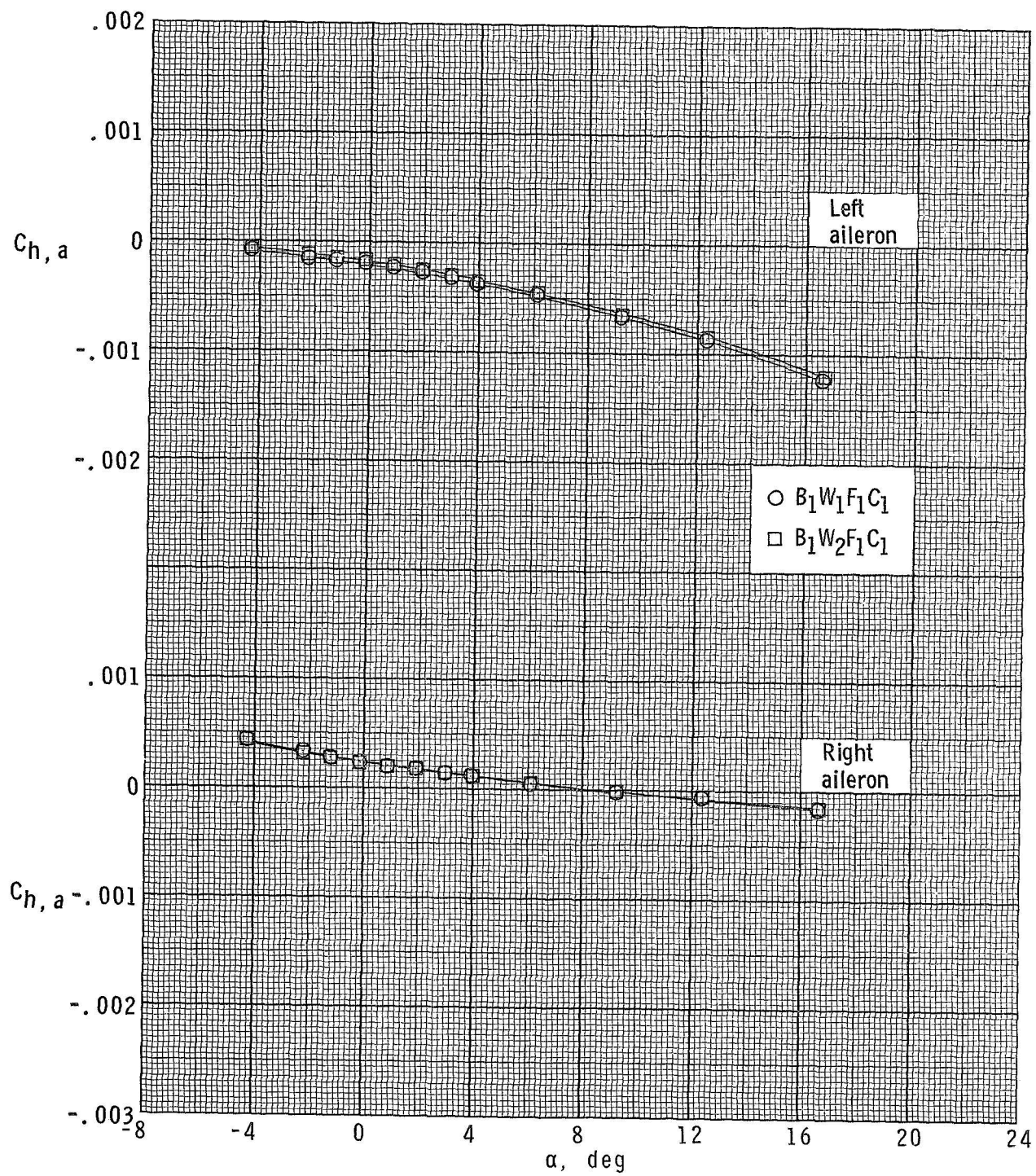
(b) $M = 2.00$.

Figure 25.- Continued.



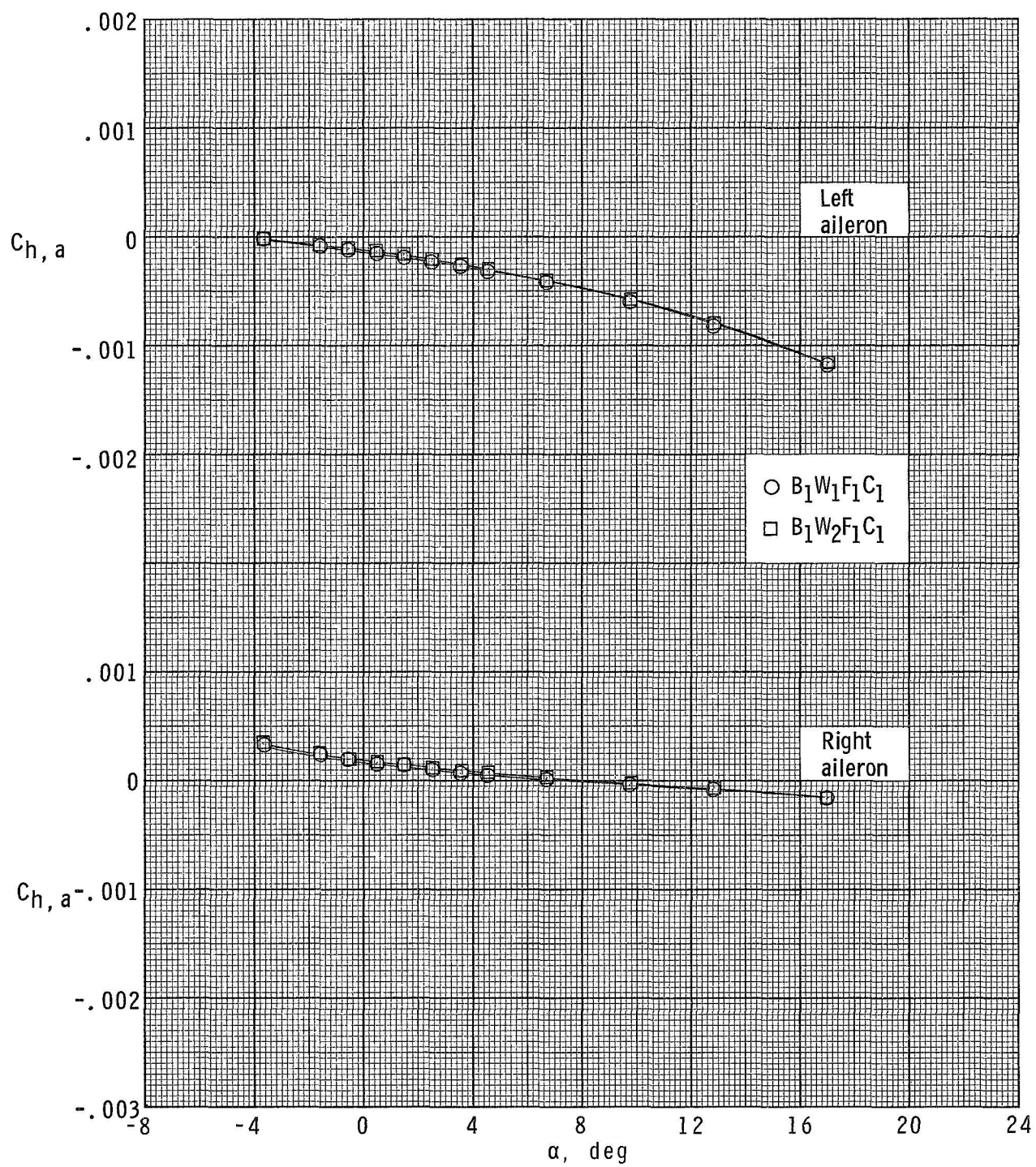
(c) $M = 2.86$.

Figure 25.- Continued.



(d) $M = 3.95$.

Figure 25.- Continued.



(e) $M = 4.63$.

Figure 25.- Concluded.